Structural studies of immunoglobulin E

Hunt, James

Structural studies of Immunoglobulin E

by

James Hunt

A thesis submitted in partial fulfilment of the

requirements for the degree of

Doctor of Philosophy in the University of London

The Randall Centre,

Division of Biomedical Sciences,

King's College London,

New Hunt's House, London, SE1 1UL

March 2004

Abstract

Immunoglobulin E (IgE) and its high-affinity receptor, FcεRI, play a key role in the allergic response. Cross-linking of FcεRI-bound IgE by multivalent antigen leads to receptor aggregation, cell activation and release of inflammatory mediators from mast cells and basophils. This can cause the immediate hypersensitivity reaction characteristic of many allergic disorders, such as asthma and acute anaphylaxis. Research into the binding of IgE to FcεRI could lead to strategies for blocking this interaction and therefore possible treatments for allergic disease.

FcεRI binds the Fc region of IgE. The smallest fragment of IgE-Fc that retains native levels of affinity for FcεRI is a mammalian-expressed dimer of Fc domains Fcε3 and Fcε4 (Fcε3-4). Surprisingly, an isolated and unfolded Fcε3 domain expressed in *E. coli* also shows binding, albeit with lower affinity. These observations highlight the following questions: What structural units and constraints within the mammalian Fcε3-4 fragment are necessary to create a fully folded Fcε3 domain, and what are the minimum requirements to produce a fragment with high affinity for FcεRI?

The work described in this thesis addressed these questions by engineering Fc fragments that lack particular structural features. Site directed mutagenesis and refolding of sub-fragments of Fcε3-4 expressed in *E. coli*, followed by biophysical characterisation, indicated that "longitudinal contacts" with a folded Fcε4 domain were sufficient to stabilise Fcε3. However, to achieve full folding, some form of "lateral" contact was required between the two Fc chains. When expressed in isolation the Fcε4 domain folded as part of a dimer, indicating that Fcε4 does not require Fcε3 for stabilisation. Therefore, Fcε4 was found to be the key to Fcε3 folding, by dimerising the Fc and providing stabilising longitudinal contacts through its intra-chain interface with the Fcε3 domain. Furthermore, it was discovered that the folding of Fcε3 domains in the context of an Fcε3-4 fragment is not dependent on glycosylation or disulphide linkage. However, circular dichroism spectroscopy, surface plasmon resonance and analytical

ultracentrifugation studies of fragments lacking these elements indicated that, although not essential for folding, they were necessary to maintain stability and full affinity for FcεRI. Surprisingly, in the absence of inter-chain disulphide linkage at the N-terminus of Fcε3-4, the fragment was found to bind two FcεRI molecules. This enabled the affinity of a single Fcε3 domain for FcεRI to be estimated; the value was found to be no greater than that previously measured for a single unfolded Fcε3 domain.

These studies have identified structural features that are required for Fcε3 domain folding, stability and high affinity binding to FcεRI. The individual contributions from interdomain contacts, glycosylation and dimerisation have been quantified. The results described within this thesis further our knowledge of IgE structure and function, and provide a structural basis for rational design of inhibitors of the allergic response.

Acknowledgements

I would first like to thank my supervisors, Brian Sutton and Hannah Gould, for providing me with the opportunity to work in their laboratories and carry out the work described in this thesis, and for aiding my progress with many useful discussions and suggestions throughout the course of my studies. This gratitude is also extended to Andrew Beavil, Rosy Calvert and Rebecca Beavil for participating in these discussions and providing many useful insights and suggestions. Further thanks go to the BBSRC for providing funding for the project.

In relation to specific experiments and materials, this work would not have been possible without the constructs created by Alistair Henry, and those of Robert Young, Justin Cook and Ray Owens. I would also like to thank Rebecca Beavil for help with the running the analytical ultracentrifuge, analysing the data, and for providing figures for the introduction; Stella Fabiane and Kate Kirwan for help in preparing the figures in Chapter 3 (Fcε3-4 interfaces) and Chapter 6 (the Fcε3 "roll") respectively; Andrew Beavil for help with operating the CD spectrometer and analysing the data, and Walter Gratzer for helpful discussions on the results; Jim McDonnell for help in analysing the Biacore data and Rosy Calvert for help with protein expression and purification. I would also like to say thank you to everyone else I have shared an office, lab (or both) with throughout my time at the Randall, both for the help they have provided and the fact they have made it such an enjoyable experience.

Finally, I would like to say thank you to my girlfriend, Chloë, and my family for the constant support I have received and the encouragement they have given me every step of the way. Thank you.

Contents

List of figures

List of Tables

Introduction

Chapter 1: Introduction

1.1 Background

Over 80 years ago Prausnitz and Küstner were able to demonstrate that a factor in the blood of allergic individuals could be transferred to the skin of a non-allergic, and render that individual sensitive to the same allergen (Prausnitz and Küstner, 1921). This cytophilic serum factor was named "reagin". It took another 46 years before the molecule was confirmed as an antibody. It was named Immunoglobulin E (IgE) after the erythema that the allergens provoke in sensitive skin. At the time the concentration of the antibody was below that detectable by protein assays, although it could be distinguished from the other known antibody isotypes: IgM, IgG and IgA (Ishizaka and Ishizaka, 1967). However, the discovery of a novel myeloma (Ig "ND") that could inhibit the classical Prausnitz Küstner reaction, and was shown to be immunochemically distinct from the other known antibodies, confirmed the existence of a new antibody class (Johannson and Bennich, 1967). The discovery of this myeloma enabled larger amounts of the antibody to become available for examination, and subsequently the cDNA from this cell line was cloned (Kenten *et al*, 1982). Recombinant preparations of IgE from cloned cDNA have formed the basis of more complex structural and functional studies aimed at understanding the nature of this molecule. This introduction aims to provide a brief overview of the structural and functional information currently available regarding IgE and its receptors, and in doing so highlight questions that have arisen from these findings and that form the basis of the research described in this thesis.

1.2 IgE structure (I)

Initial studies of IgE based on the Ig (ND) myeloma protein (reviewed in Dorrington and Bennich, 1978) demonstrated the existence of a molecule of nearly 190 kDa molecular weight, approximately 12% of which was composed of carbohydrate. The basic four-chain structure of other immunoglobulins was maintained, i.e. two light chains and two heavy chains. However, the heavy epsilon (ε) chain was shown to be nearer in size to the five domain IgM μ-chain, rather than the four domain structures of IgA, IgD and IgG. This domain structure was confirmed by protein sequencing, as was the presence of six

putative glycosylation sites (Asn 145, 173, 219, 265, 371, 383 and 394). IgE, as other antibodies, is susceptible to papain digestion, and can be cleaved into Fc (crystallisable fragment) and Fab (antigen binding fragment) sub-fragments. Digestion with pepsin yields an additional Fc'' fragment that corresponds to the "extra" heavy chain domain, Fcε2, that "replaces" the hinge region of IgG - see figure 1.1.

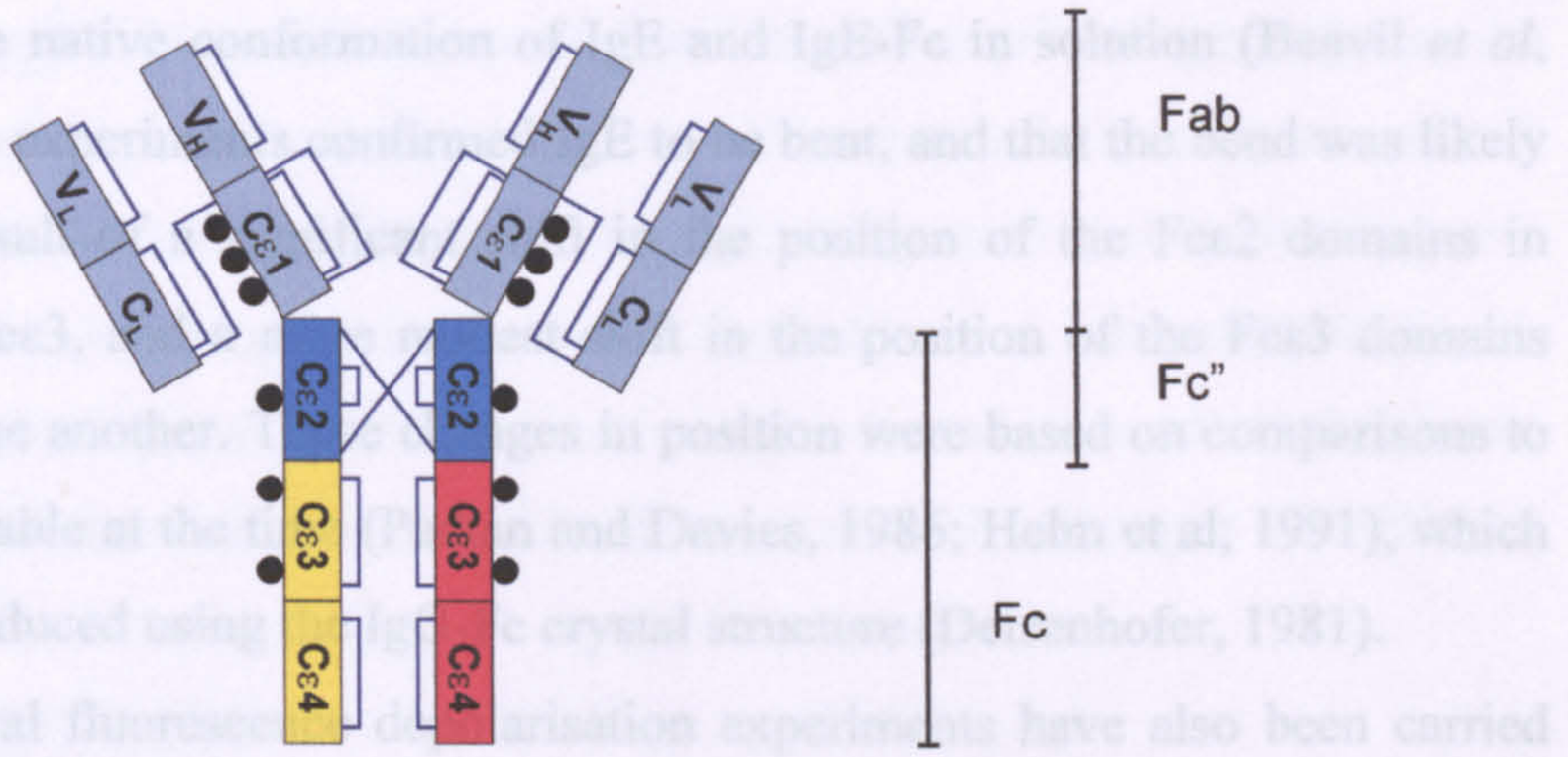

Figure 1.1: Schematic representation of IgE. Each rectangle represents a separate immunoglobulin domain; blue lines indicate disulphide bonds and black dots putative glycosylation sites. Sidebars indicate fragments generated by protease digestion.

1.3 IgE conformation

Subsequent to the initial biochemical characterisation of IgE, more detailed biophysical analyses were carried out in an attempt to determine the conformation of IgE both in solution, and when receptor-bound. The first studies used fluorescence depolarisation as an indicator of IgE flexibility. This technique relies on the measurement of re-emitted depolarised light after initial excitation from a polarised source, with the size, shape and flexibility of the protein determining the rate of depolarisation. This rate can be modelled based on the assumption that the molecule is a rigid body; therefore the degree of deviation from the model is an indication of flexibility. The source of the fluorescence was a chromophore such as dansyl, used either as a hapten or covalently coupled. The first study of this type (Nezlin *et al*, 1973) used steady state fluorescence depolarisation to show that IgE myeloma protein was much less flexible than IgM or IgG monomers. This was later confirmed using time resolved

fluorescence depolarisation (Cathou, 1978). Thus, it was shown that IgE was significantly more rigid than any IgG. Further work, using a panel of mouse anti-dansyl monoclonal antibodies with different constant regions, showed IgE to be more rigid than mouse IgG1 (Oi et al, 1984). This antibody has a shortened hinge region (whereas IgE completely lacks a hinge region) and had previously been noted for its lack of flexibility compared to other IgG sub-classes. Eventually X-ray solution scattering, allied to model fitting, provided further evidence regarding the native conformation of IgE and IgE-Fc in solution (Beavil *et al*, 1995). These experiments confirmed IgE to be bent, and that the bend was likely to be the result of a significant shift in the position of the Fcε2 domains in relation to Fcε3, and a more modest shift in the position of the Fcε3 domains relative to one another. These changes in position were based on comparisons to models available at the time (Padlan and Davies, 1986; Helm et al, 1991), which had been produced using the IgG-Fc crystal structure (Deisenhofer, 1981).

Several fluorescence depolarisation experiments have also been carried out on receptor-bound IgE. The first set of data collected indicated there to be little difference between the receptor-bound form of IgE and that found in solution (Slattery et al, 1985). Subsequently, nanosecond experiments were performed (Holowka *et al*, 1990). These enable a dissection of the modes of motion (as opposed to an average of all modes seen previously). These experiments painted a slightly more complex picture, with a variation in correlation times obtained that was attributed to different features of the bound and unbound molecule. The fastest correlation times were concluded to be representative of Fab motion, with cross-linking completely abrogating these. The difference between measurements for these motions in solution and receptor-bound was small. However, a second longer correlation time was also observed for receptor-bound IgE. This appeared to be distinct from the Fab movements, and was suggested to be the product of a reduction in segmental flexibility, probably in the Fcε2-3 region. Therefore this study concluded that the receptor-bound and solution forms of IgE could be different.

As well as the depolarisation studies of IgE, Forster resonance energy transfer (FRET) was also applied to the study of IgE conformation. The technique relies on energy transfer between fluorescent molecules with overlapping emission and excitation spectra. If a given molecule is excited at the

correct wavelength, emission occurs at a longer wavelength. If this emission spectrum overlaps with the excitation spectrum of a second fluorescent molecule, energy transfer can take place between the first and the second. If energy transfer is efficient enough, emission from the second molecule can be detected, as can a reciprocal decrease in the intensity of the emission of the first due to the transfer of energy to the second. The efficiency of this transfer is highly dependent on the distance between the probes, and thus the technique can be used as a "molecular ruler". If enough site-specific fluorescent probes with overlapping spectra can be incorporated, it is possible to map a protein of interest at the nanometre scale. A number of measurements were made for IgE using such probes, leading to a model of the receptor:IgE complex based upon distances between both the N- and C- termini of IgE, and the distance of receptor-bound molecule to the plasma membrane (Baird and Holowka, 1985; Zheng et al, 1991; Zheng et al, 1992; see figure 1.2).

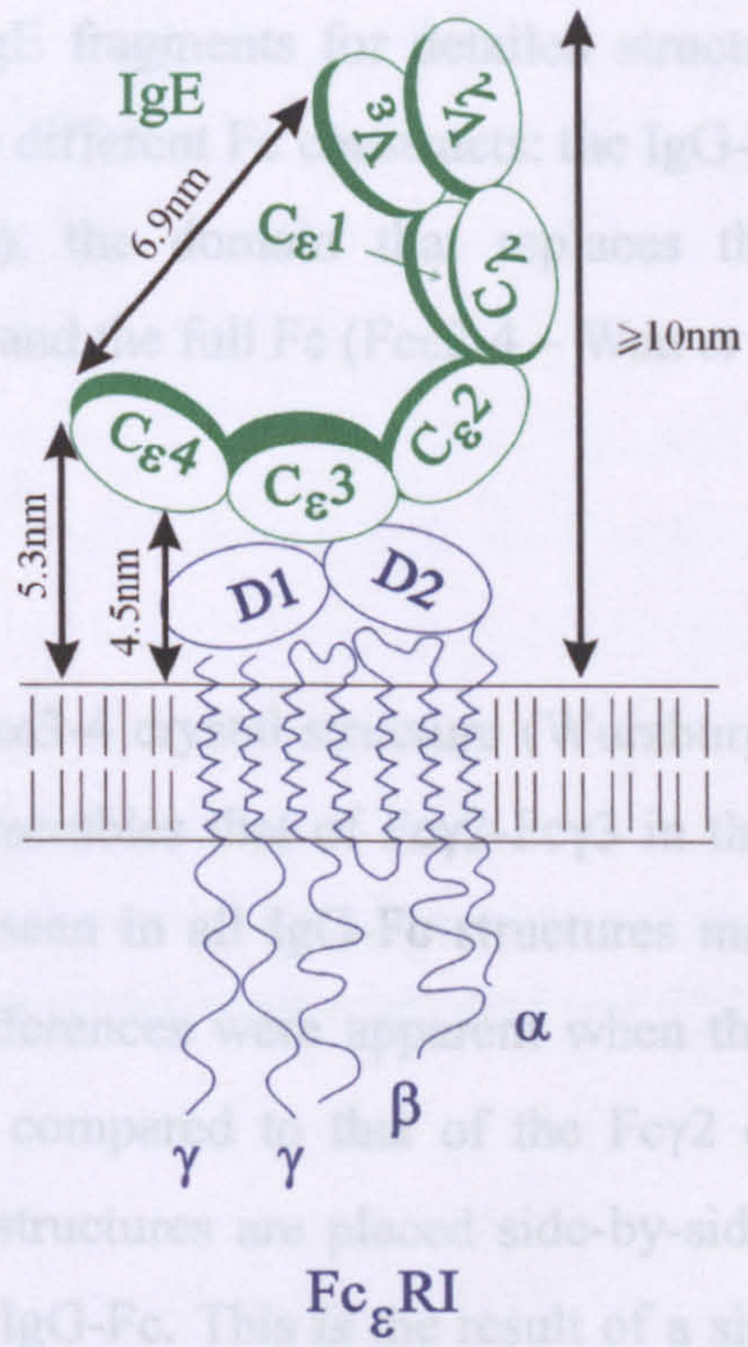

Figure 1.2: Schematic representation of receptor-bound IgE based on an illustration from Zheng et al (1991) showing distances measured by FRET between site-specific probes.

The overall conclusion derived from these FRET studies was that IgE is bent in solution, and that there is a degree of loss in the flexibility of the molecule on engagement with receptor (Baird and Holowka, 1985; Zheng et al, 1991). Furthermore, the difference in flexibility between IgG and IgE was again noted (Zheng *et al*, 1992). However, there was a degree of disagreement in the findings with respect to the overall conformation when receptor-bound. Initial experiments suggested a conformational change on receptor engagement (Baird and Holowka, 1985); however later observations using a chimeric IgE molecule indicated that the bent conformation was maintained on binding to receptor (Zheng *et al*, 1991). Further clues as to the real nature of the receptor-bound form of IgE, as compared to its solution conformation, were not to emerge until the elucidation of higher resolution structures.

1.4 IgE structure (II)

Cloning of the Fc region and expression in a variety of cell lines has led to the availability of IgE fragments for detailed structural analysis. Currently, structures exist for three different Fc constructs: the IgG-Fc homologue (Fcε3-4 – Wurzburg *et al*, 2000), the domain that replaces the IgG hinge, (Fcε2 – McDonnell *et al*, 2001) and the full Fc (Fcε2-4 – Wan *et al*, 2002).

1.4.1 Fcε3-4

The truncated Fcε3-4 crystal structure (Wurzburg *et al*, 2000) confirmed that this domain pair resembles that of Fcγ2-Fcγ3 in the IgG-Fc, with the two-fold axis of symmetry seen in all IgG-Fc structures maintained for the Fcε3-4 fragment. However, differences were apparent when the relative disposition of the Fcε3 domains was compared to that of the Fcγ2 domains in IgG-Fc (see figure 1.3). If the two structures are placed side-by-side, Fcε3-4 appears much more compact than the IgG-Fc. This is the result of a significant decrease in the angle between the Fcε3 domains and Fcε4 compared with Fcγ2-Fcγ3. It has been proposed that the difference is the result of flexibility *within* Fcε3 (Wurzburg *et al*, 2000). It is thought that Fcγ2 and Fcγ3 exhibit flexibility about their domain interface, whereas Fcε3 and Fcε4 can move with respect to one another as a

result of structural changes within Fcε3. The Fcε3-4 structure also confirmed the presence of a core of glycosylation in the cavity between opposing Fcε3 domains, as density was recorded in this region, although it could not be determined definitively. The carbohydrate chains are attached at Asn 394 of Fcε3 and mask a hydrophobic patch of ~100 $Å^2$ within this region, however, the density was not clear enough to resolve the separate residues, and therefore it was not included in the published model. The glycosylation site at Asn 394 is homologous to Asn 297 in Fcγ2 of IgG-Fc.

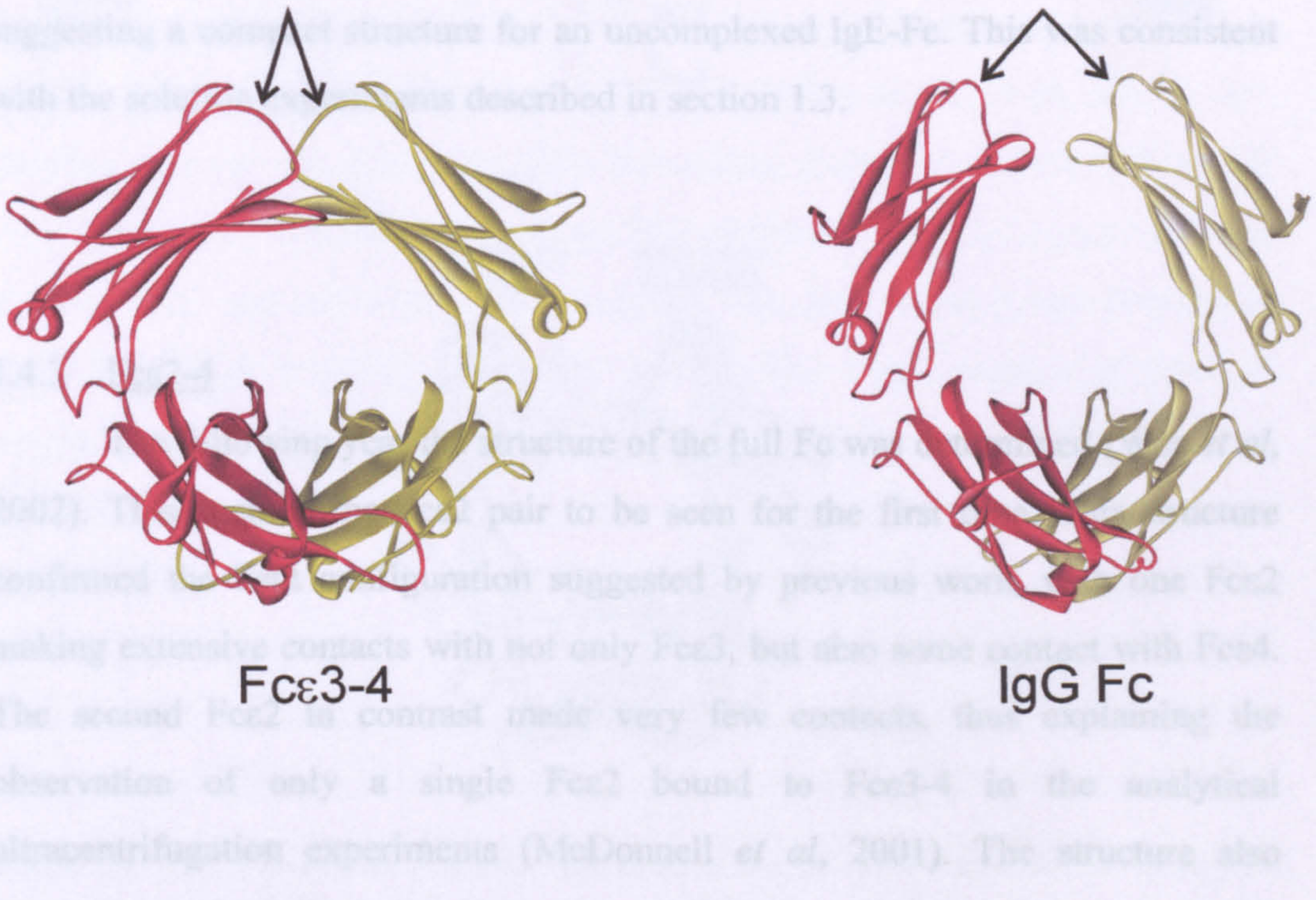

Figure 1.3: Ribbon representation of the IgG Fc (Deisenhofer et al, 1981) and Fcε3-4 (Wurzburg et al, 2000) fragments. Each chain is coloured separately, with the arrows at the N-terminus of each indicating the difference in positioning of the Fcε3 and Fcγ2 domains with respect to one another.

1.4.2 Fcε2

Shortly after the publication of the Fcε3-4 structure, that of the "extra" domain was also described (McDonnell *et al*, 2001). This was for an Fcε2 monomer, with the inter-chain disulphides mutated to serine (to aid refolding

from *E. coli* inclusion bodies). This structure was determined in solution by nuclear magnetic resonance (NMR). The structure, combined with other biophysical analyses, revealed many interesting clues to the nature of IgE's interaction with its receptor; these will be dealt with later in this chapter. Regarding the structure of the Fc, it was observed that the Fcε2 domains do not dimerise in solution, a result that was not predicted by modelling based on the comparisons between IgE and IgG-Fc (Padlan and Davies, 1986; Helm *et al,* 1991). Furthermore, it was also shown by McDonnell *at el* that in the analytical ultracentrifuge a single Fcε2 can bind to the Fcε3-4 fragment with a moderate affinity (~ 2 x 10^5 M^{-1}), which is equal to that of IgG-Fc binding to FcγRIII. This observation implied that at least one Fcε2 domain interacted directly with Fcε3-4, suggesting a compact structure for an uncomplexed IgE-Fc. This was consistent with the solution experiments described in section 1.3.

1.4.3 Fcε2-4

The following year the structure of the full Fc was determined (Wan *et al*, 2002). This enabled the Fcε2 pair to be seen for the first time. This structure confirmed the bent configuration suggested by previous work, with one Fcε2 making extensive contacts with not only Fcε3, but also some contact with Fcε4. The second Fcε2 in contrast made very few contacts, thus explaining the observation of only a single Fcε2 bound to Fcε3-4 in the analytical ultracentrifugation experiments (McDonnell *et al*, 2001). The structure also revealed an Fcε2:Fcε2 interface very different to that predicted by earlier modelling (Padlan and Davies, 1986; Helm *et al,* 1991). A much smaller area of contact was seen compared with other Fcε domain interactions (Fcε4:Fcε4, for example), mediated mostly by hydrogen bonds and electrostatic interactions and stabilised by the two inter chain disulphides (see panel A figure 1.4). This explained the lack of interaction between Fcε2 domains seen in the NMR experiments. Finally, when the packing of the Fcε2 domains against Fcε3 was examined, it was clear that this led to a distortion of the symmetry seen for the Fcε3 domains in the Fcε3-4 fragment. The result of this was that one Fcε3 domain in the Fcε2-4 structure did not assume the compact structure seen for

both Fcε3 domains in Fcε3-4. However, in the other chain Fcε3 did adopt the compact structure (see panel B figure 1.4).

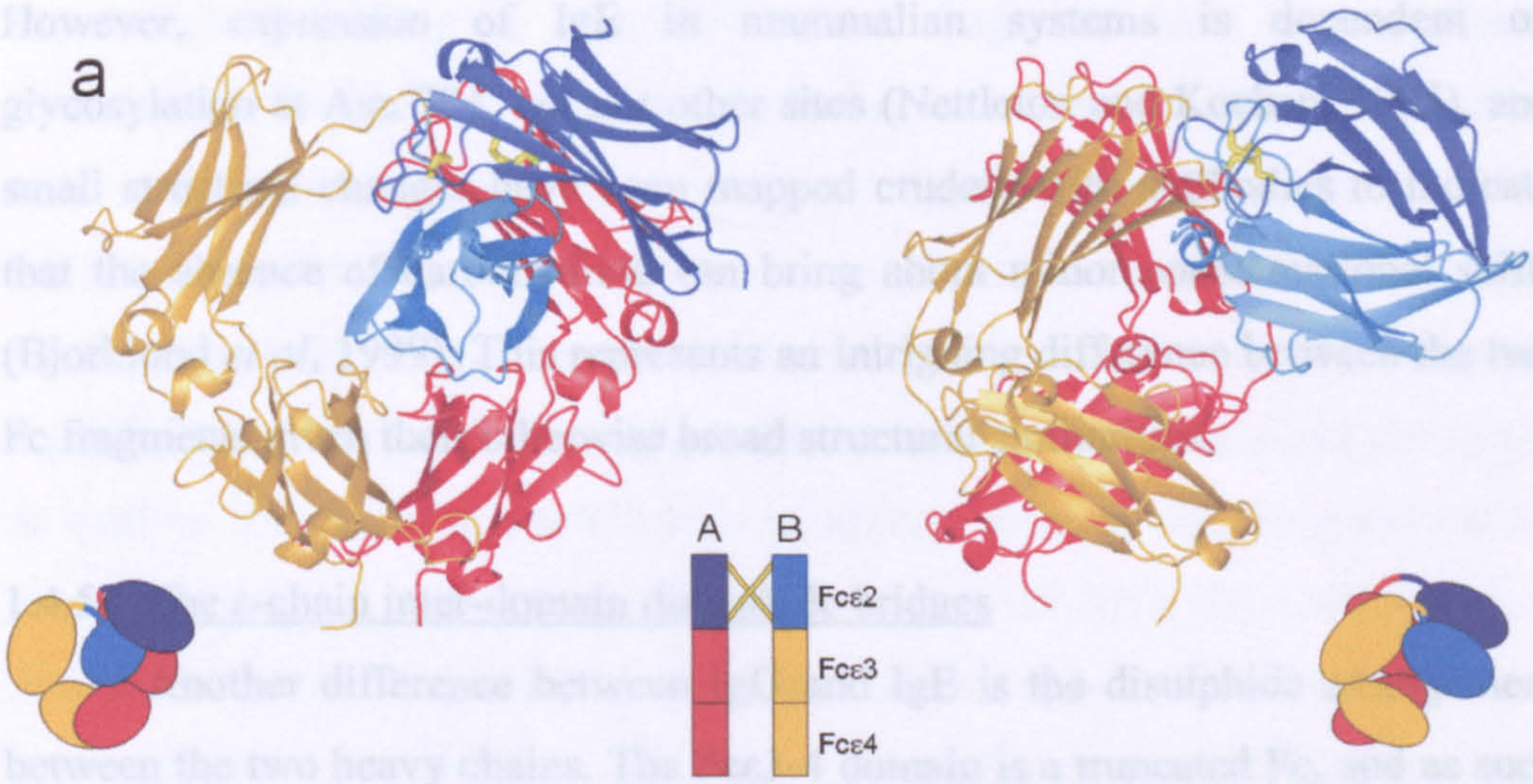

Figure 1.4: Part A represents side and front views of the full IgE-Fc structure in ribbon form with schematics included to indicate positioning of the domains relative to one another, and the position of the inter-chain disulphides. Part B represents the backbone structure of uncomplexed Fcε3-4 compared to the Fcε3-4 domains of the full Fc structure. Adapted from Wan et al, 2002.

1.4.4 IgE glycosylation

All the structures described above showed that the glycosylation of the Fc was of a high mannose type. This represents a key difference compared to IgG, which has a complex-type carbohydrate composition. The affinity of the IgG-Fc for its receptors is highly dependent on glycosylation state (Tao and Morrison, 1989; Mimura *et al*, 2001), which is something that has not been observed for the

IgE Fc. *E. coli* expressed IgE-Fc shows clear receptor binding capability (Geha *et al*, 1985; Helm *et al*, 1988; Vercelli *et al* 1989), as does deglycosylated mammalian expressed material (Basu *et al*, 1993; Bjorklund *et al*, 1999). However, expression of IgE in mammalian systems is dependent on glycosylation at Asn 394, but not other sites (Nettleton and Kochan, 1995), and small structural changes have been mapped crudely with antibodies to indicate that the absence of carbohydrate can bring about minor conformational shifts (Bjorklund *et al*, 1999). This represents an intriguing difference between the two Fc fragments given their otherwise broad structural similarities.

1.4.5 The ε-chain inter-domain disulphide bridges

Another difference between IgG and IgE is the disulphide arrangement between the two heavy chains. The Fcε3-4 domain is a truncated Fc, and as such includes only a single disulphide at the N-terminus (between residues 328 in each chain). However, in the full Fc there are two disulphide bridges between residues 241 and 328, and when the X-ray structure was determined it was found that these formed a "crossed" disulphide pairing. The hinge regions of the IgG subclasses contain parallel disulphide bridges (Kessler *et al*, 1991), although IgG4 is thought to form intra-chain linker disulphides (Aalberse and Schuurman, 2002). The IgE disulphide arrangement would simply represent a curiosity if it were not for the fact that the linker region has been implicated in receptor binding (see section 1.7), and therefore its arrangement could be a critical matter with respect to affinity and receptor recognition. It is already known that changes in the linker region for IgG4 alter effector functions (Dorai *et al*, 1992).

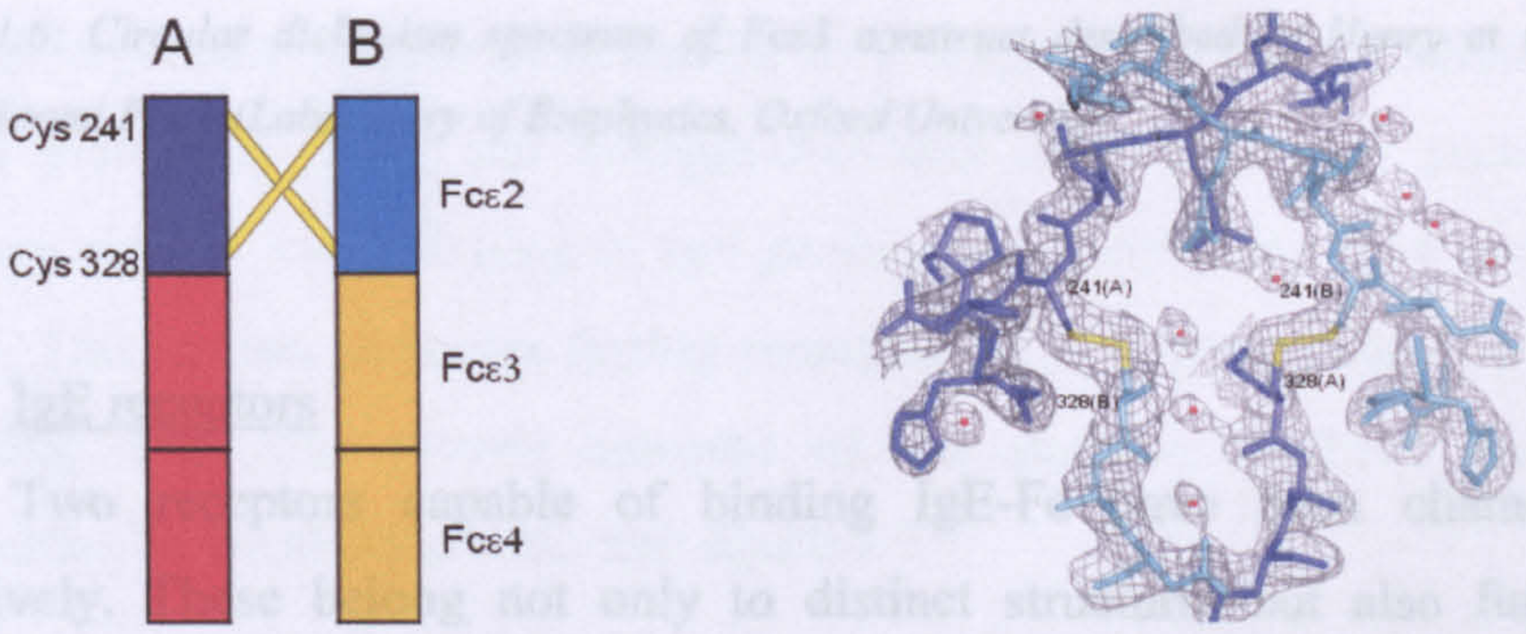

Figure 1.5: Schematic and electron density (with stick representation of residues) to indicate nature of the interdomain disulphides seen in the full Fc structure. Adapted from Wan et al, 2002.

1.4.6 Fcε3

In addition to those fragments for which atomic structures have been determined, a number of other IgE-Fc sub fragments have been produced (reviewed in Vangelista, 2003). In particular, one construct yielded surprising results; this was an *E. coli* expressed single Fcε3 domain (Henry *et al*, 2000). Although this domain was unable to fold as judged by circular dichroism (CD, see figure 1.6; for comparison standard profiles for random coil, beta sheet and alpha helix can be found in section 2.4.1), it nevertheless maintained the ability to bind an IgE receptor (FcεRI) with an affinity close to that observed for the interaction of IgG with analogous receptors (5 x 10^6 M^{-1}). This result will be discussed at greater length in the following chapters.

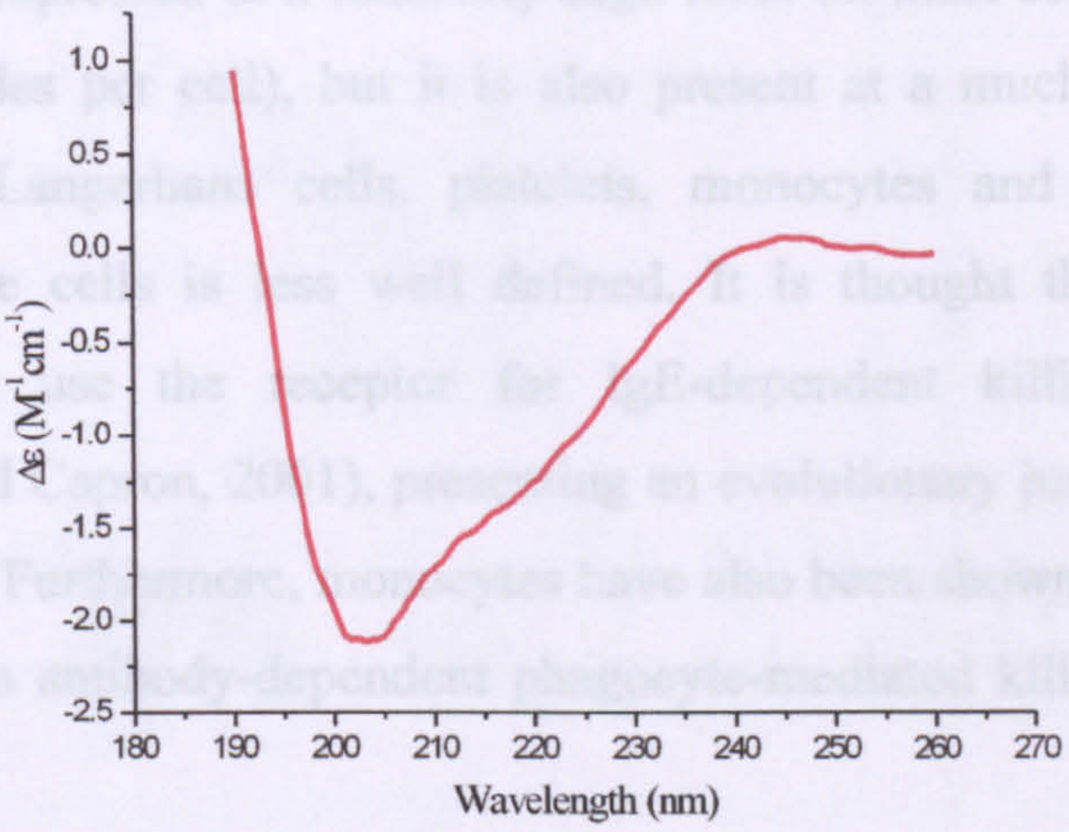

Figure 1.6: Circular dichroism spectrum of Fcε3 construct described by Henry et al, *2000; source Naomi Price (Laboratory of Biophysics, Oxford University).*

1.5 IgE receptors

Two receptors capable of binding IgE-Fc have been characterised extensively. These belong not only to distinct structural but also functional families (Reviewed by Sutton and Gould, 1993; Kinet, 1999; Novak *et al*, 2001; Gould *et al*, 2003). Firstly there is FcεRI, referred to as the "high affinity" IgE

receptor. This binds IgE with an affinity of ~ 10^{10} M^{-1} and is an Immunoglobulin type (Ig-type) receptor. The second receptor is FcεRII, or CD23, which is also referred to as the "low affinity" IgE receptor (K_A ~ 10^7 M^{-1}), and is a C-type lectin.

1.5.1 FcεRI

FcεRI is the receptor present on the surface of mast cells and basophils, and lies at the heart of the allergic reaction observed in the kind of experiment carried out by Prausnitz and Küstner. The cross-linking of FcεRI-bound IgE by multivalent antigen on the surface of these cells leads to the release of pro-inflammatory mediators that are responsible for the symptoms of an immediate hypersensitivity reaction. This reaction has a broad range of outcomes, serious in the case of anaphylactic shock, or relatively mild in the case of hayfever.

FcεRI is expressed at a relatively high level on mast cells and basophils (200,000 molecules per cell), but it is also present at a much lower level on dendritic cells, Langerhans cells, platelets, monocytes and eosinophils. Its function on these cells is less well defined. It is thought that platelets and eosinophils may use the receptor for IgE-dependent killing of parasites (Dombrowicz and Capron, 2001), presenting an evolutionary justification for the existence of IgE. Furthermore, monocytes have also been shown to be capable of harnessing IgE in antibody-dependent phagocyte-mediated killing (Karagiannis *et al*, 2003).

In addition to "killing", data has also been produced to show that FcεRI on the surface of monocytes, dendritic cells and Langerhans cells allows IgE antibody-dependent antigen presentation to T helper cells. T-cells activated by antigen presenting cells, and allergen-activated mast cells, can provide the necessary signals for switching to IgE production (specifically IL-4 and CD40 ligand). This in turn promotes further sensitisation of effector cells and antigen presenting cells. The overall outcome of this positive feedback loop is a perpetuation of the allergic state. See figure 1.7.

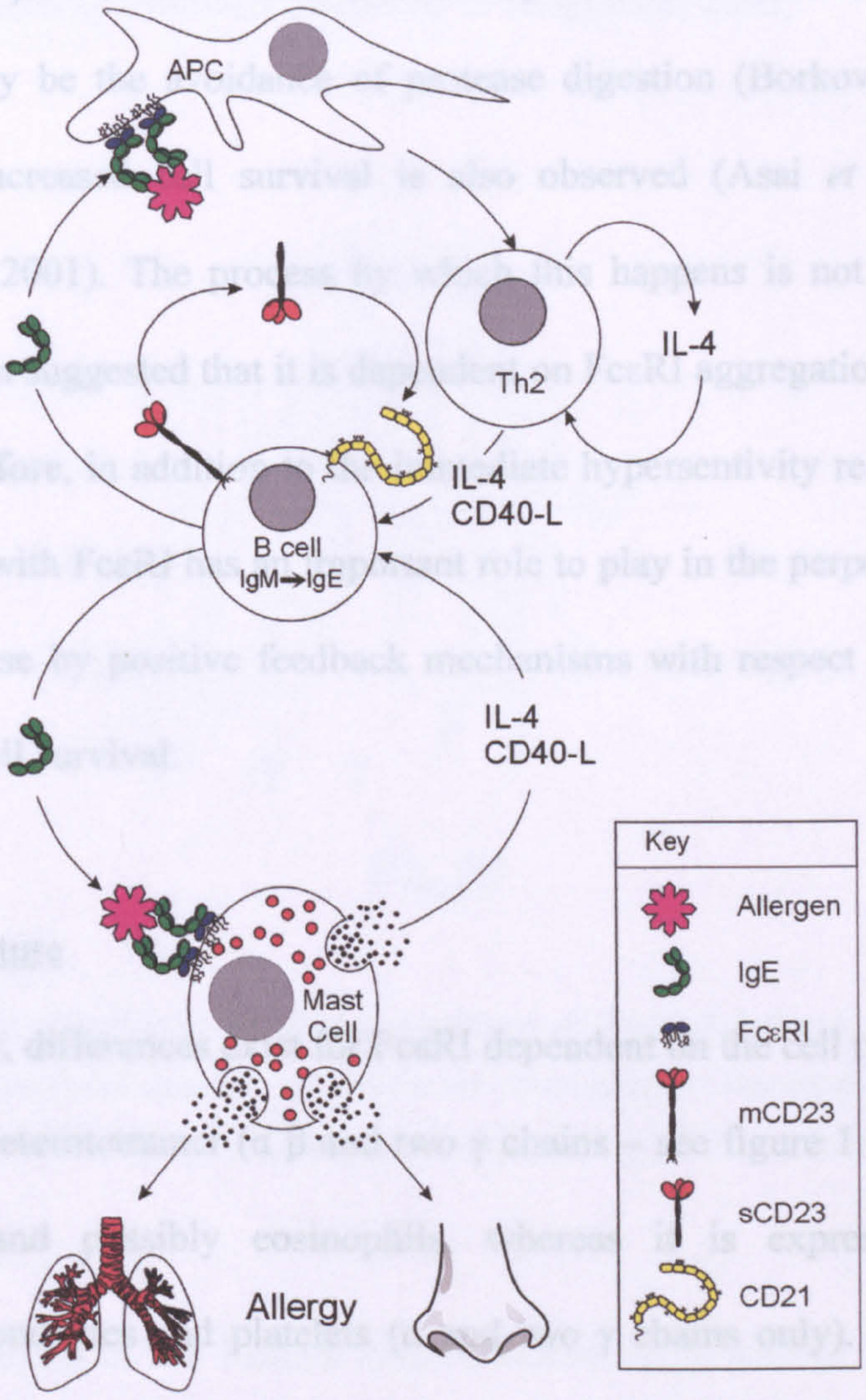

Figure 1.7: The regulation of IgE synthesis (adapted from Gould et al, *2003): Positive feedback occurs as a result of allergen uptake, mediated by FcεRI (and CD23 – see section 1.5.3) on antigen presenting cells, and activation of effector cells such as mast cells and basophils bearing FcεRI. Activated effector cells and T-cells can provide the necessary signals (IL-4 and CD40L) for induction of the switching of B-cells to IgE production. In addition, cross-linking of CD21 and membrane IgE (mIgE) on B-cells by trimeric CD23 can also up-regulate IgE synthesis, whereas cross-linking of CD23 only, or mCD23 and mIgE can down-regulate IgE synthesis (see section 1.4.3).*

Another key feature of the FcεRI:IgE complex is its ability to increase survival of the receptor on mast cells without any other additional signal. One reason for this may be the avoidance of protease digestion (Borkowski *et al*, 2001), however increased cell survival is also observed (Asai *et al*, 2001; Kalesnikoff *et al*, 2001). The process by which this happens is not yet clear, although it has been suggested that it is dependent on FcεRI aggregation (Kitaura *et al*, 2003). Therefore, in addition to the immediate hypersentivity reaction, the interaction of IgE with FcεRI has an important role to play in the perpetuation of the allergic response by positive feedback mechanisms with respect to antigen presentation and cell survival.

1.5.2 FcεRI structure

Structurally, differences exist for FcεRI dependent on the cell type. FcεRI is expressed as a heterotetramer (α β and two γ chains – see figure 1.8) on mast cells, basophils and possibly eosinophils, whereas it is expressed as a heterotrimer in monocytes and platelets (α and two γ chains only). It is the α chain, a type I integral membrane protein, that contains the Fc binding site in its N-terminal extracellular region (Riske *at al*, 1991; Hulett *et al*, 1993, Kochan *et al*, 1994). The β and γ chains in comparison are principally cytoplasmic in their function, acting in cell signalling pathways. Both the β and γ chains contain immunoreceptor tyrosine-based activation motifs (ITAMs) which can be phosphorylated by associated enzymes (normally Lyn) on receptor aggregation. These tyrosine phosphorylated ITAMs then acts as scaffolds for the binding of additional cytoplasmic signalling molecules with Src homology 2 (SH2) domains, such as Syk. Activation of Syk leads to a phosphorylation of a

multitude of signalling mediators and eventually the release of histamine or archidonic acid, or transcriptional activation leading to cytokine production, depending on the pathway followed (reviewed in Siraganian, 2003).

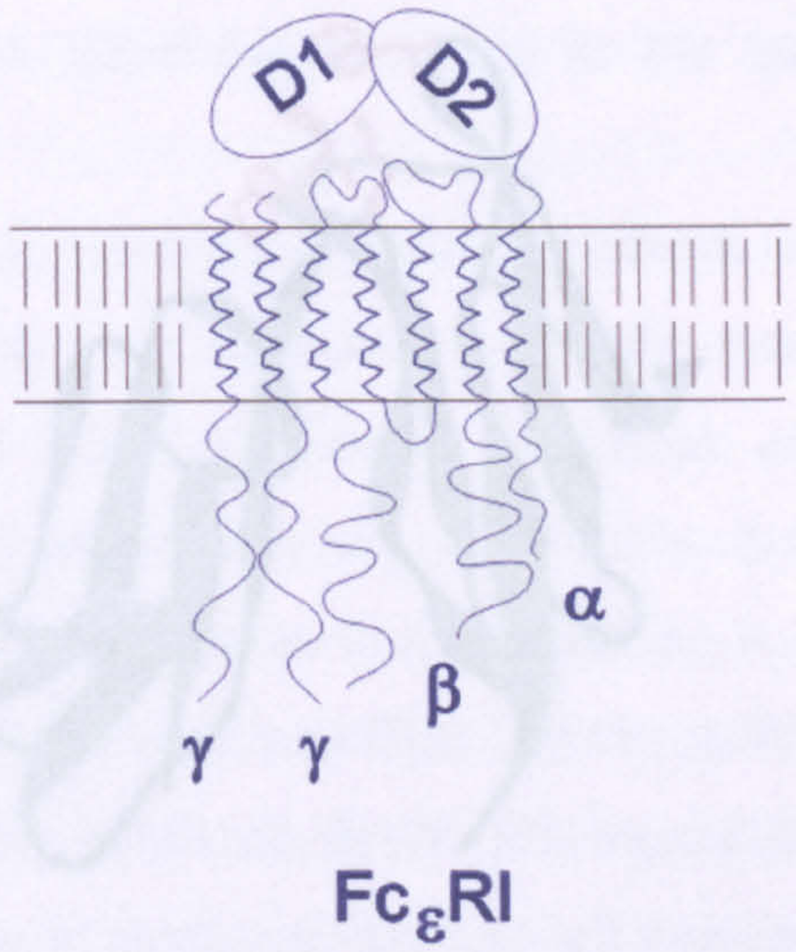

Figure 1.8: Schematic illustrating the domain structure of FcεRI relative to the plasma membrane. The extracellular portion is shown as two ellipses representative of the immunoglobulin like domains (D1 and D2) that form the IgE binding portion of the receptor.

The ectodomain of the FcεRIα chain (referred to as soluble FcεRIα, or sFcεRIα) consists of two Ig-like domains. It is this region that has been most closely examined structurally, as it forms the platform for interaction with IgE, and therefore the bridge between the allergen binding antibody and its effector cell. To date the structures of five different crystal forms of sFcεRIα have been solved (Garman *et al*, 2001). These show the two immunoglobulin domains (D1 and D2) arranged in an almost anti-parallel fashion, placing the N- and C-termini at the same end of the molecule (see figure 1.9). An extensive packing interface is seen between the two molecules, leading to a "wedge" shaped structure. The domain arrangement is apparently crucial, as it is preserved with minor variations not only throughout the differing crystal forms, but also across the domains of related IgG receptors (FcγRIIa, FcγRIIb and FcγRIII). A notable

feature of the sFcεRIα "wedge" is a "ridge" of surface exposed tryptophans at the top of the D1 – D2 interface (shown in red in figure 1.9). This region is also conserved in receptor structures related to FcεRIα, and is thought to represent a common structural motif in antibody recognition.

Figure 1.9: Ribbon representation of the FcεRI soluble alpha chain structure (Garman et al, 1998) with the surface exposed tryptophans of domain D2 important for antibody recognition coloured red (side chains shown).

1.5.3 CD23

CD23 has also been extensively characterised (Reviewed by Sutton and Gould, 1993; Novak *et al*, 2001; Gould *et al*, 2003). CD23 binds IgE with an affinity of ~10^7 M^{-1} and is not a member of the Ig superfamily like FcεRI and the Fcγ receptors, but a type II integral membrane protein composed of a calcium dependent C-type lectin head and an alpha helical stalk. The stalk has the potential to form a coiled-coil with other CD23 monomers to form trimers at the cell surface (Beavil *et al*, 1992). The role of this receptor is distinct from that of FcεRI, and there are two variants that differ in their N-termini by 7 amino acids (termed CD23a and CD23b). These differences alter signalling motifs that modify function. CD23b expression is induced by IL-4 on a broad range of cell types, whereas CD23a is only expressed on B cells. CD23a can facilitate antigen

presentation, and thus for example, CD23 on human B cells mediates IgE-dependent presentation of the Der p II allergen to Der pII specific T cell clones *in vitro* (van der Heijden *et al*, 1993). Furthermore, in human B cells, CD23 has been shown to undergo endocytosis and recycling alongside HLA-DR (Karagiannis *et al*, 2001). This may represent a method of facilitated antigen presentation due to the preferential transfer of allergenic peptides to MHC class II in recycling endosomes, ultimately resulting in the up-regulation of IgE production.

Antigen presentation, resulting in positive feedback and IgE synthesis, is not the only role CD23 has been attributed. A key function appears to be the direct regulation of IgE levels (reviewed in Gould *et al*, 1997). In a straightforward fashion, it can simply act as a buffer for IgE, mopping up unbound antibody. However, it appears that its function is more complex than this, as cross-linking of CD23, or IgE and CD23, on the surface of B cells results in the down-regulation of IgE synthesis. *In vivo* this regulatory potential has been confirmed as CD23 knock-out mice over-express IgE, whereas those engineered to over-express CD23 are deficient in IgE (Lamers and Yu, 1995; Payet and Conrad 1999). Furthermore, not only can CD23 act as a cell surface receptor, it can be cleaved from the cell surface to yield a number of soluble sub-fragments. These fragments show a complex behaviour, with an apparent role to play in the regulation of IgE synthesis. The potential of these fragments is dependent on their size and oligomeric status. The picture is complicated further by the fact that CD23 can also bind another cell surface receptor, CD21. It is known, for example, that surface cleaved CD23 acts as a B-cell growth factor up-regulating the production, but only when it is trimeric. It has been proposed that this is because trimeric CD23 has the potential to cross-link membrane IgE and CD21 on B-cells committed to IgE synthesis, leading to an up regulation of IgE production. On the other hand membrane-bound CD23 can deliver a down regulatory signal for IgE synthesis by B-cells when engaged by an allergen:IgE complex.

1.6 IgE: A therapeutic target

It is clear from the summary above that both FcεRI and CD23 have key roles to play in allergic disease. However, in this thesis, only the interaction of

IgE-Fc with FcεRI will be discussed further. The binding of IgE to FcεRI represents the first common step in the allergic cascade and thus presents a unique point for intervention in allergic disease. An increase in understanding of both the structure of the IgE-Fc, and how this affects binding to FcεRI, is key to progress in this area. In fact, some success in targeting this interaction has already been achieved with the development of an anti-IgE monoclonal antibody (mAb) (reviewed in Hamelmann *et al,* 2002). This mAb is directed to the Fcε3 domain of IgE and appears to reduce allergic symptoms markedly. Although the mode of action is unknown, the qualities of the mAb have been established; it binds serum IgE, blocks FcεRI binding and blocks degranulation of mast cells *in vitro* and *in vivo*, but does not bind to receptor-bound IgE. After treatment there is a drop in serum IgE, and therefore it appears that not only can it interfere with sensitisation, but also prevent some of the positive feedback loops described previously (Sutton *et al*, 2000). Therefore, a precedent has been set for treatment by the blocking of the IgE:FcεRI complex, confirming IgE as a valid target in allergic disease. However, more research is required, as whole antibodies cannot provide a broad range therapeutic due to their cost of production and method of administration (intra-venous). Ideally a smaller molecule is required. To enable the rational design of such a molecule, specific targets are also needed. To establish these targets a detailed knowledge of the components required to form the IgE:FcεRI interface is essential.

1.7 The IgE:FcεRI complex

An enormous amount of data has been collected with respect to the interaction of IgE with FcεRI. Early research concentrated on mapping the binding site with peptides that corresponded to fragments of the whole IgE Fc (Hamburger, 1975; Geha *et al*, 1985; Helm *et al*, 1989; reviewed in Beavil *et al*, 1993). These experiments led to the Fcε3 domains and the linker region between Fcε3 and Fcε2 being proposed as the main area of interaction with FcεRI. The binding of IgE to FcεRI through Fcε3 was further confirmed by domain swapping experiments. Utilising the observation that human IgE cannot bind rodent FcεRI, but human and murine IgE bind equally well to human FcεRI, it was found that replacement of human IgE with the Fcε3 domain of murine IgE

enabled binding to the rodent receptor. In the same study it was also demonstrated that deletion of the Fcε2 domain from this mutated IgE did not impair binding capacity, or its ability to mediate mast cell degranulation (Nissim *et al*, 1991). In a similar experiment, but this time using human Fcγ domains, it was also confirmed that Fcε4 was not essential for receptor binding (Weetal *et al*, 1990). The Fcε3 binding site was mapped to a finer degree by the use of site directed mutagenesis (Henry *et al*, 1997; Presta *et al*, 1994). The result of this was the prediction of an extensive surface area of interaction with FcεRI that covered both Fcε3 domains. This surface could be split into two distinct regions based on the two-fold axis of symmetry. At the same time studies using analytical ultracentrifugation determined the stoichiometry of the interaction, confirming it as 1:1 for both the full IgE-Fc (Keown *et al*, 1995) and Fcε3-4 (Keown *et al*, 1997). This was crucial, as degranulation of mast cells and basophils occurs in response to receptor cross-linking. It is therefore essential that non-antigen bound antibody (i.e. that with a single IgE-Fc region) is unable to cross-link receptor, otherwise allergic reactions could proceed in the absence of allergen.

The equilibrium affinity constant for the complex between Fc and FcεRI is extraordinarily high (10^{10} M^{-1}) (Ravetch and Kinet, 1991). This is especially striking when compared to those for similar IgG interactions with their Fcγ receptors: IgG1 binds FcγRIII with an affinity of around 10^5 M^{-1} (Maenaka *et al*, 2001). These measurements do vary slightly depending on the method of measurement and construct used to obtain them, but the smallest fragment that appeared to maintain close to full affinity for FcεRI was the IgE-Fc sub fragment Fcε3-4. The Fcε3-4 fragment shows an affinity from 2×10^8 M^{-1} (McDonnell *et al* 2001) to 10^{10} M^{-1} (Keown *et al*, 1997), dependent on assay format. Eventually, a crystal structure of the complex between Fcε3-4 and FcεRIα was determined (Garman et al, 2000). This revealed the basis of the 1:1 stochiometry, confirming the large surface area of interaction with both Fcε3 domains, and provided structural evidence for the high affinity between FcεRI and IgE.

As had been predicted, the surface area of interaction of Fcε3-4 with FcεRI could be split broadly into two sites by mapping contacts between Fcε3-4 and FcεRI in the complex crystal structure. These sites cover residues on both

Fcε3 domains and the Fcε2-3 linker. The contact surface is large, 1830 $Å^2$, and covers a range of electrostatic and hydrophobic residues, providing a strong indication as to why the affinity between Fcε3-4 and FcεRI is so high. In total twenty-two residues in the Fc are involved in the binding of FcεRI, of which four residues are common to both interaction sites. This is because Fcε3-4 is a homodimer, and therefore a particular residue in chain A can make a certain contact in site 1, whilst the same residue in chain B makes another in site 2. Due to the fact that contact of each Fcε3 domain with the receptor involves four identical residues (along with additional site specific interactions) an equivalent second receptor-binding site does not exist. Therefore the crystal structure of the Fcε3-4:FcεRI complex was able to explain the 1:1 stoichiometry seen between IgE and FcεRI. However, this was not the only reason why IgE is unable to engage two FcεRI receptors. Alongside the "shared" residues, the engagement of an additional receptor is sterically blocked because FcεRIα binds across the Fc symmetry axis, with the Fcε2-Fcε3 linker also bound asymmetrically.

In the complex, what is commonly referred to as binding site 1 consists of four contiguous segments and 12 residues from chain 1 of the Fcε3-4 homodimer. It is dominated by a set of loops at the top of Fcε3 that form a binding pocket for tyrosine 131 of FcεRI. These loops have been compared to the CDR loops of antibody variable domains and T cell receptors (Wurzburg and Jardetzky, 2002). Binding site 2 is formed from two segments made up of 10 residues from chain 2. This binding site is involved in the interaction with the tryptophan ridge previously described on FcεRI (see section 1.5.2). Two of these tryptophans (W87 and W110 in FcεRIα) form a pocket for proline 426 of the IgE-Fc, also known as a "proline sandwich", whereas the two other tryptophans interact with the Fcε2-3 linker. In fact, 7 of the 15 FcεRI contact residues are aromatic (including the surface exposed tryptophans) and it is thought these residues contribute greatly to the stability of the complex. In the Fcε3-4:FcεRI structure very little of the buried surface area is accounted for by interactions due to glycosylation at Asn 394 (~100 $Å^2$).

Figure 1.10: The crystal structure of the Fcε3-4:FcεRI complex (Garman et al, 2000). Soluble FcεRI alpha chain is shown in green (ribbon format). Fcε3-4 is shown in yellow and red (coloured by chain, ribbon format). Carbohydrate at Asn 394 is also coloured yellow. Proline 426 and interacting FcεRI residues, and tyrosine 131 of FcεRI and interacting residues, are shown space filled on the left and right hand side of the binding site respectively.

1.8 IgE: Conformational change

If the unbound (Wurzburg *et al*, 2000) and bound (Garman *et al*, 2000) forms of the Fcε3-4 are compared, many contact residues are found not to be fully accessible in the unbound state. It has therefore been predicted that a large conformational change is required for the full engagement of FcεRI. It is suggested that this is possible due to flexibility encoded within the Fcε3 domains (Wurzburg *et al*, 2000). The bound conformation of Fcε3 is very similar to that of the "open" chain Fcε3 in the full Fc crystal structure (Wan *et a*l, 2002). However, for full engagement of the full Fc (Fcε2-4) both Fcε3 domains would need to "open". For this to happen with respect to the conformation observed in the Wan *et al* crystal structure, the Fcε2 of the opposite chain would need to be displaced, i.e. a gross conformational change is also required with respect to the positioning of Fcε2. In fact, the determination of the structure of the full Fc (Wan *et al*, 2002), and Fcε2 (McDonnell *et al*, 2001), has led to an extension of the

hypothesis regarding conformational change and the formation of the IgE:FcεRI complex. In NMR experiments, chemical shifts were observed for Fcε2 when a N^{15} labelled Fcε2 domain was titrated into an FcεRI preparation (McDonnell *et al*, 2001). This indicated that not only do the Fcε2 domains show affinity for Fcε3 (as indicated in the analytical ultracentrifuge studies described earlier), but also FcεRI. Thus, it appears that not only does the Fcε2 move away from the opposite Fcε3 domain to allow it to bind FcεRI, but it also engages with FcεRI. Therefore an extension of the molecule must take place from the compact structure seen in the uncomplexed Fcε2-4 crystal structure, to a more elongated form in the complex in which Fcε2 can make contact with FcεRI (see figure 1.11).

Evidence for a specific role for Fcε2 in the interaction between IgE and FcεRI came from surface plasmon resonance data (McDonnell *et al*, 2001). These data show that the off-rate of the full Fc is slower than that of the Fcε3-4. However, the on-rate is also slower, so that the overall K_a remains the same, although the kinetics of interaction are altered. Therefore, while the high affinity constant for the IgE-Fc and FcεRI is mainly a result of the interaction of FcεRI with the Fcε3 domain pair, the kinetics of the interaction are markedly altered by the presence of Fcε2. This is particularly important if the *in vivo* role of IgE is considered. The immediate hypersensitivity reaction requires basophils and mast cells to be continuously primed, ready to be triggered by allergen, with the equilibrium of the IgE:FcεRI interaction *in vivo* such that it strongly favours full receptor residency (Smurthwaite *et al*, 2001). This is quite unlike IgG, which forms complexes in solution that then bind to cells triggering effector mechanisms via cross-linking receptor. Therefore, for IgE, anything that alters the rate at which the receptor ligand complex dissociates is critical. Furthermore, as outlined in section 1.5.1, it is clear that IgE:FcεRI complexes enhance receptor and cell survival. It is not known how the half-life of the complex affects these signals, nor the intensity of the immediate hypersensitivity reaction. Therefore the role of Fcε2 in slowing in the off-rate of IgE could be far more important than the small differences in affinity constants first indicate.

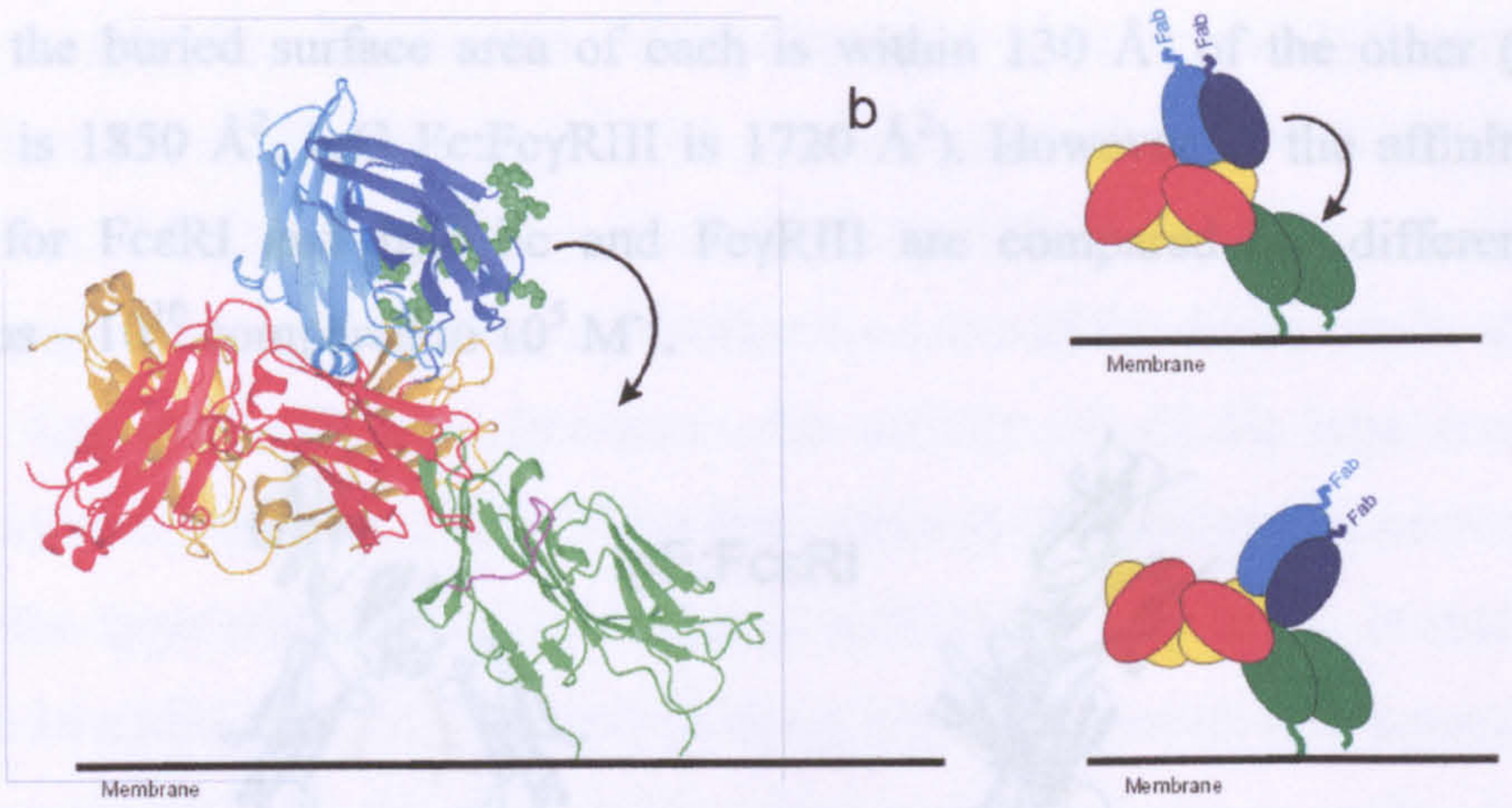

Figure 1.11: Section A shows ribbon outline of the full IgE Fc and soluble FcεRI alpha chain structures oriented on the cell surface. Residues in the Fcε2 domain predicted to interact with FcεRI are shown space filled in green. Section B represents this change in conformation in cartoon format. Adapted from Wan et al, 2002.

1.9 The role of Fcε3-4

Although knowledge of the Fcε2 domain structure suggests a functional role, and therefore novel possibilities for inhibiting the FcεRI:IgE interaction, the Fcε3-4:FcεRI complex still provides the foundation for the extraordinarily high affinity seen between these two molecules. Therefore, further investigation of how the Fcε3-4 sub-fragment maintains the majority of the binding energy for the interaction is key to discovering ways of interrupting the process of receptor binding. The IgG complex with FcγRIII is very similar to that of Fcε3-4 with FcεRI, but with an affinity that is almost five orders of magnitude less than that of IgE. Thus, there must be elements that distinguish the latter complex, and that enable such a large binding affinity to be achieved. A comparison of IgG and IgE receptor binding could therefore yield important clues as to possibilities for lowering the affinity of IgE for FcεRI.

1.10 A comparison of the IgE and IgG receptor complexes

At the time of publication of the Fcε3-4:FcεRI complex structure, a crystal complex between the IgG-Fc and one its receptors, FcγRIII, was also described (Sondermann *et al*, 2000; and subsequently by Radaev *et al*, 2001). If the complexed structures of Fcε3-4 and IgG-Fc are compared, they can be virtually overlaid, with the mode of binding replicated closely between the two.

In fact, the buried surface area of each is within 130 $Å^2$ of the other (Fcε3-4:FcεRI is 1850 $Å^2$, IgG Fc:FcγRIII is 1720 $Å^2$). However, if the affinities of Fcε3-4 for FcεRI and IgG Fc and FcγRIII are compared the difference is enormous – 10^{10} compared to 10^5 M^{-1}.

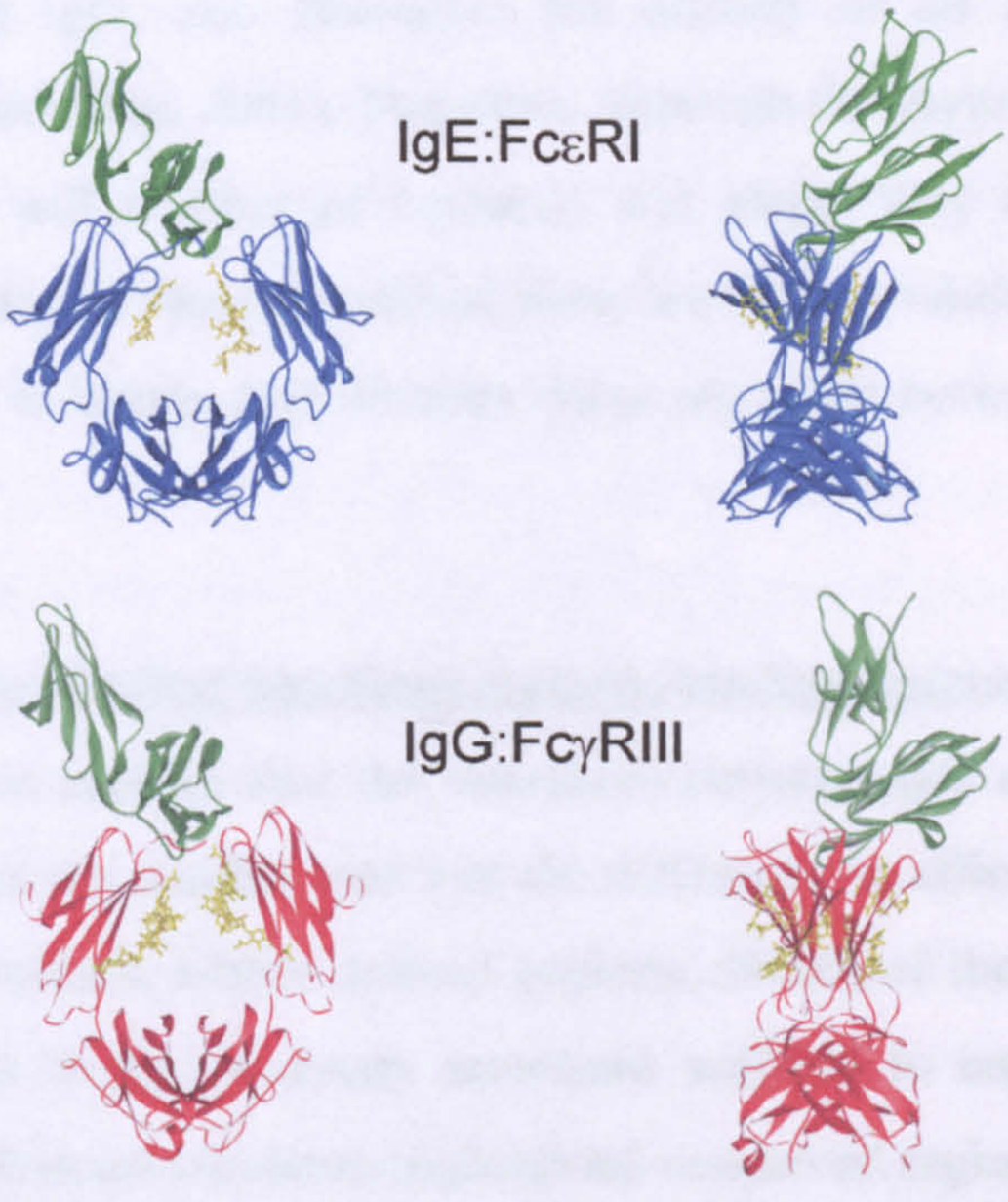

Figure 1.12: Front and side views of both the FcεRI:Fcε3-4 complex (top, Fcε3-4 coloured blue; Garman et al, 2000) and the IgG-Fc:FcγRIII complex (bottom, IgG-Fc coloured red; Sondermann et al, 2000). Carbohydrate for both complexes is shown in yellow, receptors are in green.

A closer examination of the structures revealed some small but significant differences (Radaev and Sun, 2002; Wurzburg and Jadetzsky, 2001). If the two sites described in section 1.7 are compared, it is clear that in site 2 the tryptophan "ridge", although conserved, involves more hydrophobic contacts for IgE than for the IgG-Fc. This is because in addition to the proline sandwich that is formed in both Fc complexes, a further two of the exposed tryptophans of FcεRI make contact with the N-terminal region of Fcε3-4. This region in the full Fc represents the linker between Fcε2 and Fcε3 domains. In fact, linker residues (predominantly classified as site 2) contribute 130 $Å^2$ more buried surface area to the IgG Fc interaction. However, the IgE Fc compensates for the differences by increasing the number of hydrophobic interactions and adding a salt bridge (R334-E132). This could lead to a significant increase in the binding energy

relative to IgG Fc, despite the reduced contact area in the IgE complex. Furthermore, the CDR-like site 1 has a much greater area of contact, with the surface area of Fcε3 domain interactions larger by 360 $Å^2$. It has been suggested that this region, as well as being responsible for some of the difference in affinity between IgE and IgG, also fine-tunes the affinity of all Fc type receptors (Wurzburg and Jardetzky, 2001). Therefore, although the buried surface areas are similar, the type and number of contacts, and where they arise, is markedly different. In addition to those described, there are further subtle differences, such as the number of H-bonds, and whether these are made between main chain or side chain atoms.

1.11 What is the smallest functional receptor-binding fragment of IgE?

It therefore appears that the interfaces between IgG and IgE fragments and their receptors are similar, and that the difference in affinity lies in the type and number of contacts within defined regions. Which of these interactions are crucial, and what is the necessary structural scaffold to enable them to take place? The crystal structures have highlighted conserved regions, and extra areas of contact, but they cannot quantify the relative contributions of individual structural features. This could be achieved by removing certain structural elements in a series of fragments to ascertain which are the most important. It is worth noting again here that an *E. coli* expressed fragment of a monomeric, unglycosylated Fcε3 domain that is unfolded, retains much of the binding capacity seen for a folded, glycosylated Fcε3-4 domain pair, and indeed has the same receptor affinity as IgG Fc has for FcγRIII (Henry *et al*, 2000). Defining the essential structural components required for the full, uniquely high affinity of the native IgE for FcεRI, may thus contribute to the wider aim of designing inhibitors of this interaction.

A great deal of work has been carried out to address this question for IgG (reviewed in Jefferis and Lund, 2002). In fact, despite the striking similarities in binding mode, and buried surface area in the complex structures (see section 1.10), the studies on IgG are notable for highlighting subtle, but possibly crucial differences in comparison to IgE. A key area of focus, and one that would appear to contrast strongly with findings for IgE, is the effect of glycosylation on receptor binding. Current results indicate that the minimal functional fragment of

IgG requires glyscosylation (reviewed in Jefferis and Lund, 2002), but IgE does not (Geha *et al*, 1985; Basu *et al*, 1993). As stated earlier, it has been known for some time that the absence of glycosylation at Asn 297 for IgG prevents receptor recognition, but this is not the case for IgE (see section 1.4.4). In fact, the IgG studies have progressed to a point at which different glycoforms have been analysed for stability and binding (Mimura *et al*, 2001), leading to a definition of the minimal carbohydrate requirement for full receptor binding. The crystal structures of some of these truncated glycoforms have been solved, and arguments put forward as to why differences in binding are seen (Krapp *et al*, 2003). To summarise, it is thought that a closing of the Fcγ2 domains occurs when carbohydrate is removed completely, thus preventing receptor engagement, and that disorder in the hinge proximal loops occurs for truncated glycoforms (in the C'-E loop). These loops are important for receptor recognition. What is interesting is that homologous loops in IgE are also involved in FcεRI binding (it is one of the CDR-like structures, the D-E loop). Furthermore, the closing of the "gap" between the Fcε3 domains of the IgE-Fc appears to happen even when glycosylated; a "closed" conformation is seen for one Fcε3 in the IgE-Fc crystal structure (Wan *et al*, 2002) and for both Fcε3 domains in the structure of the uncomplexed Fcε3-4 fragment (Wurzburg *et al*, 2000). This represents an interesting contradiction. Why, when Fcε3-4 is glycosylated does it adopt a closed conformation, and how is it that when it is closed, it can bind receptor with such high affinity in comparison to IgG, which in this state cannot bind receptor at all? An explanation for this may lie in the differences in flexibility and stability of the Fcε3 and Fcγ2 domains respectively, enabling Fcε3 to adjust its shape more easily. Structural differences have already been highlighted (Wurzburg *et al*, 2000, see section 1.4.1), with the suggestion that the flexibility of the Fcε3-4 fragment is due to an additional rotation from within the Fcε3 domain. In contrast, the IgG-Fc only appears to flex around inter domain regions. It is also known from differential scanning calorimetry experiments that the melting temperatures of these domains differ by 19 °C (Keown, PhD thesis, 1997 – 52 °C for Fcε3, 1997; Mimura *et al*, 2000 – 71 °C for Fcγ2), indicating that Fcε3 is less stable, and therefore perhaps a more flexible domain.

Another difference between IgE and IgG concerns the requirement for a dimer of the Fcγ2 or Fcε3 domains for receptor binding. It has been claimed that

the minimal domain requirement for Fcγ receptor recognition is a native Fcγ2 domain pair (Lund *et al*, 2000) whereas a monomeric unfolded Fcε3 domain retains affinity for FcεRI (Henry *et al*, 2000). However, neither of these fragments showed native affinity. The Fcγ2 pair functioned 30% less efficiently than full IgG in superoxide assays, and the monomeric Fcε3 domain bound FcεRI with an affinity ~200 fold lower than that of a mammalian expressed Fcε3-4 fragment. It was suggested that the difference in binding observed for the Fcγ2 pair compared to the full IgG-Fc was due to the absence of the Fcγ3 domains, which although they do not make receptor contact, may be required for the correct orientation of the Fcγ2 domain pair for receptor engagement. In the case of Fcε3, it is still not clear what components are necessary to yield full affinity for FcεRI. For example, it is possible that a single fully folded Fcε3 domain could show higher, perhaps close to native affinity levels for FcεRI. However, if two domains are required, as is strongly indicated by the crystal structure of the sFcεRIα:Fcε3-4 complex, the correct orientation of the Fcε3 domains could also be important for engagement of FcεRI. In IgE-Fc the Fcε4 domains contact extensively with Fcε3 in the same polypeptide chain, and the Fcε4 pair also forms the dimer interface between the two homologous chains of the IgE-Fc. It may be that the Fcε4 domains play a similar role to Fcγ3 in presenting the receptor binding domains. It is also possible that the extremely high affinity of the Fcε3 domain for FcεRI is the sole determinant of the interaction, and that two Fcε3 domains are sufficient for high affinity binding.

In the paper of Lund *et al* it was also shown that removing the covalent linkage in the hinge region of the IgG-Fc led to a 100-fold drop in effective competition with wild type IgG in cell binding assays. This led to the conclusion that linkage of the receptor binding domains is also critical for high affinity binding. This reveals yet another intriguing contrast with IgE, as disulphide linkage in the equivalent fragment of IgE (Fcε3-4) has been suggested to be not as important for receptor recognition (Basu *et al*, 1993). This is despite the linker region representing a critical binding motif (Garman *et al*, 2000), and the fact that it tethers the relatively unstable and flexible Fcε3 domains that constitute the two halves of the binding site.

The nature and importance of the inter-domain contacts of IgE needs to be assessed further if the structural scaffold necessary for full engagement of

FcεRI is to be understood. The comparisons and apparent contrasts with IgG provide an important insight into the factors contribute to the uniquely high affinity of IgE for FcεRI, and also highlight possible areas for further investigation in the attempt to determine the smallest fully functional receptor binding fragment of IgE.

1.12 The aims of this thesis

Prior to undertaking the studies described in this thesis, the smallest fully characterised high affinity fragment of IgE was a mammalian expressed dimer of domains Fcε3 and Fcε4 (affinity ~$10^9 M^{-1}$). In addition, an isolated Fcε3 fragment had also been produced in *E. coli*. This fragment possessed an affinity of ~$10^7 M^{-1}$ for its receptor FcεRI, and was unfolded as judged by circular dichroism and fluorescence spectroscopy. This represented a remarkable affinity for an unstructured peptide and highlighted two questions regarding IgE-Fc and its interaction with FcεRI:

a) What determines the correct folding of the Fcε3 domain in the IgE molecule?

b) What are the minimal structural requirements for a fully active Fcε3 domain?

These two questions formed the basis for the studies described in this thesis. In the course of the work, the effect of three different structural features on the folding and binding affinity of Fcε3 were examined:

i) presence of adjacent Fcε4 domains

ii) dimerisation and disulphide linkage of Fcε3

iii) glycosylation of Fcε3 at Asn 394.

The contribution that each of these features made to the structuring of Fcε3 and binding to FcεRI was assessed by circular dichroism spectroscopy, analytical ultracentrifugation and surface plasmon resonance. This has revealed new insights into the basis of IgE antibody domain folding and the formation of the FcεRI:IgE complex.

Materials and Methods

Chapter 2: Materials and Methods

2.1 Materials and stock solutions

All chemicals were obtained from Sigma unless otherwise stated.

Acrylamide: A 30% (w/v) acrylamide / 0.8% (w/v) NN'-methylenebis-acrylamide stock was used, purchased from Severn Biotech Ltd.

APS: Ammonium persulphate was prepared as a 10% (w/v) solution in deionised water.

Coomassie blue stain: 0.05% Coomassie brilliant blue R was dissolved in methanol, distilled water and acetic acid mixed at a 5:5:1 ratio.

Coomassie destain: 5% methanol 7.5% acetic acid in deionised water.

DNA loading buffer (x6): 0.25% bromophenol blue, 0.25% xylene cyanol, 30% glycerol in deionised water.

DNA molecular weight markers: λ DNA (New England Biolabs) was digested using HindIII and stored at 200 ng/µl in 20 mM EDTA at 4°C.

DTT: Dithiothreitol was prepared as a 1 M stock in deionised water and stored at -20°C.

EDTA: Disodiumethylenediaminetetra-acetate was dissolved in deionised water to a final concentration of 0.5 M at pH 8 (adjusted using NaOH).

Ethidium bromide: 10 mg/ml pre-prepared aqueous solution.

Extraction solution A: (72 ml) 10 mM Tris-HCl pH 7.9, 25% sucrose, 100 mM KCl, 2.0 mM DTT, 2.0 mM PMSF.

Extraction solution B: (18 ml) 300 mM Tris-HCl pH 7.9, 100 mM EDTA, 4 mg/ml lysozyme.

Extraction solution C: (90 ml) 1.0 M LiCl, 20 mM EDTA, 0.5% Igepal.

Extraction solution D: (200 ml) 10 mM Tris-HCl pH 7.9, 0.1 mM EDTA, 0.5M LiCl, 0.5% Igepal, 1.0 mM DTT, 1.0 mM PMSF.

Extraction solution E: (200 ml) 10 mM Tris-HCl pH 7.9, 0.1 mM EDTA, 0.5% Igepal, 1.0 mM DTT, 1.0 mM PMSF.

dFCS: Dialysed foetal calf serum, supplier Gibco.

Gel filtration run buffer: Standard buffer used in HPLC (both preparative and analytical). 0.5 M Tris-HCl pH 7.2, 250 mM NaCl 0.05% NaN_3; degassed and 0.2μm filtered.

HBS: Hepes buffer saline used for surface plasmon resonance experiments. 10 mM HEPES pH 7.4, 150 mM NaCl, 3.4 mM EDTA, 0.005% anionic surfactant p20. Sterile filtered and degassed.

IPTG: Isopropyl-beta-D-thiogalactopyranoside, made up as a 1M stock in deionised water, sterile filtered and stored at –20°C.

Luria-Bertani broth: (1l) 10g Bactotryptone, 5g yeast extract, 10g NaCl pH 7.5 (with NaOH), autoclaved to sterilise.

M9 salts: (10x, 1l) 10g NH_4Cl, 30g KH_2PO_4, 60g $Na_2HPO_4.7H_2O$, 50g NaCl in deionised water pH adjusted to 7.5 (NaOH), autoclaved to sterilise.

M9 medium: (1l) 100 ml M9 salts, casamino acids (Difco) 0.5% (w/v), 0.1 mM $CaCl_2$, 1.0 mM $MgSO_4$, 1.0 μg/ml Vitamin B_1, glucose 15% (w/v) all sterile filtered, adjusted to 1l with autoclaved deionised water.

NS0 selective medium: Iscove's medium without glutamine supplemented with glutamate (6 mg) and asparagine (6 mg); nucleosides (0.7 mg each of adenine, guanosine, cytidine uridine, and 0.24 mg thymidine); non-essential amino acids (Gibco 100 x stock); 50 ml dFCS; 100 units/ml penicillin and 100 µg/ml streptomycin. Filter sterilised.

PBS: Phosphate buffered saline, 0.14 M NaCl, 2.7 mM KCl, 1.5 mM KH_2PO_4, 8.0 mM Na_2HPO_4 pH 7.4 in deionised water.

PBS-T: As above except with the addition of 0.05% Tween 20.

PMSF: Phenylmethylsulphonyl fluoride was prepared as a 100 mM stock in isopropanol and stored at 4°C.

Protein molecular weight standards: For SDS-PAGE Invitrogen Mark 12 (200 kDa-2.5 kDa) were used (15 µl/lane), for gel filtration chromatography Sigma molecular weight standards were used at 1mg/ ml.

SDS loading buffer: (4x) 125 mM Tris pH 6.8, 2% SDS, 10% glycerol, 0.005% bromophenol blue and, for reducing gels, 1 mM DTT or 1% β-mercaptoethanol.

SDS running buffer: (10x) 30.3g Tris, 144.1g glycine, 10g lauryl sulphate made to 1l with deionised water.

SOC: 2g bactotryptone, 0.55g yeast extract, 10 mM NaCl, 10 mM KCl in deionised water (97 ml). 10 mM $MgSO_4$, 10 mM $MgCl_2$ and 20 mM glucose added and filter sterilised.

TAE: (10x) 48.4g Tris, 11.4 ml glacial acetic acid, 20 ml 0.5M EDTA made to 1l with deionised water.

TBS: Tris buffered saline, 20 mM Tris-HCl pH 8.6, 100 mM NaCl.

TE: 10 mM Tris-HCl pH 8.0, 1 mM EDTA

TEMED: NNN'N'-tetramethylethylenediamine

Tris-acetate: 2.0 M Tris-base was adjusted to pH 8.6 with glacial acetic acid for use in protein refolding protocols.

Western blot: Cathode buffer: 25 mM Tris-Cl pH 9.4, 40 mM ε-aminocaproic acid, 20% methanol. Anode buffer: 0.3 M Tris-Cl pH 10.4, 20% methanol.

2.2 DNA methods

All sequences coding for the cDNA of either FcεRIα or IgE-Fc had already been cloned into expression vectors (see tables 2.1 and 2.2). Subsequently the only manipulation of these vectors that took place was the introduction of point mutations.

2.2.1 Site directed mutagenesis

Site directed mutagenesis was carried out using the Quikchange system (Stratagene). The procedure is outlined in figure 2.1.

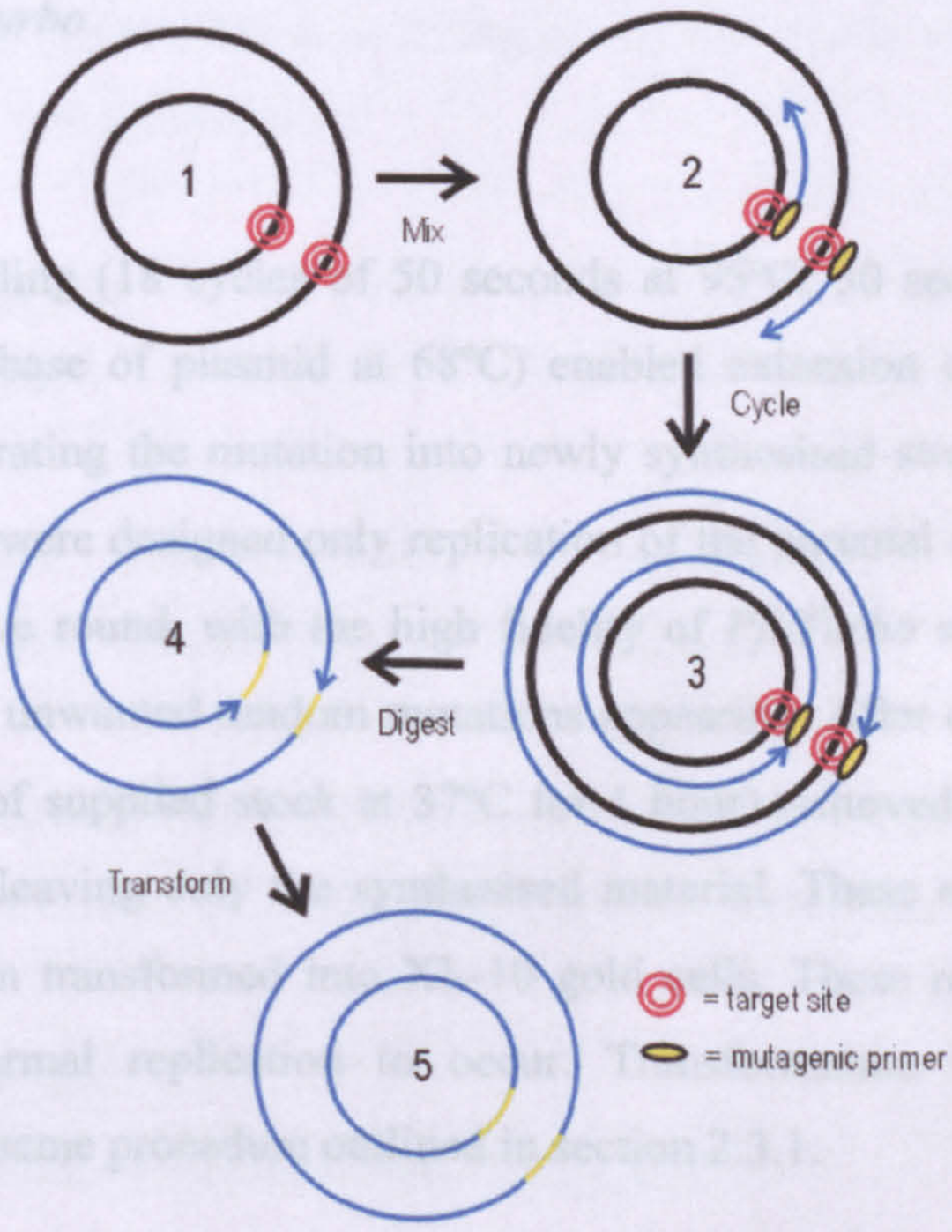

(see previous page)

Figure 2.1: Model for Stratagene Quikchange mutagenesis. 1: Gene is targeted within a plasmid. 2: After denaturation plasmid is annealed with primers coding for a specific mutation. 3: Thermal cycling is carried out to extend and incorporate mutation primers resulting in nicked circular strands. 4: The parental DNA template is digested. 5: The resulting double stranded nicked plasmids containing the mutation are transformed into competent cells. 6: The XL-10 strain repairs nicks in the plasmid.

A mix was prepared according to the manufacturer's instructions using reagents supplied with the kit:

5 µl reaction buffer
10 ng template plasmid DNA
125 ng Primer 1
125 ng Primer 2
1 µl dNTP mix
3 µl Quicksolution
autoclaved deionised water to 50 µl
added last
1 µl *PfuTurbo*

Temperature cycling (18 cycles of 50 seconds at 95°C; 50 seconds at 60°C; 2 minutes per kilobase of plasmid at 68°C) enabled extension of the mutagenic primers, incorporating the mutation into newly synthesised strands. Because of the way primers were designed only replication of the parental strand took place in each successive round, with the high fidelity of *PfuTurbo* severely reducing the likelihood of unwanted random mutations appearing. After cycling treatment with *DpnI* (1µl of supplied stock at 37°C for 1 hour) removed *dam*-methylated parental strands leaving only the synthesised material. These nicked mutagenic strands were then transformed into XL-10 gold cells. These repaired the nicks and allowed normal replication to occur. Transformation was carried out according to the same procedure outlined in section 2.3.1.

2.2.2 Plasmid purification

Single colonies were picked and cultured in LB broth supplemented with ampicillin (50 μg/ml) overnight at 37°C. Plasmid DNA was prepared using QIAGEN plasmid purification kits; mini- midi- or maxi- depending on the required amount of DNA, with culture volume adjusted accordingly.

2.2.3 DNA electrophoresis

A solution of 0.5-1.5% agarose (dependent on the size of fragment to be identified) was prepared in TAE buffer, melted and cooled, then set in a gel tray with a plastic comb. Once set the gel was placed into electrophoresis apparatus and covered with TAE buffer supplemented with ethidium bromide (1-5μl stock solution). Samples (5μl) diluted in DNA loading buffer were separated alongside appropriate markers by applying 50 volts across the gel until different sized fragments could be resolved; as judged by viewing the incorporation of ethidium bromide into the DNA under UV illumination.

2.2.4 DNA sequencing

DNA sequencing was carried out by the in-house molecular biology unit using the fluorescent DNA dideoxy termination method. Sequencing primer was used at 3.2ρmol/μl and plasmid DNA at 250ng/μl and the results viewed using ABI prism technology (PE biosystems)

2.2.5 Primers for PCR

All for pET vectors:

Sequencing:

T7 promoter: GTAATACGACTCACTATAGGGC

T7 terminator: TATGCTAGTTATTGCTCAG

Mutagenesis:

F506R (Forward): CCGGCTTCTTCGTCCGCAGCCGCCTGGAGG

F506R (Reverse): CCTCCAGGCGGCTGGCGACGAAGAAGCCGG

2.3 Protein methods

2.3.1 Expression of recombinant protein in *E. Coli*

Fragments of the IgE-Fc ε chain were expressed as inclusion bodies in the *E. coli* strain BL21* (DE3) (Invitrogen) using either the pET 5a or pET 15 vector (Invitrogen). The table below details the name, vector and fragment residue range:

Name	ε residues*	Vector
Fcε4	438-547 (plus His tag)	pET 15
Fcε4 F506R (F506R mutation)	438-547 (plus His tag)	pET 15
Fcε3-4ΔC (C328S mutation)	328-547	pET 5a
Fcε3-4ΔC F506R (C328S F506R mutations)	328-547	pET 5a

*Table 2.1: Constructs used for expression of IgE-Fc subfragments. * Numbered according to Dorrington and Bennich (1978).*

For each fragment preparation competent *E. coli* were transformed with 500ρg of plasmid DNA using a heat shock method:

Aliquots of the competent cell line were defrosted from storage at –70°C on ice, plasmid was added to the cell suspension and left on ice for a further 30 minutes. Cells were then heat shocked (42°C) in a heating block for 1 minute and the left to recover for 60 minutes in 300µl of SOC in a 37°C shaking incubator set to 200 rpm. The cell suspension was then plated out on LB agar supplemented with ampicillin to 50µg/ ml and left overnight in a 37°C oven. Transformed *E. coli* grew up as single colonies due to ampicillin resistance encoded within the transformed plasmid DNA.

The following day a single colony was picked and used to inoculate 1 ml of M9 medium supplemented with ampicillin (50µg/ ml); this was grown again at 37°C in a shaking incubator. After 10 hours the culture was expanded into a larger (500 ml) flask containing Amp^+ M9 medium and left overnight under identical conditions. The following day the culture was expanded again, using the overnight culture (2% of the final volume) to inoculate a larger flask of Amp^+ M9 medium. This culture was grown until mid log density ($OD_{600nm} \sim 0.6$) then

induced with 0.4 mM IPTG. Cells were harvested after 5 hours at 6,000*g* in a GSA rotor (Sorvall) at 4°C for 10 minutes and pellets stored at –70°C.

2.3.2 Purification of recombinant protein from *E. Coli*

All protein expressed in *E. coli* formed inclusion bodies. Isolation was carried out using a procedure adapted from Bohmann and Tjian (1989). All solutions were kept on ice throughout the procedure and all centrifuge runs were carried out at 4°C.

The cell pellet was resuspended in extraction solution A and incubated for 10 minutes with extraction solution B. Extraction solution C was then applied to the mix and sonication was carried out in pulses for 5 minutes (MSE soniprep) and the inclusion body protein pelleted by centrifugation at 16,000*g* for 10 minutes. The pellet was then washed by resuspending in extraction solution D, followed by sonicating in pulses for a further 5 minutes and pelleting by centrifugation. This procedure was repeated with extraction solution E and the pellet stored at –70°C.

The pellet obtained from the extraction procedure was thawed on ice and solubilised in 4 ml of 6 M guanidine hydrochloride, 20% sucrose, 1 mM DTT by sonicating in pulses for 5 minutes. The protein solution was then centrifuged at 12,000*g* for 15 minutes and the supernatant removed. This supernatant was passed over a Sephacryl S300 column (C30 x 100 – Pharmacia) equilibrated with 6 M guanidine hydrochloride at 0.5 ml/min (room temperature) to remove contaminating nucleic acids. Elution peaks were monitored by absorbance at 280 nm. Fractions were then selected and analysed by SDS-PAGE with those corresponding to the molecular weight of the desired protein pooled for refolding.

2.3.3 Refolding of purified recombinant protein from *E. Coli*

Refolding of solubilised inclusion body material was carried out by a mixed disulphide rapid dilution method adapted from Taylor *et al* (1992). Extracted protein (2 ml at 10 mg/ ml in 6 M GuHCl) was pH adjusted with Tris-acetate (final concentration 200 mM) and reduced by addition of DTT (final

concentration 1 mM) at 37°C for 1 hour. Mixed disulphide bonds were formed overnight by diluting the protein to 1 mg/ml in 6 M GuHCl, 100 mM Tris-acetate, pH8.6, containing 0.1 M oxidised glutathione. The following day denaturant (GuHCl) was removed and native disulphides formed by rapid dilution to 10 μg/ml in 100 mM Tris-acetate, 3 mM L-cysteine, pH 8.6. After removal of the denaturant, protein was concentrated to 5 mg/ml. This protein was then purified by gel filtration in 0.5 M Tris-HCl, 0.25 M NaCl, pH 7.4, on a Superdex HR-75 1 x 30 cm gel filtration column. Fractions containing monomeric protein units were identified by non-reducing SDS-PAGE. In the case of Fcε3-4ΔC this protein was also assessed for integrity by nanospray mass spectrometry carried out by the proteomics facility at the Institute of Psychiatry (University of London).

2.3.4 Expression of recombinant protein in mammalian cells

All mammalian expressed proteins were from stable NS0 cell lines established using the glutamine synthetase expression system (Bebbington *et al* 1992). The $(sFc\varepsilon RI\alpha)_2IgG_4$-Fc chimera is a fusion of an IgG4-Fc with two sFcεRIα subunits replacing the Fabs. See table 2.2.

Name	Residues	Reference
Fcε3-4	328-547	Shi *et al* (1997)
sFcεRIα	1-176	Cook *et al* (1997)
$(sFc\varepsilon RI\alpha)_2IgG_4$-Fc	α = 1-176·IgG-Fc = 235-446	Shi *et al* (1997)

Table 2.2: Constructs used for NS0 expression of IgE-Fc and FcεRI subfragments.

Cells were grown in NS0 selective medium at a cell count of 5 x 10^5/ml in roller bottles maintained at 37°C. Every other day cells were gassed with sterile 5% CO_2 in air for one minute and growth was maintained for up to 2 weeks, cell counts were carried out regularly by haemocytometer using 2% v/v trypan blue. Supernatant was then harvested by centrifugation at 6,000*g* to remove cell debris, 0.2μm filtered and stored at 4°C after supplementation with sodium azide to a final concentration of 0.05% to inhibit bacterial growth.

2.3.5 Purification of recombinant protein from mammalian cells

Supernatants from mammalian cell culture were purified in a two-step procedure. Firstly, affinity chromatography was used to isolate the desired species; table 2.3 details the specific capture agents for each protein:

Protein	Capture	Source
Fcε3-4	$(sFc\varepsilon RI\alpha)_2IgG_4$-Fc	Shi *et al* (1997)
sFcεRIα	3B4 monoclonal antibody	Prof. P. M. Hogarth (Austin Research institute – Victoria, Australia)
$(sFc\varepsilon RI\alpha)_2IgG_4$-Fc	Protein G	Amersham
Fcε3-4(4)	Ni^+ matrix	Qiagen

Table 2.3: Ligands for affinity purification of IgE-Fc and FcεRI sub-fragments.

Monoclonal 3B4 and $(sFc\varepsilon RI\alpha)_2IgG_4$-Fc affinity matrices were prepared by amine coupling ~50mg of capture agent to ~12.5ml of either a affi-gel or affi-prep 10 support (Biorad) and then packing into a glass column. Identical purification procedures were used for Fcε3-4, sFcεRIα and $(sFc\varepsilon RI\alpha)_2IgG_4$-Fc. Each column was loaded with supernatant by cycling pH adjusted material (pH 8.6 using 10 x TBS) overnight at 0.5 ml/min followed by thorough washing of the column (10 column volumes) with TBS. Captured ligand was then eluted using 0.2 M glycine pH 2.5 and immediately neutralised by addition of 1 M Tris pH 8 (to a final concentration of 100 mM). The column was re-equilibrated by cycling with TBS (10 column volumes). Fcε3-4(4) was purified under slightly different conditions; the run buffer was changed to 50mM Sodium Phosphate, 50mM Imidazole, 500mM Sodium Chloride pH 7.4, with elution carried by increasing the Imidazole concentration to 0.5M. Eluted materials were concentrated using a Amicon (Millipore) stirred cell (fitted with the appropriate molecular weight cut-off membrane) and purified on a Gilson HPLC with either a Superdex HR-75 (Fcε3-4 and sFcεRIα) or a Superdex HR-S200 ($(sFc\varepsilon RI\alpha)_2IgG_4$-Fc) gel filtration column (Pharmacia). Relevant fractions were identified by SDS-PAGE.

2.3.6 Deglycosylation of mammalian expressed protein

Native NS0-derived proteins were deglycosylated using PNGaseF (New England Biolabs) – 1 µl of enzyme preparation per 20µl (~1mg/ml) of protein sample buffered with supplied concentrate. Samples were incubated overnight at 37°C in sealed tubes and HPLC purified using either a S75-HR or S200-HR gel filtration column. Samples were assessed for carbohydrate removal by SDS-PAGE followed by either protein (Coomassie) or glyco (Schiff base) staining (see section 2.3.7). Finally, Fcε3-4 samples were also analysed for residual carbohydrate by denaturing PNGaseF digestion followed by mass spectrometry (R. Boehm, Glycobiology Unit, Department of Biochemistry, Oxford University).

2.3.7 SDS-PAGE

Sodium dodecyl sulphate polyacrylamide gel electrophoresis was used to characterise proteins based on their size. The method applied was based on that of Laemmli (1970) and was carried out using Atta protein gel eletrophoresis apparatus. Protein gels were prepared from stock solutions, see table 2.4:

Percentage acrylamide	Acrylamide	2 M Tris pH 8.8	10% SDS	APS	Temed
12.5 %	10 ml	4.7 ml	0.25 ml	0.16 ml	20 µl
15 %	12.5 ml	4.7 ml	0.25 ml	0.16 ml	20 µl
20 %	16.7 ml	4.7 ml	0.25 ml	0.16 ml	20 µl
Stack	1 ml	1.25 ml (Tris pH 6.8)	0.1 ml	0.064 ml	15 µl

Table 2.4: Polyacrylamide gel composition from stock (all made up to 25 ml with deionised water, except stack 10 ml; see section 2.1 for APS and acrylamide concentrations).

Once the gel was prepared and placed in the gel tank, sample (20-30 µl) was loaded after boiling (1') in SDS loading buffer (reducing or non-reducing depending on requirements). Samples were run (150 volts) alongside markers until loading dye had reached the bottom of the gel plate. Separated protein was visualised by staining either with Coomassie blue for 2 hours followed by

washing with water and incubation overnight with destain or, if identifying glycosylation, a Glyco-staining kit was used (Pierce) that applies a Schiff base staining method. Western blotting was also carried out to positively identify IgE proteins using the Dako HRP conjugated anti-IgE polyclonal antibody P295 and semi-dry blotting apparatus onto activated nitrocellulose (0.45 μm pore size, Schleicher and Schuell). The blot was developed using SuperSignal (Pierce) chemoluminescence reagent and detected using autoradiography film (Kodak) and a X-omat developing machine.

2.3.8 Quantification of proteins

Purified preparations of recombinant protein were quantified by virtue of their molar extinction coefficient (calculated according to Sedenterp – ftp://alpha.bbri.org/rasmb/spin_ms/sednterp). Absorbance at OD_{280nm} was measured in a Cary 1E UV visible spectrophotometer using a 1cm pathlength quartz cell. Protein concentration was assessed using the Beer-Lambert law:

$$A = \varepsilon c l \qquad [2.3.1]$$

Where absorbance A is equal to the molar extinction coefficient ε (units $M^{-1}cm^{-1}$) multiplied by the concentration c (mg/ml) and the path length of the cell (cm). Therefore the absorbance of 1 mg/ml can be determined by the ratio of ε to molecular weight *i.e* in a 1 cm cell 1 mg/ml Fcε3-4 of a mw 49,100 and a ε of 64520 has an absorbance of 1.3. See table below for all values:

Protein	A_{280} of 1mg/ml protein solution
sFcεRIα	2.56
$(sFc\varepsilon RI\alpha)_2$IgG4-Fc	1.81
Fcε3-4ΔC	1.31
Fcε3-4ΔCF506R	1.31
Fcε3-4	1.31
Fcε4	1.48
Fcε4F506R	1.48

Table 2.5: Absorbance values to obtain mg/ml measurement of protein concentration for expressed fragments.

2.4 Biophysical techniques

Once fragments of IgE had been expressed and purified they were examined for variations in stability and structure. This was carried out using circular dichroism (CD) spectroscopy. Fragment preparations were also assessed for homogeneity and their molecular weight determined by analytical ultacentrifugation (AUC). AUC was also used in addition to surface plasmon resonance (SPR) studies to determine the affinity constants for high affinity receptor (FcεRI) binding.

2.4.1 Circular dichroism spectroscopy

Background: Electromagnetic waves are characterised by the amplitude and orientation of their component electric and magnetic fields, with the electric and magnetic components always perpendicular to the direction of propagation. It is by orientation with respect to an external reference that polarisation can be described. In plane-polarised light the oscillations of both the magnetic and electric waves occur within a single plane perpendicular to the direction of propagation, whereas in circularly polarised light they rotate about this axis (see figure 2.2).

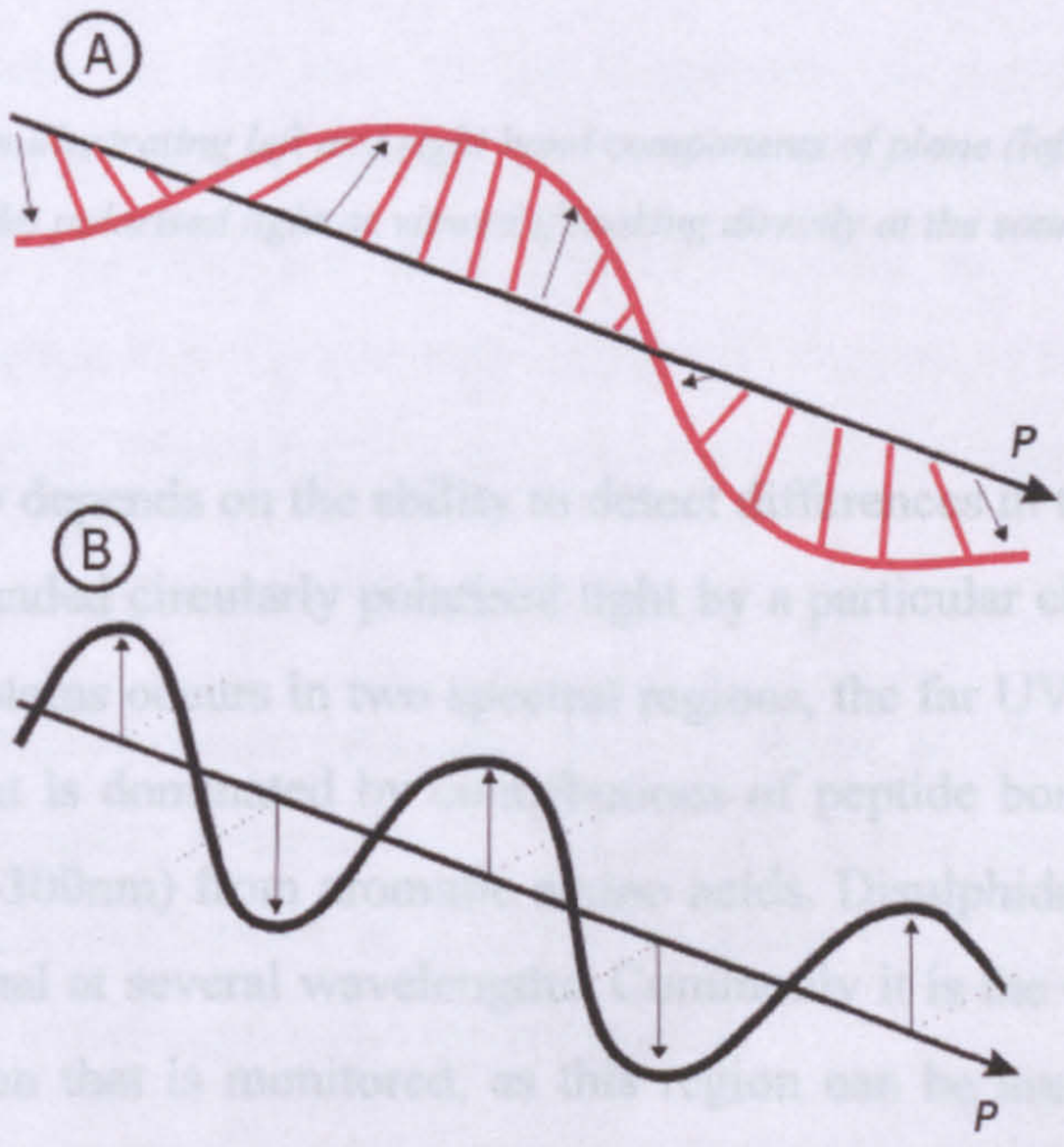

Figure 2.2: Diagram illustrating a single field component of A: Circularly polarised light and B: Plane polarised light

Circular polarisation can be left- or right-handed depending on the sense of rotation about the direction of propagation. If left- and right-handed polarised waves of equal amplitude are combined, the result will be plane-polarised light. If two circularly polarised components of unequal amplitude are combined, the result is elliptically polarised light, characterised both by the ellipticity and the direction of the major axis (see figure 2.3).

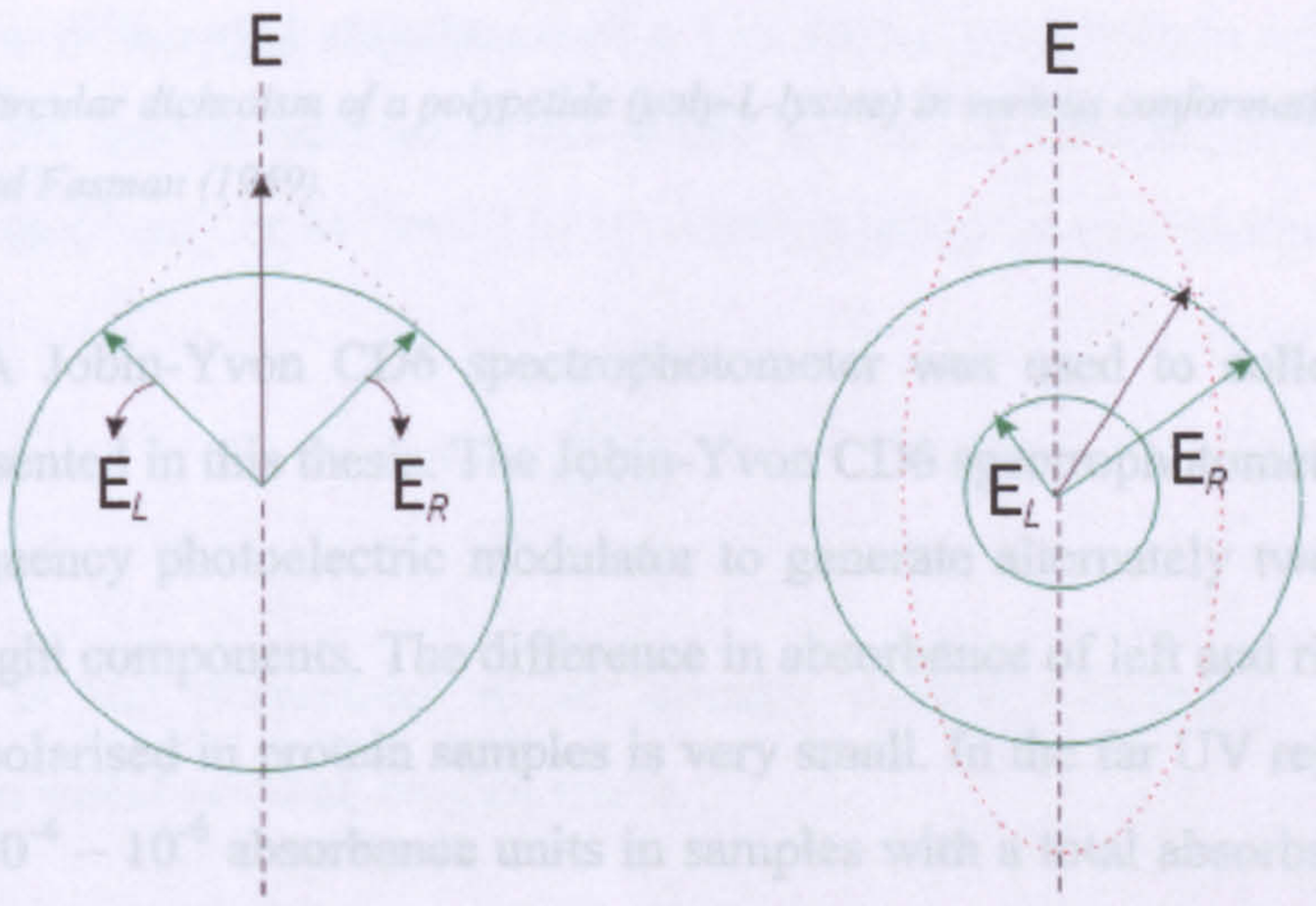

Figure 2.3: Diagram illustrating left and right hand components of plane (left side) and elliptically (right side) polarised light as viewed if looking directly at the source.

CD spectroscopy depends on the ability to detect differences in the absorbance of left- and right-handed circularly polarised light by a particular chromophore. The CD signal of proteins occurs in two spectral regions, the far UV or amide region (170-250nm) that is dominated by contributions of peptide bonds, and the near UV region (250-300nm) from aromatic amino acids. Disulphide bonds also give rise to a CD signal at several wavelengths. Commonly it is the CD signal within the far-UV region that is monitored, as this region can be used to characterise secondary structure. The characteristic CD spectra of different secondary structural elements is shown overleaf.

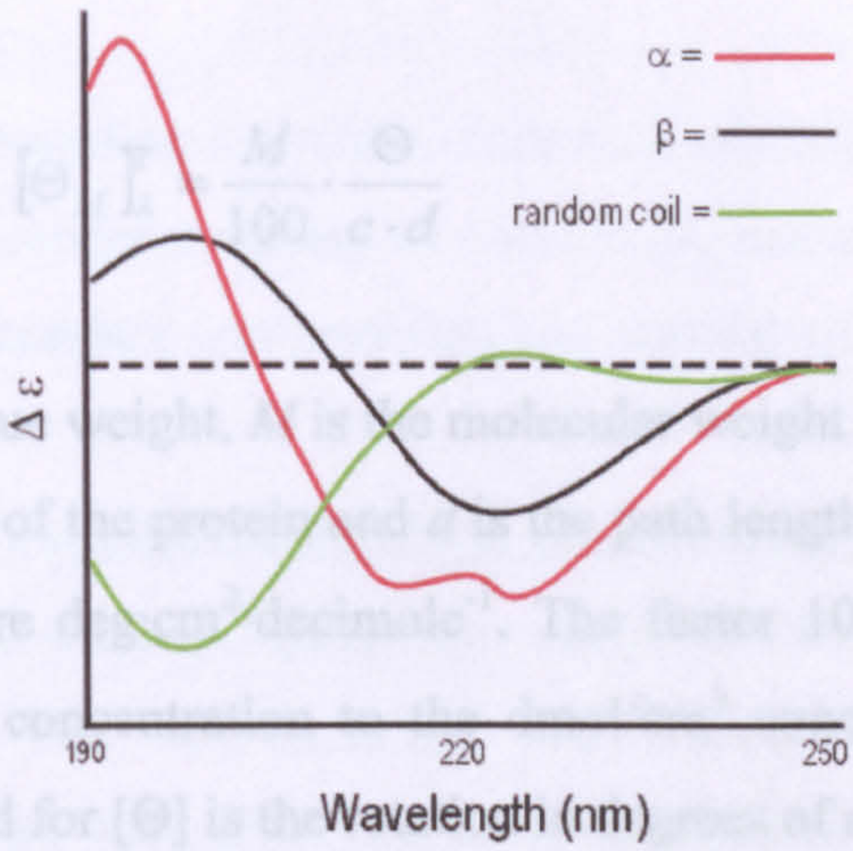

Figure 2.4: Circular dichroism of a polypetide (poly-L-lysine) in various conformations – after Greenfield and Fasman (1969).

Method: A Jobin-Yvon CD6 spectrophotometer was used to collect the CD spectra presented in this thesis. The Jobin-Yvon CD6 spectrophotometer employs a high frequency photoelectric modulator to generate alternately two circularly polarised light components. The difference in absorbance of left and right handed circularly polarised in protein samples is very small. In the far UV region it is in the range $10^{-4} - 10^{-6}$ absorbance units in samples with a total absorbance of 1.0. Therefore careful sample preparation is necessary to obtain accurate and reproducible results. In the case of IgE fragments, all samples were HPLC purified, dialysed into a non-absorbing buffer (20 mM Sodium Phosphate pH 7.4, 50 mM Sodium Fluoride) and their spectra recorded at a concentration of ~0.5mg/ml of protein in a 0.5 mm path length cell to obtain a reasonable signal-to-noise ratio. Scans were taken in 0.2 nm steps with an integration time of 1 second.

The CD6 spectrophotometer measures the CD signal as ellipticity, $[\Theta_{obs}]$, in millidegrees. To enable comparison of values, this measurement can be scaled such that it is expressed either as a molar ellipticity $[\Theta_M]$ or residue ellipticity $[\Theta_{mrw}]$ at a given wavelength λ and temperature T:

$$[\Theta_{mrw}]_{\lambda}^{T} = \frac{mrw}{100} \cdot \frac{\Theta}{c \cdot d} \qquad [2.4.1]$$

$$[\Theta_M]_\lambda^T = \frac{M}{100} \cdot \frac{\Theta}{c \cdot d} \qquad [2.4.2]$$

mrw is the mean residue weight, *M* is the molecular weight of the protein studied, *c* is the concentration of the protein and *d* is the path length of the cell. The units of molar ellipticity are deg·cm^2·decimole^{-1}. The factor 100 originates from the conversion of molar concentration to the dmol/cm^3 concentration unit, as the concentration standard for [Θ] is the rotation in degrees of a 1 dmol/cm^3 solution, and Δε is the differential absorbance of a 1 mol/l solution, both in a 1cm cell. In the case of the spectra reported in this thesis, the values were expressed in terms of Δε (litre·mol^{-1}·cm^{-1} or M^{-1} cm^{-1}) by conversion using the expression:

$$\Delta\varepsilon = \frac{[\Theta]}{3300} \qquad [2.4.3]$$

where Δε is the differential molar circular dichroic extinction coefficient expressed in molar or mean residue terms.

In addition to providing an estimate of the amount of secondary structure in a protein, CD can also be used to monitor transitions in protein structure. This means that the stability of one protein relative to another can be determined, and the impact of the removal of specific structural elements can be assessed. If the $[\Theta_{obs}]$ at a particular wavelength is monitored (in this case 215nm, a recognised minimum with respect to β structure) and temperature increased incrementally (20-80°C in 2°C steps) the denaturation profile of the protein can be plotted. Readings can be normalised for comparison using the following expression:

$$F_u = \frac{\Theta - \Theta_N}{\Theta_D - \Theta_N} \qquad [2.4.4]$$

F_u refers to the fraction of protein unfolded, Θ the observed ellipticity at a given temperature, and Θ_N Θ_D the ellipticity of fully folded and denatured species calculated from linear regression of the baselines before and after transition.

The relative ease of recording a circular dichroism spectrum allied to the ability to take measurements under a variety of conditions, makes CD a powerful tool for the study of the secondary conformation and stability of a protein.

2.4.3 Sedimentation equilibrium analytical ultracentrifugation

Background: In sedimentation equilibrium analytical ultracentrifugation speeds are controlled such that sedimentation and back-diffusion forces are of comparable magnitudes. This gives rise to an equilibrium distribution of solute concentration dependent on mass, with no net transport. This concentration distribution is independent of molecular shape, and therefore it is possible to accurately determine the molecular weight and degree of homogeneity of a protein preparation. Furthermore, for an interacting system, the distribution is an absolute function of the mass action relationship between species participating in the equilibrium, with concentration as well as molecular mass determining position. This means it is also possible to calculate the equilibrium affinity constant of an interacting system. Thus, sedimentation equilibrium analytical ultracentrifugation is an extremely valuable technique for studying protein:protein interactions.

The forces placed on a molecule in the centrifuge are outlined in figure 2.5 and are described as follows:

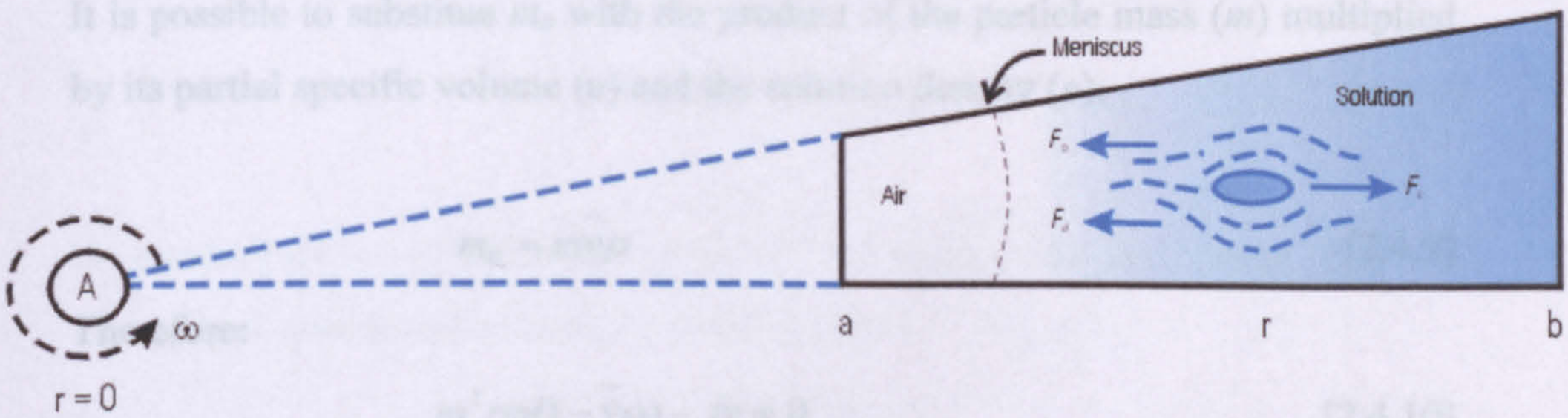

Figure 2.5: Diagram of a sedimentation experiment. The sector shaped cell spins about axis A at an angular velocity ω. The molecule is acted on by centrifugal (F_c), buoyant (F_b) and frictional drag (F_d) forces. See equations 2.4.5 - 2.4.7.

In a rotor turning with an angular velocity ω (radians per second) a molecule will experience a centrifugal force proportional to the product of its mass (m) and the distance (r) from the centre of rotation:

$$F_c = \omega^2 rm \qquad [2.4.5]$$

The molecule also displaces some solution, giving rise to a force equal to that exerted on the mass of solution displaced:

$$F_b = -\omega^2 rm_0 \qquad [2.4.6]$$

Finally, if as a result of these forces the molecule acquires a velocity (v) through the solution, a frictional force will be exerted:

$$F_d = -fv \qquad [2.4.7]$$

where f is the frictional coefficient. This situation will result in the molecule acquiring a velocity just great enough to make the total force zero:

$$F_c + F_b + F_d = 0$$

$$\omega^2 rm - \omega^2 rm_0 - fv = 0 \qquad [2.4.8]$$

It is possible to substitue m_o with the product of the particle mass (m) multiplied by its partial specific volume (υ) and the solution density (ρ):

$$m_0 = m\bar{v}\rho \qquad [2.4.9]$$

Therefore:

$$\omega^2 rm(1 - \bar{v}\rho) - fv = 0 \qquad [2.4.10]$$

If this is then multiplied by Avogadro's number and rearranged to place the molecular parameters on one side and the experimentally measured on the other:

$$\frac{M(1-\bar{v}\rho)}{Nf} = \frac{v}{\omega^2 r} = s \qquad [2.4.11]$$

This gives *s*, the sedimentation coefficient; s is measured in seconds and is experimentally determined as the ratio of velocity to centrifugal force. Values are commonly around 1 x 10^{-13} seconds, and therefore every 1 x 10^{-13} is referred to as a Svedberg unit (S).

In an equilibrium situation this centrifugally driven force is balanced by a diffusion driven counterflow, D (cm^2sec^{-1}), which is also governed by the translational frictional coefficient:

$$D = \frac{RT}{Nf} \qquad [2.4.12]$$

Where R is the universal gas constant and T the absolute temperature. The influence of f on the individual magnitudes of S and D cancels within the ratio:

$$\frac{S}{D} = \frac{M(1-\bar{v}\rho)}{RT} \qquad [2.4.13]$$

Therefore the parameter to emerge from the analysis of solvent distribution at sedimentation equilibrium is buoyant molecular weight:

$$M(1-\bar{v}\rho) \qquad [2.4.14]$$

At equilibrium the concentration gradient for a single component in an ideal two component system can be described as follows

$$\frac{1}{C}\frac{dC}{dr} = \frac{\omega^2 r M(1-\bar{v}\rho)}{RT} \qquad [2.4.15]$$

where C is the concentration.

Integrating this between the meniscus (a) and point r shows that C depends on r in an exponential fashion:

$$C(r) = C(a)e^{\omega^2 M(1-\bar{v}\rho)(r^2-a^2)/2RT} \qquad [2.4.16]$$

or:

$$\ln\frac{C(r)}{C(a)} = \frac{\omega^2 M(1-\bar{v}\rho)(r^2-a^2)}{2RT} \qquad [2.4.17]$$

More simply, a plot of *ln* concentration against the square of the radial distance will give a straight line, the gradient of which is proportional to molecular weight.

Method: Experiments carried out as part of this thesis were performed using a Beckman XL-A. UV visible absorbance was measured as a function of radial position. During the experiment the solution redistributes such that an increasing concentration gradient travelling away from the centre of rotation is formed. This is read relative to a control cell that contains only the buffer into which the species are dialysed. This system is illustrated in figure 2.5:

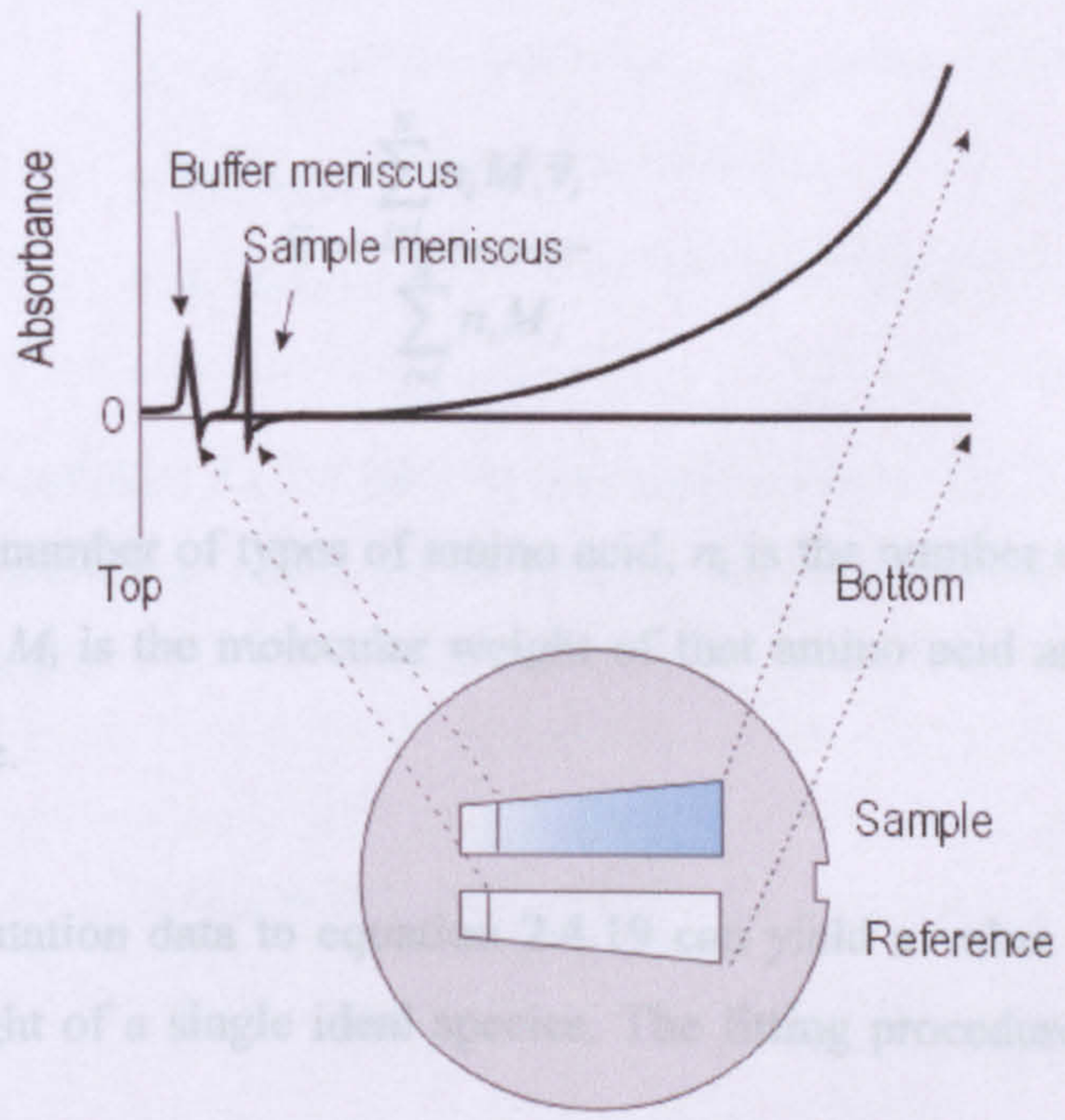

Previous page.

Figure 2.6: Diagram illustrating the concentration gradient observed in a two sector AUC cell

In the Beckman XL-A measurements are made in absorbance units, therefore equation 2.4.16 becomes:

$$A_r = A_{r0} e^{[M(1-\bar{\nu}\rho)\omega^2/2RT](r^2 - r^2{}_0)} \qquad [2.4.18]$$

where A_{r0} is the absorbance at a radial reference point and A_r is the absorbance at a given radial position. Absorbance is proportional to concentration according to the Beer-Lambert equation 2.3.1.

In curve fitting, the term $\omega^2/2RT$ is constant (H) and a baseline term is added (E); this is obtained by performing an overspeed (42,000 rpm) spin and measuring the background absorbance in the cell. Thus:

$$A_r = A_{r0} e^{[HM(1-\bar{\nu}\rho)(r^2 - r^2{}_0)]} + E \qquad [2.4.19]$$

Values for solvent density (ρ) and ($\bar{\nu}$) are determined prior to fitting, ρ from standard values and $\bar{\nu}$ from the following equation:

$$\bar{\nu} = \frac{\sum_{i=1}^{N} n_i M_i \bar{\nu}_i}{\sum_{i=1}^{N} n_i M_i} \qquad [2.4.20]$$

where N is the number of types of amino acid, n_i is the number of a certain type of amino acid, M_i is the molecular weight of that amino acid and $\bar{\nu}_i$ its partial specific volume.

Fitting sedimentation data to equation 2.4.19 can yield a value for the buoyant molecular weight of a single ideal species. The fitting procedure can be carried

out using a computer and a non-linear least squares analysis, with a residual plot used to evaluate the quality of the fit (as applied for Biacore data, see section 2.4.2). In the case of a single ideal system, plotting ln A versus r^2 will produce a straight line. If the plot observed is curved this indicates either a non-ideal system or mass action association between species.

If the sample is simply a mixture of ideal species the observed distribution is a sum of the exponentials for each species

$$A_r = E + \sum A_{r0i} e^{[(HM(1-\bar{v}\rho))_i (r^2 - r^2{}_0)]} \qquad [2.4.20]$$

where i refers to the i^{th} component.

If the system is interacting, for example in the case below

$$A + 2B \leftrightarrow AB + B \leftrightarrow AB_2 \qquad [2.4.21]$$

the sedimentation equilibrium profile as a function of radius can be described as the sum of the contributions of A alone, B alone, the AB complex and the AB_2 complex. This can be described as the sum of the exponentials as before:

$$\begin{aligned} A_r &= A_{0,A} e^{[HM_A(1-\bar{v}\rho)(r^2 - r^2{}_0)]} + A_{0,B} e^{[HM_B(1-\bar{v}\rho)(r^2 - r^2{}_0)]} \\ &+ A_{0,A} A_{0,B} e^{[\ln k_1 H(M_A + M_B)(1-\bar{v}\rho)(r^2 - r^2{}_0)]} \\ &+ A_{0,A} (A_{0,B})^2 e^{[\ln k_2 H(M_A + 2M_B)(1-\bar{v}\rho)(r^2 - r^2{}_0)]} + E \end{aligned} \qquad [2.4.22]$$

The association constant K_A for each of the reactions thus can be calculated from the apparent equlibrium constants k_1 and k_2, as these are on an absorbance concentration scale:

$$\ln K_{AB} = \ln k_1 + \ln\left(\frac{\varepsilon_A \varepsilon_B l}{\varepsilon_A + \varepsilon_B}\right) \qquad [2.4.23]$$

$$\ln K_{AB2} = \ln k_2 + \ln\left(\frac{\varepsilon_A \varepsilon_B{}^2 l}{\varepsilon_A + 2\varepsilon_B}\right) \qquad [2.4.24]$$

where ε refers to the molar extinction coefficients of each of the species and l is the path length of the cell.

For IgE fragments interacting with sFcεRIα, samples were exhaustively dialysed into PBS supplemented with 0.05% azide. Fragments were then mixed in molar ratios of 1:1, 2:1 and 3:1 FcεRIα:Fcε3-4, with an overall loading corresponding to an A_{280} of ~0.6. For an estimation of the molecular weight of the single species sample preparation was identical. Rotor speeds were adapted depending on the expected fragment or complex size using equation 2.4.25, incorporating an estimate of $M(1-\bar{v}\rho)$ as one quarter the molecular weight:

$$speed(rpm) = \frac{\sqrt{2.336x10^{12}}}{M(1-\bar{v}\rho)} \qquad [2.4.25]$$

In addition, $1/\sqrt{2}$ of this speed and the average of the two speeds was calculated to give three separate speeds to measure $M(1-\bar{v}\rho)$ accurately. Data were collected as an average of 25 absorbance measurements at a wavelength of 280 nm and a radial spacing of 0.001 cm.

2.4.2 Surface plasmon resonance

Background: If two transparent media of different refractive indexes are taken and light passed through the material of higher refractive index towards that of lower refractive index, above a certain critical angle of incidence, total internal reflection occurs at the interface. When the incident light is totally reflected, an evanescent wave penetrates a short distance into the medium of lower refractive index. If the interface between the two is coated with a thin layer of metal, and the light monochromatic and polarised such that the electric vector component is parallel to the plane of incidence, the intensity of the reflected light dips at a specific incident angle due to excitation of surface plasmons propagating within

the gold surface. This phenomenon is known as surface plasmon resonance (SPR), with the angle at which the dip is observed known as the SPR angle.

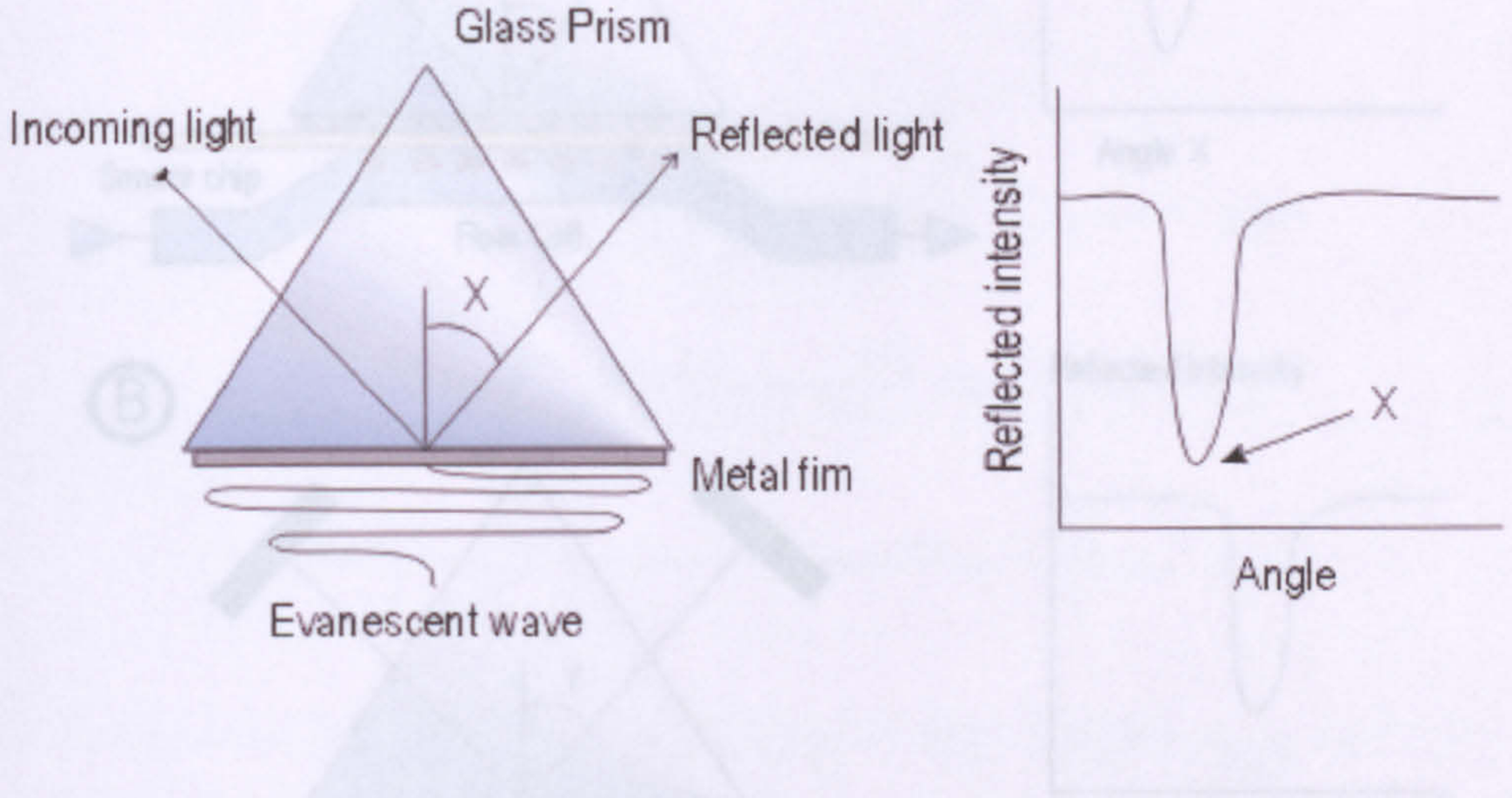

Figure 2.7: Under conditions of total internal reflection an evanescent wave propagates into the material of lower refractive index on the non-illuminated side. The angle of the minimum in reflected intensity has a sharp "shadow" at a specific point – this is the SPR angle X.

This phenomenon can be used for studying protein-protein interactions, as the SPR angle is dependent on a number of factors including temperature, the wavelength of the incident light and, critically, the refractive index of the medium into which the evanescent wave propagates (on the non-illuminated side). Therefore, if all other factors are controlled, it is possible to measure changes in surface concentration in real time by monitoring the SPR angle.

In a Biacore instrument a biomolecule (ligand) is immobilised close to the interface and the binding of specific analyte is monitored as a result of the change in refractive index at the surface (see figure 2.8).

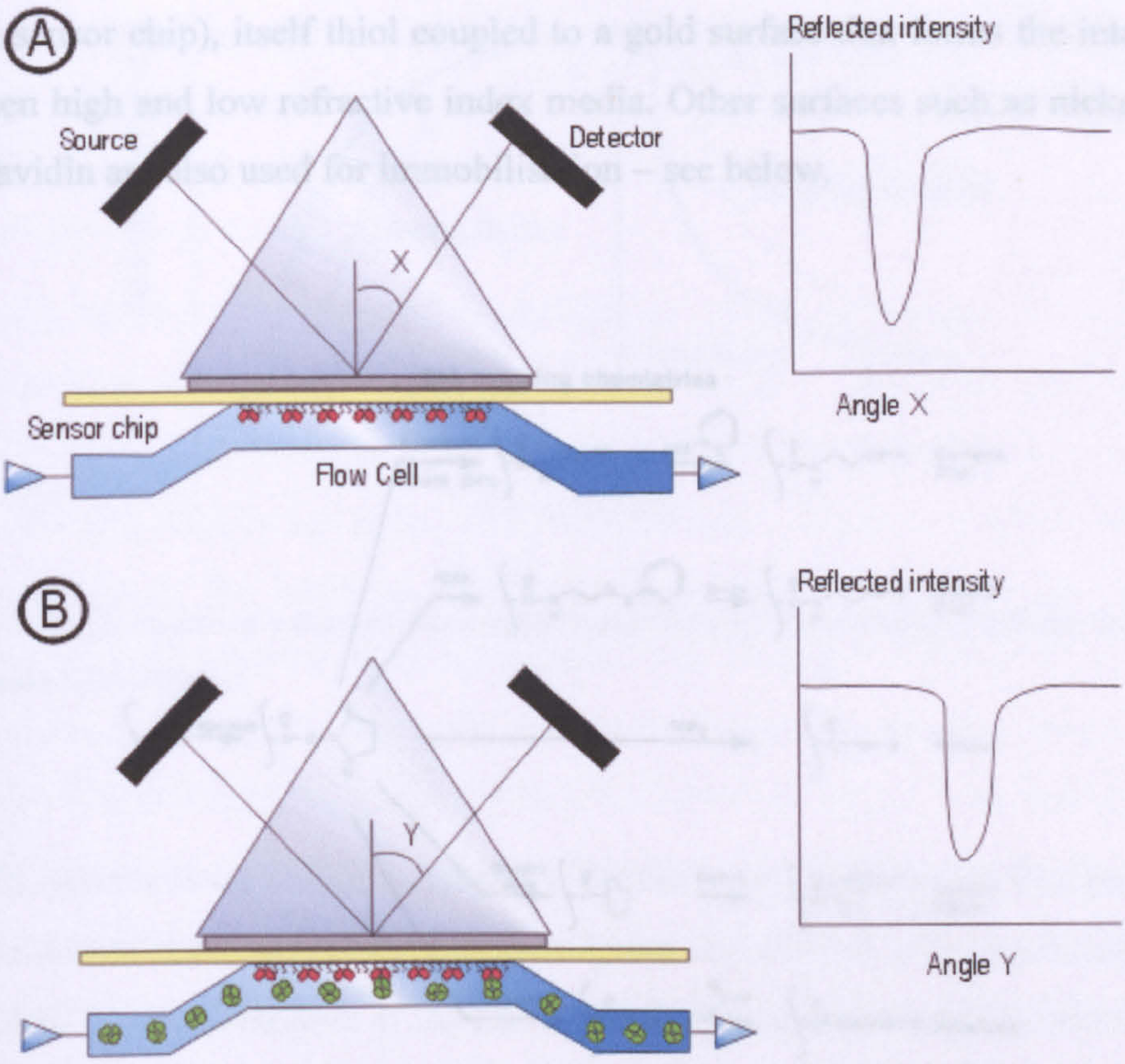

Figure 2.8: Changes in refractive index are monitored by the shift in the SPR angle. These measurements are proportional to the mass of ligand bound at the receptor surface. Therefore, real time interactions can be observed using the phenomenon of SPR. The yellow bar represents a sensor chip onto which the protein of interest is immobilised (red elipses), analyte is then flowed over the sensor chip (green elipses) and binding is monitored using a CCD to monitor the shift in SPR angle.

The ligand is commonly immobilised onto a carboxymethylated dextran matrix (CM5 sensor chip), itself thiol coupled to a gold surface that forms the interface between high and low refractive index media. Other surfaces such as nickel and streptavidin are also used for immobilisation – see below.

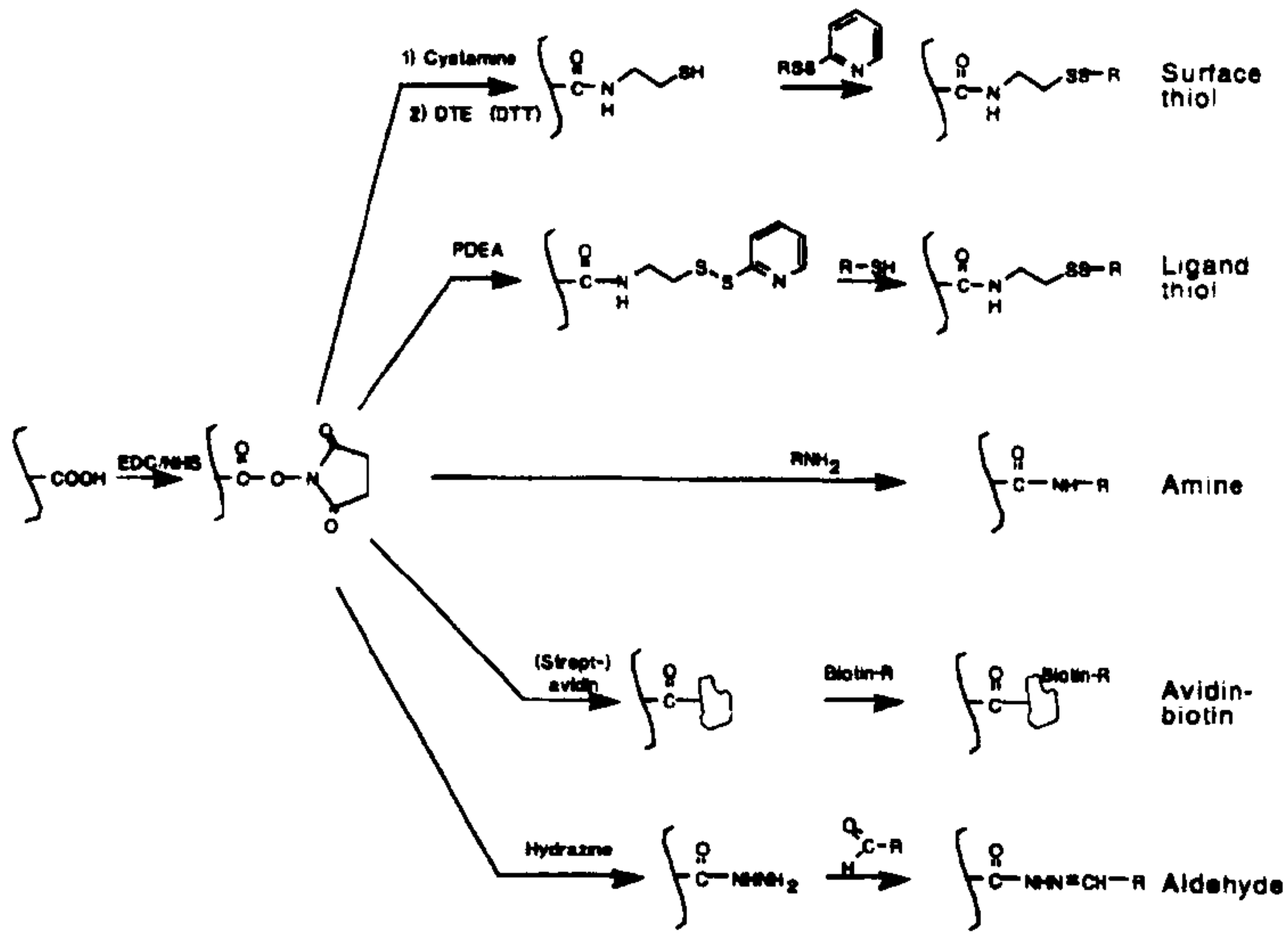

Figure 2.9: Coupling chemistries possible using a CM5 Biacore sensorchip.

A Biacore assay commonly follows a method in which the chip surface is exposed to analyte for a defined period of time; dissociation is then monitored when the flow is stopped, again for a defined period of time. This yields a trace known as a sensorgram with the association and dissociation of analyte corresponding to a rise and fall in the SPR angle measured in resonance units (RU). Bulk effects are also sometimes observed due to differences in buffers when analyte is injected. These artefacts are usually dealt with by carrying out control experiments in which a protein with similar properties, but no binding capability, is immobilised at identical levels on a separate surface. This enables the bulk effect to be subtracted from the signal; in addition it allows the removal of signal that corresponds to non-specific binding to the dextran matrix. From the curve it is then possible to derive kinetic parameters to describe the binding and dissociation phases of the observed interaction.

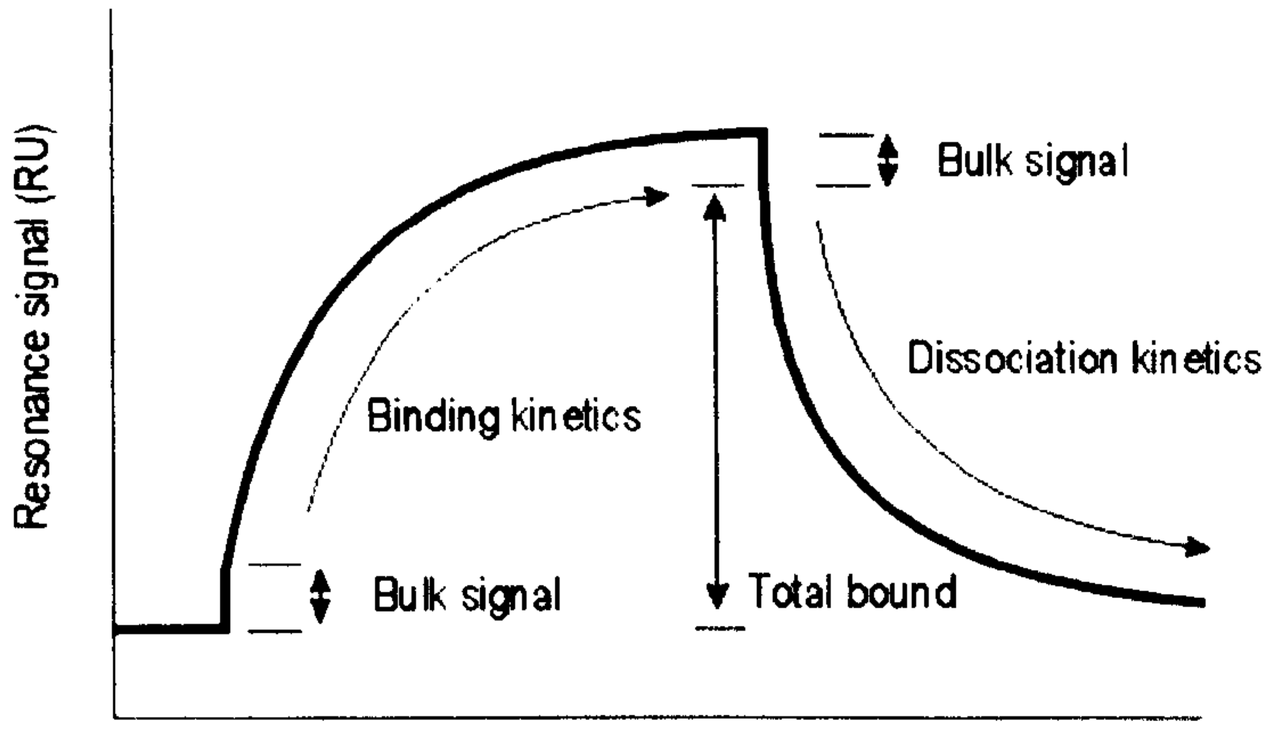

Figure 2.10: Schematic of a Biacore experiment to monitor real time binding of specific analyte to an immobilised ligand.

Careful experimental design is crucial if curves are to be obtained that are truly representative of the interaction between ligand and analyte. One key factor to be controlled is mass transport. If the rate of mass transport of analyte to the surface is slower than the rate of interaction, then the observed SPR signal will be significantly affected. In this situation analysis of the data would provide incorrect kinetic constants. However, these artefacts can be minimised. Inside the flow cell the key feature to be dealt with is the diffusion distance to the ligand. Within the flow cell, a laminar flow effect is observed and therefore even high flow rates do not deliver ligand to the surface directly, but depend on diffusion from the area of laminar flow to the surface. By increasing the flow rate, the diffusion distance to the matrix can be decreased significantly, as the laminar flow region is extended closer to the matrix surface.

In addition to diffusion distance, the initial interaction rate is critical. If there are a high number of sites available for interaction at the start of the assay, the process may be mass transport limited. By reducing the immobilisation level of ligand this effect is diminished. This reduces the consumption of ligand and therefore impacts positively on the problems associated with mass transport limitation due to diffusion. Furthermore, low immobilisation levels reduce the possibility of rebinding events that could also skew the data. Varying the flow

rate and immobilisation level, and monitoring the consequent shift in initial binding rates, can be used to assess the effects of mass transport. The balancing of these effects however has also to take into consideration the signal required to observe the interaction and the availability of material for analysis.

A good dataset for analysis comprises a series of curves at different concentrations of analyte that cover a broad range, from near saturation to minimal binding. This is important because a variety of parameters are essential when deriving affinity constants. Using a high concentration of analyte will give an indication of the point at which maximal binding (R_{max}) occurs. Before experimentation, the level of immobilisation can be used to estimate R_{max}, as the SPR response is proportional to the mass concentration at the chip surface. For example, if a protein of 150,000 mw is immobilised at 500RU, and binding of a 50,000 mw protein monitored which is known to bind with a 1:1 stochiometry, the maximal theoretical response would be ~160 RU. When fitting data the goodness of fit can then be assessed by comparing the observed and theoretical R_{max} values to those derived from the fitting procedure. Observation of saturation binding also provides a check on whether the surface has been compromised, by comparing the difference between theoretical and observed R_{max} values. However, binding curves with higher analyte concentrations contain less information with respect to the association phase of binding. This is because saturation or equilibrium is reached too quickly. Therefore inclusion of lower concentrations into the dataset enables a more accurate assessment of the on-rate, as more information is available for fitting. Finally, a broad range of dissociation phases also provides a better assessment for the fitting of off-rates for the same reason. Commonly an analyte concentration range of between zero and 10 – 100 times the K_D is thought to be sufficient (van der Merwe, 2000)

The on and off rates for the formation of a binary complex can be described by the following equations:

$$A + B \longleftrightarrow AB \qquad [2.4.26]$$

where the association rate is:

$$\frac{d[AB]}{dt} = k_a[AB] \qquad [2.4.27]$$

and the dissociation rate is:

$$-\frac{d[AB]}{dt} = k_d[AB] \qquad [2.4.28]$$

At equilibrium, association and dissociation rates are equal:

$$k_a[A][B] = k_d[AB] \qquad [2.4.29]$$

This equation can be rearranged to give the equilibrium dissociation constant:

$$\frac{k_d}{k_a} = \frac{[A][B]}{[AB]} = K_D \qquad [2.4.30]$$

or the equilibrium association constant:

$$\frac{k_a}{k_d} = \frac{[AB]}{[A][B]} = K_A \qquad [2.4.31]$$

The equilibrium constant defines the balance of free components and complexed components at equilibrium, whilst the rate constants define how fast the forward and backward reactions occur. In the Biacore it is possible to obtain the equilibrium affinity constant simply by injecting different concentrations of ligand over the chip surface until equilibrium is achieved and then carry out a steady state analysis based on a plot of concentration versus ligand bound. However, the real advantage the Biacore has is that it is able to monitor the formation and decay of receptor ligand complexes in real time. Therefore it can provide a direct assessment of rate constants. Equilibrium constants can then be calculated from their constituent rate contants (see 2.4.30 - 31). For fitting purposes, terms used in SPR analysis can be substituted into the combined form of the rate equation. Thus (overpage):

$$\frac{d[AB]}{dt} = k_a \cdot [A][B] - k_d[AB] \qquad [2.4.32]$$

becomes:

$$\frac{dR}{dt} = k_a \cdot C \cdot (R_{max} - R) - k_d \cdot R \qquad [2.4.33]$$

where C equates to the concentration of ligand $[A]$, R_{max} equates to the concentration of immobilised receptor $[B]$ and R equates to the SPR signal associated with the formation of complex $[AB]$. The BIAevaluation software supplied with the machine can solve this differential rate equation. To do this the BIAevaluation software uses a standard least squares minimisation routine, which optimises parameter values by minimising the sum of the squared residuals. When a minimum is reached, a plot of the residuals between the fit and the data can assess the quality of the fit: points on this plot should be randomly distributed around the baseline if the fit is good.

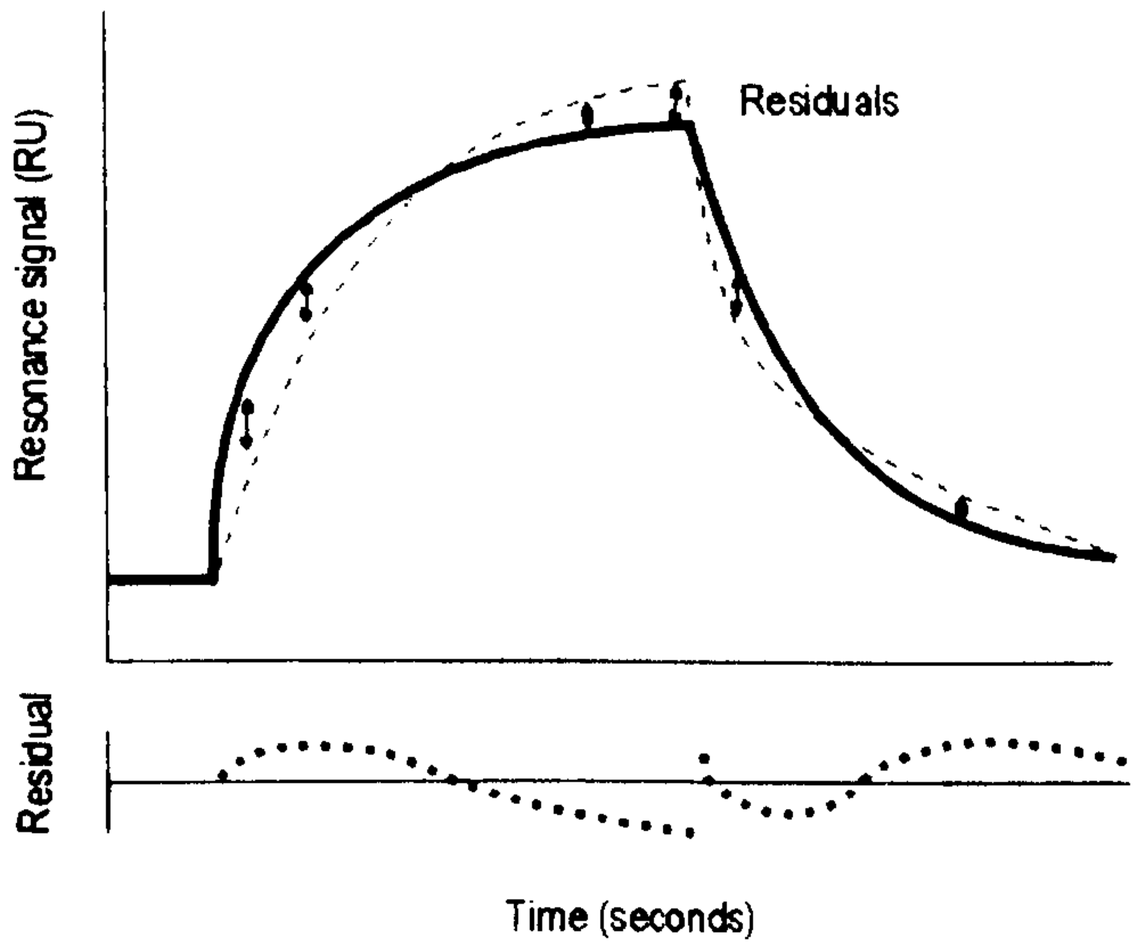

Figure 2.11: Schematic to illustrate fit procedure for Biacore data. Dashed line represents the fit line; arrows indicate values taken from which sum of squares is calculated. Dotted line represents a plot of the residuals.

A χ^2 value can also be calculated from the residuals, which acts as a numerical indicator of the goodness of fit. To minimise error and the chance of obtaining unrealistic rate constants it is better to fit a concentration series globally rather

than individually. However, sometimes this is not possible, as small inconsistent variations in the dataset (such as differences in drift, injection artefacts or small deteriorations in the surface) mean it is not possible to resolve the data into a global minimum when fitting. In such cases curves can be fitted individually. However, care needs to be taken to ensure the fitting procedure does not produce too great an error in the determination of constants. Calculating the standard deviation of the average rate constant, and checking for trends related to concentration, can be used to assess this.

Method: In the case of experiments described in this thesis, only CM5 chips were used to immobilise the $(sFc\varepsilon RI\alpha)_2$-$IgG_4$-Fc fusion protein via primary amine groups. $(sFc\varepsilon RI\alpha)_2$-$IgG_4$-Fc fusion was used because amine coupling destroys $sFc\varepsilon RI\alpha$ binding capability (only a more complex, and less easy to control, hydrazide coupling method works for this protein, Cook *et al*, 1997). Immobilisation was achieved by activating the CM5 matrix with a 1:1 mixture of N-hydroxysuccinimide (NHS) and N-ethyl-N'- (3-diethyl-aminopropyl)-carbodiimide (EDC) for 1 minute at a flow rate of 5µl/min. The ligand was then passed over the activated matrix at a concentration of 50µg/ml in 10mM sodium acetate pH 4.5 until the resonance signal reached approximately 500 RU. This immobilisation level corresponds to ~ 0.5 ng of protein per mm^2 of the matrix. In fact the matrix extends for 100 nm from the chip surface, and therefore strictly an immobilisation of this degree is equal to a surface concentration of ~5mg/ml. Once the correct response level had been reached, remaining activated sites were blocked with 35µl of 1.0M ethanolamine-hydrochloride pH 8.5 and the surface washed with HBS at 5µl/min. A control surface was prepared in an identical manner using IgG_4-Fc.

Data were collected for IgE fragments within the concentration range 100 nM to 6 nM using a 500 RU surface and a flow rate of between 10 and 30 µl/min. This is sufficient to provide assessment of binding kinetics for IgE (McDonnell *et al* 2001).

The model previously described (equation 2.4.33) applies to a simple Langmuir isotherm for absorption to a surface, and is the simplest description of a 1:1

interaction. However, it has already been demonstrated through both Biacore analysis and subsequent structural studies that the interaction of IgE with FcεRI is more complex than this (Henry *et al*, 1997; Garman *et al*, 2000). A biphasic model better describes the interaction, but fitting involves a larger number of variables. It is important to choose the model that best describes the system. IgE binding to FcεRI is a 1:1 interaction that is formed by at least two distinct binding sites. The model that best describes this situation would incorporate biphasic kinetics and competition between the two sites. This model exists in the BIAevaluation software and can be described as follows:

$$A + B \longleftrightarrow AB \qquad [2.4.34]$$

plus:

$$C + B \longleftrightarrow CB \qquad [2.4.35]$$

Where A and C represent the two different modes of IgE binding and B respresents FcεRI. From this the following differential rate equations can be derived:

$$\frac{dR_1}{dt} = k_{a1} \cdot C_A \cdot (R_{max} - R_1 - R_2) - k_{d1} \cdot R_1 \qquad [2.4.36]$$

$$\frac{dR_2}{dt} = k_{a2} \cdot C_c \cdot (R_{max} - R_1 - R_2) - k_{d2} \cdot R_2 \qquad [2.4.37]$$

The total response is:

$$R = R_1 + R_2 \qquad [2.4.38]$$

However, in this scheme the number of parameters to fit has obviously increased, and it is necessary to obtain values for not one, but two association and dissociation constants. A good fit can only be achieved in circumstances like this if a reasonable estimate of the constants is available initially. This is because as the number of parameters rises, so does the number of minima into which the fitting procedure can resolve itself. One method for controlling this issue is to

derive some of the components individually. The R_{max} should not vary between fits carried out using the same ligand on the same surface. Therefore the R_{max} should also ideally be determined experimentally, or by estimating a value based on the immobiliation and molecular weight of ligand (as detailed earlier). It is also possible to assess off-rates separately, as they can be fitted independently of concentration or knowledge of R_{max}. Values can then be fed back into the full equation and used as constants, or the values compared to those derived from the simultaneous fitting of association and dissociation data. To enable the fitting of off-rates separately from on-rates it is necessary to derive an equation for the fitting procedure to solve. From a normal Langmuir isotherm that describes the dissociation of a single simple 1:1 complex:

$$\frac{dR}{dt} = -k_d R \qquad [2.4.39]$$

the following expression can be derived:

$$R = R_0 \cdot e^{-kd(t-t_0)} \qquad [2.4.40]$$

where R is the SPR response at time t and R_0 is the response at t_0. However, the IgE:FcεRI interaction is biphasic, and therefore the "off" phase must be treated as two independent events whose individuals rates can combine to form an overall response. This can be done by simply creating an expression for a dual exponential decay. The expression does not have to take into account the competitive step observed for the on-rate and is simply a parallel dissociation composed of two distinct kinetic events:

$$R = R_1 \cdot e^{-kd_1(t-t_0)} + (R_0 - R_1) \cdot e^{-kd_2(t-t_0)} \qquad [2.4.41]$$

where R_1 is the contribution to R_0 from component 1 and $R_0 - R_1$ is the contribution from component 2. The model calculates a value for R_1. The relative contribution for each of the components can be assessed by the ratio of R_1/R_0.

Biacore analysis provides a practical way of analysing protein:protein interactions with relatively small amounts of material, and is ideal for comparing panels of molecules with slight variations in structural features. The "real time" nature of the recording of the receptor:ligand interaction, in both association and dissociation, enables subtle differences to be observed that would not be obvious if only the overall affinity constant were derived. Furthermore, the method not only provides comparative data, but can also lead to the derivation of absolute rate constants, in addition to the affinity constants that can be obtained using other methods. The method also has drawbacks. In respect of mass transport, these can be circumvented by careful experimental design. However, there are intrinsic problems associated with the immobilisation of ligand by chemical coupling methods. Therefore, the experiments can appear compromised if compared to solution methods that do not require adaptation of one of the components (such as AUC). However, it is possible to check data by reversing the orientation of the experiment (something already achieved for IgE: Henry *et al*, 1997; Cook *et al*, 1997). Also, immobilised receptor is an approximation of the situation at the cell surface. If used alongside other techniques, and controls are carefully carried out, the comparisons possible from the direct observation of rate constants by surface plasmon resonance can provide a powerful tool in protein:protein interaction analysis.

Production and characterisation of a Fcε3-4 monomer

Chapter 3: Production and characterisation of a Fcε3-4 monomer

3.1 Introduction

An Fcε3-4 dimer of IgE-Fc can be produced from mammalian cells and is folded according to its circular dichroism (CD) spectrum (Keown *et al*, 1997). Furthermore, an *E. coli* expressed Fcε3-4 also refolds with an indistinguishable CD spectrum (Henry, PhD thesis, 1997), indicating that a bacterially expressed fragment has all the features necessary for folding Fcε3. However, an isolated Fcε3 fragment produced in *E. coli* is unfolded according to the same criteria (Henry *et al*, 2000). Therefore, given the aim to produce a fully folded Fcε3 with the minimal structural requirements, which of the structural components present within the Fcε3-4 fragment are necessary to create a folded Fcε3 domain?

The crystal structure of an (insect cell expressed) Fcε3-4 fragment (Wurzburg *et al*, 2000) has enabled the inter-relationship of Fcε3 with other domains to be determined within this fragment. This is clearly a very useful tool for suggesting what features may be essential for Fcε3 stabilisation. One area that could potentially be critical for the scaffolding of Fcε3 is the longitudinal interface between Fcε3 and Fcε4 domains within the same polypeptide chain. There are 14 contacts in this region, burying a surface are of ~ 873 $Å^2$ in each Fcε3-4 chain (Wurzburg *et al*, 2000), see figure 3.1.

Figure 3.1: Contacts between Fcε3 and Fcε4 within the same polypeptide chain (Fcε3 = blue, Fcε4 = red, contacts space-filled, C-α trace only for non contact residues).

There are no direct contacts between the two Fcε3 domains in either the unbound Fcε3-4 structure (Wurzberg *et al*, 2000), the Fcε3-4:FcεRIα complex (Garman *et al,* 2000) or the full IgE-Fc (Wan *et al*, 2001). However, the carbohydrate chains attached to Fcε3 domains in the uncomplexed Fcε3-4 crystal structure may make contact with each other, although no electron density is visible, and this region is presumably disordered. In the complex structure (Garman *et al*, 2000) no contact is seen between the carbohydrate chains, nor is there contact in the unbound IgE-Fc (Wan *et al*, 2002). This suggests that lateral contacts between Fcε3 domains may be less important for folding. The carbohydrate does cover a large surface area (450 $Å^2$ in the IgE-Fc) approximately half of which shields hydrophobic residues. However, as stated previously, the Fcε3-4 fragment can be refolded from *E. coli* inclusion bodies (Henry, 1997), indicating that carbohydrate is not essential for folding. In fact, the only lateral interaction observed in the crystal structures is that between opposing Fcε4 domains. This appears to be the region that enables dimerisation of the Fcε3-4 chains. The possible interactions necessary for stabilising Fcε3 are outlined in the schematic below, figure 3.2.

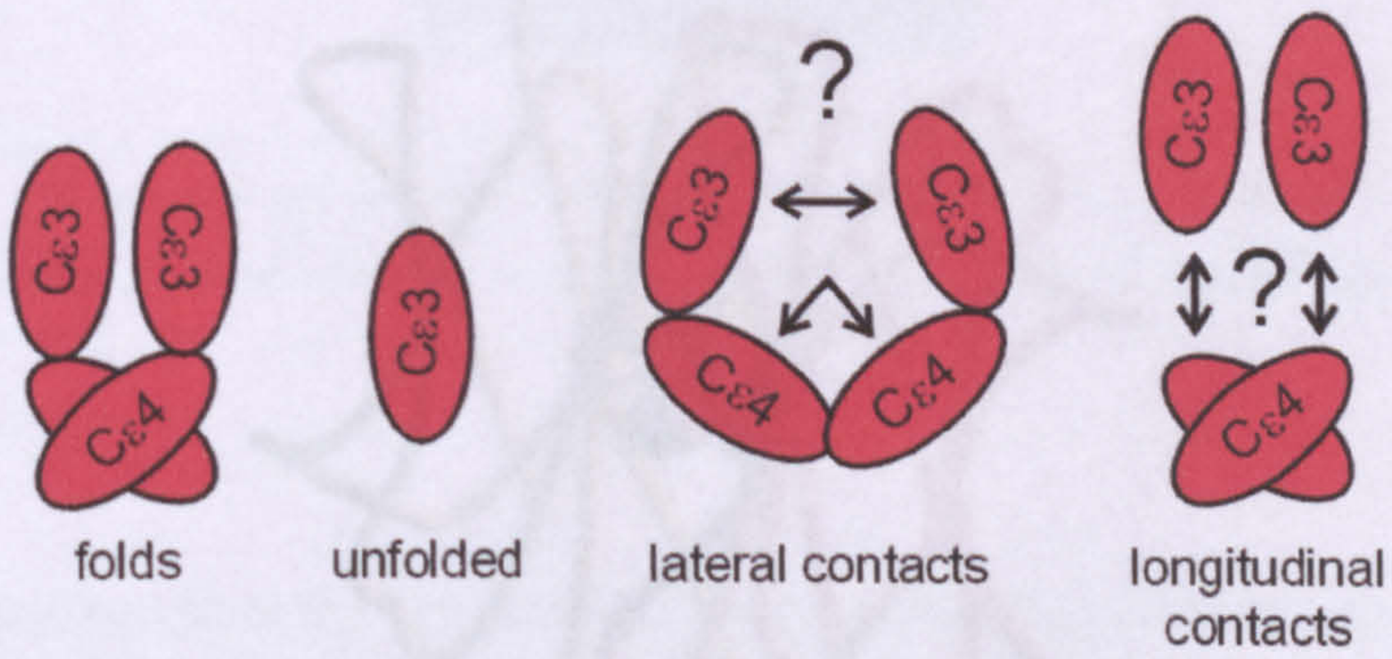

Figure 3.2: Possible contacts necessary for folding Fcε3. A red ellipse represents each domain; arrows indicate contacts that could be essential for folding.

If the factors that lead to the folding of Fcε3 are to be determined, it would appear a method in which the lateral and longitudinal contacts within the Fcε3-4 dimer could be isolated, might provide an answer. In order to isolate the effects of these contacts on the folding of Fcε3, novel sub-fragments were

designed and expressed in *E. coli*. Initially it was decided to investigate the effect of longitudinal contacts on the folding of Fcε3 to determine whether the broad interface between Fcε3 and Fcε4 could act as a scaffold for folding of Fcε3.

3.2 Production of a Fcε3-4 monomer

To isolate the effect of longitudinal contacts from those of lateral contacts it was necessary to produce a monomeric Fcε3-4 population. To achieve this, the most promising way appeared to be disruption of the Fcε4:Fcε4 interface, as from the crystal structures this interaction seemed to provide the platform for non-covalent dimerisation of the Fcε3-4 fragment. It was hypothesised that if a single point mutation was introduced into the structure at the appropriate place, dimerisation could be prevented, thus yielding a monomeric fragment. When the interface was examined closely, the ideal candidate looked to be a phenylalanine at position 506. This packed closely with its twin in the opposing chain (see figure 3.3). It was predicted that introduction of a large, charged side chain such as arginine in its place would yield a monomeric fragment by like-charge repulsion.

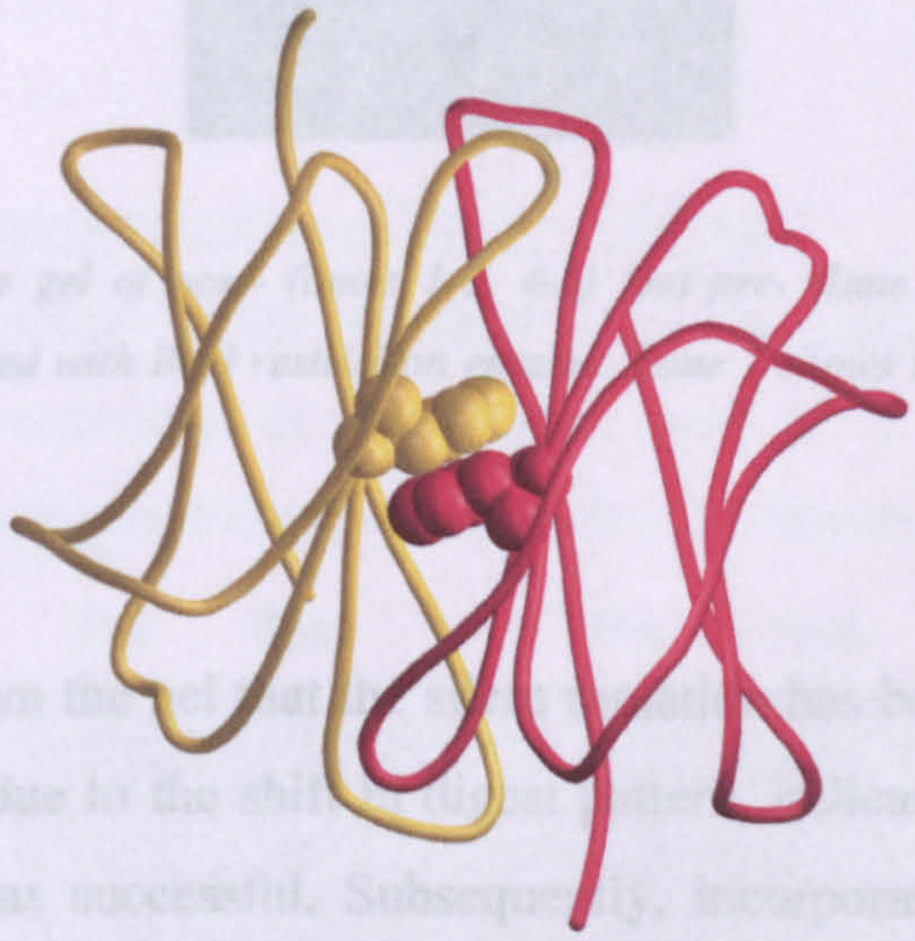

Figure 3.3: Fcε4 dimer with phenylalanine 506 space-filled (opposing chains are coloured red and yellow- C-α only).

3.3 Introduction of the F506R mutation into pET Cε3-4ΔC

The phenylalanine to arginine (F506R) mutation was introduced into the Cε3-4ΔC pET vector using the Quickchange™ system from Stratagene; this method is outlined in section 2.1. The Fcε3-4ΔC vector was engineered previously for expression of Fcε3-4 in *E. coli* (Henry, 1997), with the N-terminal cysteine residues removed to aid the refolding process by reducing the potential for aggregation due to the formation of non-native disulphides. Silent mutations were also incorporated into the vector using the mutation encoding primers to enable quick identification of F506R positive clones. These silent mutations knocked out a restriction site (BbsI). Digests of pre-and post mutation vectors can be seen in figure 3.4.

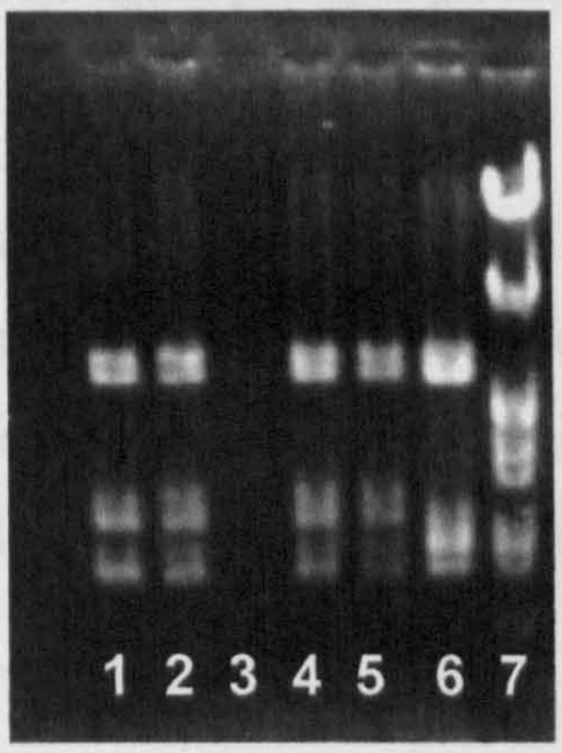

Figure 3.4: 1% agarose gel of post- (lanes 1-2, 4-5) and pre- (lane 6) mutated Fcε3-4 pET expression vector digested with BbsI restriction enzyme. Lane 7 shows Hind III digested lambda DNA.

It is clear from the gel that the silent mutation has been incorporated into the mutated vector due to the shift in digest pattern, indicating that the directed mutation process was successful. Subsequently, incorporation of the mutation and fidelity of replication was confirmed by sequencing of the targeted region, see figure 3.5.

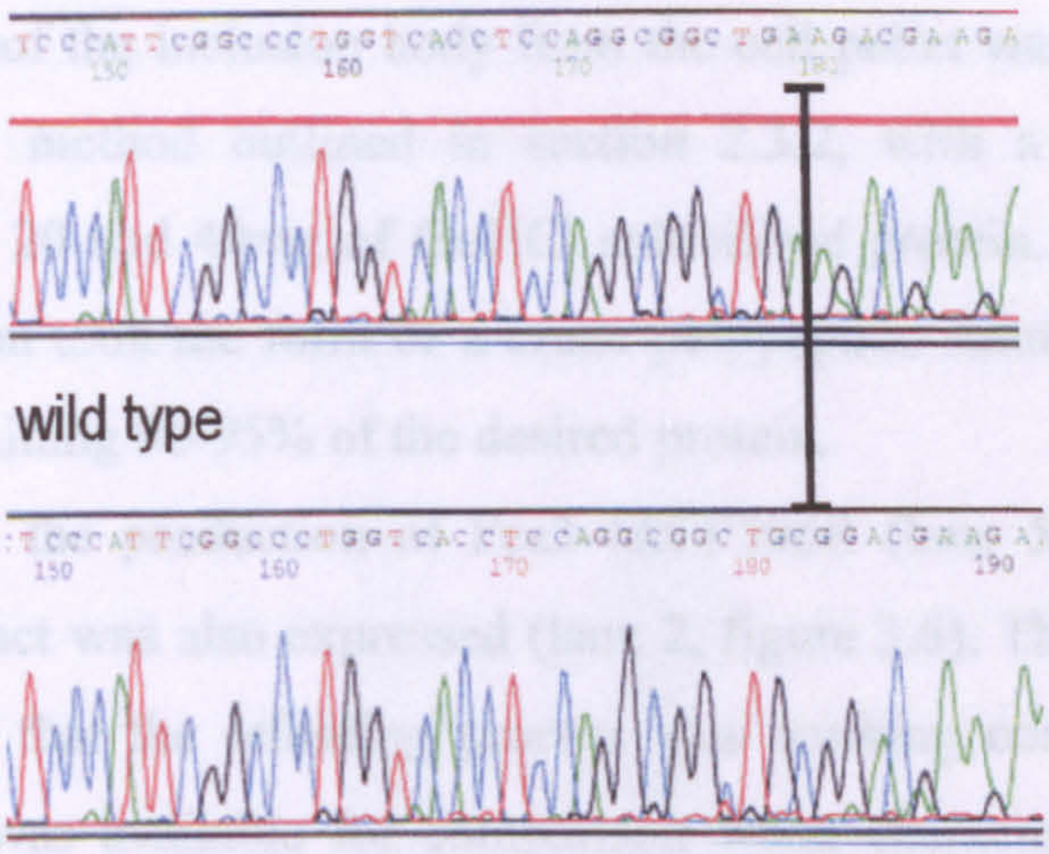

Figure 3.5: Sequence profiles of wild type and mutated Fcε4 in the domain interface target region. The black bar indicates the mutagenic primer target sequence.

The sequence obtained from the mutated and wild type pET vectors were identical except for the shifts intended. The phenylalanine codon has been switched to an arginine codon in the mutated vector. In addition the restriction site BbsI had been knocked out with the silent mutation. Other coding regions were not mutated.

3.4 Expression and purification of Fcε3-4 F506RΔC

After confirmation of the introduction of the mutation into the Fcε3-4 vector, protein was expressed as an inclusion body in *E. coli*. (BL21* DE3). SDS-PAGE of pre- and post induction cell pellets are shown in figure 3.6.

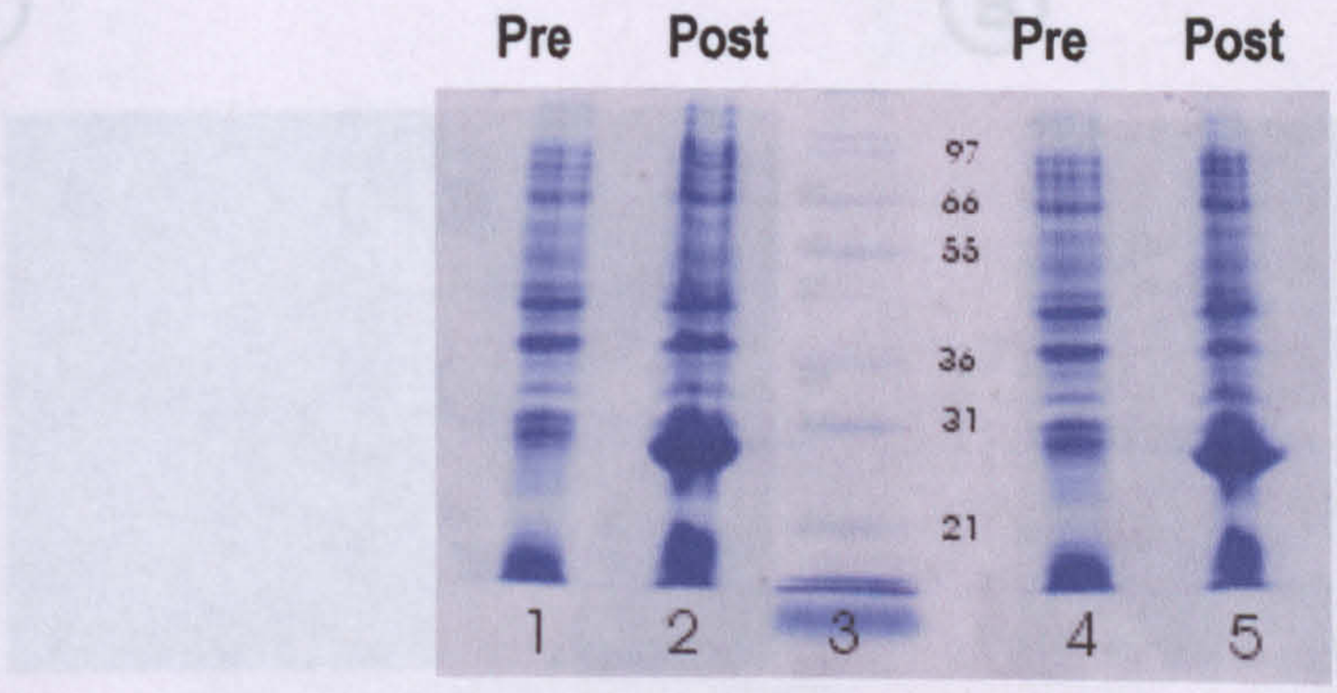

Figure 3.6: 12% SDS-PAGE of pre-induction (lanes 1 and 4) and post-induction (lanes 2 and 5) cultures of Fcε3-4ΔC (left) and Fcε3-4ΔC F506R (right), molecular weight markers lane 3.

Recovery of the inclusion body from the cell pellet was then carried out according to the method outlined in section 2.3.2, with a one-litre culture yielding between 20 and 40mg of GuHCl solubilised protein. At this stage the protein preparation took the form of a crude polypeptide solution solubilised in 6 M GuHCl containing 90-95% of the desired protein.

Alongside the production of Fcε3-4ΔCF506R (lane 5, figure 3.6), the Fcε3-4ΔC construct was also expressed (lane 2, figure 3.6). This was to act as a control, ensuring that the refolding process was working correctly and that a suitable species was available for comparison when characterising the F506R mutant. Once inclusion body material had been solubilised, a further purification step was carried out to isolate protein material from nucleic acid. This step is illustrated both for Fcε3-4ΔC and the F506R mutant in figure 3.7. The main benefit of this was that it enabled more accurate determination of protein concentration for the refolding process, which is critical for assessing the ratio of DTT and oxidised glutathione to free sulphydryl groups in the target protein.

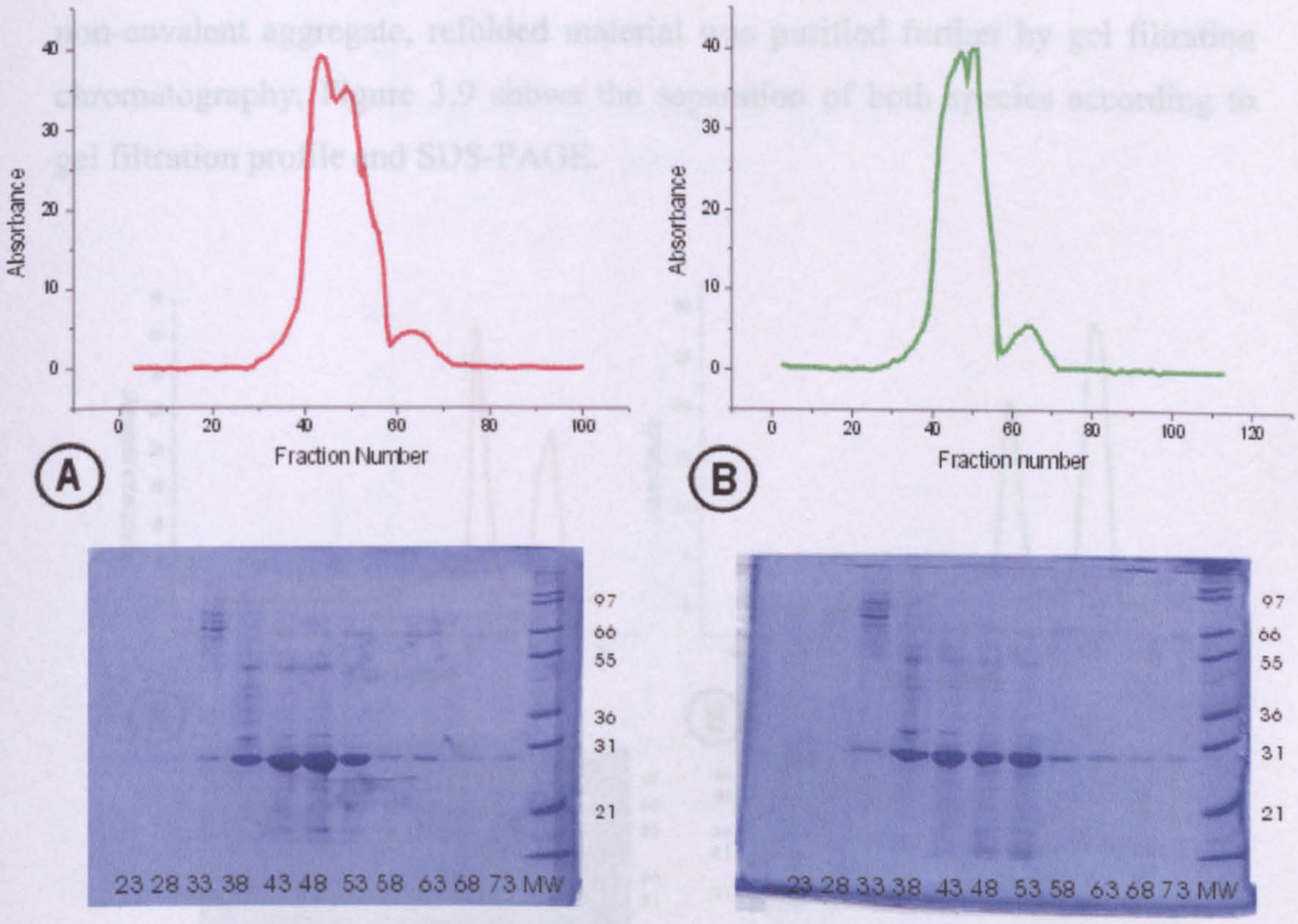

Figure 3.7: Panel A = Fcε3-4ΔC F506R, panel B = Fcε3-4ΔC. Gel filtration (S300 – see section 2.3.2 for conditions) profiles above, corresponding SDS-PAGE of peak fractions below.

After separation, material of the correct molecular weight was combined and subjected to the refolding protocol outlined in section 2.3.3. The material was also Western blotted with an anti-IgE polyclonal antibody (P293 – Dako) to ensure isolation of the correct species (see below):

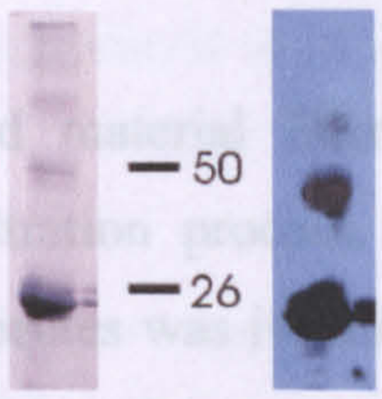

Figure 3.8: Non-reducing SDS-PAGE (left) and corresponding Western blot (right) of Fcε3-4ΔC F506R.

The blot in figure 3.8 shows a non-reduced sample of Fcε3-4ΔC F506R after refolding but prior to HPLC purification. Because this sample has not been treated with either DTT or mercaptoethanol, covalent aggregates can be seen above the major monomeric fraction at 26 kDa. To remove both covalent and non-covalent aggregate, refolded material was purified further by gel filtration chromatography. Figure 3.9 shows the separation of both species according to gel filtration profile and SDS-PAGE.

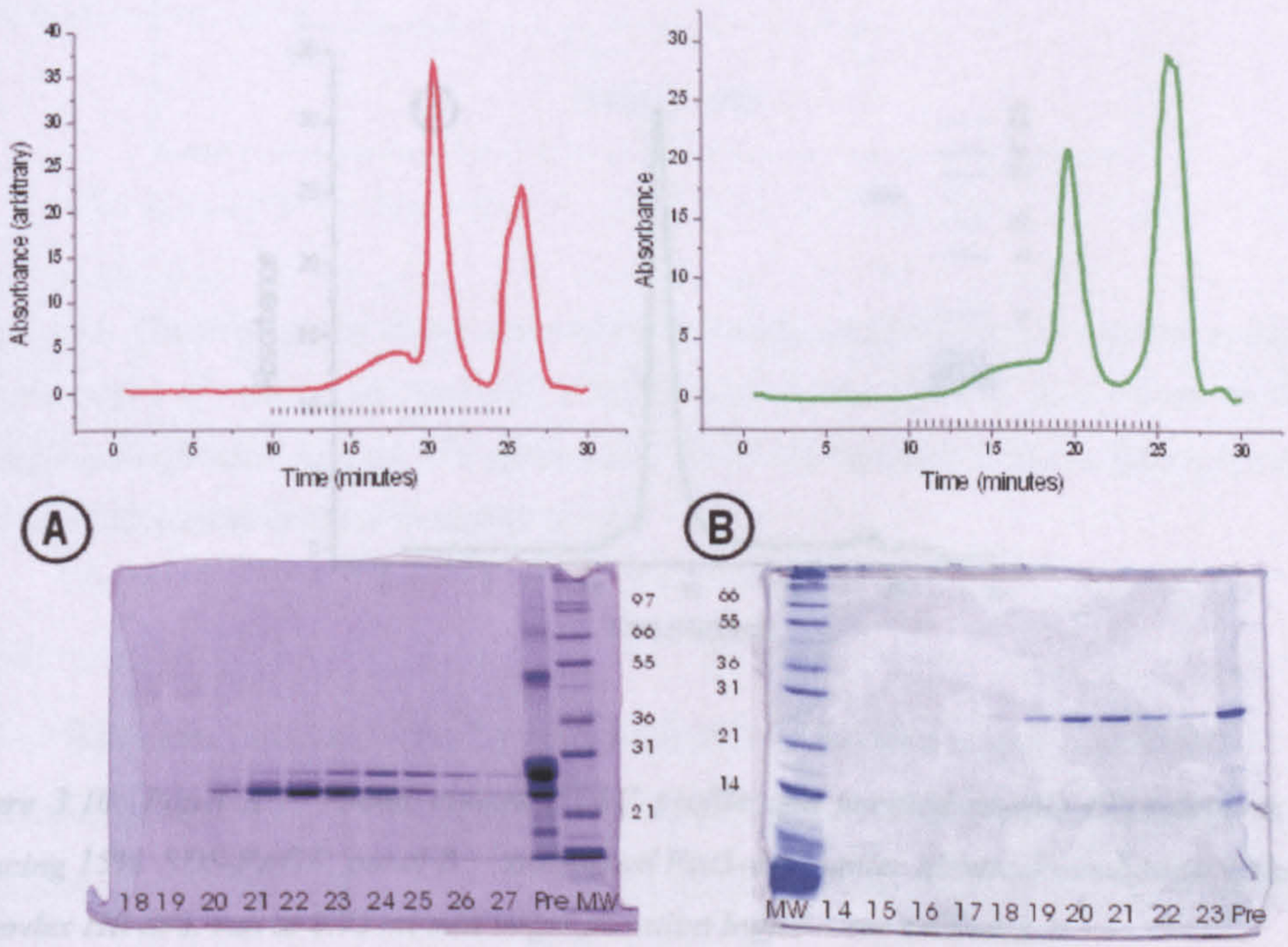

Previous page.

Figure 3.9: Panel A = gel filtration profile (above) and 12% non-reducing SDS-PAGE (below) of Fcε3-4ΔC F506R. Panel B = identical to A except now the Fcε3-4ΔC construct. Marks on the x-axis indicate fractions taken; these correspond to the fraction number shown at the bottom of each gel lane. Column – Superdex HR S200, run at 0.75 ml/min in gel filtration buffer – see section 2.1.

To separate the desired material from aggregate it was sometimes necessary to repeat the gel filtration process, depending on the preparation. However, eventually a single species was isolated for both constructs according to both SDS-PAGE and gel filtration chromatography, see figure 3.10.

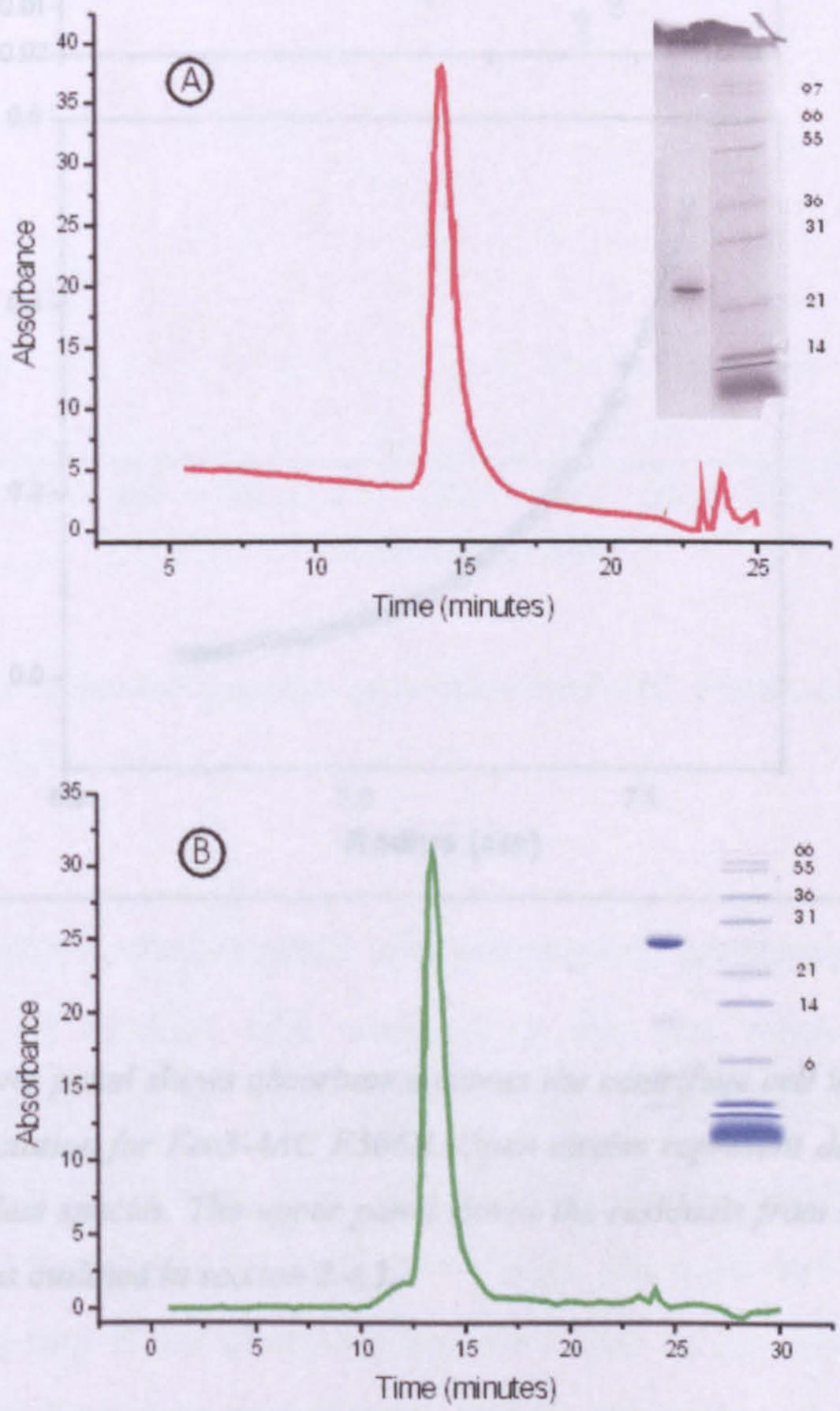

Figure 3.10: Panel A = F506R mutant HPLC profile and purified sample of protein on non-reducing 15% SDS-PAGE, panel B = unmutated Fcε3-4ΔC under identical conditions. Column – Superdex HR S75, run at 0.75 ml/min in gel filtration buffer – see section 2.1.

3.5 Characterisation of Fcε3-4 F506RΔC

Isolation of purified material enabled a more detailed characterisation to be carried out. Firstly the Cε3-4ΔCF506R mutant was analysed by sedimentation equilibrium analytical ultracentrifugation to obtain an accurate assessment of the isolated protein's molecular weight. From this it would be possible to ascertain whether the material was truly monomeric in solution. A representative trace for this can be seen in figure 3.11.

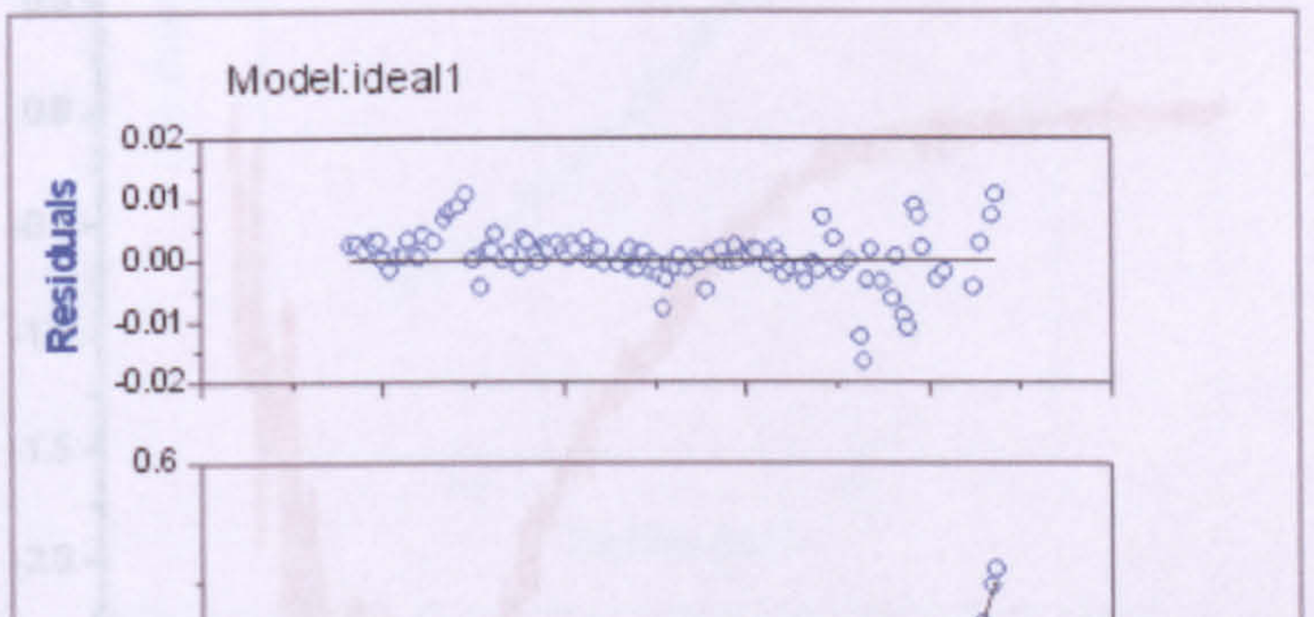

Figure 3.11: The lower panel shows absorbance across the centrifuge cell in relation to distance from the centre of rotation for Fcε3-4ΔC F506R. Open circles represent data points, the line is the fit for a single ideal species. The upper panel shows the residuals from the fitting procedure. Data was collected as outlined in section 2.4.3.

The data obtained fitted a single ideal species model and yielded a molecular weight of 27500 ± 1100. This is a slight overestimate compared to the calculated molecular weight of 24,561 (Sedenterp), but does confirm the protein

to be monomeric, i.e. a single Fcε3-4 chain. The overestimate may be due to a small amount of aggregate forming in the sample over time; this was reflected in the fact higher speeds produced data that delivered more satisfactory fits. An explanation for this observation presented itself when the circular dichroism spectrum of the F506R fragment was measured, see figure 3.12.

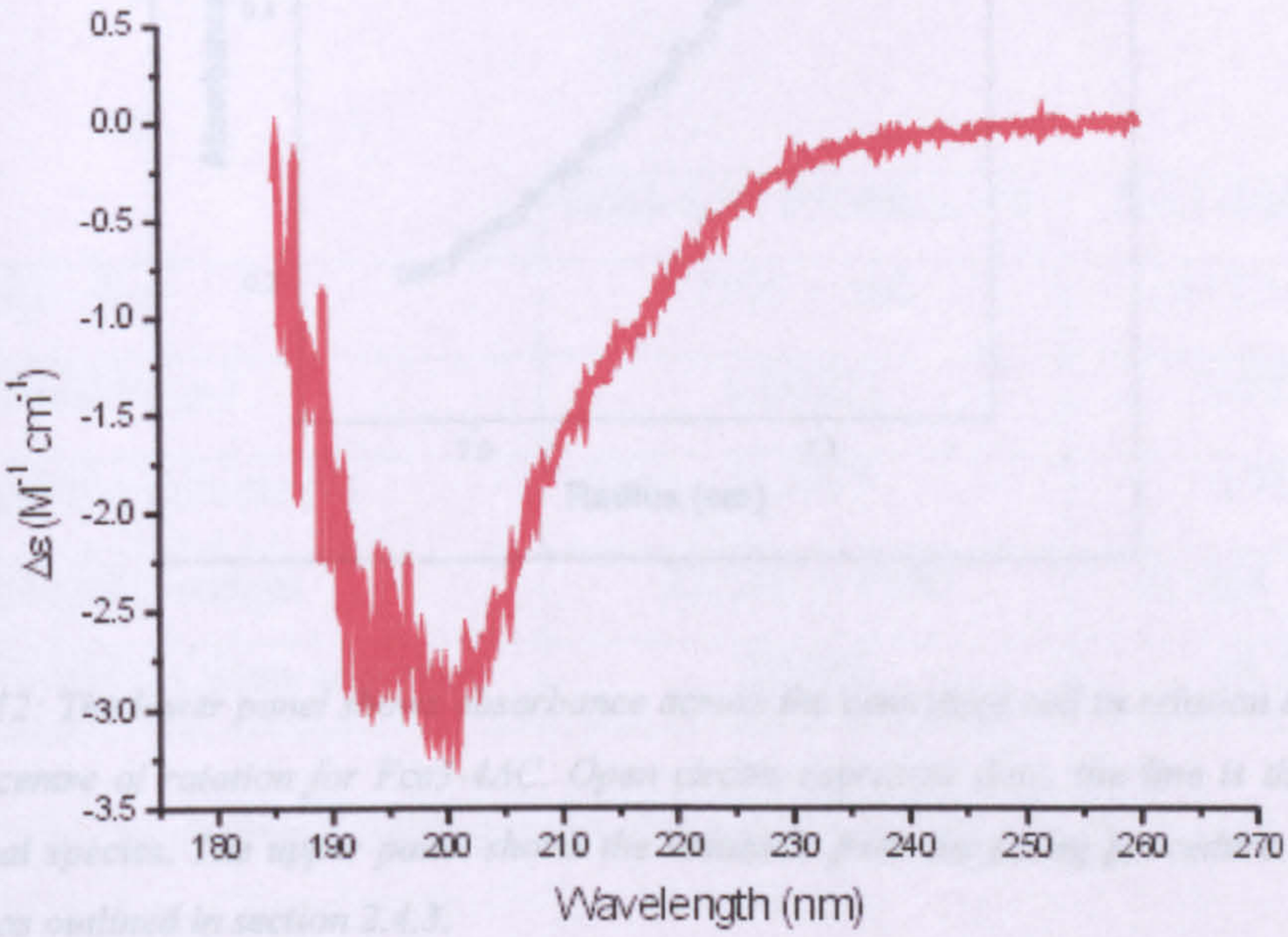

Figure 3.12: Circular dichroism spectrum of purified Fcε3-4ΔC F506R. Data was collected as outlined in section 2.4.1.

The spectrum is characteristic of a polypeptide preparation composed of a large proportion of random coil, suggesting that the monomeric species is unfolded. It is therefore of little surprise that some degree of aggregation occurred in the ultracentrifuge over the lifetime of the experiment (~3 days), probably due to hydrophobic interactions between the unfolded monomers.

To ensure that these observations were due to the incorporation of the F506R mutation, rather than an incorrect refold procedure, they were compared to results from refolding the Fcε3-4ΔC dimer. This was carried out under identical conditions, see figures 3.12 and 3.13

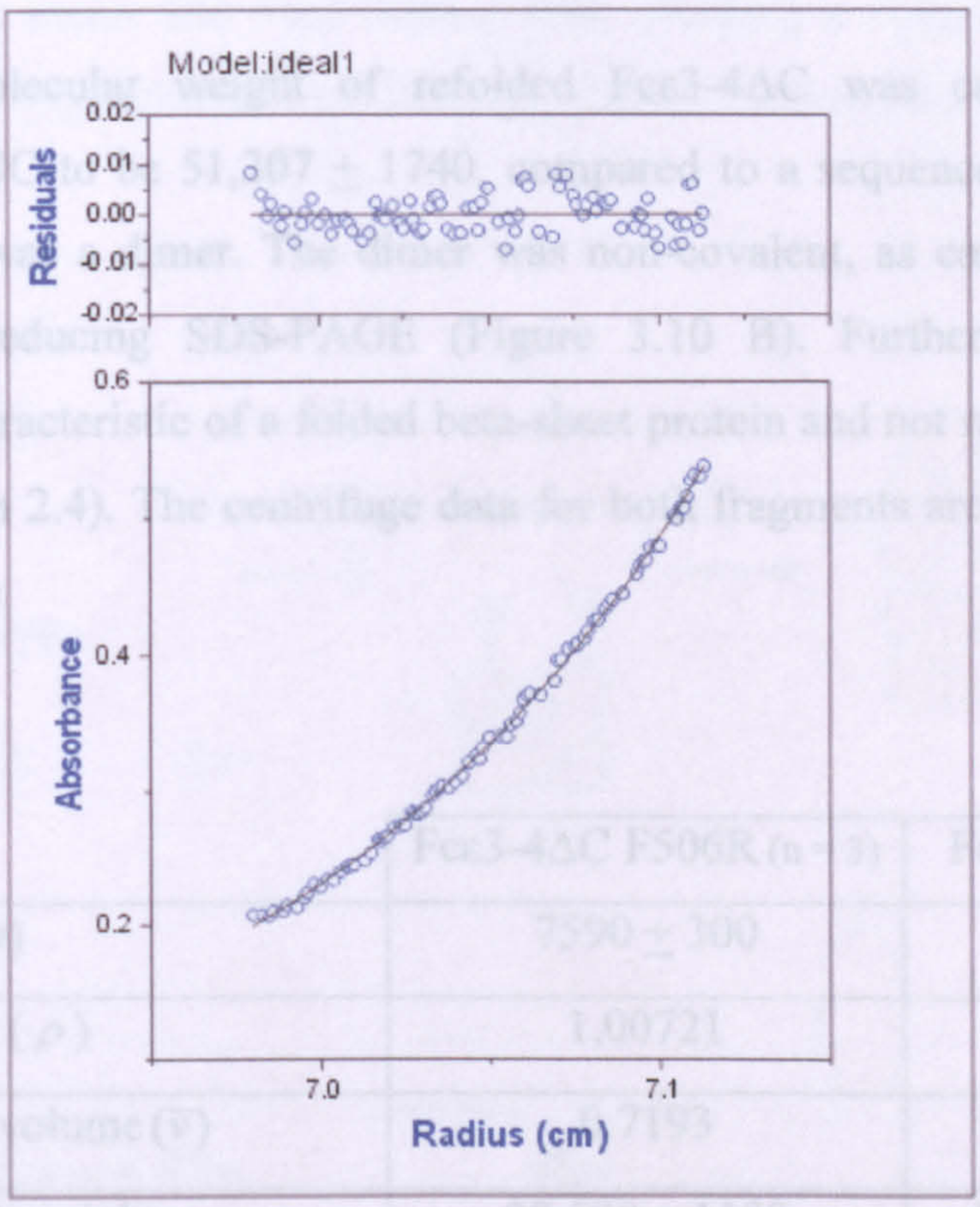

Figure 3.12: The lower panel shows absorbance across the centrifuge cell in relation to distance from the centre of rotation for Fcε3-4ΔC. Open circles represent data, the line is the fit for a single ideal species. The upper panel shows the residuals from the fitting procedure. Data was collected as outlined in section 2.4.3.

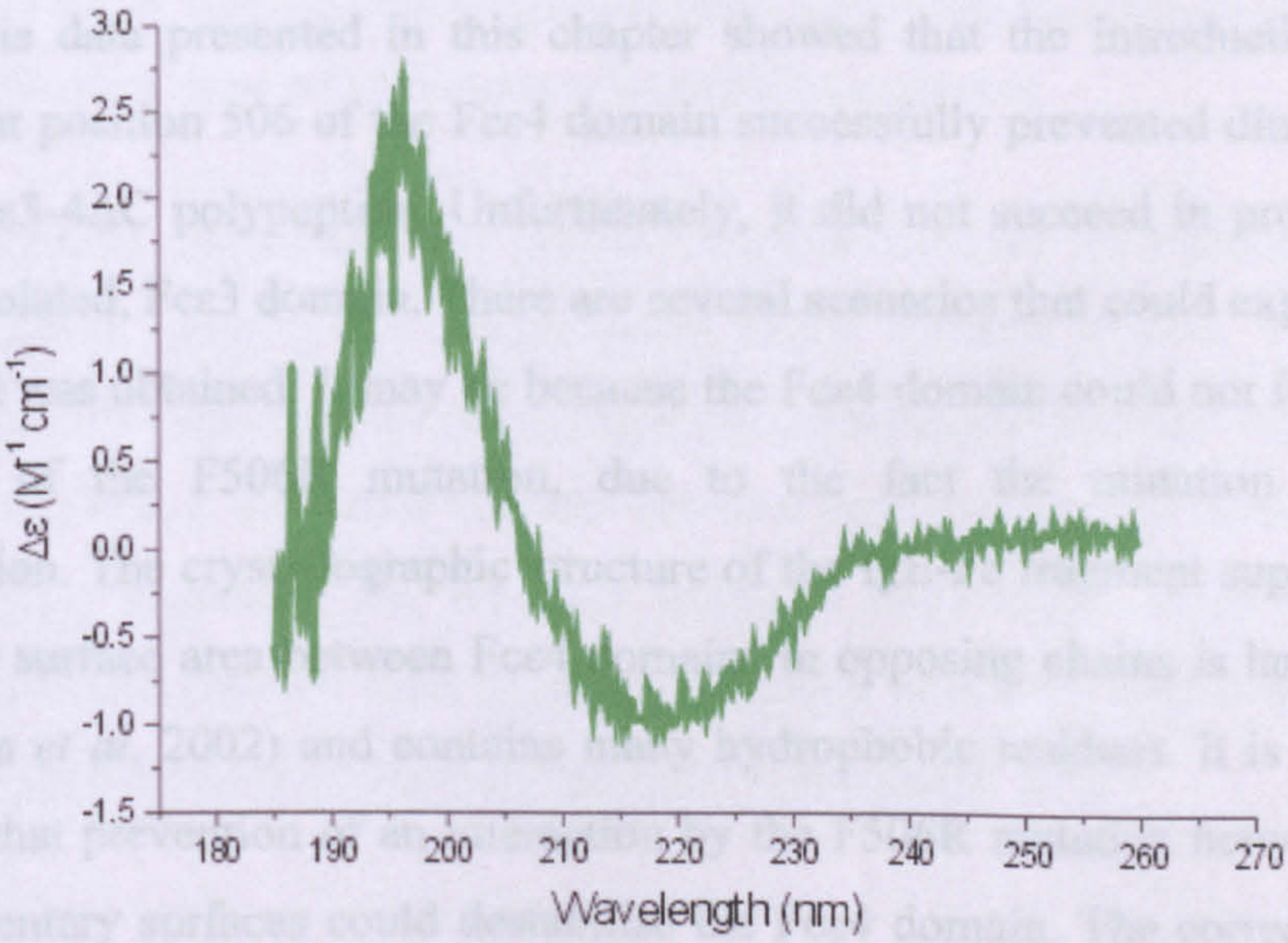

Figure 3.13: Circular dichroism spectrum of Fcε3-4ΔC. Data was collected as outlined in section 2.4.1.

The molecular weight of refolded Fcε3-4ΔC was calculated using equilibrium AUC to be 51,307 ± 1740, compared to a sequence calculation of 49,106, i.e. it was a dimer. The dimer was non-covalent, as can be seen from previous non-reducing SDS-PAGE (Figure 3.10 B). Furthermore, the CD spectrum is characteristic of a folded beta-sheet protein and not random coil (see methods section 2.4). The centrifuge data for both fragments are summarised in the table below:

	Fcε3-4ΔC F506R (n = 3)	Fcε3-4ΔC (n = 5)
Mean $M(1-\bar{v}\rho)$	7590 ± 300	14115 ± 480
Solvent density (ρ)	1.00721	1.00721
Partial specific volume ($\bar{v}$)	0.7193	0.7197
Mean molecular weight	27,500 ± 1100	51,307 ± 1740
Molecular weight from sequence	24,561	49,106

Table 3.1: Data for analytical centrifuge runs with mutated and unmutated Fcε3-4ΔC.

3.6 Discussion

The data presented in this chapter showed that the introduction of an arginine at position 506 of the Fcε4 domain successfully prevented dimerisation of the Fcε3-4ΔC polypeptide. Unfortunately, it did not succeed in producing a folded, isolated, Fcε3 domain. There are several scenarios that could explain why this result was obtained. It may be because the Fcε4 domain could not fold in the presence of the F506R mutation, due to the fact the mutation prevents dimerisation. The crystallographic structure of the IgE-Fc fragment supports this idea. The surface area between Fcε4 domains in opposing chains is large (2326 $Å^2$ – Wan *et al*, 2002) and contains many hydrophobic residues. It is therefore possible that prevention of an interaction by the F506R mutation between these complementary surfaces could destabilise the Fcε4 domain. The correct folding of the Fcε4 domain may normally provide a contact surface area for Fcε3 within the same chain to stabilise folding of the Fcε3 domain. Absence of a folded Fcε4

might therefore mean that Fcε3 cannot fold, yielding a completely unfolded, monomeric Fcε3-4 fragment. This folding pathway is illustrated schematically in figure 3.14.

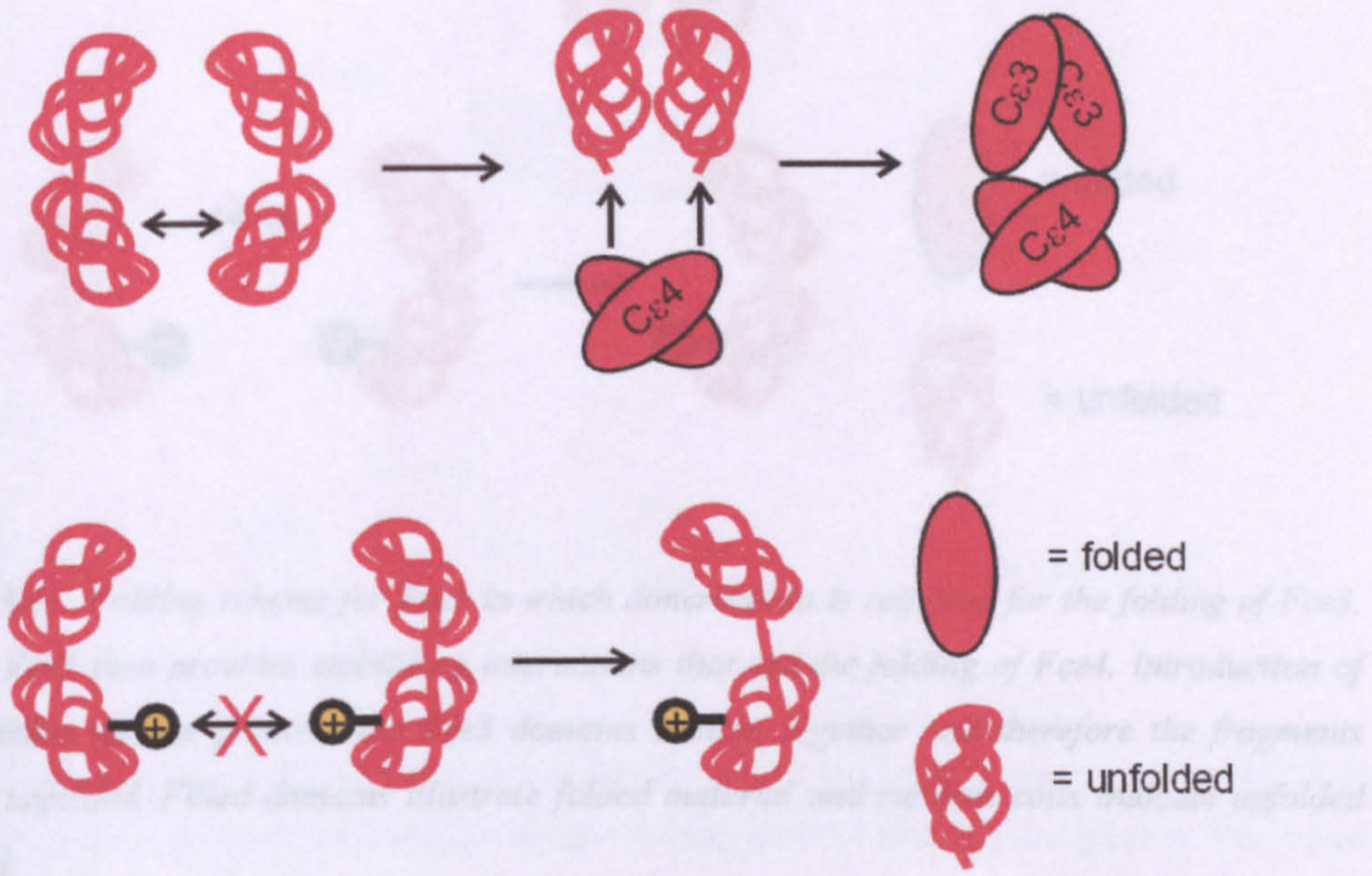

Figure 3.14: Folding scheme for Fcε3 in which folded, dimerised Fcε4 is required as a contact surface to fold Fcε3. Filled domains illustrate folded material, random coils indicate unfolded material. The upper row represents unfolded (or partially folded) Fcε3-4 monomers coming together; the dimerised Fcε4 domains fold completely and then provide contacts for Fcε3 to fold. In the second row the arginine mutation prevents dimerisation of the Fcε4 domain and therefore the chain of events is disrupted, resulting in unfolded Fcε3-4 monomers.

However, there are other possible explanations for the observed result. For example, it may be that Fcε3 requires lateral contacts to fold. The folded Fcε3 could then stabilise Fcε4 using the same intra-domain contacts described in figure 3.14. Thus, if the lateral contacts between Fcε3 domains are prevented due to the charge repulsion, the resultant unfolded Fcε3 might mean that Fcε4 remains unfolded because there is no inter-domain interface. This is basically a reverse of the processes outlined in figure 3.14, see figure 3.15.

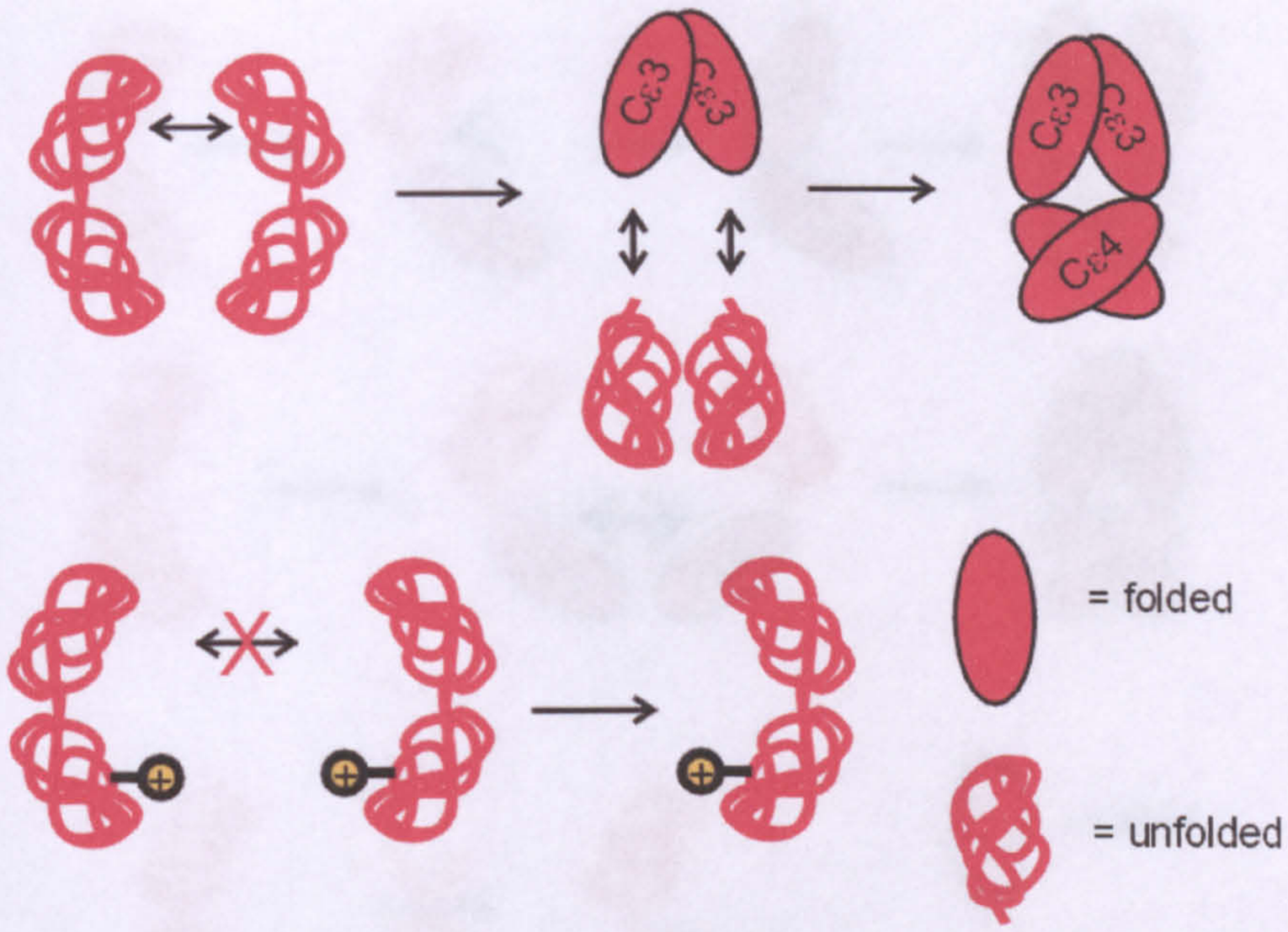

Figure 3.15: Folding scheme for Fcε3 in which dimerisation is required for the folding of Fcε3. Folded Fcε3 then provides stabilising interactions that aid the folding of Fcε4. Introduction of the arginine residue prevents the Fcε3 domains coming together and therefore the fragments remain unfolded. Filled domains illustrate folded material and random coils indicate unfolded material.

This scheme is less likely as direct contacts between Fcε3 domains have not been observed in three IgE-Fc domain crystal structures (Garman *et al*, 2000; Wurzburg *et al*, 2000; Wan *et al*, 2002). Furthermore, the Fcε3 domains are unable to pair together and fold in isolation, as demonstrated by work carried out on an isolated Fcε3 domain (Henry *et al*, 2000).

A more complicated situation could also exist, in which a reciprocal relationship involving Fcε3 and Fcε4, dimerisation and intra-domain contacts are all necessary for folding. Put simply, if one or all of these stabilising factors is removed by the introduction of the arginine mutation it could cause the system to unravel.

Finally, the F506R mutation may have a more direct effect on Fcε4 folding by interfering with, or preventing initiation of the folding pathway of the domain itself. This would then have downstream effects on the folding of Fcε3 by removing any favourable inter- or intra-chain contacts that Fcε4 can provide when folded either as a dimer or monomer, see figure 3.16.

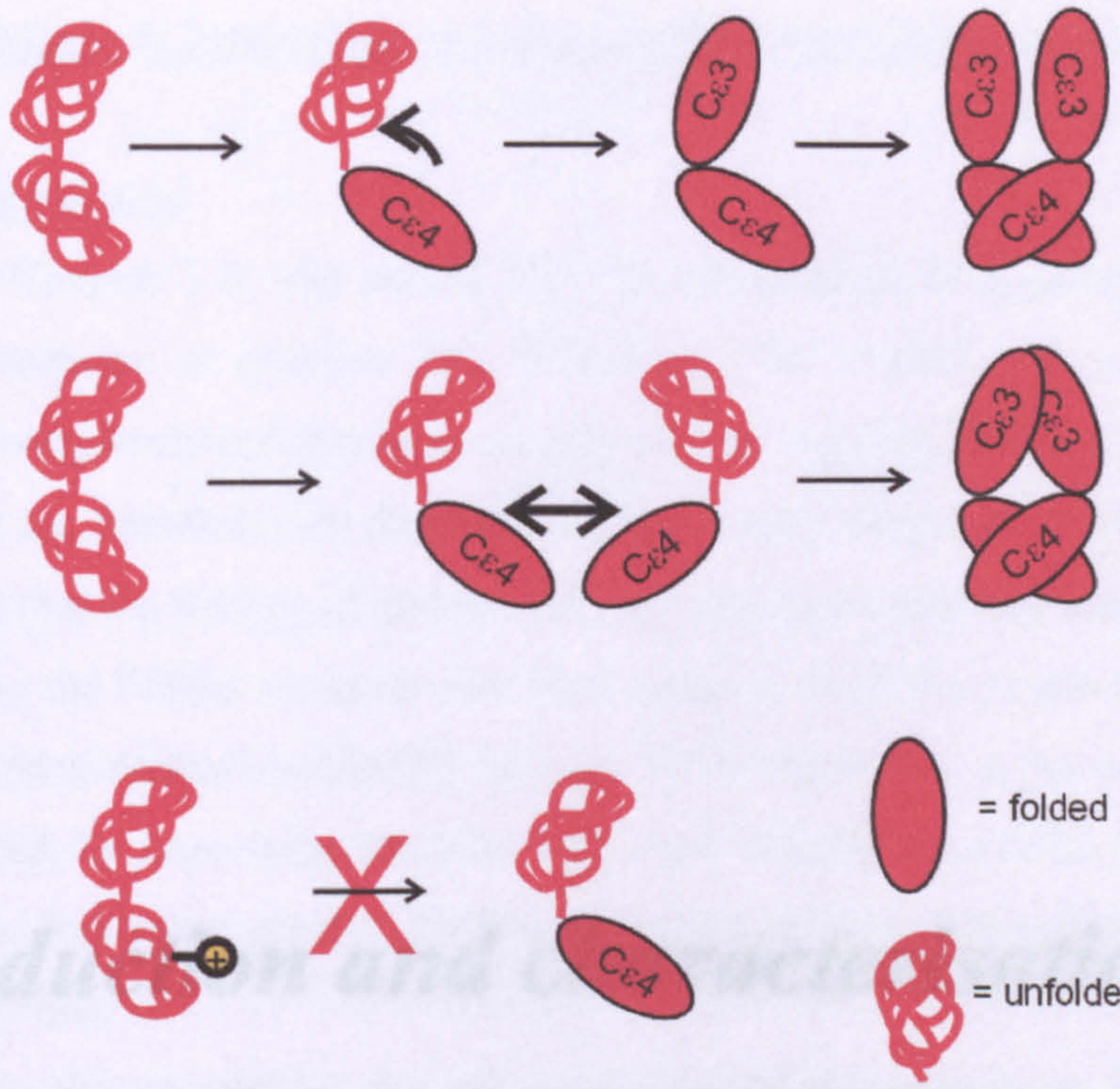

Figure 3.16: Possible mode of F506R destabilisation of the Fcε3-4ΔC fragment. Introduction of the arginine mutation prevents the Fcε4 domain folding and the downstream effect of this is that Fcε3 cannot fold as a result of the prevention of favourable inter- or intra-chain contacts (or both) provided either directly by Fcε4, or by the fact that it causes the chains to dimerise once folded.

The most straightforward outcome from these experiments on the monomeric Fcε3-4 fragments would have been the observation of either two folded domains, or a polypeptide in which one domain was folded and the other was not. However, the whole fragment appears to be unfolded. Thus it is impossible to distinguish whether lateral contacts between Fcε4 domains, Fcε3 domains, or a mixture of both effects are mediating folding, or indeed whether the F506R destabilises the fragment in a way that is not dependent upon contacts between Fcε4 domains. To help resolve the issue of the effect of F506R on Fcε4 folding, it was decided to investigate the Fcε4 fragment in isolation. By incorporating the F506R mutation into a single Fcε4 domain, the effect of the mutation could be observed in the absence of any influence of unstructured Fcε3. Furthermore, folding of an Fcε4 wild type domain could also be studied for comparison, yielding information about the necessity of Fcε3 for the folding of wild type Fcε4.

Production and characterisation of Fcε4 and Fcε4 F506R

Chapter 4: Production and characterisation of Fcε4 and Fcε4 F506R

4.1 Introduction

In Chapter 3 it was shown that the introduction of a phenylalanine to arginine mutation at position 506 (F506R) of the Fcε3-4 polypeptide chain yielded a completely unfolded monomeric protein fragment. However, it was not clear how the mutation was destabilising the Fcε3-4 fragment. It was therefore concluded that the folding of an isolated Fcε4 domain would be investigated. By introducing the F506R mutation into Fcε4 alone it would be possible to identify whether this mutation was directly responsible for destabilising the Fcε4 domain. Furthermore, by expressing the wild type Fcε4 domain in parallel, it would be possbile to determine whether Fcε3 has any role to play in the stabilisation and folding of Fcε4.

In order to analyse the effect of the F506R mutant on Fcε4 it was necessary to express the wild-type domain in isolation. Although an isolated Fcε3 domain had been expressed (Henry *et al*, 2000), Fcε4 had not been produced before. This was essential in order to determine whether any destabilisation observed in a F506R mutant was solely due to the incorporation of the mutation, rather than removal of beneficial Fcε3 contacts. It would also ensure that the refolding process was functioning correctly for the truncated fragment.

If the Fcε4 domain folded in isolation it would indicate that this domain has the potential to structure itself first within the Fcε3-4 fragment. It could then perhaps serve to facilitate Fcε3 folding. Evidence from the crystal structures (Garman *et al*, 2000; Wurzburg *et al*, 2000; Wan *et al*, 2002 – as discussed in Chapter 3) indicates the Fcε4 region is responsible for dimerisation. However, it is not clear what relation this dimerisation process has to folding. In Chapter 3 it was proposed that one possible reason for the observed results was that dimerisation is essential for Fcε4 folding. However, if a folded Fcε4 monomer were obtained it would indicate dimerisation was not essential for folding. It would also imply a more complex process of dimer formation involving Fcε3. Thus, expression of an Fcε4 domain in isolation would provide more information regarding the Fcε3-4 folding pathway, in addition to providing a basis for evaluating the effect of the F506R mutation (see figure 4.1).

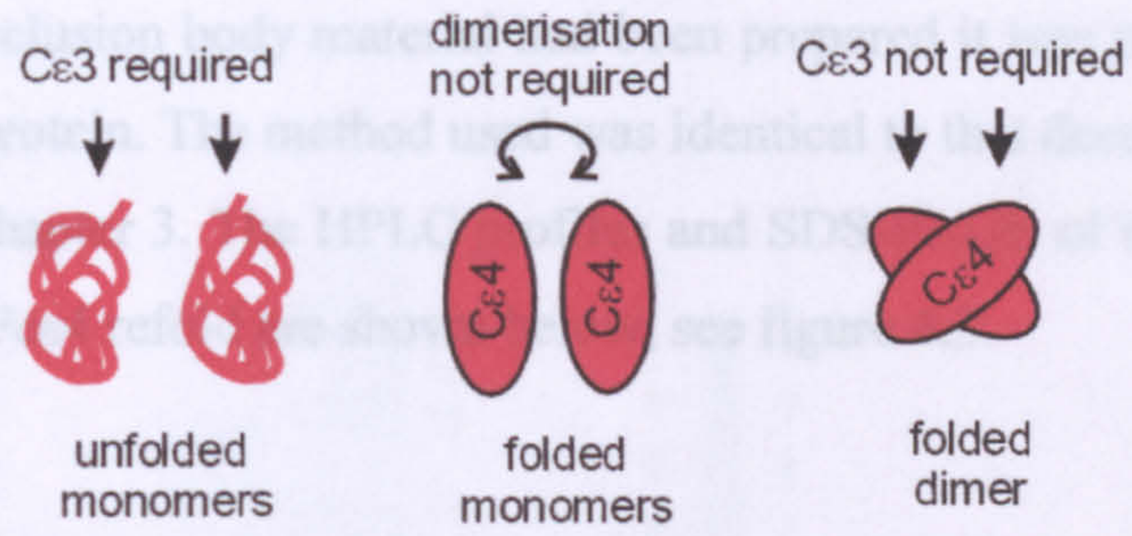

Figure 4.1: Schematic indicating possible results from folding Fcε4 in isolation.

4.2 Expression and purification of a Fcε4 domain

The Fcε4 domain had previously been cloned into the pET 15 expression vector (Alistair Henry - unpublished). This construct included a hexa-histidine tag at the C-terminus to enable easy purification of the fragment. The pET 15 vector was otherwise used in an identical fashion to the pET 5a vector. However, this construct had not been fully characterised previously and therefore the first step was to express the protein and isolate pure material for biophysical characterisation. Initially, purification was carried out according to the same protocol used for the larger Fcε3-4 fragments, rather than a nickel affinity column method. This involved isolating and solubilising inclusion bodies over-expressed in transformed BL21* (DE3) *E. coli*, see figure 4.2.

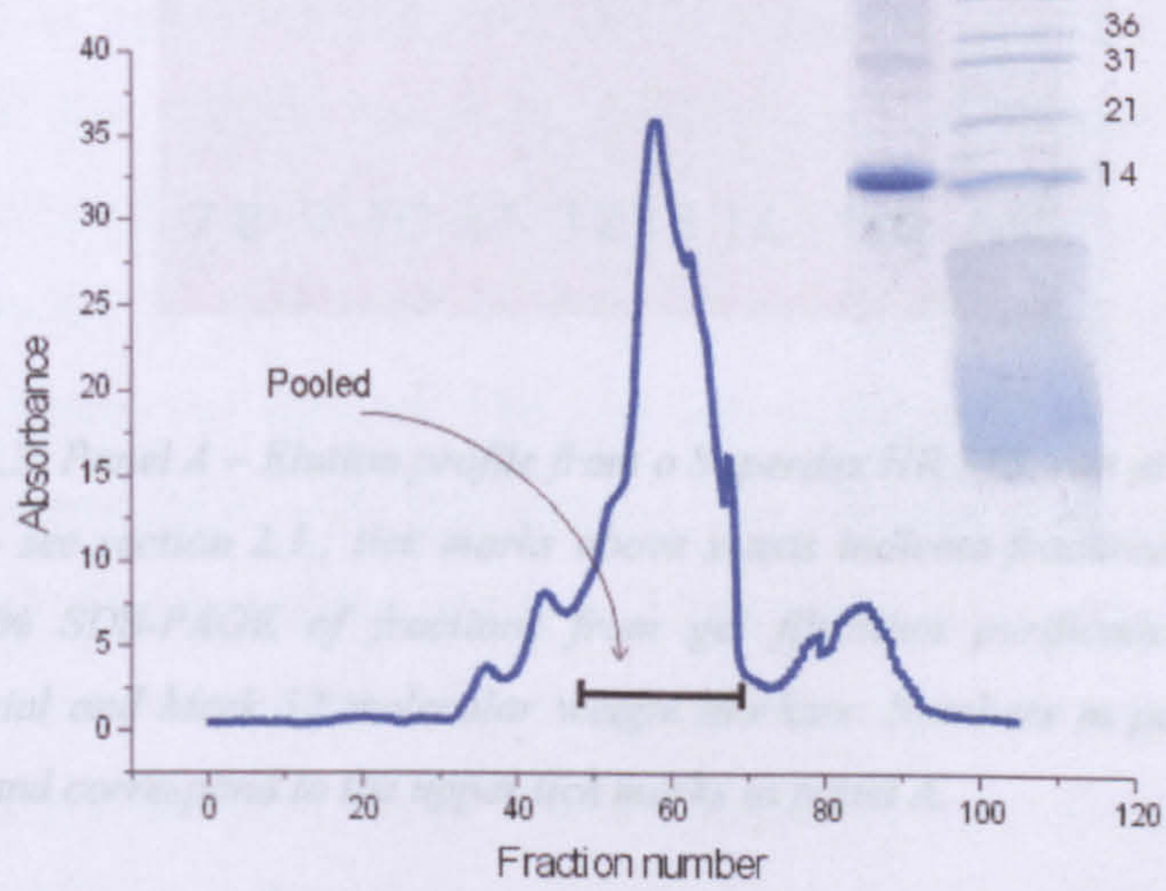

Figure 4.2: Gel filtration profile (S300 – see section 2.3.2 for conditions) indicating pooled fractions of GuHCl solubilised E. coli expressed material. Inset: reducing 20% SDS-PAGE of pooled fractions.

Once inclusion body material had been prepared it was possible to refold the denatured protein. The method used was identical to that described for Fcε3-4 fragments in Chapter 3. The HPLC profiles and SDS-PAGE of isolated fractions from a typical Fcε4 refold are shown below, see figure 4.3.

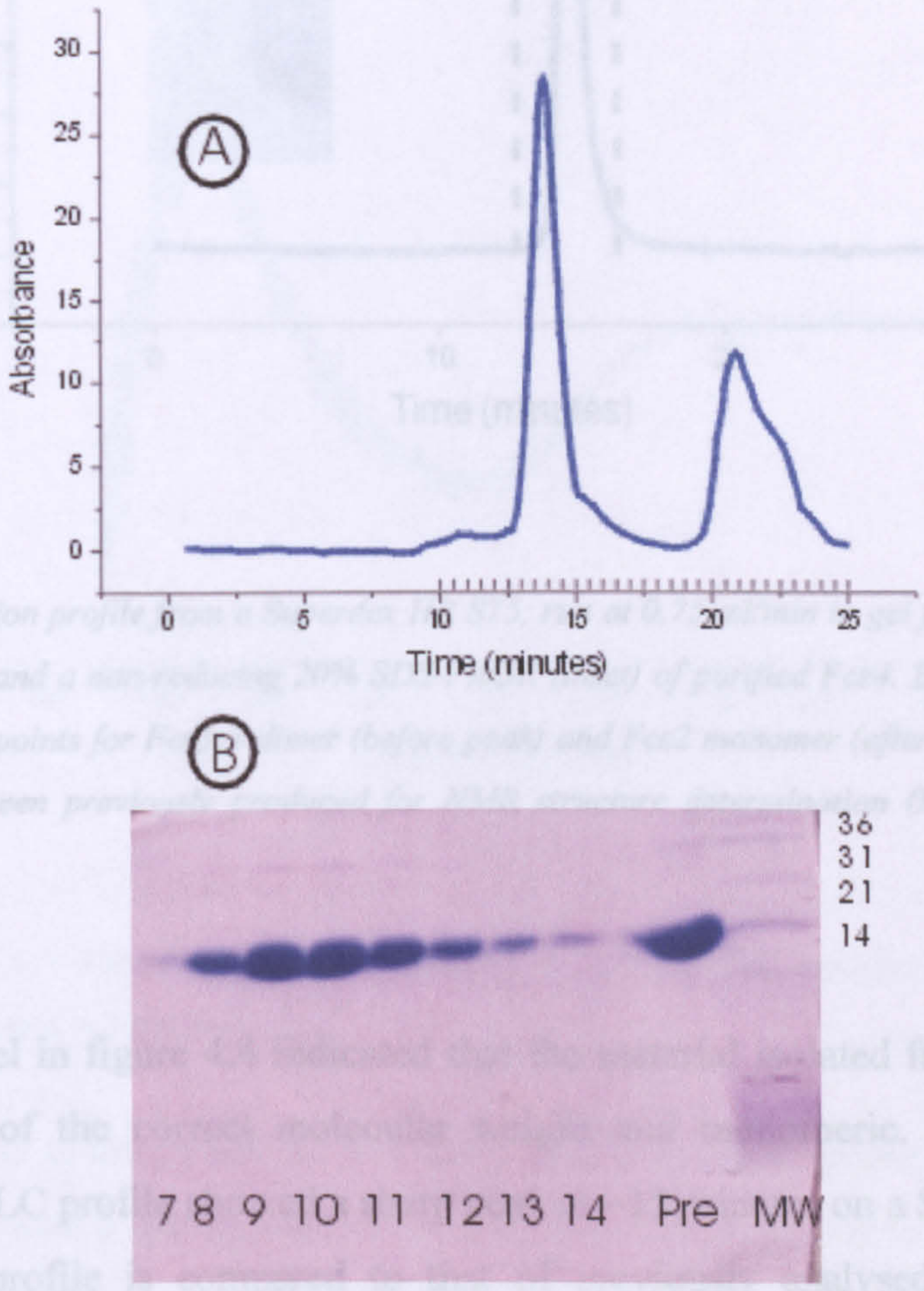

Figure 4.3: Panel A – Elution profile from a Superdex HR S75, run at 0.75 ml/min in gel filtration buffer – see section 2.1.; tick marks above x-axis indicate fractions taken. Panel B – non-reducing 20% SDS-PAGE of fractions from gel filtration purification, including pre-purifcation material and Mark 12 molecular weight markers. Numbers in panel B refer to the fraction number and correspond to the upper tick marks in panel A.

Fractions relating to the HPLC profile peak were combined and concentrated yielding high purity material (see figure 4.4).

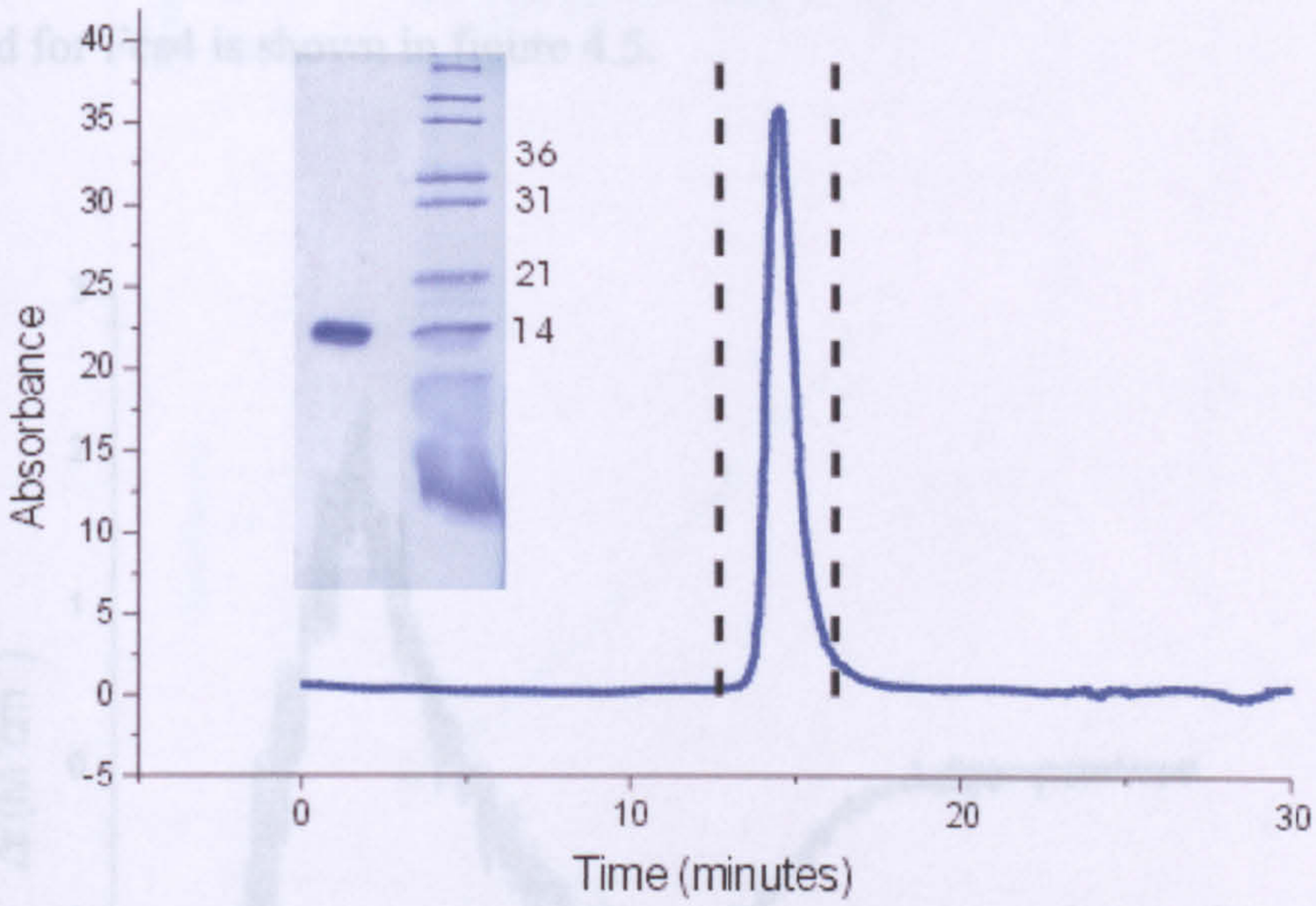

Figure 4.4: Elution profile from a Superdex HR S75, run at 0.75 ml/min in gel filtration buffer – see section 2.1. and a non-reducing 20% SDS-PAGE (inset) of purified Fcε4. Black dotted lines indicate elution points for Fcε3-4 dimer (before peak) and Fcε2 monomer (after peak). The Fcε2 monomer had been previously produced for NMR structure determination (McDonnell et al, 2001).

The gel in figure 4.4 indicated that the material isolated from the refold process was of the correct molecular weight and monomeric. However, the analytical HPLC profile showed a sharp peak at ~15 minutes on a S75 column. If this elution profile is compared to that of previously analysed fragments it appears that a dimer was formed. The line before the peak on the profile shows where Fcε3-4 elutes (MW ~48,000) and the line after the peak indicates where a monomeric Fcε2 domains elutes (MW ~12,000 – characterised in McDonnell *et al*, 2001). However, this method has inaccuracies; for example the elution time of an unfolded protein (Fcε3-4ΔC F506R) appeared very similar to its folded partner (Fcε3-4ΔC) even though it was half the molecular weight – see Chapter 3. Fortunately, the purity of the Fcε4 material made it suitable for further biophysical analysis in order to confirm the folding and dimerisation state.

4.3 Characterisation of Fcε4

Firstly the material was assessed for folding by CD. The spectrum obtained for Fcε4 is shown in figure 4.5.

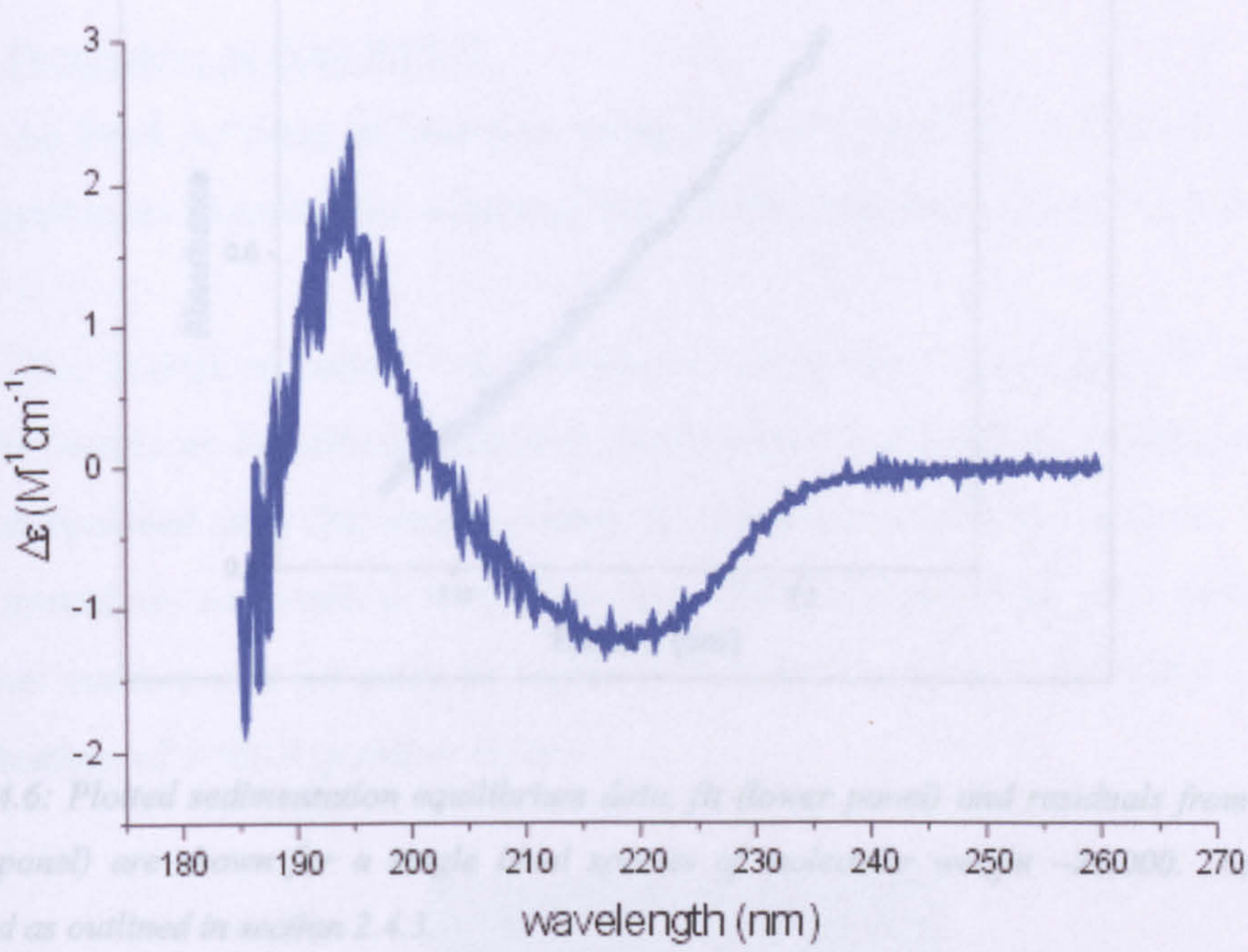

Figure 4.5: Circular dichroism spectrum of isolated and refolded Fcε4. Data was collected as outlined in section 2.4.1.

The CD spectrum for the isolated fragment is characteristic of a folded β-sheet protein, with a strong positive peak around 195nm falling to a minimum at 215 nm, and rising again to plateau at zero ellipticity at longer wavelength. Therefore the elution profile in the gel filtration experiments was not due to the species being unfolded, and is more likely to reflect a dimeric species. To confirm this, analytical ultracentrifugation was used. This would also enable accurate assessment of molecular weight. If the material was completely dimeric, as would be expected from previous experiments, the distribution profile should fit that for a single ideal species of approximate molecular weight 24,000. A representative fit and data obtained for Fcε4 are shown in figure 4.6 and table 4.1 respectively.

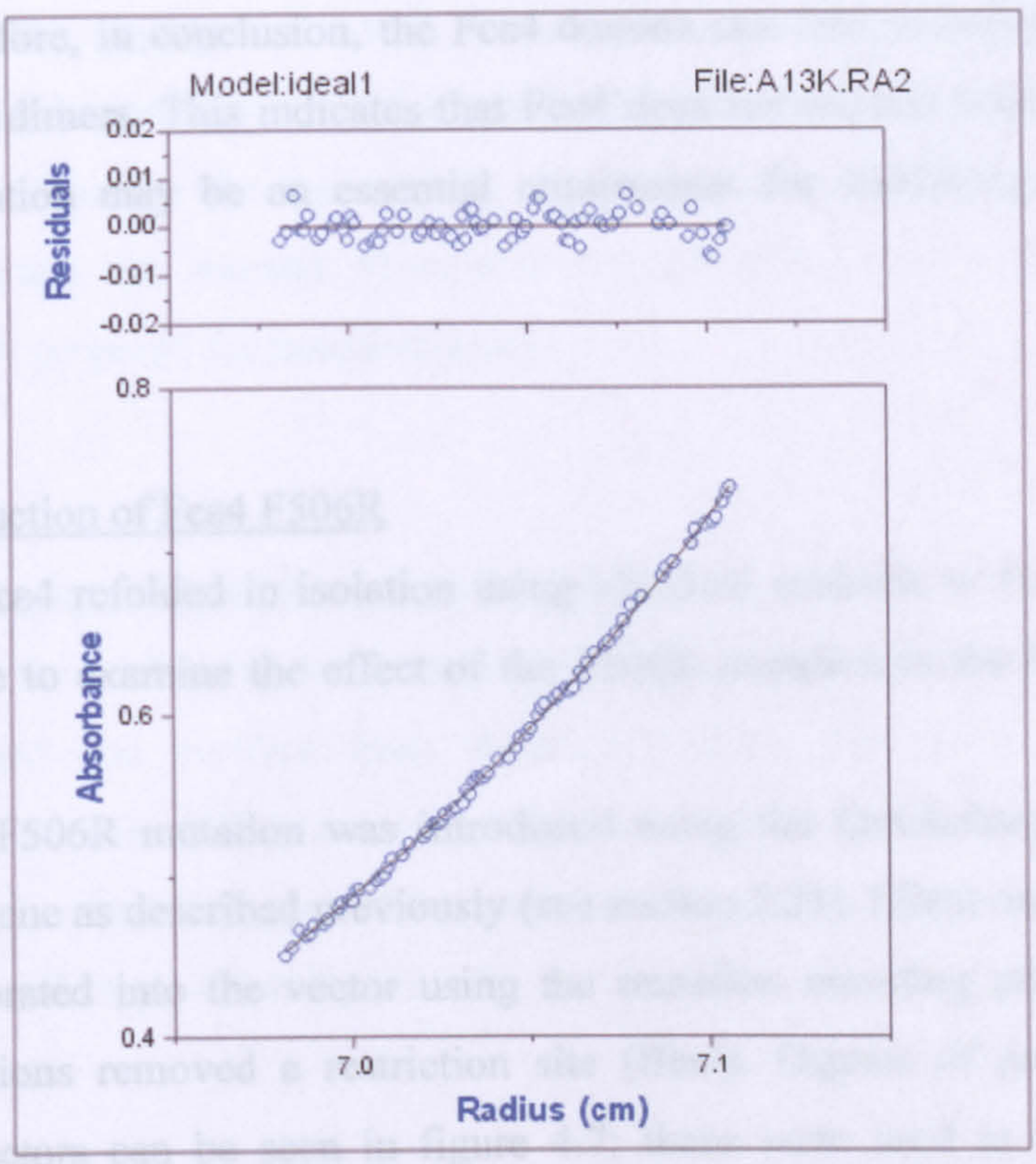

Figure 4.6: Plotted sedimentation equilibrium data, fit (lower panel) and residuals from the fit (upper panel) are shown for a single ideal species of molecular weight ~26,000. Data was collected as outlined in section 2.4.3.

The data obtained from a series of sedimentation equilibrium experiments fitted a single ideal species model. The best fit data yielded an average molecular weight that agreed with that calculated for a Fcε4 dimer; these data are summarised in table 4.1.

	Fcε4 (n = 9)
Mean $M(1-\bar{v}\rho)$	7339 $\pm$ 421
Solvent density (ρ)	1.00721
Partial specific volume ($\bar{v}$)	0.7225
Mean molecular weight	26,953 $\pm$ 1547
Molecular weight from sequence	24844 (dimer)

Table 4.1: Data obtained from single ideal species fit for Fcε4 sedimentation equilibrium data (n = number of datasets analysed).

Therefore, in conclusion, the Fcε4 domain can fold in isolation to form non-covalent dimers. This indicates that Fcε4 does not require Fcε3 to fold and that dimerisation may be an essential requirement for stabilising the Fcε3-4 fragment.

4.4 Production of Fcε4 F506R

As Fcε4 refolded in isolation using identical methods to Fcε3-4, it was thus possible to examine the effect of the F506R mutation in the Fcε4 domain alone.

The F506R mutation was introduced using the Quickchange™ system from Stratagene as described previously (see section 2.21). Silent mutations were also incorporated into the vector using the mutation encoding primers. These silent mutations removed a restriction site (BbsI). Digests of pre- and post-mutation vectors can be seen in figure 4.7; these were used to enable quick identification of F506R positive clones.

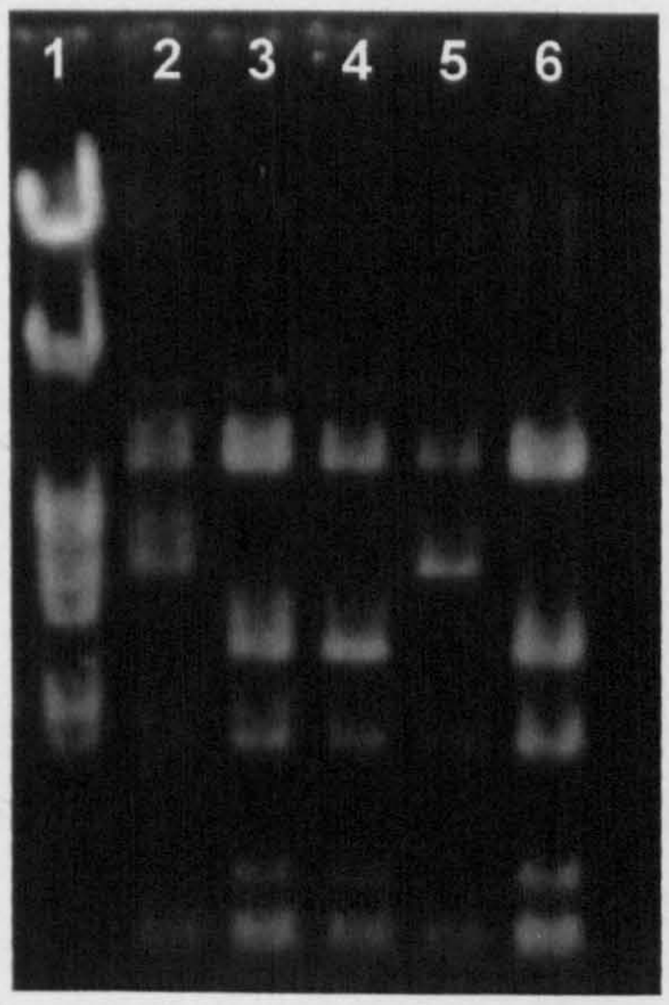

Figure 4.7: 1% agarose gel of pET 15a Fcε4 vectors pre (lane 2) and post (lanes 3-6) mutation digested with BbsI. HindIII digested lambda DNA lane 1.

From the digests in lanes 3, 4 and 6 it was clear that mutation of the vector DNA had been successful, but not for the reaction in lane 5. Subsequently the fragment sequence for successfully altered fragments was verified by DNA sequencing (data not shown). From this a single clone was isolated and the plasmid DNA prepared for transformation.

4.5 Expression and purification of Fcε4 F506R

Once the relevant mutation had been incorporated, the material was again over-expressed and purified from inclusion bodies. The process used was identical to that described previously. Figure 4.8 shows the final product of the inclusion body extraction procedure, and this was almost identical in yield and purity to the wild type Fcε4 (figure 4.4).

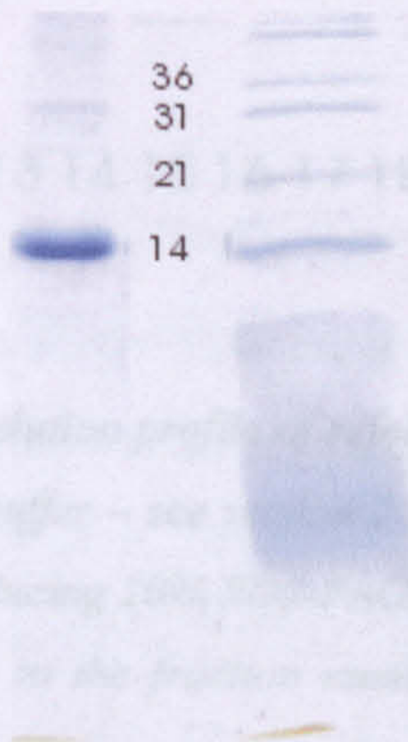

Figure 4.8: Reducing 20% SDS-PAGE of inclusion body purified Fcε4 F506R

This material was subjected to the refolding protocol used for all previous fragments. The dilute refolded material was then concentrated and HPLC purified by gel filtration on a S75 HR column. The elution profile for the refolded product alongside SDS-PAGE of the fractions is shown in figure 4.9.

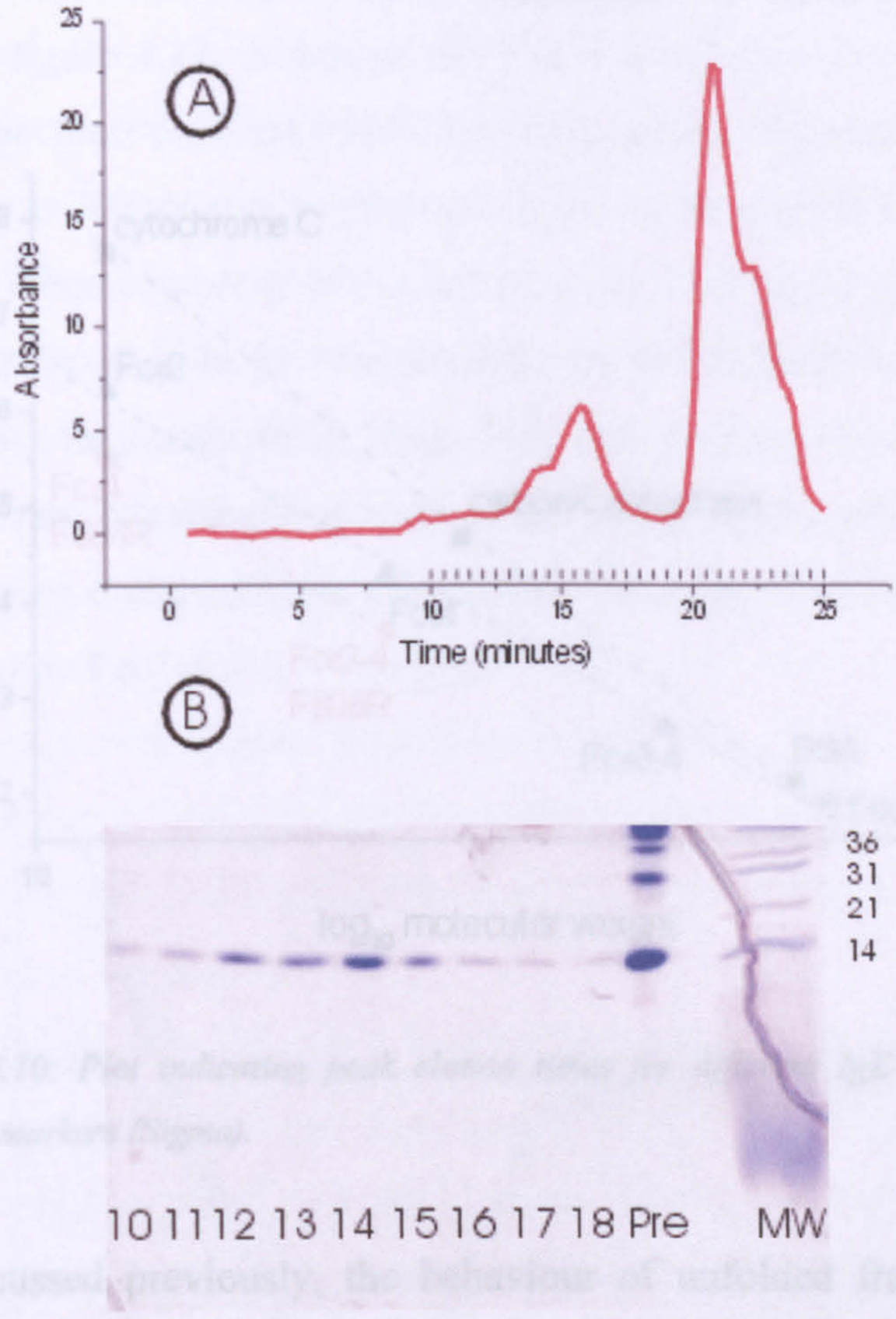

Figure 4.9: Panel A – Gel filtration elution profile of refolded Fcε4 F506 run on a Superdex HR S75 at 0.75 ml/min in gel filtration buffer – see section 2.1.; upward ticks on the x-axis indicate fractions collected. Panel B- non-reducing 20% SDS-PAGE of HPLC fractions and pre-injection material. Numbers in panel B refer to the fraction number and correspond to the upper tick marks in panel A.

The profile obtained for Fcε4 F506R was very different from that of wild type Fcε4. The SDS-PAGE of the refolded product prior to gel purification shows a number of covalent aggregates, identifiable by a ladder of species of different molecular weight in panel B of figure 4.9. This material formed a precipitate that could be removed from the protein solution by filtration prior to injection onto the gel filtration column; this explains the absence of covalent aggregates in the elution profile. The remaining protein represented only a small fraction of that subjected to the refold (less than 0.5 mg from a total 20 mg). This kind of aggregation and covalent oligomerisation is behaviour charateristic of an unfolded protein, such as Fcε3 (Henry, PhD thesis, 1997). The elution point of

the protein was also later than would be expected, even for a folded monomer, see figure 4.10.

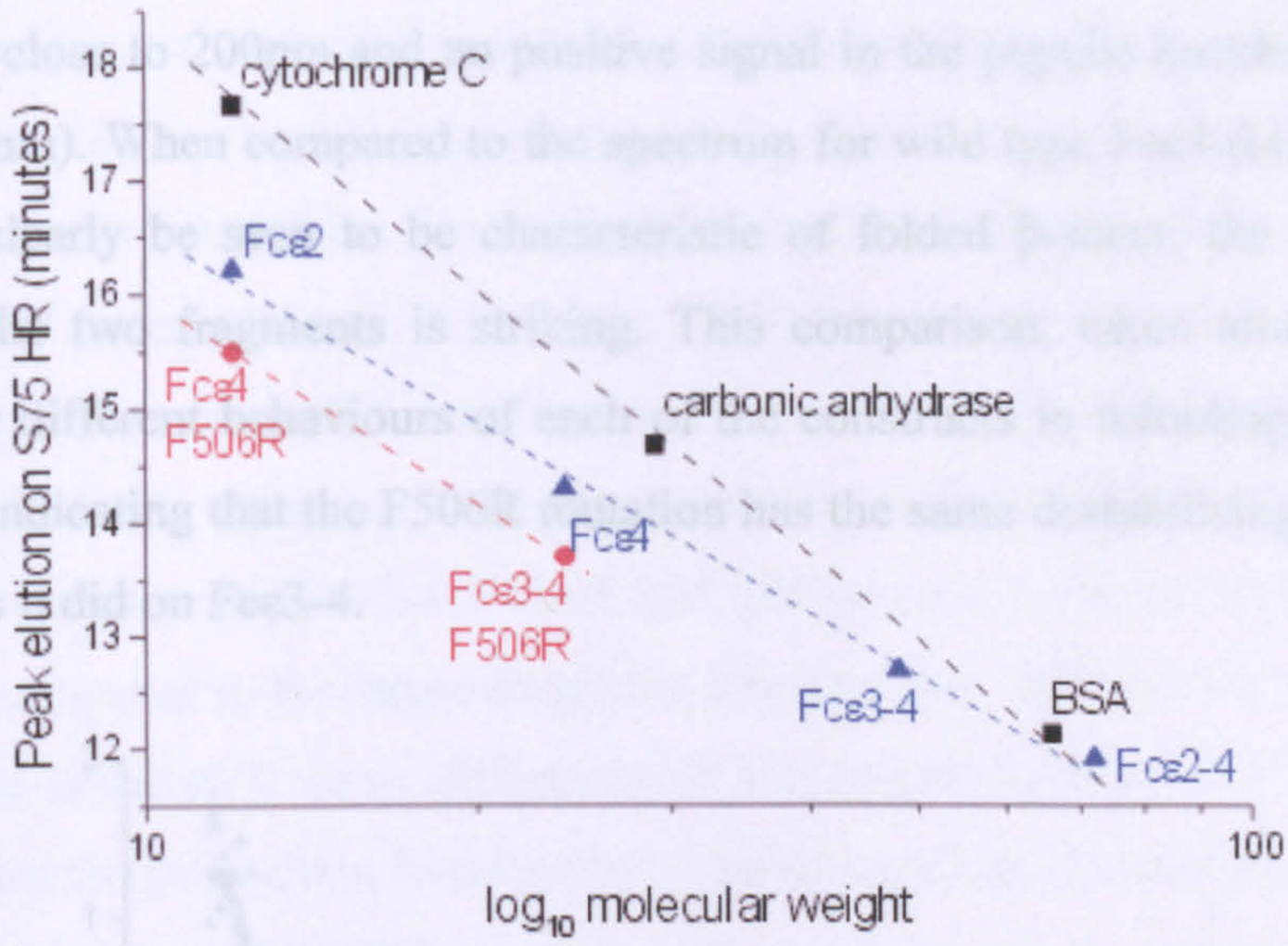

Figure 4.10: Plot indicating peak elution times for different IgE-Fc fragments and molecular weight markers (Sigma).

As discussed previously, the behaviour of unfolded fragments is very different in gel filtration from those that have formed globular domains. The peak elution time for F506R Fcε4 mutant is much later than that for a folded Fcε4, and but earlier than that of a single Fcε2 domain. This is very similar behaviour to the unfolded, monomeric Fcε3-4 F506R construct. Therefore, from the gel filtration elution profile it was concluded that Fcε4 F506R was unfolded and was unable to form dimers in solution. Fortunately, enough covalently monomeric material was obtained from the refold to carry out circular dichroism analysis on the fragment to categorically determine the folded state of the protein.

4.6 Characterisation of Fcε4 F506R

Although recovery levels were poor, the Fcε4 F506R could be analysed at lower concentrations in a longer path length cell than that normally used (10mm). The material was not amenable to concentration, and thus it was not possible to carry out the complementary sedimentation equilibrium experiments that require a concentration of around 0.5mg/ml. Therefore the CD spectrum of

Fcε4 was also recorded at low concentration, to act as a control. The CD traces can be seen in figure 4.11. Although the signal obtained was sub-optimal it is clear that the spectrum for Fcε4 F506R is characteristic of a random coil, with a minimum close to 200nm and no positive signal in the peptide backbone region (200- 240nm). When compared to the spectrum for wild type Fcε4 (blue), which can still clearly be seen to be characteristic of folded β-sheet, the difference between the two fragments is striking. This comparison, taken alongside the drastically different behaviours of each of the constructs in refolding, is strong evidence indicating that the F506R mutation has the same destabilising influence on Fcε4 as it did on Fcε3-4.

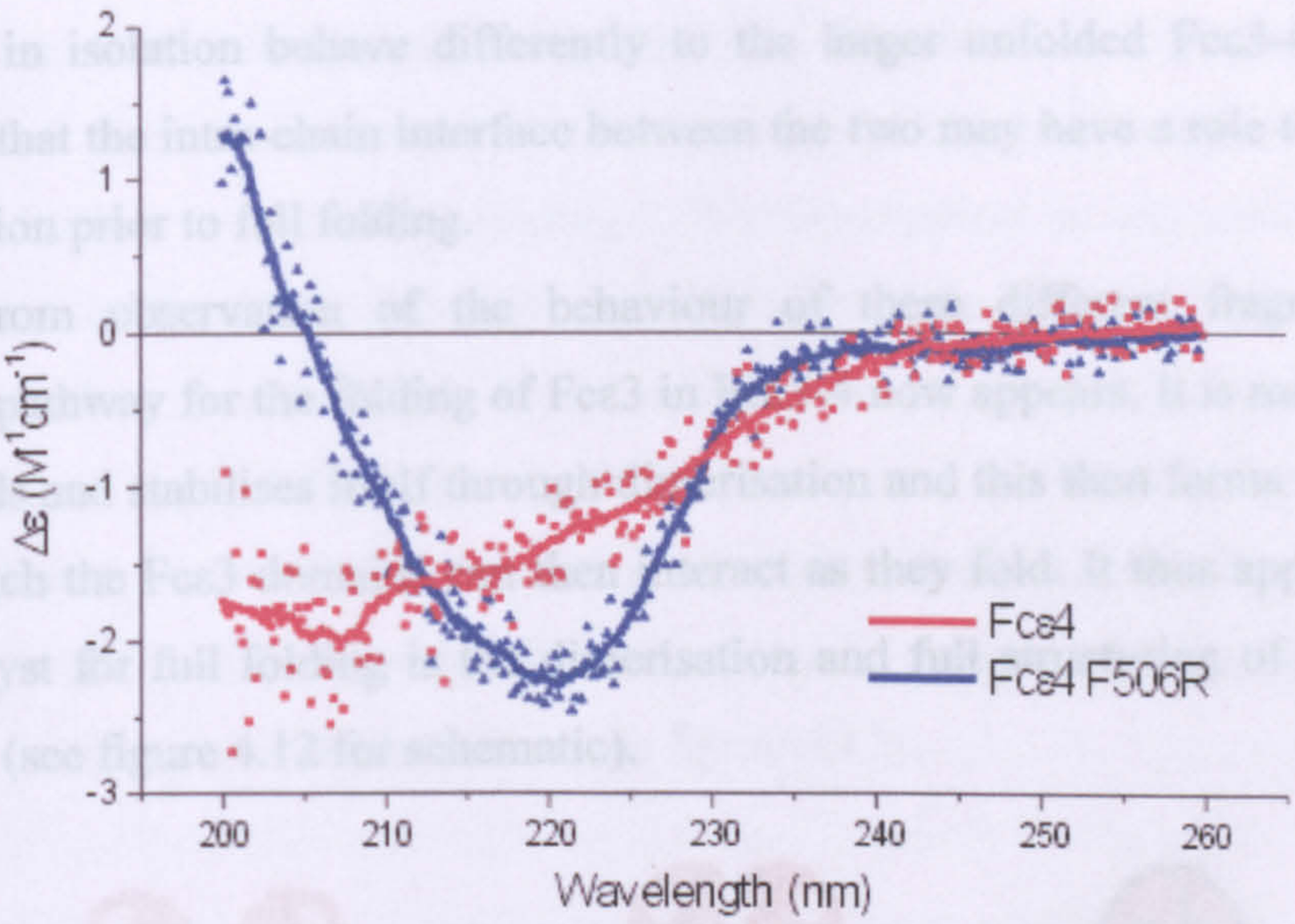

Figure 4.11: Circular dichroism spectra of Fcε4 wild type and Fcε4 F506R. Trend-line for each set of data (points also plotted individually) calculated using adjacent averaging. Other than concentration (protein concentration was determined to be 50 μg/ml by absorbance) and cell pathlength (10mm), data was collected as outlined in section 2.4.1.

4.7 Discussion

The aim of the work detailed in this chapter was to analyse the folding of Fcε4 in isolation from Fcε3 and use this as a basis for assessing the effect of the F506R mutation. Fcε4 folded fully in the absence of Fcε3 to form non-covalent dimers. This result demonstrated that Fcε3 was not essential for stabilising Fcε4 and confirmed the Fcε4 domain as a key mediator for dimerisation of the IgE-Fc. In comparison, the Fcε4 F506R mutant was extremely difficult to handle. This

construct did not fold properly (as judged by CD) and remained monomeric in solution (according to gel filtration data), indicating a strong relationship between stability and dimerisation. This result confirmed that the effect of the F506R mutation on Fcε3-4ΔC was due to destabilisation of Fcε4, and that Fcε4 would appear to have a role in stabilising Fcε3.

The behaviour of the Fcε4 F506R mutant was very similar to that of an isolated Fcε3 domain (Henry, PhD thesis, 1997) that also does not fold. The Fcε4 F506R fragment was notably harder to handle than the larger unfolded Fcε3-4ΔC F506R mutant. On refolding, a larger proportion of Fcε4 F506R was found to precipitate compared to Fcε3-4 F506R, and furthermore, stability over time was also poor compared to the larger fragment. The fact that unfolded Fcε3 and Fcε4 domains in isolation behave differently to the larger unfolded Fcε3-4 further suggests that the intra-chain interface between the two may have a role to play in stabilisation prior to full folding.

From observation of the behaviour of these different fragments, a possible pathway for the folding of Fcε3 in Fcε3-4 now appears. It is most likely Fcε4 folds and stabilises itself through dimerisation and this then forms a surface with which the Fcε3 domains can then interact as they fold. It thus appears that the catalyst for full folding is the dimerisation and full structuring of the Fcε4 domains (see figure 4.12 for schematic).

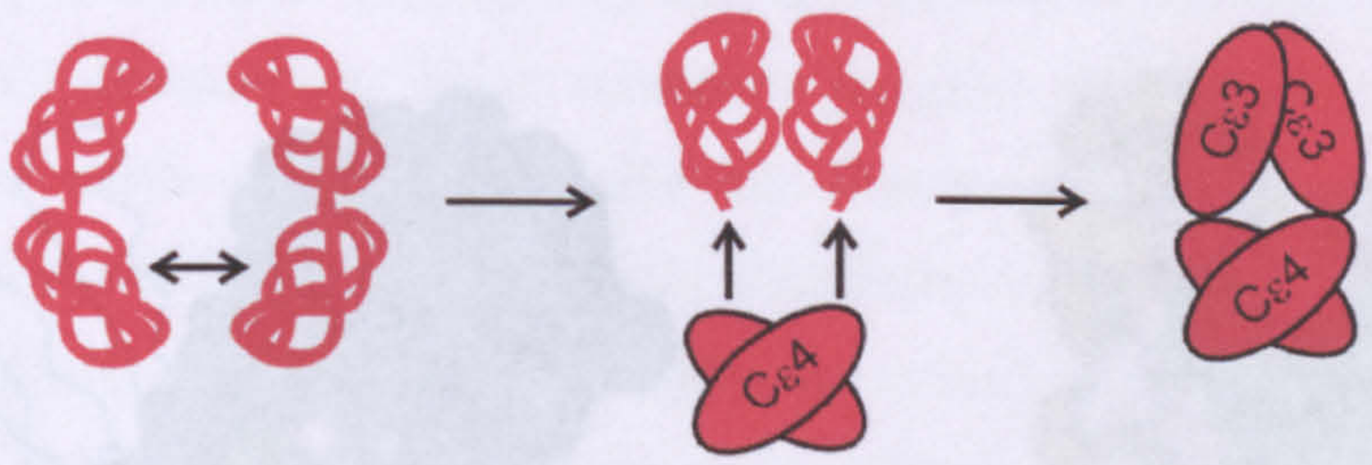

Figure 4.12: Suggested pathway for the folding of Fcε3.

One problem with this scheme is that it is not clear how the two Fcε4 domains that are unfolded could come together before folding. It is apparent from the CD spectra of Fcε3-4 F506R (figure 3.12) and Fcε3 (figure 1.6) that although these fragments are not completely folded, neither are they a complete random coil (see figure 2.4 in section 2.4.1), as the ellipiticity observed at shorter wavelengths is less negative than that for a pure random coil. This could

represent a residual structuring of the domains. The intra-domain disulphide of Fcε3 is also known to be crucial to maintaining the binding capacity of this essentially unfolded fragment (Henry *et al*, 2000), further indicating that there is some structuring at least at the core of the domain. Such a core of structuring may exist for Fcε4, although at present there is no evidence for this. If this were true, it is possible that this minimal structuring of the fragments may provide motifs for recognition that are sufficient to allow initial contact to be made between monomers and the folding pathway to continue to completion. The presence of a large charge in the chain, in the form of the F506R mutation, may prevent these contacts and therefore stall the folding process.

Fcε4 monomers were not seen in solution either by gel filtration or analytical centrifugation, confirming that this domain is a key mediator in dimerisation. Furthermore, the lack of monomers is consistent with a necessity for dimerisation to complete folding. This observation is supported by an examination of the Fcε4 dimer interface. The interface between Fcε4 domains buries a surface area of 2326 $Å^2$, of which 63% is non-polar and no water molecules are trapped (Wan *et al*, 2002). In contrast, for Fcε2, a domain that does fold as a monomer (McDonnell *et al*, 2001), the interface between Fcε2 domains is 1760 $Å^2$, and crucially only 25% is non-polar, with nine water molecules are buried at the interface (see figure 4.13).

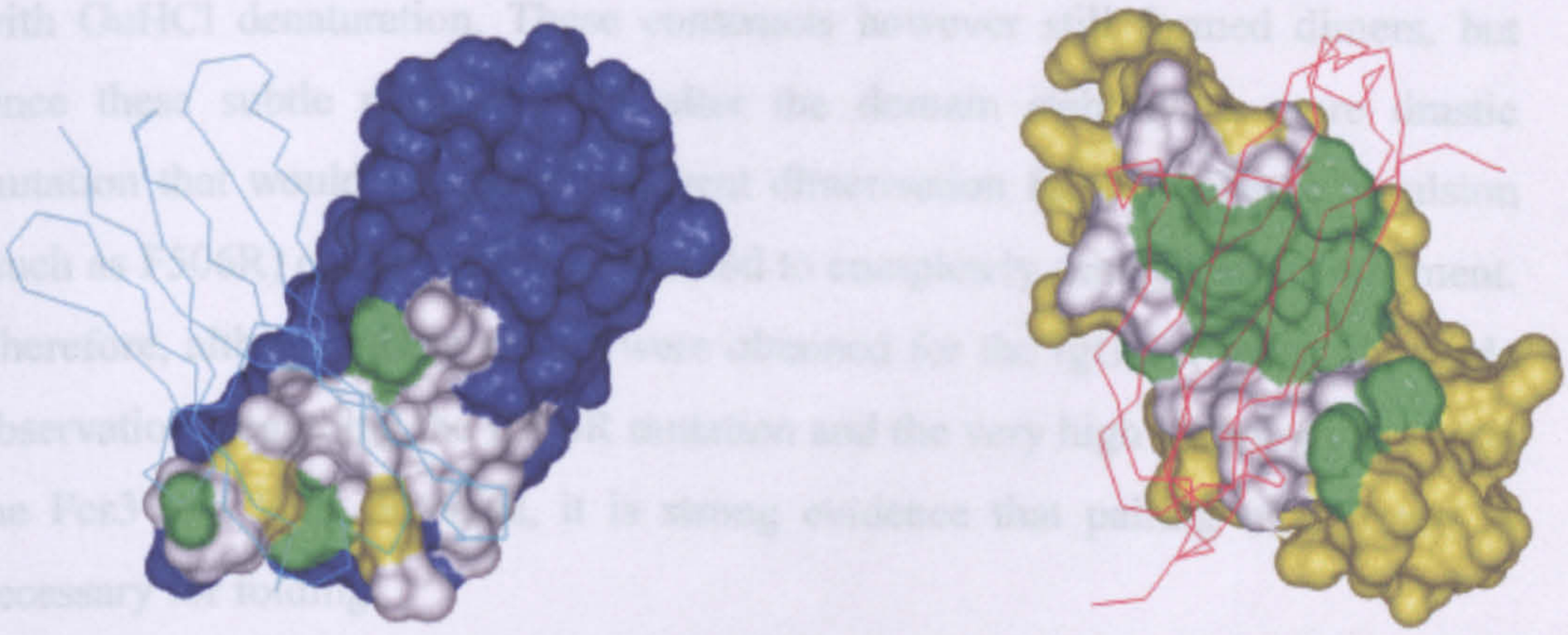

Figure 4.13: Fcε2 (left) and Fcε4 (right) domain pairs (one space-filled the other a Cα trace) from the Fc crystal structure (Wan et al, 2002). Hydrophobic residues are green; hydrophilic residues white; yellow non-contact in Fcε4; blue non-contact in Fcε2 (yellow in Fcε2 are cysteines).

Although the results so far indicate that the F506R mutation prevents folding due to interfering with favourable Fcε4:Fcε4 domain interface interactions, there is still the possibility that the F506R mutation affects folding simply by disrupting local domain structure, rather than domain pairing. This is an important question to consider when assessing whether forming a fully folded Fcε3-4 monomer is at all possible.

Previous work carried out on IgG has shown that the homologous Fcγ3 domain interface is amenable to point mutation (reviewed in Carter 2001). Carter showed that alteration of residues in this interface to create complementary "knobs" (for example trytophan) and "holes" (for example valine) can be used to form bispecfic antibodies. In fact, one of the key residues used in this method is a tyrosine at the position homologous to phenylalanine 506 of Fcε4. This residue in Fcγ3 makes a stabilising hydrogen bond with a threonine in the same chain, as well as packing closely with the opposing chain, so in terms of domain stability it appears to be as important as phenylalanine 506 in Fcε4. Yet, mutations in this region that are complementary with respect to interaction with the opposing domain do not cause unfolding.

Investigation of non-complementary mutations has shown that these do alter the stability of the domain (Dall'Acqua *et al*, 1998). Mutations formed on one side of the Fcγ3 domain to create a cavity in the domain interface reduced the stability of the dimer as judged by circular dichroism spectroscopy combined with GuHCl denaturation. These constructs however still formed dimers, but since these subtle mutations did alter the domain stability, a more drastic mutation that would completely prevent dimerisation fully by charge repulsion (such as F506R) could easily be expected to completely destabilise the fragment. Therefore, although these results were obtained for the IgG-Fc, taken alongside observations regarding the F506R mutation and the very high homology between the Fcε3 and Fcγ2 domains, it is strong evidence that pairing of domains is necessary for folding.

In conclusion, the Fcε4 domain does not require Fcε3 for folding, as an isolated fragment refolds from *E. coli* expressed inclusion bodies to display a circular dichroism spectrum characteristic of a fully folded domain. Furthermore, this fragment spontaneously forms non-covalent dimers, confirming this region as the key mediator of dimerisation for the Fc fragment. The fact that no

intermediate species (*i.e.* folded monomers) were observed in solution (as judged by AUC and gel filtration chromatography), and that the incorporation of like charges at the domain interface prevents folding (Fcε4 F506R construct) suggests that the dimerisation process is integral to the folding of the Fcε4 domain. The results obtained for Fcε3-4ΔC F506R show that without a folded Fcε4 domain, the Fcε3 domain in this construct could not fold (see Chapter 3), whereas a dimeric Fcε3-4ΔC does fold. It is therefore concluded that the minimum scaffold required for a fully folded Fcε3 domain must include a dimer of Fcε4 domains and that Fcε4 may play a role in promoting the folding of Fcε3.

Production and characterisation of a Fcε4-Fcε3-4 heterodimer

Chapter 5: Production and characterisation of a Fcε3-4-Fcε4 heterodimer

5.1 Introduction

In Chapter 4 it was shown that Fcε4 only folds correctly as a dimer. Thus, in order to discover whether a single Fcε3 will fold when attached to a folded Fcε4 domain, it was necessary to create a heterodimer of Fcε3-4 and Fcε4. In such a fragment, the single Fcε3 domain is free from any lateral contact with another Fcε3 domain, and so the effect of the longitudinal contact with Fcε4 alone can be investigated.

If contact from a folded Fcε4 is the sole requirement for the stabilisation of Fcε3, a fully folded Fcε3-4:Fcε4 heterodimer (referred to as Fcε3-4(4)) would be observed, see figure 5.1.

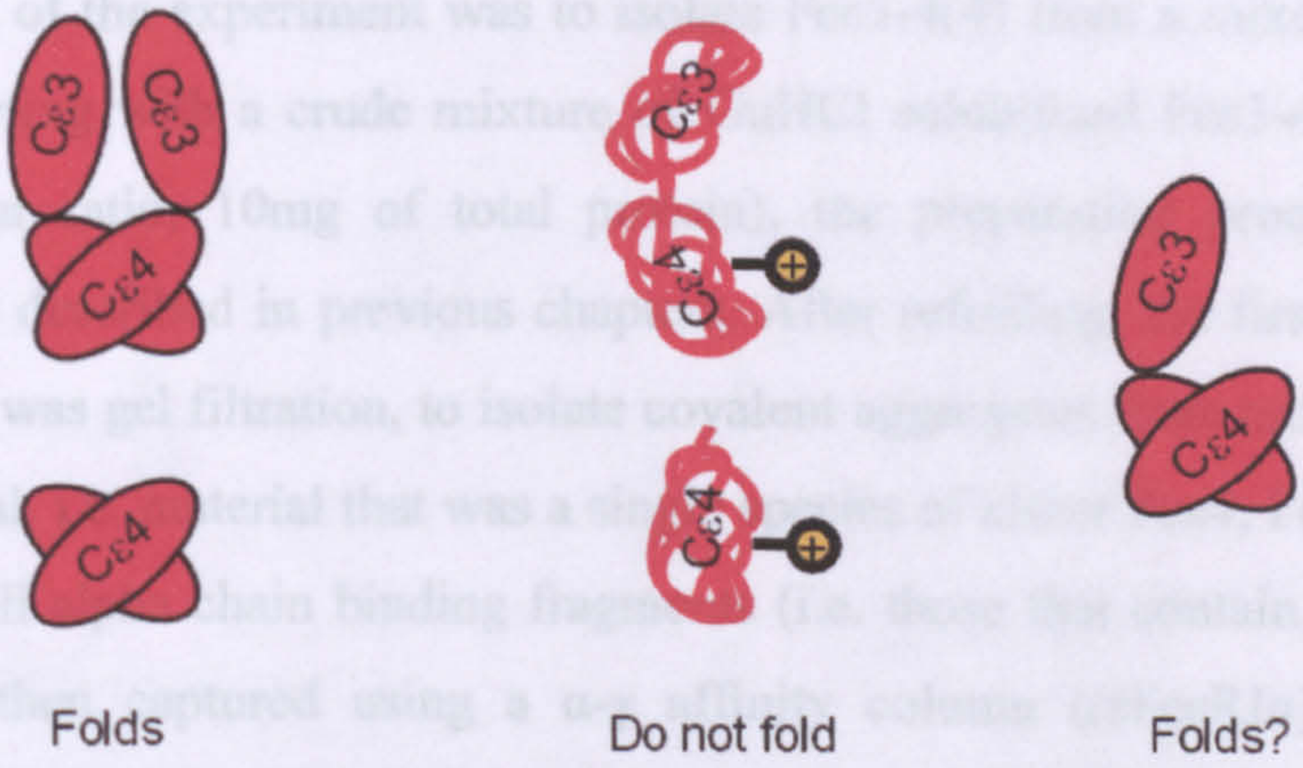

Figure 5.1: Cartoon illustrating the various Fc sub-fragments described in Chapters 3 and 4, alongside the heterodimer (Fcε3-4(4)).

5.2 Refold and purification trial

E. coli expression and refolding had previously provided clear results for both folded and unfolded IgE fragments, and therefore this system was also used for the heterodimer experiments. The protocol devised for isolating the heterodimer is outlined in figure 5.2.

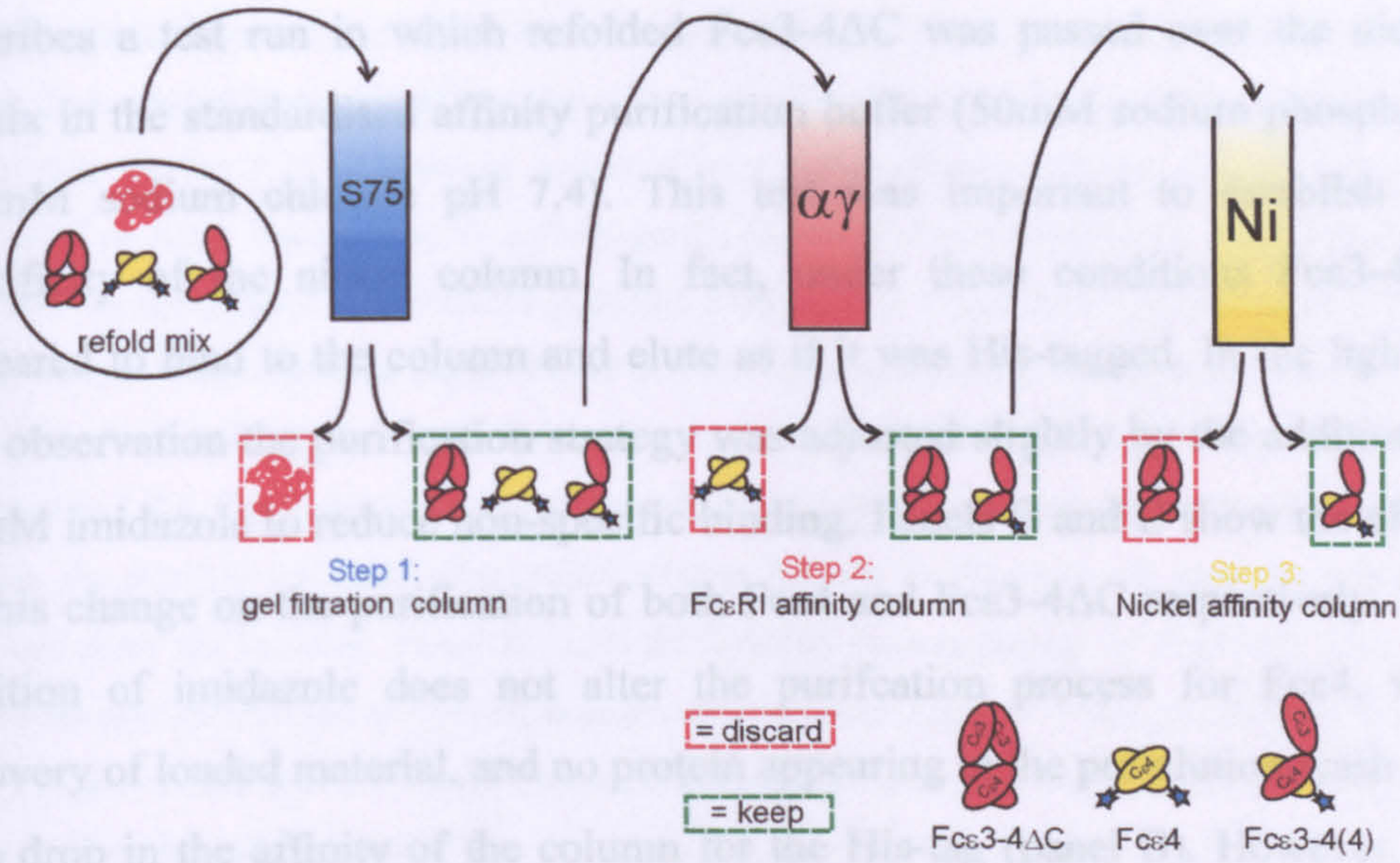

Figure 5.2: Process for isolating Fcε3-4(4) from a mixed refold population. The blue star indicates a His-tag, ellipses folded domains and random coil unfolded polypeptide chain.

The aim of the experiment was to isolate Fcε3-4(4) from a mixed refold population. Starting with a crude mixture of GuHCl solubilised Fcε3-4ΔC and Fcε4 (1:1 molar ratio, 10mg of total protein), the preparation process was identical to that described in previous chapters. After refolding, the first step in the purification was gel filtration, to isolate covalent aggregates from monomeric refolded material, i.e. material that was a single species of either Fcε4, Fcε3-4ΔC or Fcε3-4(4). All alpha chain binding fragments (i.e. those that contain an Fcε3 domain) were then captured using a α-γ affinity column ($(sFc\varepsilon RI\alpha)_2IgG_4Fc$ amine coupled to Fast Flow Sepharose (Pharmacia)). The folding status of Fcε3 at this point is not critical as the domain maintains FcεRI binding capability even when not fully structured (Henry *et al*, 2000). Positively selected material was then passed over a nickel affinity column, thus isolating only His-tagged material. Only the Fcε4 vector attaches this motif. From this selection procedure it should only be possible to isolate a Fcε3-4(4) heterodimer, as by the time of the nickel affinity step all Fcε4 dimers should have been removed due to their inability to bind the α-γ fusion column.

To ensure that the purification process worked in the intended manner, a number of control experiments were carried out. The results of these are displayed in figure 5.3. Panels A-C illustrate gel filtration profiles of the purification products from different runs over the nickel affinity matrix. Panel A

describes a test run in which refolded Fcε3-4ΔC was passed over the nickel matrix in the standardised affinity purification buffer (50mM sodium phosphate, 500mM sodium chloride pH 7.4). This test was important to establish the specificity of the nickel column. In fact, under these conditions Fcε3-4ΔC appeared to bind to the column and elute as if it was His-tagged. In the light of this observation the purification strategy was adjusted slightly by the addition of 50mM imidazole to reduce non-specific binding. Panels B and C show the effect of this change on the purification of both Fcε4 and Fcε3-4ΔC respectively. The addition of imidazole does not alter the purifcation process for Fcε4, with recovery of loaded material, and no protein appearing in the pre-elution wash due to a drop in the affinity of the column for the His-tag (panel B). However, the addition of imidazole did stop the Fcε3-4ΔC sticking to the column, as all the loaded material came through in the wash and none in the elution fraction (panel C).

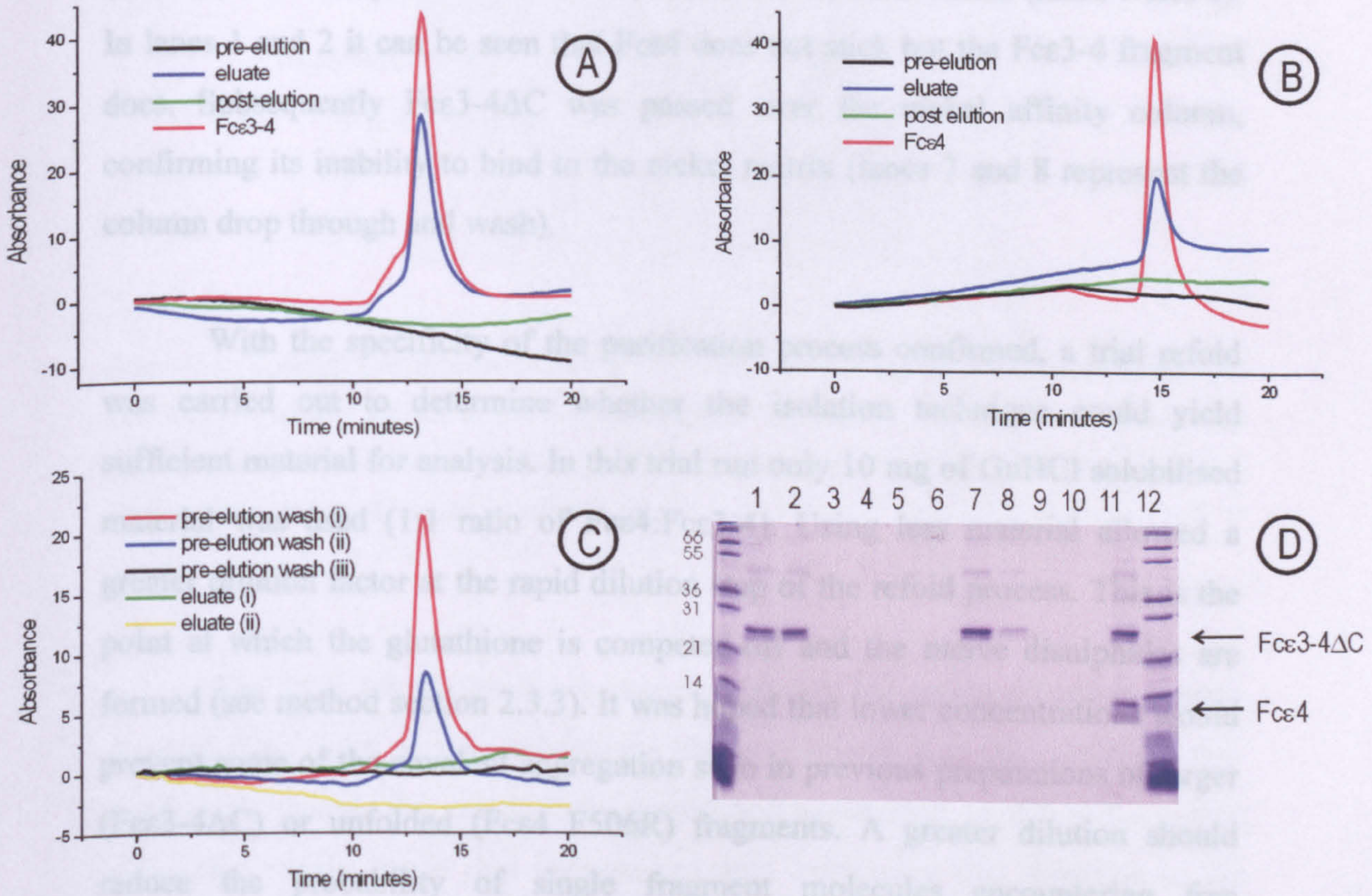

Legend overpage.

Previous page. Figure 5.3: Control experiments for the Fcε3-4(4) isolation process. A – C are traces from analytical gel filtration using a Superdex HR S75, run at 0.75 ml/min in gel filtration buffer (see section 2.1) of fractions collected from nickel Hi-trap columns loaded with either Fcε3-4ΔC or Fcε4. Traces from the affinity purification are shown alongside a control profile of the relevant IgE fragment to indicate expected elution time. Panel A: Fcε3-4ΔC applied to the nickel matrix in standardised buffer. Panel B: Fcε4 applied to nickel matrix in imidazole buffer. Panel C: Fcε3-4ΔC applied to nickel matrix in imidazole buffer. All buffer compositions are outlined in 2.3.4. Pre-elution represents the unbound fraction, eluate the bound fraction and post elution the fraction collected after initial elution (shown to illustrate all material had been removed from the column). Panel D: 15% SDS-PAGE (non-reducing) of Fcε3-4ΔC and Fcε4 fragments applied as a mix to α-γ fusion and nickel columns. Lane 11 = mix prior to purification, lane 1 = α-γ eluate, lane 2 = nickel column unbound fraction, lanes 3-6 = nickel column eluate, lanes 7-10 nickel column wash.

Finally, it was also established that the α-γ column did not allow cross contamination due to non-specific binding. The results are outlined in panel D of figure 5.3. Here the two fragments (Fcε4 and Fcε3-4ΔC) were mixed together (lane 11) and then passed over the α-γ fusion column and eluted (lanes 1 and 2). In lanes 1 and 2 it can be seen that Fcε4 does not stick but the Fcε3-4 fragment does. Subsequently Fcε3-4ΔC was passed over the nickel affinity column, confirming its inability to bind to the nickel matrix (lanes 7 and 8 represent the column drop through and wash).

With the specificity of the purification process confirmed, a trial refold was carried out to determine whether the isolation technique could yield sufficient material for analysis. In this trial run only 10 mg of GuHCl solubilised material was used (1:1 ratio of Fcε4:Fcε3-4). Using less material allowed a greater dilution factor at the rapid dilution step of the refold process. This is the point at which the glutathione is competed-off and the native disulphides are formed (see method section 2.3.3). It was hoped that lower concentrations would prevent some of the covalent aggregation seen in previous preparations of larger (Fcε3-4ΔC) or unfolded (Fcε4 F506R) fragments. A greater dilution should reduce the probability of single fragment molecules encountering free sulphydryls from another molecule and forming cross-links prior to formation of the correct intra-chain disulphide. The refold was carried out using the same protocol as established for other IgE fragments (Henry, 1997) and was then

subjected to gel filtration to remove covalent aggregate. The gel filtration elution profile and SDS-PAGE analysis of fractions are shown in figure 5.4.

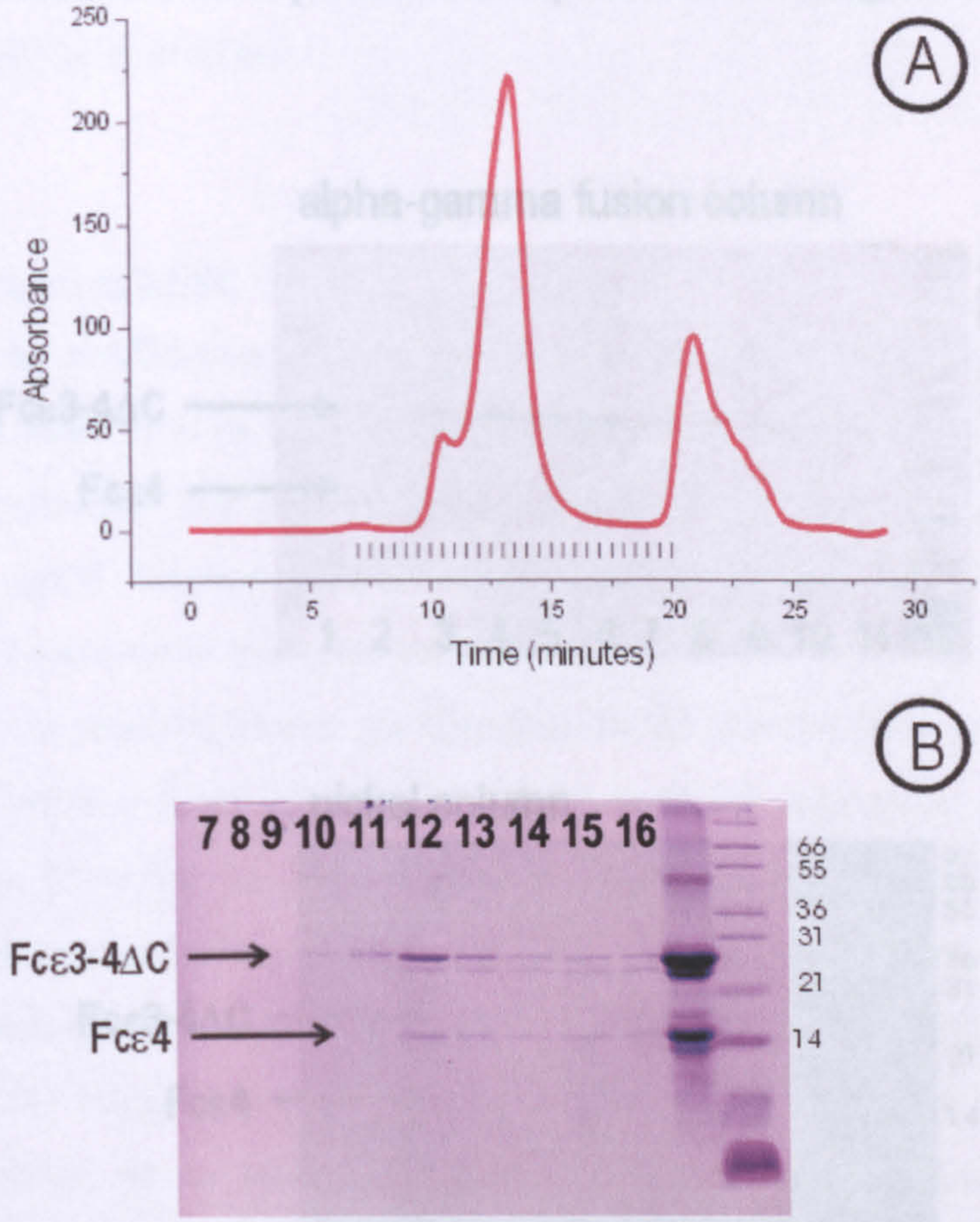

Figure 5.4: Panel A: Gel filtration profile of Fcε3-4ΔC and Fcε4 mixed refold run on a Superdex HR S75, run at 0.75 ml/min in gel filtration buffer – see section 2.1. Upward ticks on x-axis indicate fraction collection points. Panel B: 15% non-reducing SDS-PAGE of fractions, numbers correspond to tick marks on the profile in panel A.

The SDS PAGE profile in panel B shows the pre-purification sample (second from right) and the subsequent eluted fractions. It is clear from the pre-purification sample that much of the protein still aggregated, visible in the higher molecular weight bands that indicate covalent aggregates and smearing in the gel. The subsequent recovery of much of the sample confirmed this (~3mg protein total prior to the two-step affinity purification, as assessed by absorbance at 280nm). Fortunately the gel filtration step enabled all of this aggregate to be

removed from the eluted fractions. After gel filtration, fractions containing Fcε4 and Fcε3-4ΔC identified by SDS-PAGE were combined and then passed over the α-γ affinity column; eluted fractions were recombined and passed over the nickel column. The results of these purification steps are shown in figure 5.5.

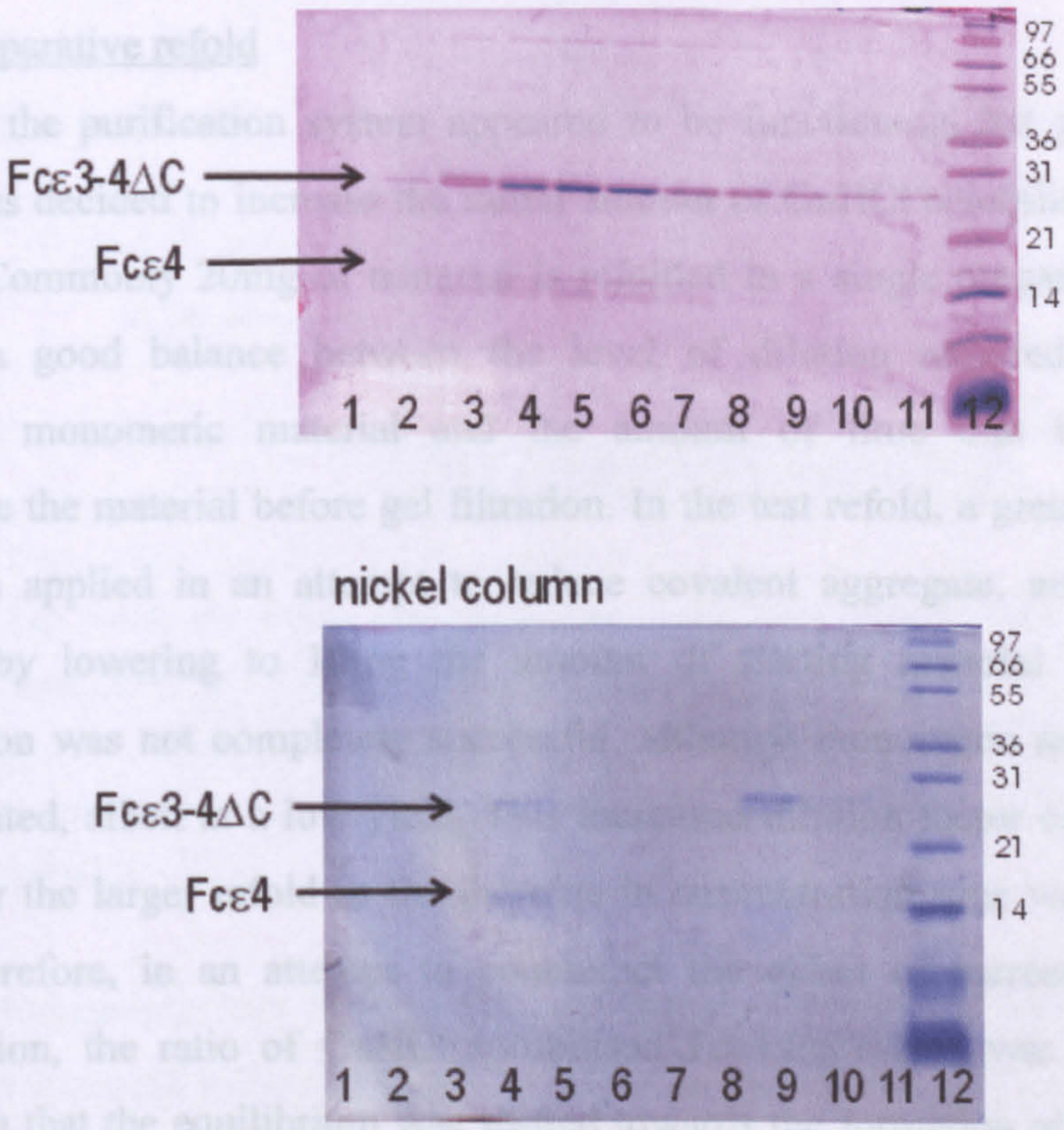

Figure 5.5: Top panel: eluted fractions collected from α-γ fusion column (lanes 1-11). Bottom panel: Fractions collected from nickel column after purification of collected material eluted from α-γ fusion purification step. Lane 1-6 = eluate fractions, lanes 7-11 = unbound fractions.

The SDS-PAGE of the α-γ and nickel columns clearly shows that the isolation process has captured heterodimeric fragments. The α-γ column would not be able to co-elute Fcε4 with Fcε3-4 unless the two had associated. This association was non-covalent as the gels run are non-reducing. The positive selection process is most clear in the nickel column step, with lane 9 showing Fcε3-4ΔC coming though in the column wash, and the Fcε3-4(4) material

appearing in the eluted fraction (lane 4). Unfortunately only very small amounts of material were obtained. In total ~50μg was recovered, which was sufficient for detection using SDS-PAGE, but represented only a fraction of the intial 10mg of GuHCl solubilised material. Due to the very low recovery, no biophysical analysis could be carried out.

5.3 Preparative refold

As the purification system appeared to be functioning, but yields were poor, it was decided to increase the initial amount of GuHCl solubilised starting material. Commonly 20mg of material is refolded in a single preparation. This provides a good balance between the level of dilution required to obtain covalently monomeric material and the amount of time that it takes to concentrate the material before gel filtration. In the test refold, a greater dilution factor was applied in an attempt to reduce covalent aggregate, and this was achieved by lowering to 10mg the amount of starting material used. This modification was not completely successful, although monomeric material was still separated, albeit at a low yield. This increased dilution factor could not be applied for the larger refold as the increase in concentration time would be too great. Therefore, in an attempt to counteract the effect of increased protein concentration, the ratio of GuHCl solubilised Fcε4:Fcε3-4ΔC was altered (to 1.5:1) such that the equilibrium was shifted towards the formation of Fcε4. This was because Fcε4 yields much less aggregated material when refolded than Fcε3-4ΔC, thus lowering the potential for the appearance of nucleation points for aggregation. The refold should then also favour the formation of Fcε3-4(4) over Fcε3-4ΔC due to the excess Fcε4 in the mix. This might result in a small drop in the yield of Fcε3-4(4), but by reducing the potential for aggregation and increasing the total protein, it was anticipated that the experimental yield would be higher.

After gel filtration and isolation of the covalently monomeric fraction (data not shown), the refolded material was affinity purified by the same two-step procedure, the results of which are presented in figure 5.6. Again monomeric fragments co-purified, indicating the formation of a heterodimer.

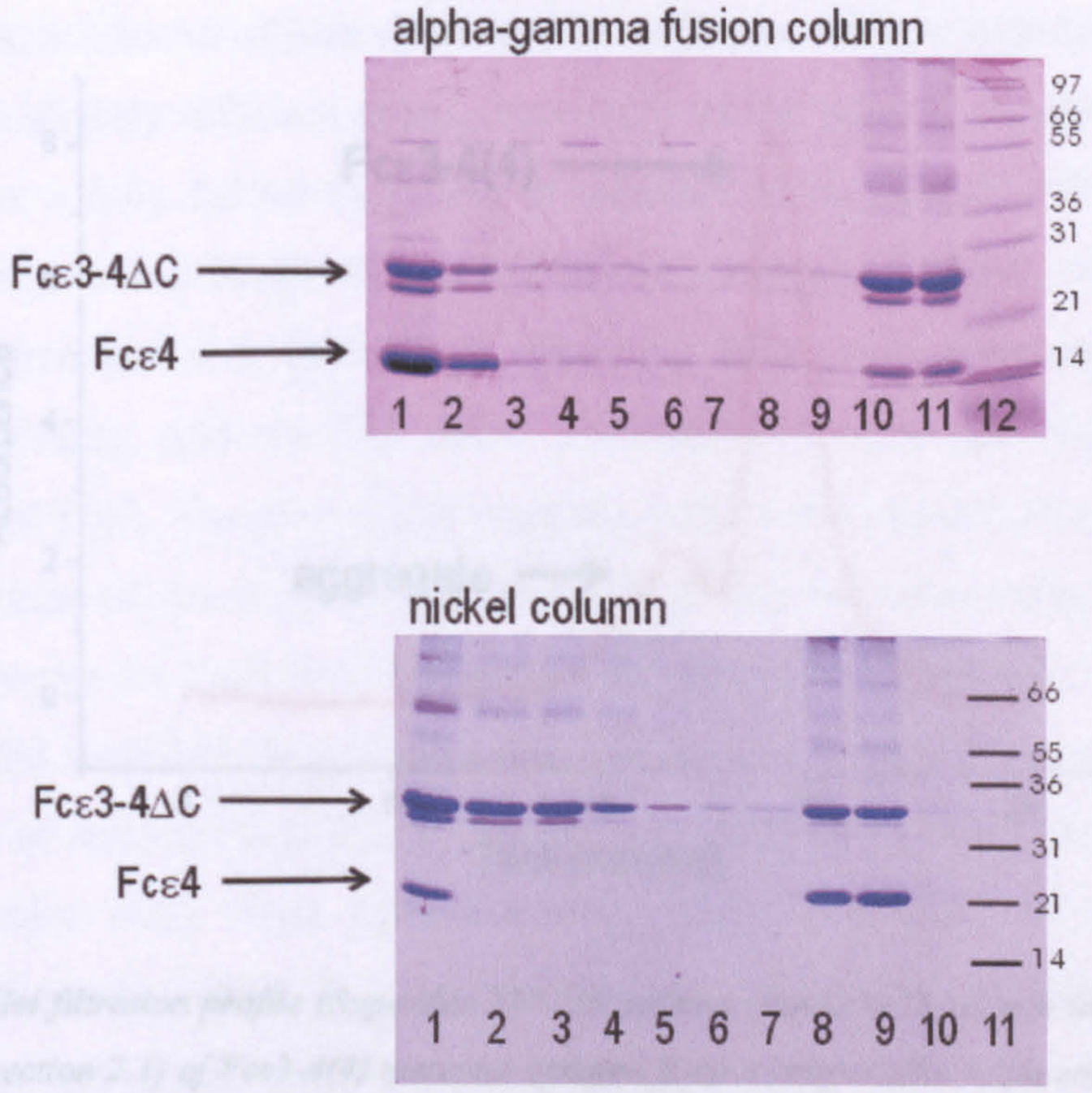

Figure 5.6: Top panel: α-γ fusion purification step in Fcε3-4(4) refold: lanes 1 and 2 are unbound fractions (note Fcε3-4 appears in the drop through due to saturation of the α-γ matrix), lanes 3-9 wash fractions and lanes 10 and 11 eluted fractions. Bottom panel: nickel column step from Fcε3-4(4) purification: lane 1 pre-purification sample, lanes 2-7 unbound fraction, lanes 8 and 9 eluted fractions.

Unfortunately, the increase in the amount of protein meant that the preparation appeared to be more prone to covalent aggregation, as can be seen in the smearing in the gel and higher molecular weight bands corresponding to covalently linked fragments (lanes 10 and 11 in the top panel, lanes 8 and 9 in the lower panel; smears from 36kDa and upwards according to the markers – figure 5.6). This occurred after elution from the α-γ fusion column as the material that was applied was composed of monomeric material collected from the gel filtration step.

Once all purified material had been combined, there was sufficient material for biophysical analysis, but recovery levels meant it was not possible to re-purify the material by gel filtration to reduce the amount of covalent aggregate. An analytical gel filtration profile of the material collected was obtained; this can be seen in figure 5.7. A total yield of less than 200μg was recovered from a refold of 20mg, due to the aggregation problems.

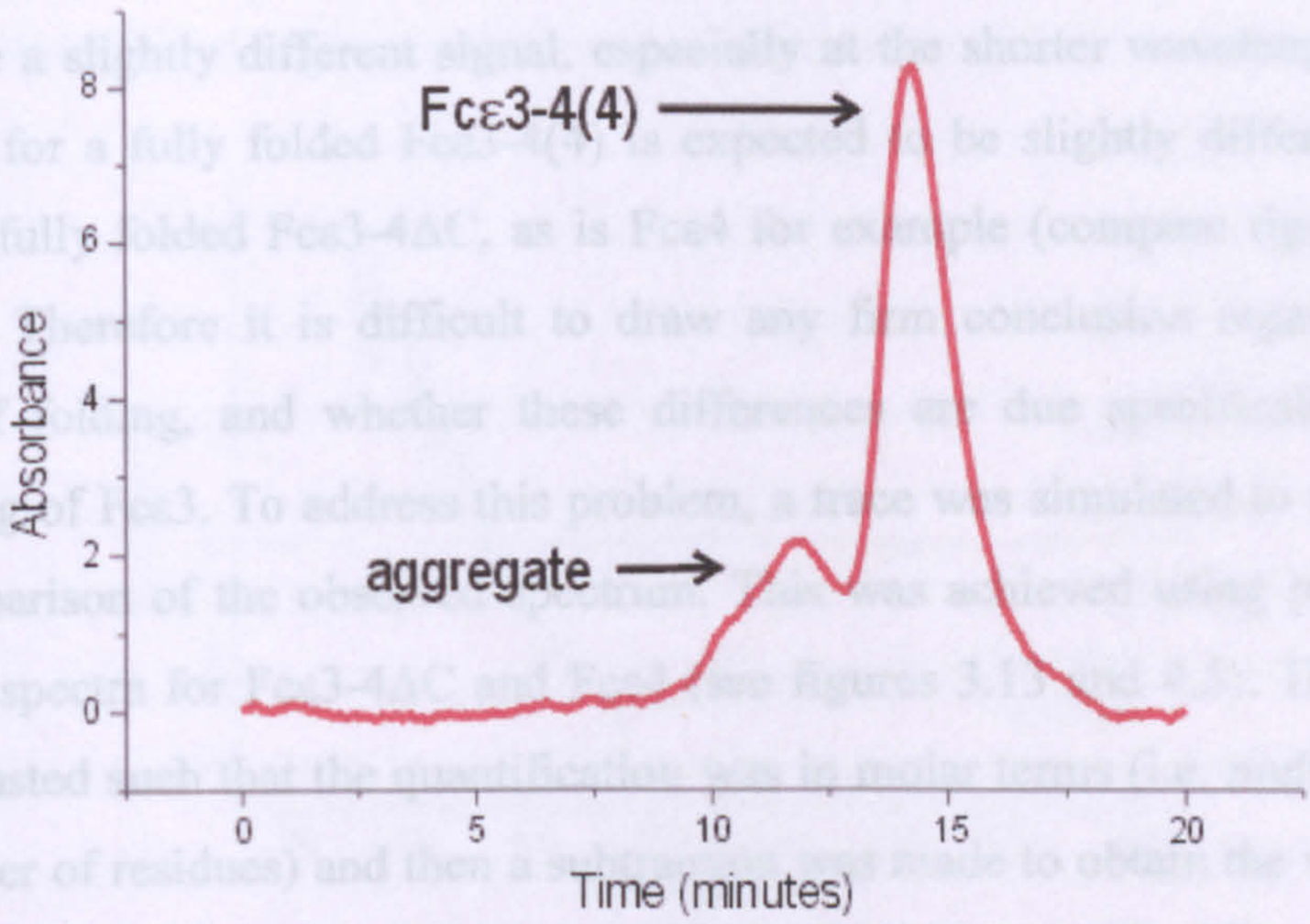

Figure 5.7: Gel filtration profile (Superdex S75 HR column, run at 0.75 ml/min in gel filtration buffer – see section 2.1) of Fcε3-4(4) material isolated from a preparative scale combined refold of GuHCl solubilised Fcε4 and Fcε3-4ΔC fragments.

Of the total yield ~10% appeared to be aggregate. Although not ideal, the recovery did provide enough material to carry out further structural and functional characterisation.

5.4 Characterisation

The first step in characterising the heterodimer was circular dichrosim spectroscopy. This was carried out using a larger path length cell because the material obtained was dilute and prone to precipitation if concentrated. The result of this was a noisy spectrum, as observed for Fcε4 F506R. Therefore the trace is cut off at 200nm because from that point onwards the data was not of sufficient quality. As a control, the spectrum for a fully folded Fcε3-4ΔC fragment was also recorded at an identical protein concentration. The values were then scaled to account for the longer path length cell and lower protein concentration. After scaling, the results obtained for the control were (virtually) identical to those collected under ideal conditions (Chapters 3 and 4; figures 3.13 and 4.5) indicating that the correction process had worked satisfactorily. The data can be seen (both Fcε3-4ΔC and Fcε3-4(4)) in the top panel of figure 5.9. It is clear that both fragment preparations are composed of folded material, with the

characteristic minimum of beta-sheet seen at ~215 nm. However, the heterodimer does have a slightly different signal, especially at the shorter wavelengths. The spectrum for a fully folded Fcε3-4(4) is expected to be slightly different from that of a fully folded Fcε3-4ΔC, as is Fcε4 for example (compare figures 3.13 and 4.5). Therefore it is difficult to draw any firm conclusion regarding the degree of folding, and whether these differences are due specifically to the structuring of Fcε3. To address this problem, a trace was simulated to provide a fair comparison of the observed spectrum. This was achieved using previously recorded spectra for Fcε3-4ΔC and Fcε4 (see figures 3.13 and 4.5). The values were adjusted such that the quantification was in molar terms (i.e. multiplied by the number of residues) and then a subtraction was made to obtain the values for a single folded Fcε3 when part of a fully folded Fcε3-4ΔC. This was then subtracted from the Fcε3-4ΔC spectrum to yield a theoretical spectrum for Fcε3-4(4). The process of subtraction is outlined in figure 5.8.

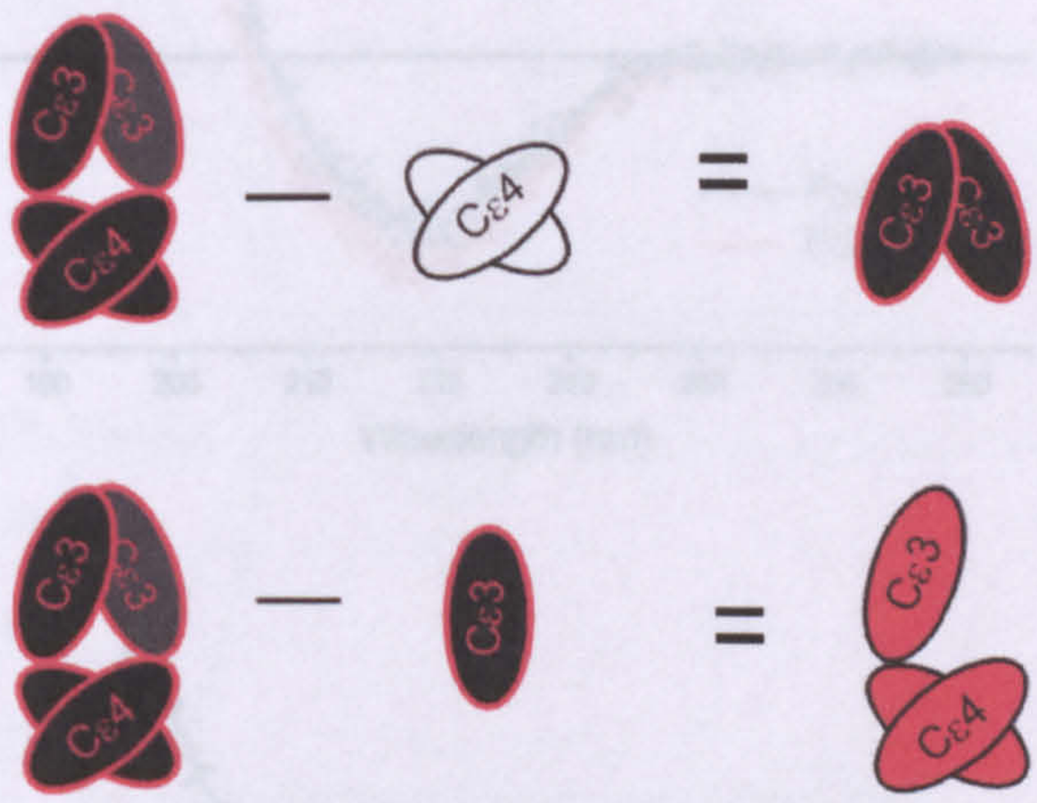

Figure 5.8: Process of subtraction used to create a simulated spectrum for a fully folded Fcε3-4(4). Firstly the spectrum for the Fcε4 dimer was subtracted from that of Fcε3-4ΔC to give the spectrum for a folded Fcε3. This value was then adjusted to provide the spectrum for a single folded Fcε3 domain, and was then subtracted from the original Fcε3-4ΔC spectrum to yield the theoretical value for Fcε3-4(4).

The result of this simulation is displayed in the middle panel of figure 5.9, alongside the experimental trace for a fully folded Fcε3-4ΔC. The data are plotted together with a trend line calculated using an adjacent averaging algorithm. This enables a straightforward comparison to be made between the

simulated and collected datasets (see bottom panel for collected data presented in the same style) but also gives an indication of the error within the data collected.

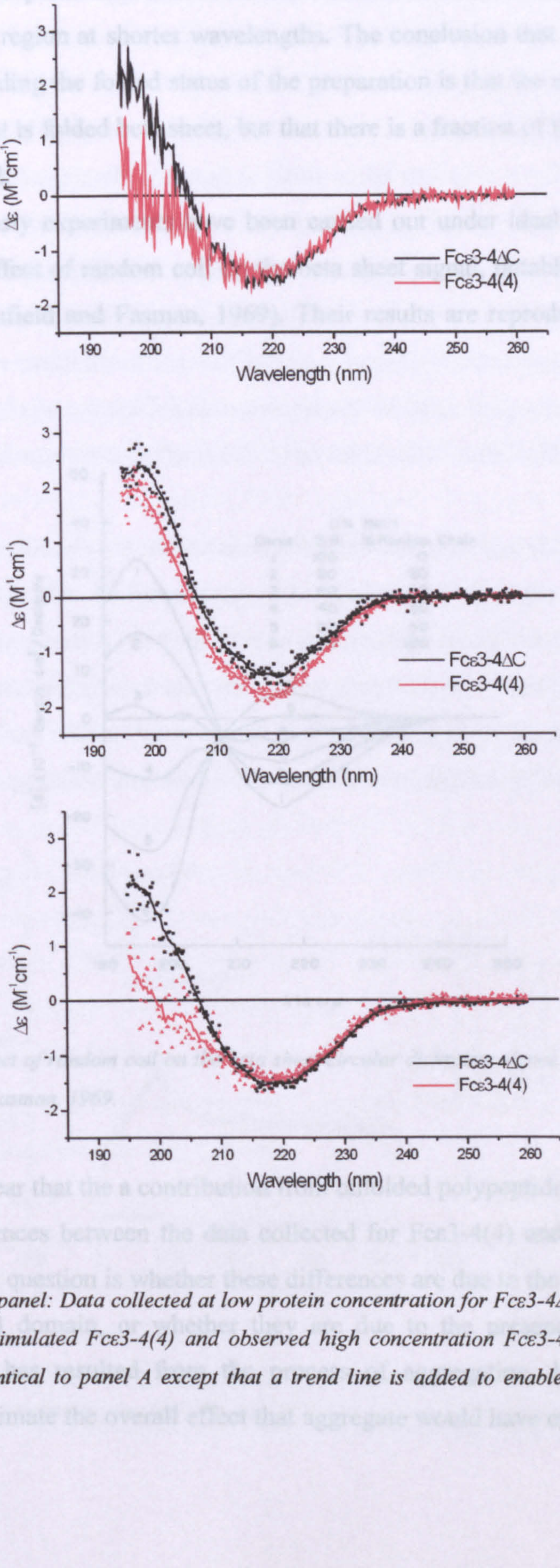

Figure 5.9: Top panel: Data collected at low protein concentration for Fcε3-4ΔC and Fcε3-4(4). Middle panel: Simulated Fcε3-4(4) and observed high concentration Fcε3-4ΔC data. Bottom panel: Data identical to panel A except that a trend line is added to enable comparison with panel B data.

Comparison of the simulated trace for Fcε3-4(4) (middle panel figure 5.9) with the experimental data (lower panel figure 5.9) shows that there is a shift upwards in the experimental data at the 215 nm minimum, and a shift downwards in the positive region at shorter wavelengths. The conclusion that can be drawn from this regarding the folded status of the preparation is that the majority of the material present is folded beta sheet, but that there is a fraction of the preparation that is unfolded.

Previously experiments have been carried out under ideal conditions to establish the effect of random coil on the beta sheet signal, notably the work by Fasman (Greenfield and Fasman, 1969). Their results are reproduced in figure 5.10.

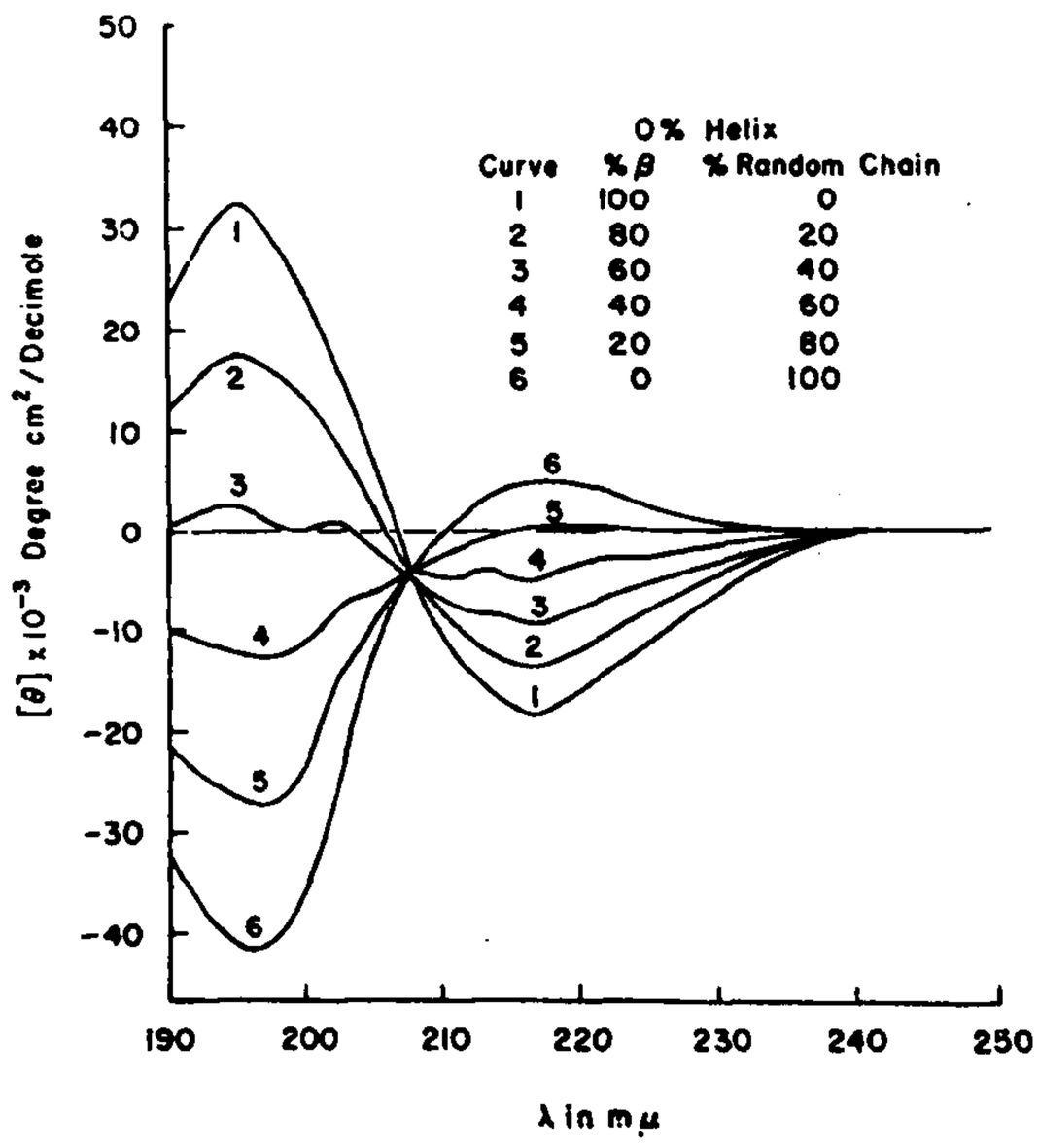

Figure 5.10: Effect of random coil on the beta sheet circular dichroism signal, reproduced from Greenfield and Fasman, 1969.

It is clear that the a contribution from unfolded polypeptide could account for the differences between the data collected for Fcε3-4(4) and the simulated spectrum. The question is whether these differences are due to the presence of an unfolded Fcε3 domain, or whether they are due to the presence of unfolded material that has resulted from the process of aggregation. It is extremely difficult to estimate the overall effect that aggregate would have on the signal for

the folded species, as it may represent a mixture of partially folded material alongside random coil. It must also be noted that if the Fcε3 were unfolded it would be very prone to aggregation. However, from Fasman's data it is clear that the difference between the observed and calculated spectrum represents a contamination of less than 20%. If the Fcε3 were fully unfolded one would expect to see a 33% decrease in signal, assuming no aggregate. Since it may be assumed that the aggregate material is likely to be unfolded it indicates that the Fcε3 domain within Fcε3-4(4) is at least partially folded for the signal to be as strong as it is (aggregate makes ≤10% of the final preparation, see figure 5.7). Equally, it is clear that the fragment isolated is not completely folded. It therefore appears that the presence of Fcε4 is having a beneficial effect on the folding of Fcε3, but is perhaps not sufficient to completely stabilise the preparation. It may even be that the aggregate is the result of an incomplete stabilisation of the Fcε3 domain.

Further analysis was undertaken with this fragment to estimate its affinity for FcεRI using SPR. Unfortunately, either due to the aggregate, the unstable nature of the preparation, or both, it was not possible to collect data due to the non-specific accumulation of material on the chip surface – see figure 5.11. This behaviour was not unlike that seen for Fcε3-4 F506R (data not shown), adding weight to the suggestion that the Fcε3 domain is not completely folded.

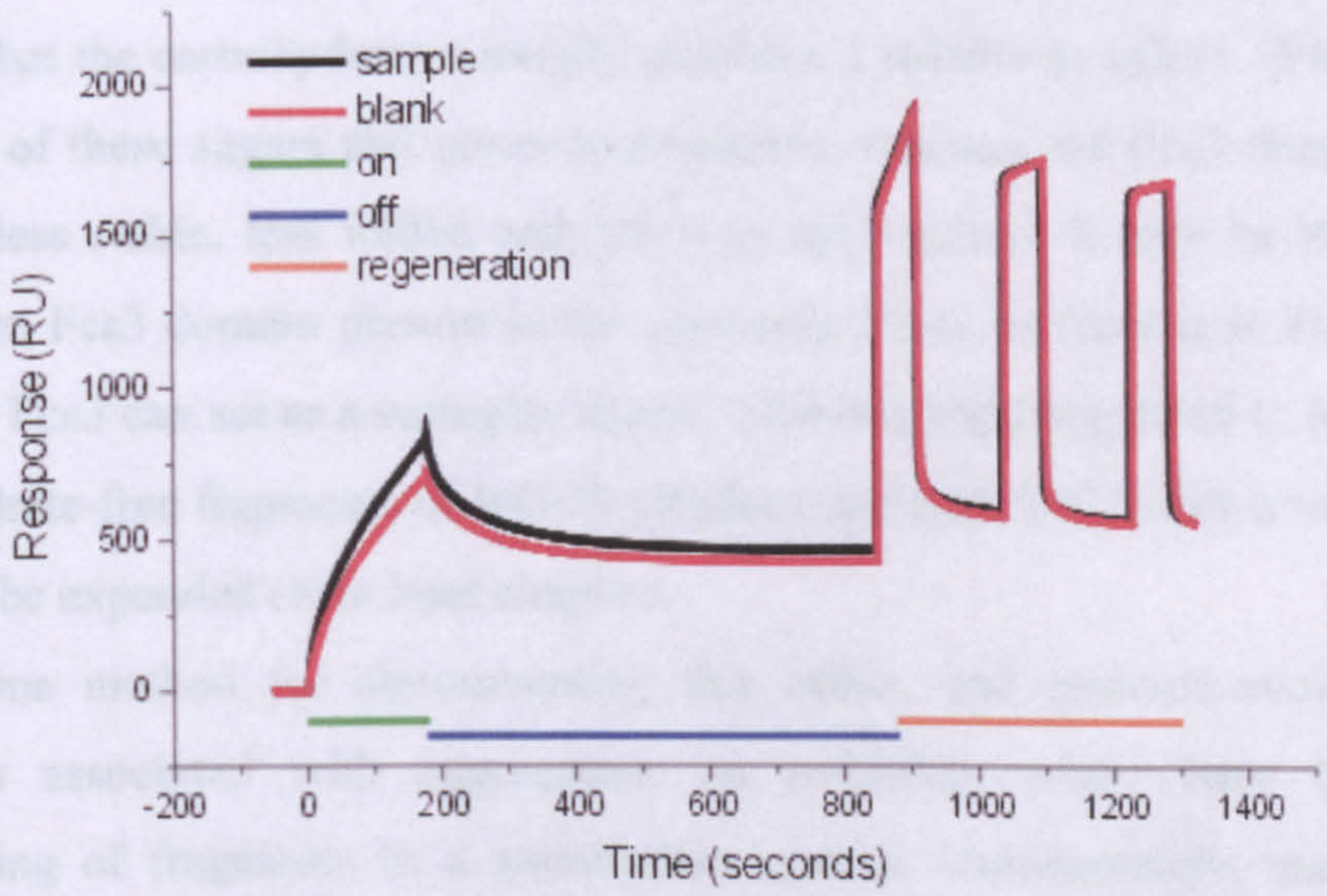

Figure 5.11: Biacore trace obtained for Fcε3-4(4) passed over immobilised α-γ fusion protein. Blank refers to a coupled surface (IgG4Fc only) that acts as a control for non-specific binding.

Several attempts were made at repeating the preparation to obtain a smaller amount of aggregate, but unfortunately it appears that the method is only able to yield material that is prone to this type of behaviour. The consistent appearance of aggregate suggests an inherent instability of the Fcε3-4(4) fragment.

5.5 Discussion

The data presented in this chapter indicate that longitudinal contact between a folded Fcε4 and Fcε3 domain at least partially stabilises the folding of the latter. This does therefore also imply that the Fcε3 domain of IgE-Fc is not able to completely fold in the absence of lateral contacts. However, Fcε4 is able to stabilise Fcε3 to some degree, and the Fcε3-4(4) fragment is clearly more folded than the monomers described in previous chapters. Unfortunately the fragment obtained from the mixed refold method is not stable in solution for prolonged periods. This prevented storage and the accumulation of material that would have enabled a more rigorous analysis to be undertaken.

The Fcε4 domains were presented in such way that they were expected to fold, as discussed in previous chapters. It is therefore reasonable to assume that the problems observed with the Fcε3-4(4) are the result of the behaviour of Fcε3. One possible reason for this effect may the absence of carbohydrate. Although the fragment commonly folds without glycosylation in the form of Fcε3-4ΔC, it may be that the carbohydrate normally provides a stabilising effect. Without the presence of these sugars that cover hydrophobic residues, the Fcε3 domain may become less stable, less folded and prone to aggregation. It may be that when there is an Fcε3 domain present in the opposing chain, as there is in Fcε3-4ΔC, the other Fcε3 can act as a surrogate shield. This has been suggested to happen in carbohydrate-free fragments of IgG-Fc (Radaev and Sun, 2001) and is something that will be expanded on in later chapters.

One method for circumventing this effect, and perhaps avoiding the problems associated with aggregation on refolding, might have been the engineering of fragments in a mammalian system. Unfortunately, mammalian systems have only yielded fragments when the protein can fold and/or solubilise correctly; little success was achieved when expressing Fcε3 for example (R. Young, personal communication), or fragments without glycosylation at Asn 394

(Nettleton and Kochan, 1995; Sayers *et al*, 1998). Previously, the fragments produced in *E.coli* had provided unequivocal answers regarding folding status, both for fully folded and unfolded proteins. *E. coli* expression was therefore the appropriate system, especially as carbohydrate had not been essential for the folding of other IgE-Fc fragments (Geha *et al*, 1985, Helm *et al*, 1988). However, it may be that the production of a heterodimer, following the strategy of Carter (Carter, 1997), by engineering the Fcε4 domain interface to favour the association of heterodimers, could be used to produce a Fcε3-4(4) with a glycosylated Fcε3 domain. Such a fragment might provide a more definitive answer regarding the need for longitudinal contacts.

Given the result obtained with Fcε3-4(4), it appears that the Fcε3-4ΔC fragment remains the minimal fragment of the IgE-Fc within which Fcε3 folds completely. Therefore, the functional properties of this fragment were investigated further in an attempt to discover why Fcε3 remains stable within this context, but becomes increasingly unstable when further structural features are removed.

The effect of disulphide linkage and glycosylation on high affinity receptor binding and folding of Fcε3-4

Chapter 6: The effect of disulphide linkage and glycosylation on high affinity receptor binding and folding of Fcε3-4

6.1 Introduction

The results presented in chapter 5 indicated that it is not possible to fold Fcε3 completely without lateral contacts. Therefore the minimal fragment within which Fcε3 appears to be fully structured remains the *E. coli* expressed Fcε3-4ΔC. This fragment is particularly interesting in that it lacks two structural features of the more extensively studied mammalian Fcε3-4; disulphide linkage at the N-terminus (Cys 328) and glycosylation at Asn 394. Previously it has been suggested these are of little consequence with respect to stability and the binding of FcεRI (Henry, PhD thesis, 1997; Basu *et al*, 1993). However, the results described in Chapter 5 indicated the possibility that carbohydrate may have an important role in the stabilisation of Fcε3. Furthermore, it has recently been discovered that the disulphide pairing present in the mammalian Fcε3-4 fragment is not replicated in the full Fc (Wan *et al*, 2001). In the light of these recent findings, it appeared that a re-examination of the properties of this molecule might yield vital clues as to the basis of the high affinity of Fcε3-4 for FcεRI, and the stability of Fcε3 within the Fcε3-4 fragment.

6.2 Expression and purification of mammalian Fcε3-4

To enable a fair examination of the *E. coli* Fcε3-4ΔC, it was also necessary to produce a mammalian Fcε3-4 fragment, i.e. an Fcε3-4 fragment that is glycosylated at Asn 394 and disulphide-linked at the N-terminus. The mammalian fragment was expressed from permanently transfected NS0 mouse myeloma cells, a procedure previously established for a number of investigations within the laboratory (Keown *et al*, 1997, Shi *et al*, 1997). This fragment has an identical number of residues (328-547) to Fcε3-4ΔC, but has an Asn-Gln mutation at 371 so that the fragment is only glycosylated at Asn 394. The Cys is maintained at 328 to allow covalent linkage of the homodimer. The method for isolating material involved a simple two-step purification using a α-γ fusion affinity column (as used in Chapter 5), followed by gel filtration on an HPLC system, as outlined in section 2.3.5. The final isolated fragment is shown in figure 6.1 as a single band on a non-reducing 15% SDS-PAGE in comparison

with an isolated Fcε3-4ΔC fragment run under identical conditions. Crucially, this demonstrates the formation of the inter-chain disulphide at position 328.

Figure 6.1: 15% non-reducing SDS-PAGE of mammalian Fcε3-4 (left) and E. coli *Fcε3-4ΔC (right).*

The formation of the disulphide was confirmed by reducing the fragments (inset figure 6.2), lowering the apparent molecular weight of the mammalian fragment from around 50 kDa to less than 30 kDa. This agreed closely with the size of Fcε3-4ΔC, although the band for the mammalian material was slightly higher due to the presence of glycosylation (confirmation of the glycosylation status can be found in Chapter 7, section 7.2). Finally, the purified fragments were run back-to-back on an S200 gel filtration column – see below:

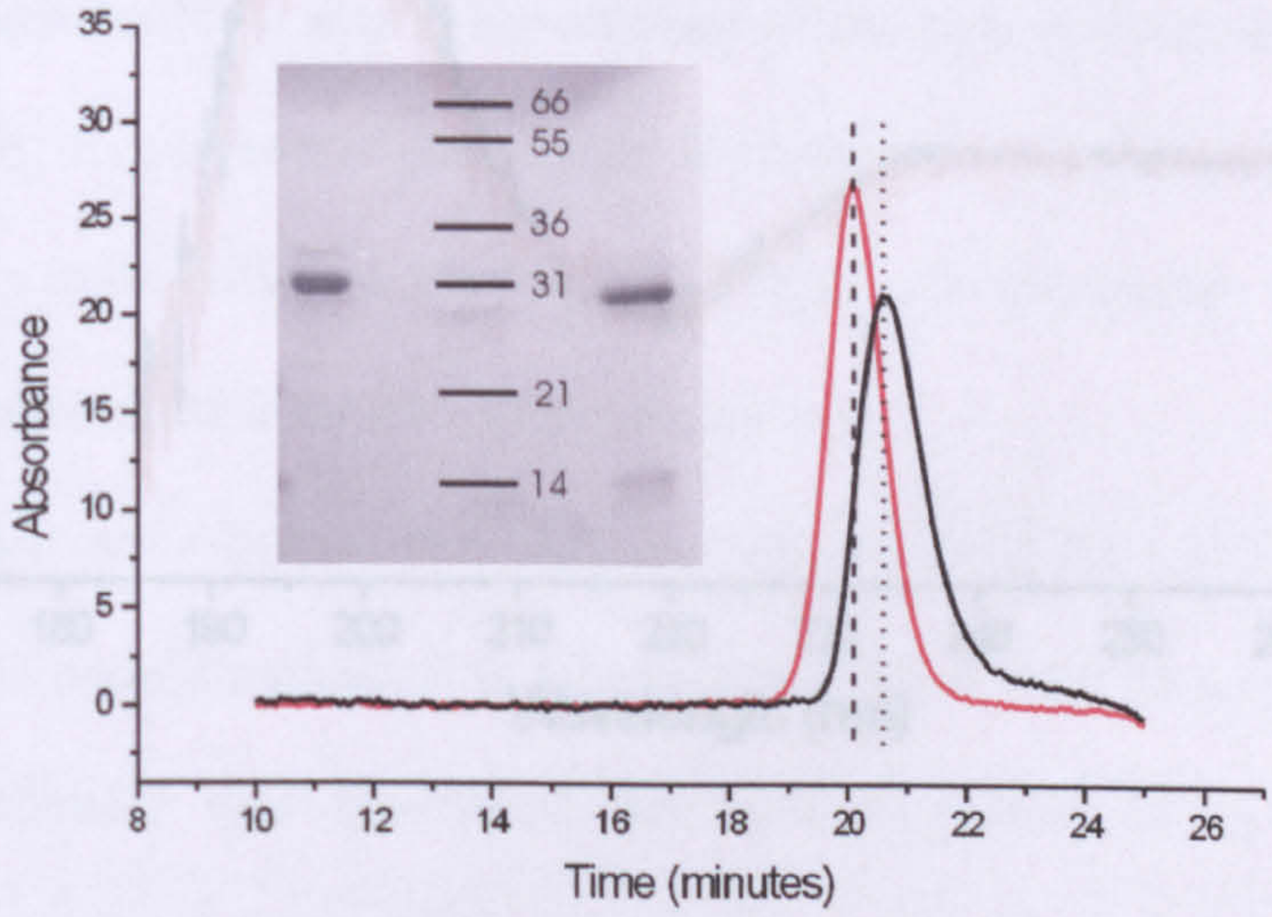

Figure 6.2: Gel filtration profile (Superdex S200 HR column, run at 0.75 ml/min in gel filtration buffer – see section 2.1) of mammalian Fcε3-4 (red) and E. coli *Fcε3-4ΔC (black). Inset: 15% reducing SDS-PAGE of mammalian Fcε3-4 (left) and* E. coli *Fcε3-4ΔC (right).*

Under analytical gel filtration conditions the apparent molecular weight of mammalian Fcε3-4 was slightly higher than that of *E. coli* Fcε3-4ΔC, with a time difference of ~ 30 seconds. This difference was larger than expected given the minor shift seen on SDS-PAGE. This could be the result of a difference in the conformation of the Fcε3-4ΔC molecule compared with mammalian Fcε3-4, i.e. to one that is more compact, due to the release of the constraints imposed by the disulphide bond at position 328, or the absence of carbohydrate. It is not the result of the "monomerisation" of Fcε3-4ΔC, as this fragment has already been confirmed to be a dimer in solution – see Chapter 4, section 3.3.2.

6.3 Folding and stability of mammalian Fcε3-4 and *E. coli* Fcε3-4ΔC

Initially the interest in these two fragments stemmed from speculation that the absence of carbohydrate could be having a negative impact on the structuring of the Fcε3 domains. Therefore the two isolated fragments were examined by circular dichroism spectroscopy, see figure 6.1:

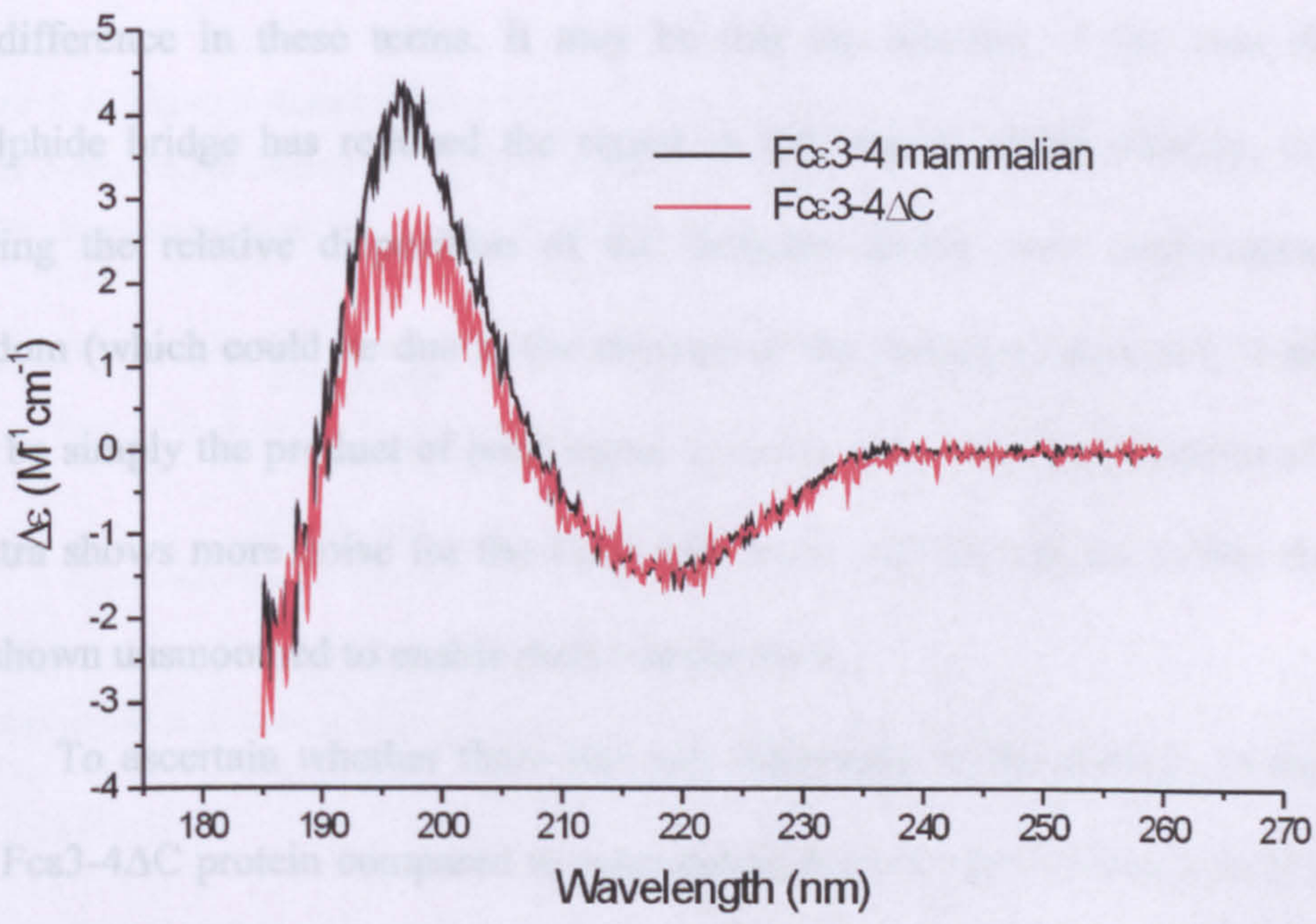

Figure 6.3: Circular dichroism spectra of E. coli *Fcε3-4ΔC (red line) and mammalian expressed Fcε3-4 (black line). Data were collected according to the method outlined in section 2.4.1.*

In comparing the spectra it is clear that there is a difference in the magnitude of the signal between 195nm and 205nm. This region corresponds to the signal obtained from an ordered arrangement in the peptide backbone. If the protein is disordered (i.e. random coil), a strong negative band is seen; a strong positive signal is observed in a folded protein (see Chapter 2, figure 2.4). The lower signal in this region may be explained for *E. coli* Fcε3-4ΔC by the presence of a small amount of residual random coil from the refolding process, but the beta sheet signal is of an identical magnitude. If the drop at 200nm were due to the presence of random coil, it would be associated with a change in the magnitude of the signal in the β-sheet region (see the Greenfield and Fasman data reproduced in Chapter 5, figure 5.10). It is therefore difficult to rationalise the difference in these terms. It may be that the absence of the inter-chain disulphide bridge has reduced the signal in this region, either directly, or by altering the relative disposition of the domains and/or their conformational freedom (which could be due to the absence of the carbohydrate also). It might also be simply the product of poor signal to noise, as a close examination of the spectra shows more noise for the Fcε3-4ΔC trace. All the spectra in this thesis are shown unsmoothed to enable such comparisons.

To ascertain whether there was any difference in the stability of the *E. coli* Fcε3-4ΔC protein compared to mammalian Fcε3-4, the CD signal at 215nm (β-sheet minimum) was monitored for both fragments as a function of temperature, see figure 6.4 and table 6.1.

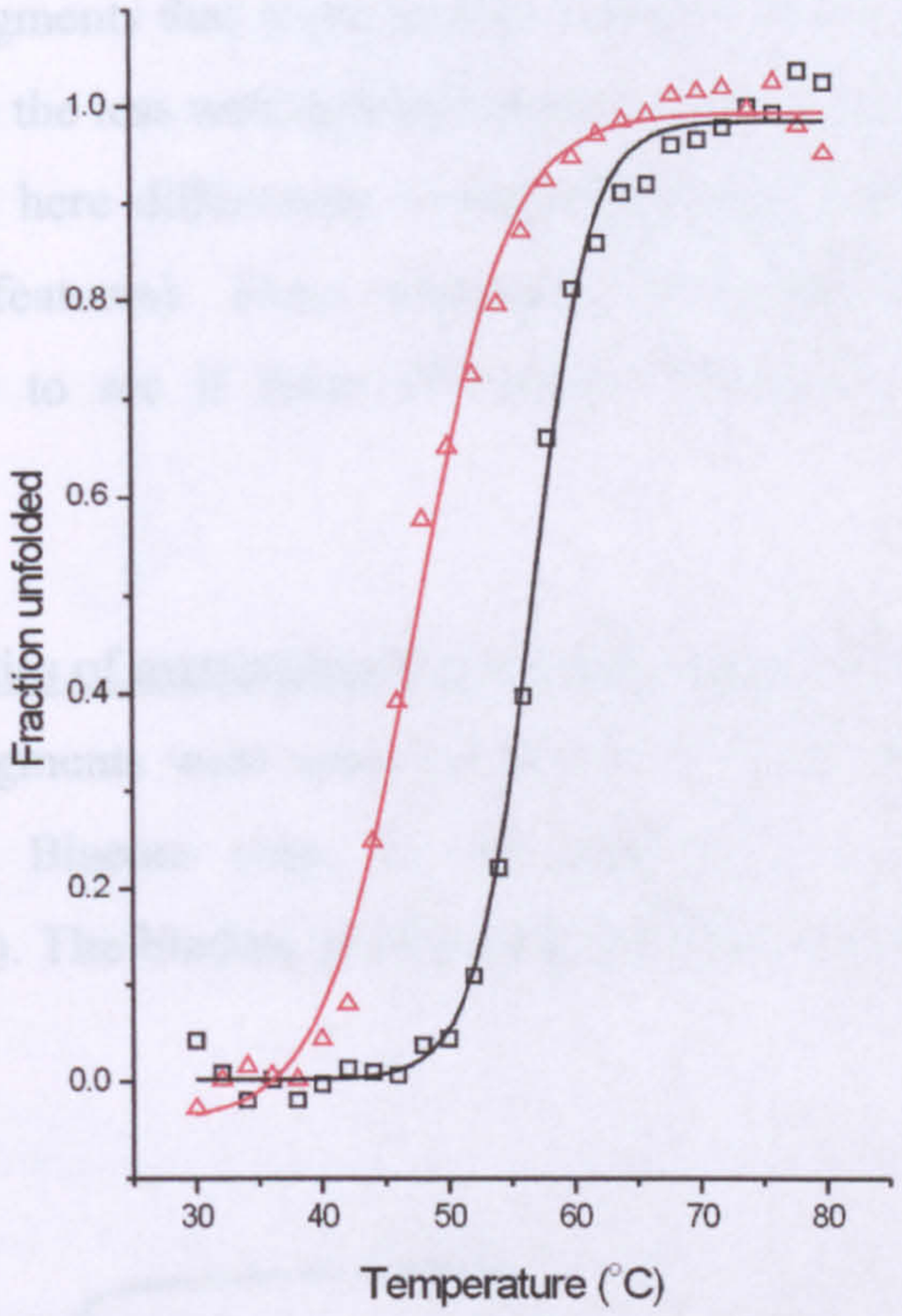

Figure 6.4: Thermal denaturation profile of E. coli *Fcε3-4ΔC (red) and mammalian Fcε3-4 (black) based on the monitoring of the CD signal of each protein at 215 nm; sigmoidal curve fitted to demonstrate transition between folded and unfolded baselines.*

Fragment	T_m (°C)
Fcε3-4	56.7
Fcε3-4ΔC	47.6

Table 6.1: Melting points for E. coli *Fcε3-4ΔC and mammalian Fcε3-4. Temperatures represent the point at which protein is 50% unfolded according to the circular dichroism signal at 215nm.*

It is apparent from the transitions that the *E. coli* Fcε3-4ΔC fragment is not as stable as the mammalian Fcε3-4 fragment. It may be that this is due to the absence of carbohydrate, the inter-chain disulphide, or a combination of both. At the wavelength at which denaturation was monitored (215nm), the signal recorded was identical for the two fragments prior to denturation (see figure 6.3, recorded at room temperature). This wavelength represents the point at which

beta structure is normally assessed by CD, and thus there are obvious differences between the two fragments that relate to their stability of their β-sheet structures (this is in contrast to the less well defined region where divergence was observed for the full spectra; here differences in signal are much harder to attribute to specific structural features). These fragments were also examined for their binding capabilities to see if these differences impacted on overall binding function.

6.4. Binding studies of mammalian Fcε3-4 and *E. coli* Fcε3-4ΔC

The two fragments were analysed firstly for their ability to bind FcεRI immobilised on a Biacore chip, in the form the of α-γ fusion protein ($(sFc\varepsilon RI\alpha)_2IgG_4$-Fc). The binding profiles and fits obtained are shown in figures 6.5 and 6.6.

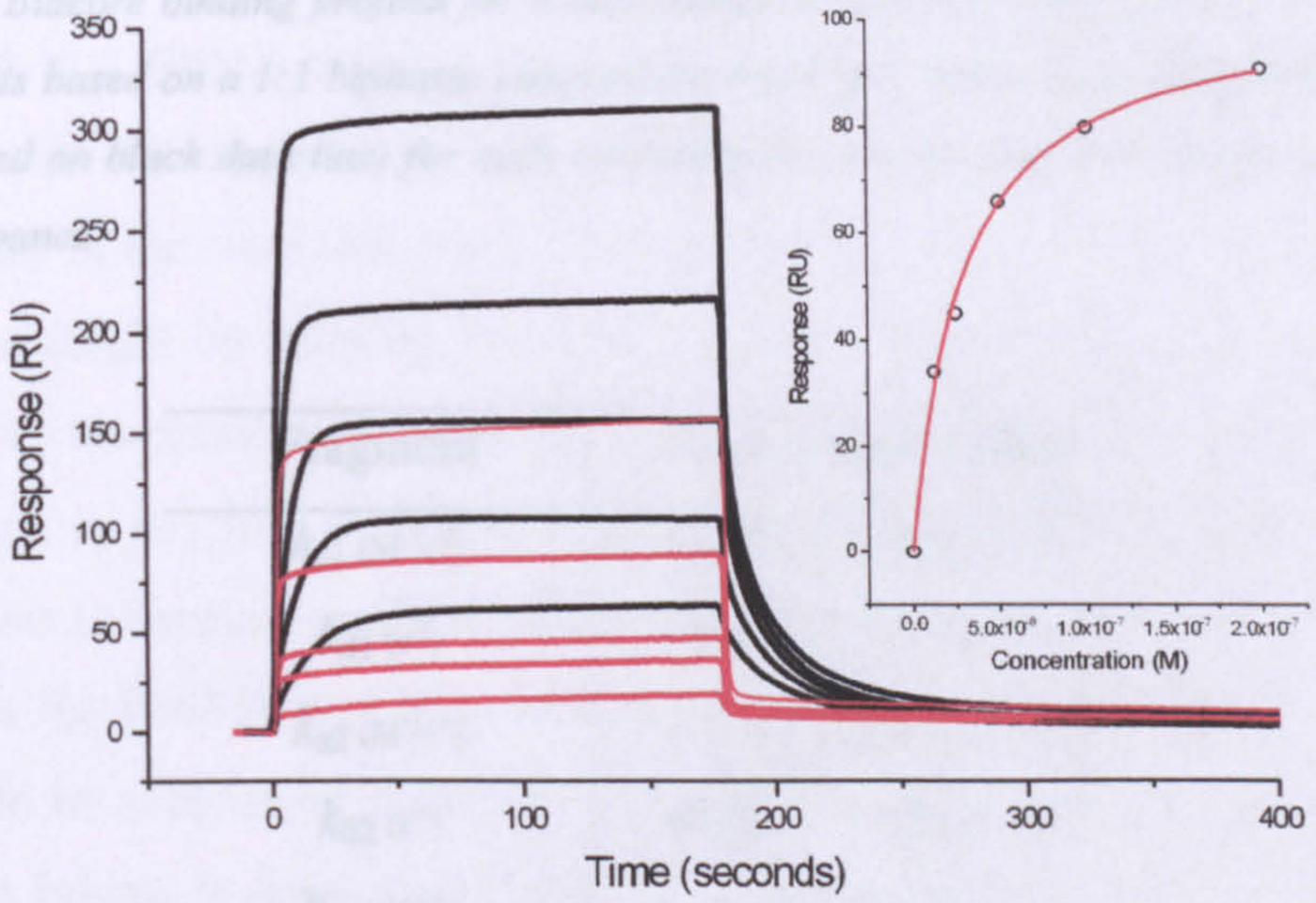

Figure 6.5: Biacore binding profiles for a concentration series of Fcε3-4ΔC (100nM to 6.25nM) showing binding to blank (red) and FcεRI (black) surfaces. Inset is the steady state fit (R_{eq} versus concentration) used to derive affinity constants.

Surface	K_A ($M^{-1} \pm$ SE)	R_{max} (RU)
α-γ fusion (436 RU)	$(2.66 \pm 0.24) \times 10^7$	180 (± 5)
α-γ fusion (216 RU)	$(3.43 \pm 0.30) \times 10^7$	104 (± 3)

Table 6.2: Affinity constants derived from steady state analysis of Fcε3-4ΔC. Two surfaces were used at different immobilisation levels, with five concentrations for each surface.

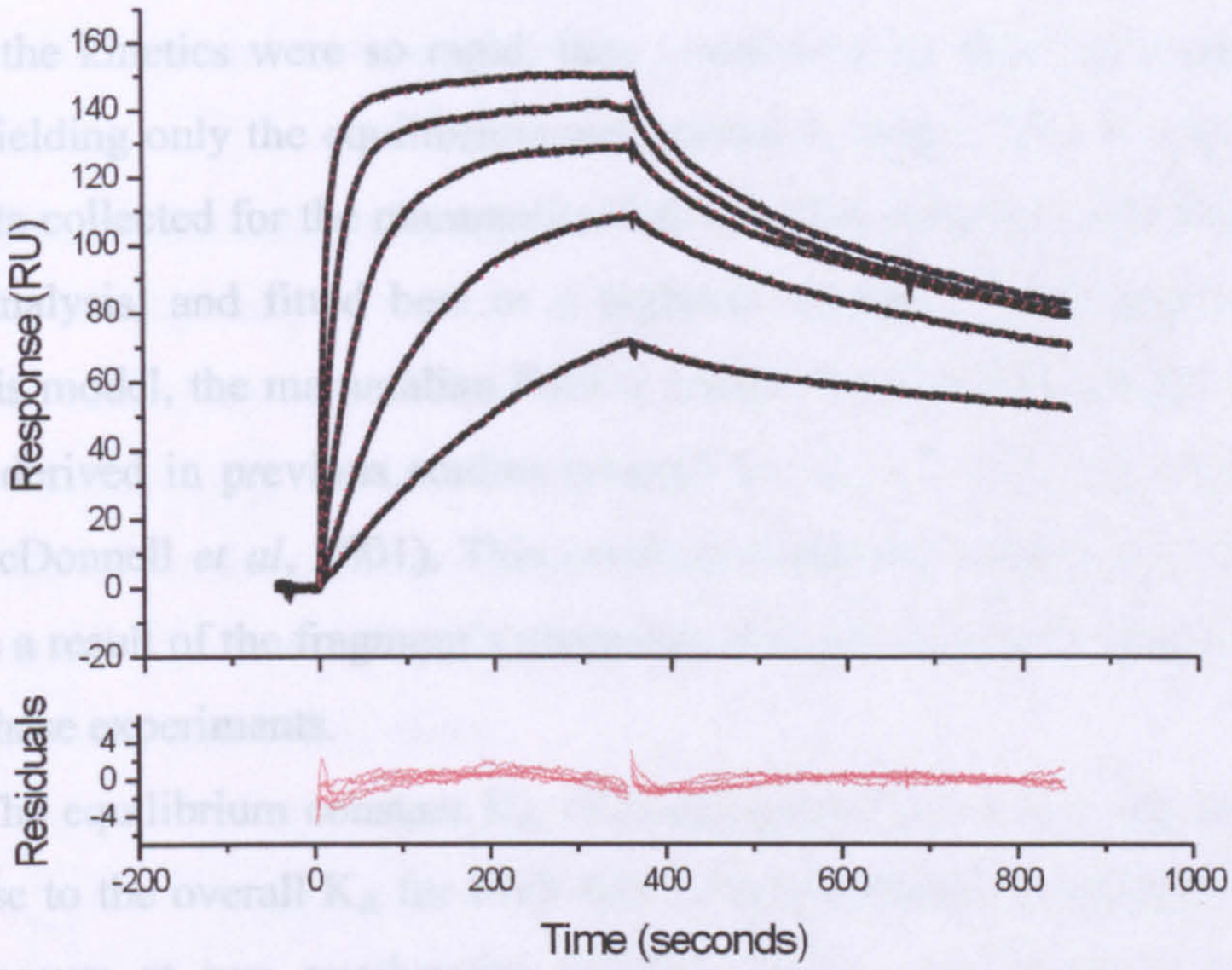

Figure 6.6: Biacore binding profiles for a concentration series of mammalian Fcε3-4 (100nM - 6.25nM). Fits based on a 1:1 biphasic competition model are shown as a red dotted line (visible superimposed on black data line) for each concentration and residuals for the fits are shown in the bottom panel.

Fragment	Fcε3-4 mammalian
k_{a1} ($M^{-1}s^{-1}$)	$(4.77 \pm 1.88) \times 10^{5}$
k_{d1} (s^{-1})	$(1.21 \pm 0.19) \times 10^{-2}$
k_{a2} ($M^{-1}s^{-1}$)	$(3.08 \pm 0.65) \times 10^{5}$
k_{d2} (s^{-1})	$(6.26 \pm 1.29) \times 10^{-4}$
K_{a1} (M^{-1})	3.94×10^{7}
K_{a2} (M^{-1})	4.92×10^{8}
R_1/R_0	0.15 ± 0.03
Overall K_A (M^{-1})	4.2×10^{8}

Table 6.3: Affinity constants derived from kinetic analysis of mammalian Fcε3-4. The R_1/R_0 ratio describes relative contribution from each component of the biphasic fit; the overall K_A represents an average of the two individual K_a based on this ratio.

Striking differences can be seen when the *E. coli* Fcε3-4ΔC and mammalian Fcε3-4 binding profiles are compared. The Fcε3-4ΔC fragment has

very fast on and off rates and appears to be a simple monophasic interaction. Because the kinetics were so rapid, they could only be fitted to a steady state model, yielding only the equilibrium association constant. This is very different to the data collected for the mammalian Fcε3-4. This could be subjected to a full kinetic analysis, and fitted best to a biphasic competitive association model. Using this model, the mammalian Fcε3-4 yielded very similar affinity constants to those derived in previous studies (overall K_A of ~ 5 x 10^8 M^{-1}; Cook *et al*, 1997; McDonnell *et al*, 2001). This confirmed that the behaviour of the Fcε3-4ΔC was a result of the fragment's properties and was not due to the chip surface used in these experiments.

The equilibrium constant K_{a1} of mammalian Fcε3-4 was calculated to be very close to the overall K_A for Fcε3-4ΔC. The interaction between FcεRIα and Fcε3-4 occurs at two overlapping binding sites on the basis of the crystal structure of the complex (Garman *et al*, 2000). The observation of this two-site interaction is a strong justification for the application of the biphasic binding model. In this crystal structure, one of these interaction sites is composed almost solely of the N-terminal linker and it was therefore a concern that some, or all, of this region might be missing from the fragment expressed in *E. coli*. For the mammalian fragment it is easy to ensure the integrity of this region after purification, as any loss of residues would result in a shift in apparent molecular weight. This is because the N-terminal residue in the linker region is the cysteine that forms the disulphide bridge between the two chains, and therefore a large shift would be seen under non-reducing SDS-PAGE. However, in Fcε3-4ΔC this disulphide bridge is not present, and therefore it is difficult to tell if important binding residues are still present, as the loss of a part of the linker would not lead to a dramatic shift in molecular weight. If this site were absent, a gross change in binding kinetics would be expected. The fragment would still be active in binding FcεRIα, as the other binding sub-site within the Fcε3 domain would still be present, but loss of the N-terminal residues might be expected to lead to a difference in affinity and loss of biphasicity. In fact, a significant difference between the gel filtration profiles of the two fragments had already been noted (see figure 6.2), although this was thought to represent a difference in conformation. Therefore, to confirm that the difference in kinetics and gel

filtration profile was not simply due to the loss of important N-terminal residues, the Fcε3-4ΔC fragment was subjected to examination by mass spectrometry.

6.5. Mass spectrometry of Fcε3-4ΔC

The homogeneity and integrity of the refolded Fcε3-4ΔC preparation was assessed by nanospray mass spectrometry (figure 6.7 courtesy of Malcolm Ward of the proteomics unit, Institute of Psychiatry). The analysis gave a final value within 2 Da of the expected molecular weight for Fcε3-4ΔC (MW 24557 with the N-terminal Cys mutated to Ser). This confirmed that the fragment had not lost any of the N-terminal residues.

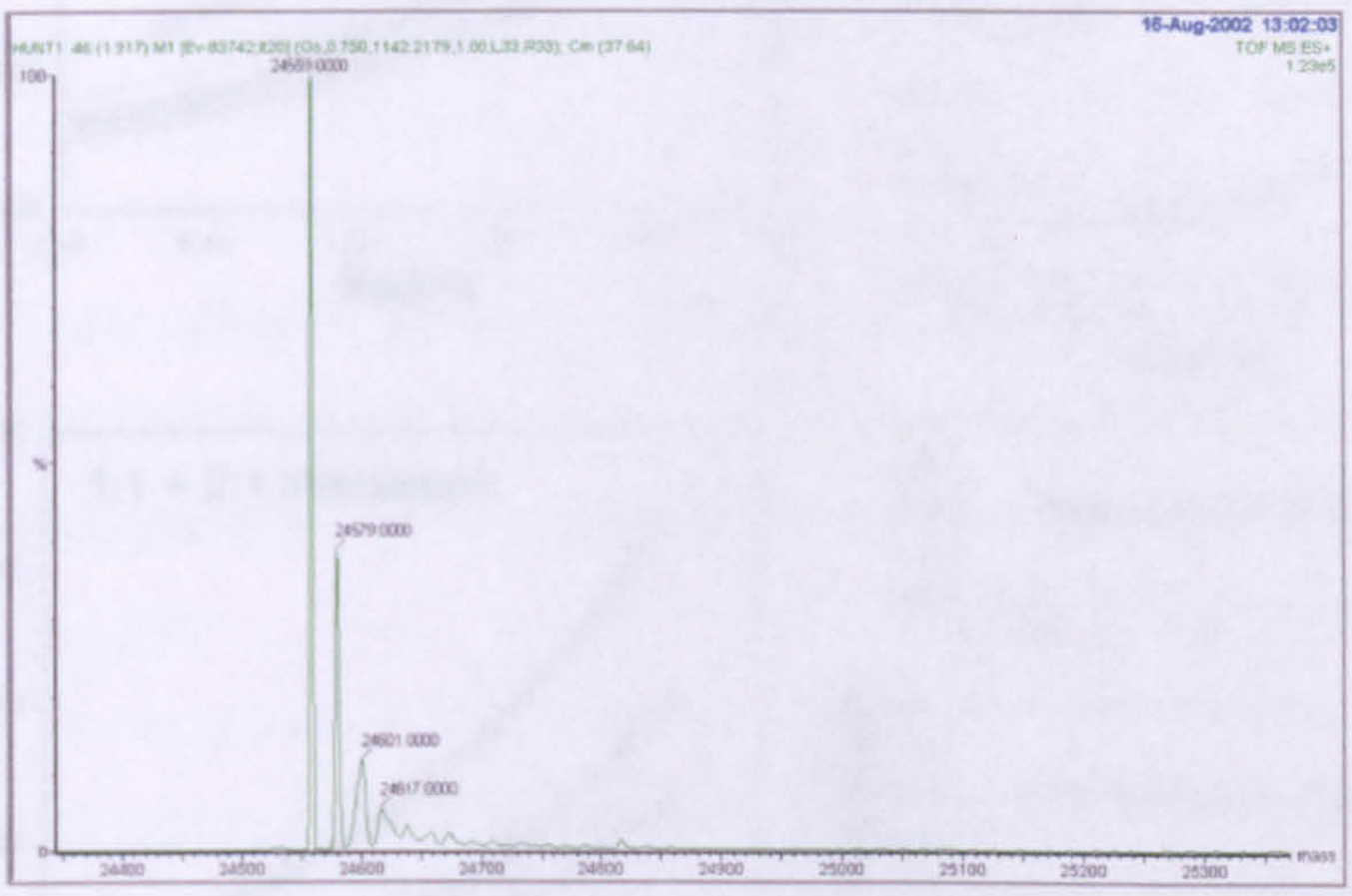

Figure 6.7: Readout from nanospray mass spectrometric analysis of Fcε3-4ΔC. See section for 2.3.3 for the method.

6.6. Analytical ultracentrifugation of Fcε3-4, Fcε3-4ΔC and sFcεRIα

Once the Fcε3-4ΔC fragment was shown to be intact it was important to investigate the binding properties of both fragments under different conditions, to ensure that the differences observed so far were not an artefact of the Biacore assay. Therefore Fcε3-4ΔC binding to sFcεRIα was analysed under equilibrium conditions in the analytical ultracentrifuge. Previous studies of the mammalian Fcε3-4 fragment in the analytical centrifuge had yielded data demonstrating a 1:1 stochiometry with sFcεRIα (Keown *et al*, 1997). Once the data were collected for *E. coli* Fcε3-4ΔC, a very different behaviour was immediately apparent. During the fitting of the equilibrium data to various interaction models, it became clear

that a 2:1 stoichiometry between Fcε3-4ΔC and sFcεRIα was occurring (compare top and middle panels in figure 6.8). Although the residual distribution is similar, statistically the best fit to the data yielded was a mix of 2:1 and 1:1 stoichiometries (see lower panel figure 6.8). The affinity data extracted from this fit are shown in table 6.4.

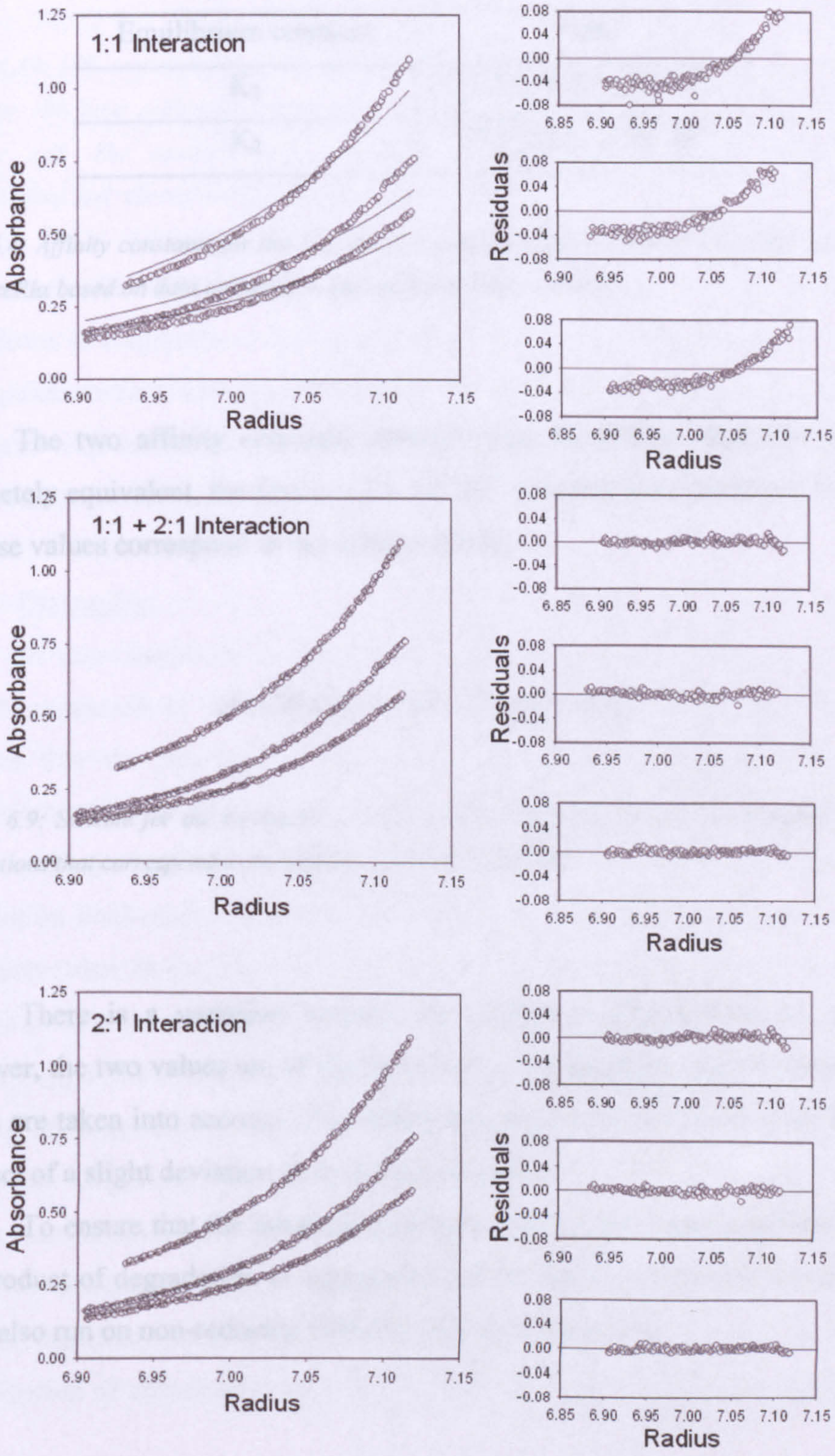

Previous page.

Figure 6.8: Sedimentation equilibrium analytical ultracentrifugation datasets for E. coli *Fcε3-4ΔC binding to sFcεRIα. Data fits based on an interaction stoichiometry of either 1:1, 2:1 or 1:2 are shown for mixes of Fcε3-4ΔC:sFcεRIα at 1:1, 2:1 and 1:2. Residuals for each fit are shown in adjacent panels.*

Equilibrium constant	Value
K_1	$(1.8 \pm 0.4) \times 10^5\ M^{-1}$
K_2	$(7.2 \pm 2.2) \times 10^5\ M^{-1}$

Table 6.4: Affinity constants for the 1:1 and 2:1 complexes formed between sFcεRIα, Fcε3-4ΔC and sFcεRIα based on data collected in the analytical ultracentrifuge.

The two affinity constants derived from the fitting procedure are not completely equivalent, the first is ~ $2 \times 10^5\ M^{-1}$, whereas the second is $7 \times 10^5\ M^{-1}$. These values correspond to the scheme below:

$$A + 2B \underset{K_1}{\longleftrightarrow} AB + B \underset{K_2}{\longleftrightarrow} AB_2$$

Figure 6.9: Scheme for the formation of a 2:1 complex between Fcε3-4 and sFcεRIα showing interactions that correspond to the affinity constants K_1 *and* K_2.

There is a variation between the affinities observed for K_1 and K_2 however, the two values are of the same order of magnitude, and are close when errors are taken into account. The difference observed therefore is most likely a product of a slight deviation in the fitting procedure.

To ensure that the interaction observed during the centrifuge run was not the product of degradation or aggregation of the sample in the cell, the contents were also run on non-reducing SDS-PAGE, see figure 6.10:

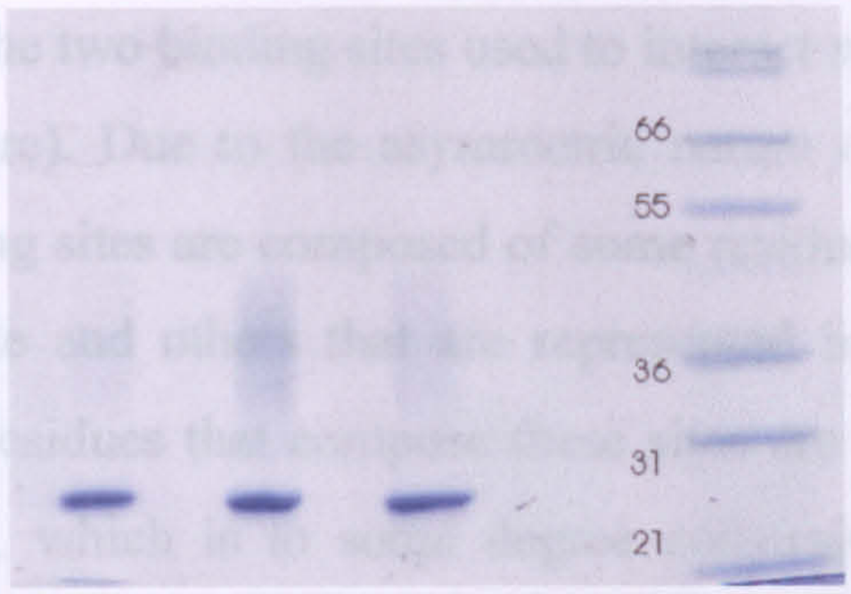

Figure 6.10: 15% non-reducing SDS-PAGE of Fcε3-4ΔC:sFcεRIα mixes from the ultracentrifuge cell after 100 hour sedimentation equilibrium experiments. Each lane is the protein from a different cell. The smeared band represents sFcεRIα (smeared due to heterogeneous glycosylation) and the resolved is band Fcε3-4ΔC.

From the SDS-PAGE there appeared to be no evidence of a gross breakdown of fragments occurring during centrifugation, nor was there covalent aggregation. In fact, any significant degree of aggregation in the cell would have interfered with the model fitting procedure to an extent that no data fitting would have been possible.

6.5 Discussion

In this chapter, a comparison of Fcε3-4ΔC expressed in *E. coli*, and Fcε3-4 expressed in a mammalian cell line yielded striking differences. It appears that the absence of disulphide linkage and/or carbohydrate has a deleterious effect on the affinity of Fcε3-4 for FcεRI. In the Biacore and AUC analyses the mode of interaction with FcεRIα appeared to be altered drastically. In solution Fcε3-4ΔC was able to bind sFcεRIα with a mixture of 1:1 and 2:1 stoichiometries. In the Biacore, which is a surface interaction assay, the binding only showed a 1:1 stoichiometry. This conclusion is based on the values derived for the R_{max} in the steady fit, as these were equivalent to the R_{max} expected for the amount of immobilised α-γ fusion protein based on the ratio of each proteins's molecular weight. In both cases the overall affinity observed was significantly lower than that recorded for the mammalian expressed fragment that possesses these two structural features.

The functional properties of the Fcε3-4ΔC fragment could be the result of a combination of structural factors. For example, the cysteine 328 disulphide acts

as a bridge between the two binding sites used to interact with FcεRI (as revealed in the crystal structure). Due to the asymmetric nature of the interaction with FcεRI, the two binding sites are composed of some residues which are exclusive to each particular site and others that are represented in both (Garman *et al*, 2000). Many of the residues that compose these sites are in the linker region of the Fcε3-4 molecule, which is to some degree constrained by the disulphide linkage. Therefore, removal of this structural feature present in the linker would be expected to have some effect on binding.

The extremely rapid kinetics and potential for 2:1 stoichiometry seen for Fcε3-4ΔC may be explained in terms of only one site, or one particular set of residues, being engaged. In Fcε3-4, steric hindrance is responsible for preventing a second sFcεRIα from binding, but if non-disulphide linked Fcε3-4 can engage a second receptor, there must be a greatly increased distance between the binding sites. A clue to how this may arise lies in the crystal structures of the Fcε3-4 fragment. If the unbound state of Fcε3-4 (Wurzburg *et al*, 2000) is compared to that of the bound (Garman *et al*, 2000) a large conformational shift is necessary to engage receptor, with the Fcε3 domains moving from a "closed" to an "open" conformation. This assumption is supported by the crystal structure of the full Fc (Fcε2-4, Wan *et al,* 2002), as this displays an intermediate structure in which one domain is "open" and the other "closed". If the unbound and bound structures are examined further, there appears to be evidence for an inherent flexibility within the Fcε3 domains, especially when compared to that of the homologous IgG-Fc (Wurzburg *et al*, 2000). It is possible that without the constraint of either a disulphide bridge at residue 328, attached carbohydrate, or a combination of both, that an even greater degree of freedom could be observed for Fcε3 domains, allowing the binding of a sFcεRIα molecule to each Fcε3 domain. Further evidence for a conformational difference between Fcε3-4 and Fcε3-4ΔC appears in the gel filtration data (figure 6.2). In comparison to mammalian Fcε3-4, the non-disulphide linked construct has a smaller apparent molecular weight that suggests a more compact structure. If the Fcε3 domains in Fcε3-4ΔC were compacted to a high enough degree, it is easy to imagine that the two sub-sites (one on each Fcε3 domain) would be too far apart to both contact a single sFcεRIα, but that being far apart they could each bind an sFcεRIα using only one

of the sub-sites. Thus the Fcε3 domains might "roll" past one another as the inter-domain region closes. This is illustrated in figure 6.11.

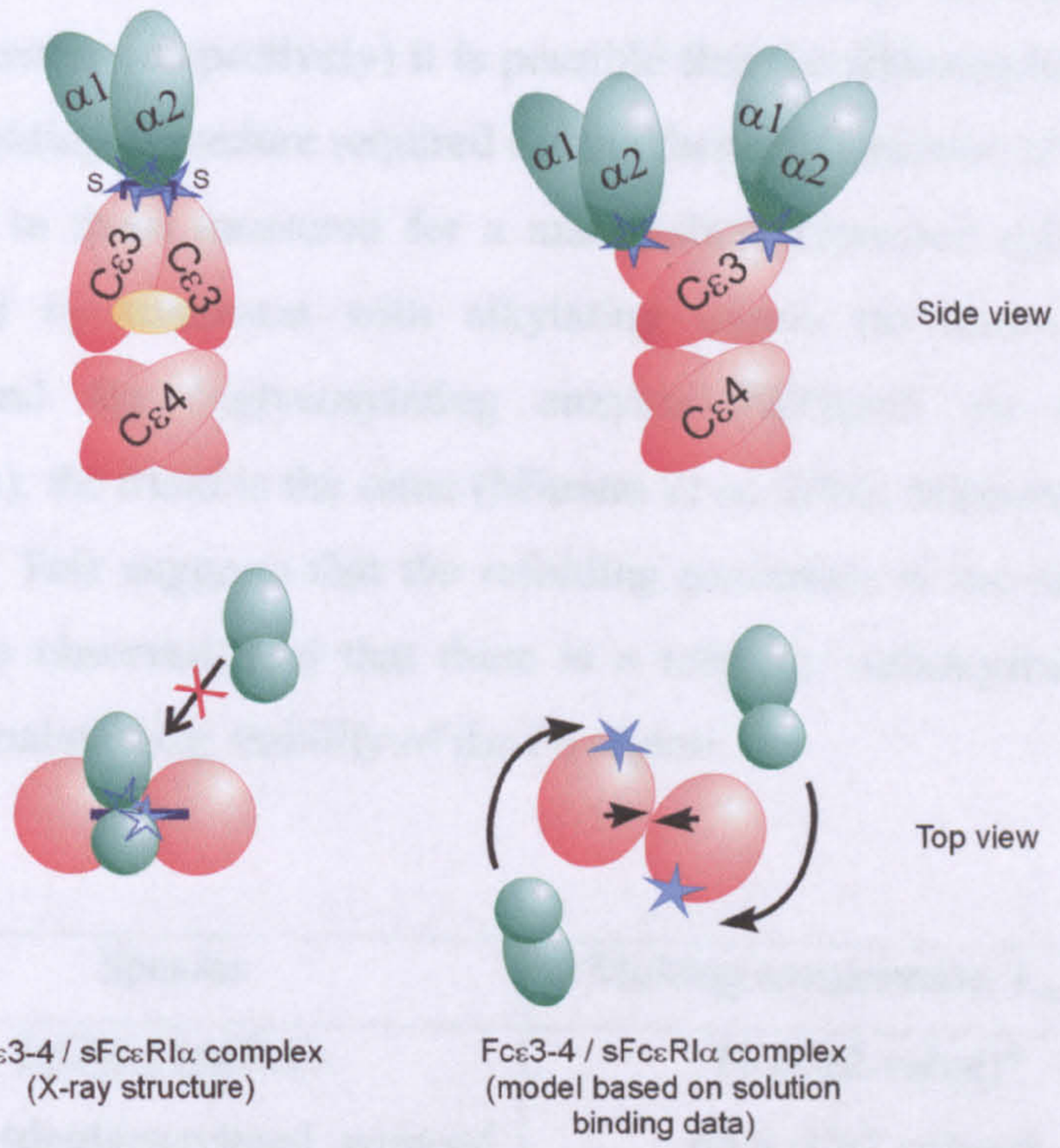

Figure 6.11: Schematic illustrating a potential interaction model for sFcεRIα with Fcε3-4ΔC and mammalian Fcε3-4. Blue stars indicate binding sites on individual Fcε3 domains, yellow ellipse indicates carbohydrate at Asn 394. There are in fact two sub-sites on each Fcε3 domain, but from the experiment carried out it is not clear which site is being engaged and therefore the single blue star represents both sites in this case.

A possible role for carbohydrate in determining these conformational differences is apparent if work carried out on the IgG-Fc is taken into account. Deglycosylation of IgG-Fc leads to a closing of the molecule (Jefferis and Lund, 2002). In fact, on complete deglycosylation, the IgG-Fc is thought to close to such an extent that engagement of a receptor is not possible at all due to occlusion of the binding site. This closing results in a shift in apparent molecular weight (Radaev and Sun, 2001) similar to that seen for Fcε3-4ΔC. It was suggested this closing could be a result of the need to cover hydrophobic residues normally shielded by the core glycosylation. A similar mechanism may be at work for Fcε3-4ΔC, in figure 6.11 the black inward facing arrows in the bottom left illustration indicate such a potential movement.

If the CD data for both fragments is examined it is clear there are structural differences between the two molecules, notable especially in terms of their relative stabilities. As the Fcε3-4ΔC and Fcε3-4 come from different sources (*E. coli* and mammalian respectively) it is possible that the differences observed are due to the refolding procedure required for the former. However, if the T_m values are compared to those measured for a mammalian expressed IgG-Fc that was then modified by treatment with alkylating agents (to remove the linker disulphide) and the deglycosylating enzyme PNGaseF (to remove core glycosylaytion), the trend is the same (Mimura *et al*, 2000; Mimura *et al*, 2001 – see table 6.5). This suggests that the refolding procedure is not responsible for the differences observed, and that there is a role for carbohydrate and/or the disulphide in maintaining stability of the Fc region.

Species	Melting temperature T_m (°C)
IgG-Fc (native)	71 (Cγ2 value)*
IgG-Fc (deglycosylated, reduced and alkylated)	63.5 (Cγ2 value)*
Fcε3-4 (mammalian)	56
Fcε3-4ΔC (*E. coli*)	48

*Table 6.5: DSC (IgG-Fc) and CD (Fcε3-4) thermal denaturation values. DSC can provide individual T_m values for each domain and therefore the lower value for Fcγ2 is given (*Data from Mimura et al, 2000; Mimura et al, 2001).*

It is also worth noting from these data that the relative thermal stabilities of these isotypes are very different, with the IgE-Fc values 15°C lower than those for their IgG-Fc homologues in each case. It could be that the flexibility of Fcε3 compared to that of Fcγ2 in IgG is reflected in a lower overall thermal stability.

Some of the results obtained for Fcε3-4ΔC with different techniques are seemingly at odds with one another. In the Biacore assay although the affinity and binding mode were altered, as was the case in the centrifuge experiments, only a single mode of engagement was observed. The reason for this is likely to

be that the ligand spacing between either the Fab arms that hold each sFcεRIα subunit, or the spacing between active immobilised α-γ fusion at the chip surface, would have prevented Fcε3-4ΔC being able to contact two sFcεRIα domains at the same time. In the centrifuge 2:1 is more likely because the experiment was carried out using the smaller sFcεRIα construct and neither component was immobilised.

In addition to differences in the stoichiometry, a difference in the overall affinities obtained using AUC and Biacore was also observed (Biacore ~ 10^7 M^{-1}, AUC ~ 10^5 M^{-1}). This is not the first time that such a difference has been observed, and may again simply be a result of the way in which ligand is presented to the receptor. In AUC experiments on CD23, analysed using the same model applied here, the affinity of a single binding site on the IgE-Fc was determined to be ~ 10^5 M^{-1} (Shi *et al*, 1997), whereas in a Biacore assay the affinity of the same construct was determined found to be ~ 10^7 M^{-1} (McDonnell *et al*, 2001).

Previous experiments carried out either using this Fcε3-4ΔC construct (Henry, PhD Thesis, 1997), or a similar mammalian ΔC construct (Basu *et al*, 1993) also highlighted differences in the affinity of non-disulphide linked Fcε3-4 for FcεRI compared to the wild type molecule. In cell binding assays a three-fold reduction in the affinity of the ΔC construct was observed by Basu *et al* (with the shift attributed to an increase in the off-rate of the molecule). This change is not as drastic an effect as described in this thesis. The difference in results could be explained by the assay approaches applied. Basu *et al* used a saturation cell-binding assay. In this system an avidity effect could have been seen due to the bivalent nature of the non-disulphide linked construct, as suggested by the results obtained from the centrifuge experiments described in this thesis. In fact saturation binding levels determined with their non-disulphide linked form of Fcε3-4 (329-547) were almost always half of the value for their disulphide linked Fcε3-4 (315-547). This indicates a very different mode of binding for the Fcε3-4 (329-547) construct. In fact, when assayed in competition ELISA (Henry, PhD thesis, 1997) the Fcε3-4ΔC fragment gave similar IC_{50} values to those of Basu *et al* (see table 6.6). This suggests that these two molecules (Fcε3-4ΔC and Fcε3-4

329-547) are functionally very similar, if not identical, and that it is only the method of assay that leads to differences of affinity.

Species	IC_{50} (nM)
Fcε3-4 wt (Henry, PhD thesis)	20.7 ± 9.8
Fcε3-4 ΔC (Henry, PhD thesis)	89.6 ± 1.5
Fcε3-4 315-547 (Basu *et al*)	7.7 ± 4.5
Fcε3-4 329-547 (Basu *et al*)	32.9 ± 25.8

Table 6.6: Table comparing the IC_{50} values obtained for Fcε3-4ΔC (Henry, PhD thesis, 1997) and Fcε3-4 329-547 (Basu et al, *1993) in competition ELISA and cell binding assay respectively. Results shown are ± standard error.*

One exciting result to come from the experiments carried out on Fcε3-4ΔC is that because a 2:1 stochiometry has been observed, this has enabled the affinity of a single folded Fcε3 domain for sFcεRIα to be measured. This value is either ~2 x 10^5 M^{-1}, or ~2 x 10^7 M^{-1}, depending on the method used for measurement (AUC or Biacore). These values bracket that quoted for a single unfolded Fcε3 domain (5 x 10^6 M^{-1}, Henry *et al*, 2000), as measured by Biacore. This highlights the interesting proposition that the affinity of a single folded Fcε3 is no greater than that of an unfolded isolated domain. This will be discussed further in the next chapter.

Finally, one further question that needs to be addressed is to what degree the carbohydrate and disulphide-bridge contribute to the effects reported in the chapter. Possible roles for both have been outlined in this discussion with respect to constraint of the N-terminal linker, and conformational changes with respect to the Fcε3 domains. To determine the individual contribution that each of these structural features makes to the interaction with FcεRIα, experiments were carried out on a molecule lacking just one of these components. The results of these experiments will be described in Chapter 7.

Distinguishing the effects of disulphide linkage and glycosylation on high affinity receptor binding and folding of Fcε3-4

Chapter 7: Distinguishing the effects of glycosylation and disulphide linkage on high affinity receptor binding and folding of Fcε3-4

7.1 Introduction

In Chapter 6 it was demonstrated that *E. coli*-expressed Fcε3-4ΔC has a reduced stability and a lower affinity for FcεRI than a mammalian expressed Fcε3-4 fragment. Furthermore, the mode of interaction of Fcε3-4ΔC with FcεRI compared to that of mammalian Fcε3-4 was altered such that a single monophasic binding relationship was observed when assayed by SPR, and a 2:1 stochiometry was observed when assayed in solution by analytical ultracentrifugation. The Fcε3-4ΔC fragment lacked two structural features present in the mammalian expressed Fcε3-4 fragment – disulphide linkage at the N-terminus and glycosylation at Asn 394. It was not clear from the comparison made in chapter 6 to what degree the differences observed for Fcε3-4ΔC were due to the absence of carbohydrate or the absence of the disulphide bridge. Therefore mammalian expressed fragments were prepared with and without carbohydrate to distinguish the roles of glycosylation and disulphide linkage on the interaction with the high affinity receptor.

7.2 Deglycosylation of mammalian Fcε3-4

Fcε3-4 was expressed and isolated from mammalian culture as described in the previous chapter. This fragment runs on non-reducing SDS-PAGE at about the 55kDa marker. There are three discernible glycoforms, dependent on the preparation (see figure 7.1 A). Treatment with the endoglycanase PNGase F resolves this pattern into a further lower band corresponding to the deglycosylated form; this can be seen in the partial digest in 7.1 B. This process of carbohydrate removal has been investigated in detail previously, with PNGase F established as the most suitable enzyme (Basu *el al*, 1993; Keown, PhD thesis, 1997; Bjorklund *et al*, 1999). During this treatment, much of the material is lost as precipitate, as has also been described by others (Basu *et al*, 1993). A sample of this precipitate can be seen on non-reducing SDS-PAGE in panel C. All the Fcε3-4 material corresponds to the lower band in the precipitated sample,

suggesting that it is the loss of sugars that has a deleterious effect on the solubility of the fragment.

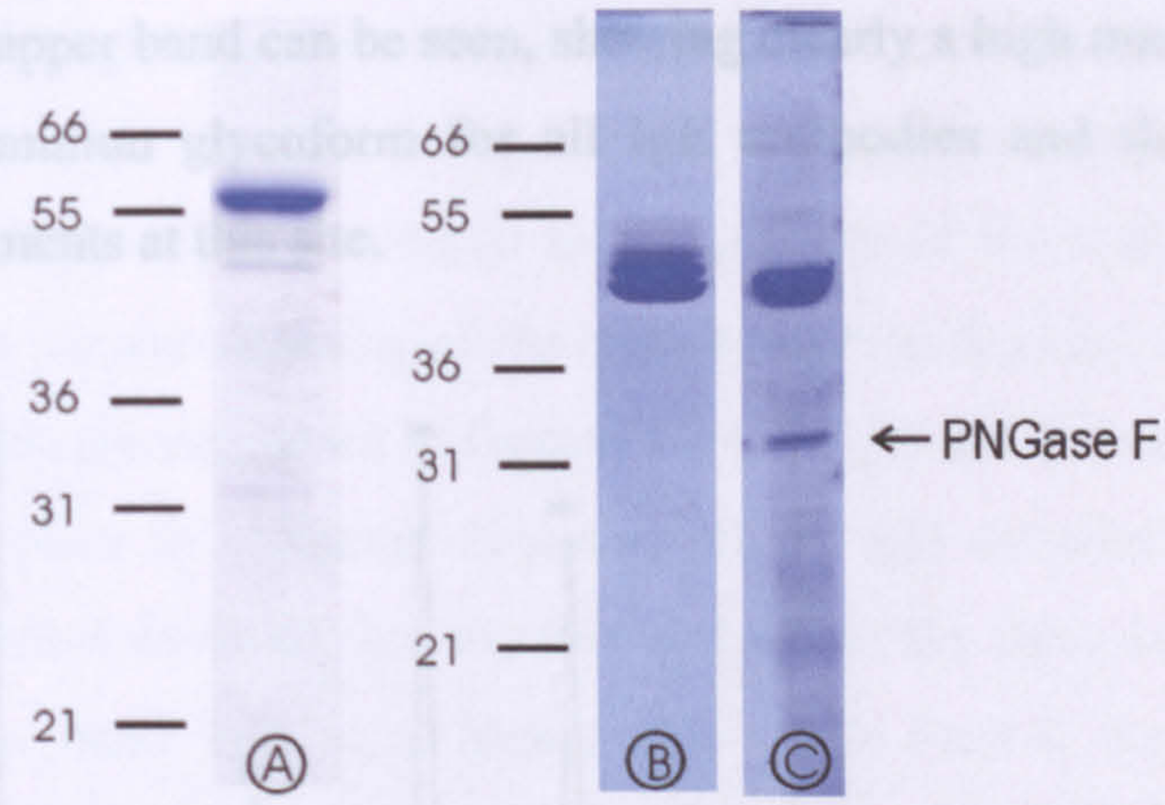

Figure 7.1: 15% non-reducing SDS-PAGE of Fcε3-4 mammalian samples at various stages of deglycosylation. Lane A = prior to digestion, lane B = partial digestion, lane C: precipitated material. For method see section 2.3.6.

Repeated digestion with PNGase F finally resolves all the protein into the lower band. In figure 7.2 a partially digested fragment resolved by SDS-PAGE can be seen both Schiff stained (stains only carbohydrate) and Coomassie stained gels (all protein). The two upper bands stain with the Schiff's reagent, whereas the lower band does not. In the two right hand panels a completely deglycosylated sample is shown; no Schiff staining is seen for this fragment, with a single band resolved in the Coomassi stained sample.

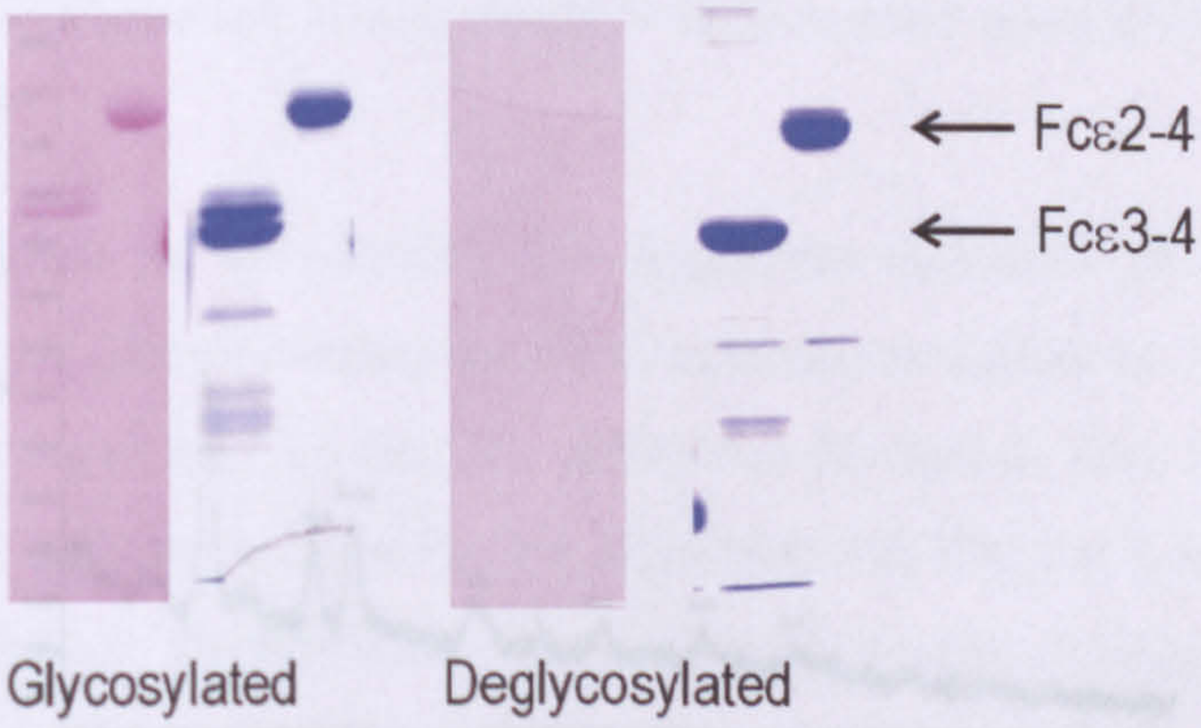

Figure 7.2: Coomassie (blue) and Schiff (pink) stained Fc fragments (the full Fc, Fcε2-4, and Fcε3-4) 15% non-reducing SDS-PAGE.

Prior to a final round of PNGase F digestion, the upper and lower bands of the partial digest (figure 7.1 – panel B) were analysed for their carbohydrate composition (R. Boehm – Oxford Glycobiology Institute). In figure 7.3 the profile for the upper band can be seen, showing clearly a high mannose structure. This is the common glycoform for all IgE antibodies and their mammalian expressed fragments at this site.

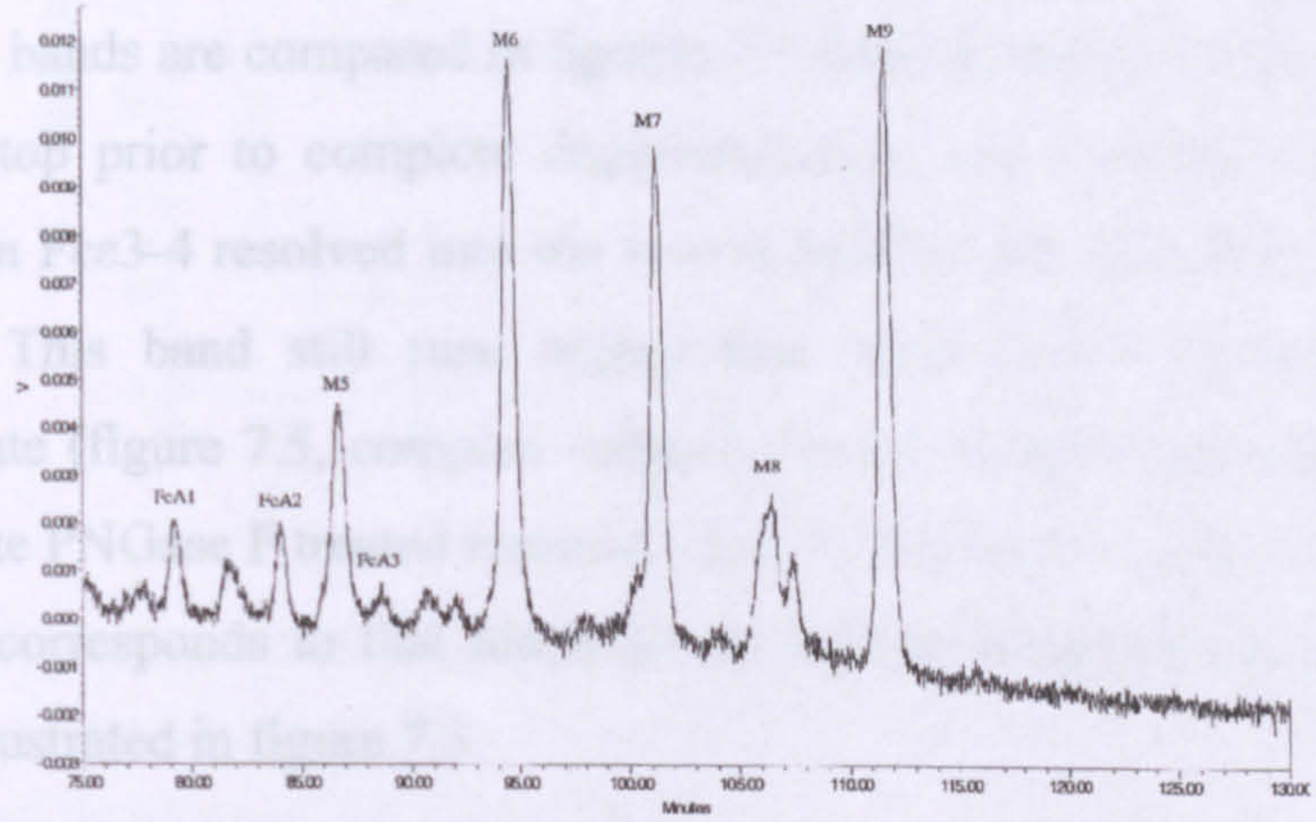

Figure 7.3: HPLC profile of released carbohydrate from glycosylated Fcε3-4 after initial PNGase F treatment.

Figure 7.4 shows the carbohydrate profile of the lower band from the gel shown in figure 7.2, i.e. the non-Schiff stained band. Here virtually all of the high mannose structures have been removed, and only a residual core fucose and a small amount of mannose remains, indicating that the lower band that appears after PNGase F treatment corresponds to the deglycosylated form of Fcε3-4.

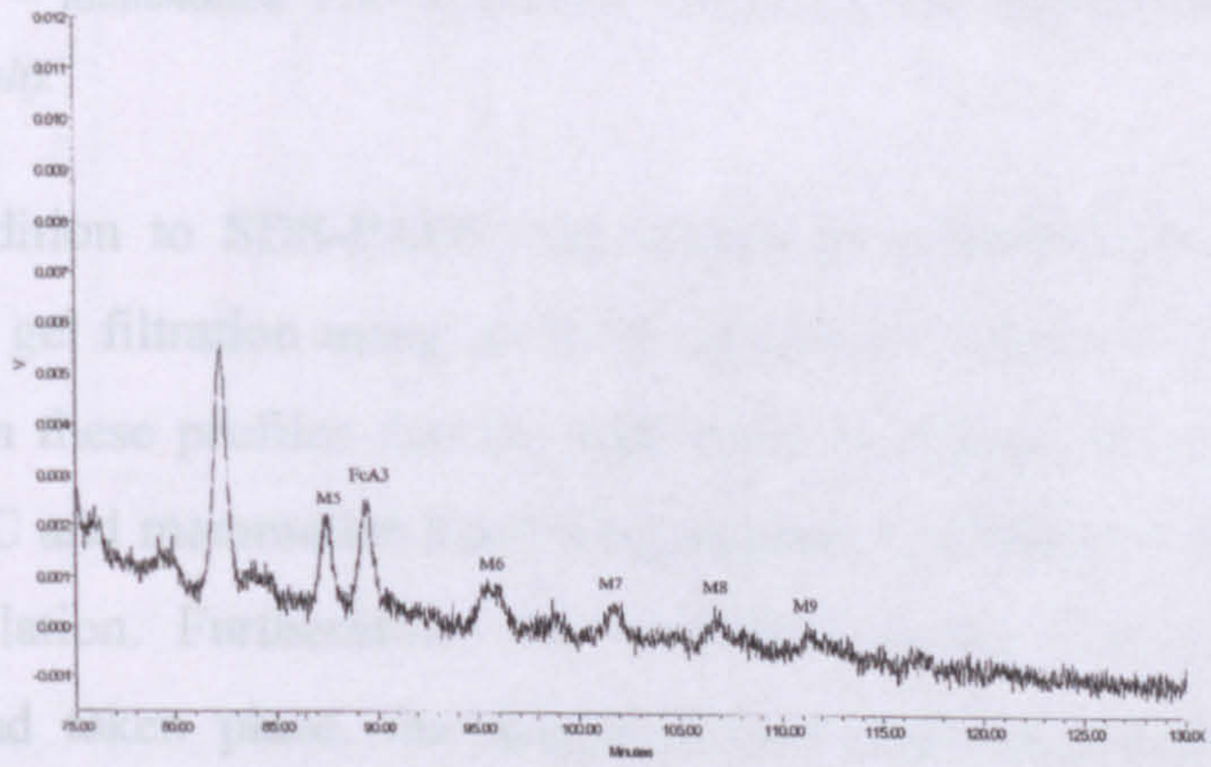

Figure 7.4: HPLC profile of released carbohydrate from lower, non-Schiff staining Fcε3-4 band seen in figure 7.2.

Once deglycosylation was complete, with all material resolved into the lower band, the remaining Fcε3-4 was re-purified by gel filtration. To confirm the purity, the material was run out on both reducing and non-reducing SDS-PAGE alongside glycosylated Fcε3-4 and *E. coli* expressed Fcε3-4ΔC. The deglycosylated material runs smaller than the glycosylated, with reduction resolving the deglycosyated material to the position of Fcε3-4ΔC. Over time it appeared that a natural trimming of the carbohydrate took place, as can be seen if the Fcε3-4 bands are compared in figures 7.1 (lane A) and 7.5 (lane A). This did however stop prior to complete deglycosylation, and eventually, most of the mammalian Fcε3-4 resolved into the lowest band of the three seen in figure 7.1 (lane A). This band still runs higher than both Fcε3-4 fragments without carbohydrate (figure 7.5, compare reduced Fcε3-4 samples; glycosylated – lane D, complete PNGase F treated material –lane E, Fcε3-4ΔC – lane F) and it is this band that corresponds to that identified as high mannose by the glycosylation analysis illustrated in figure 7.3.

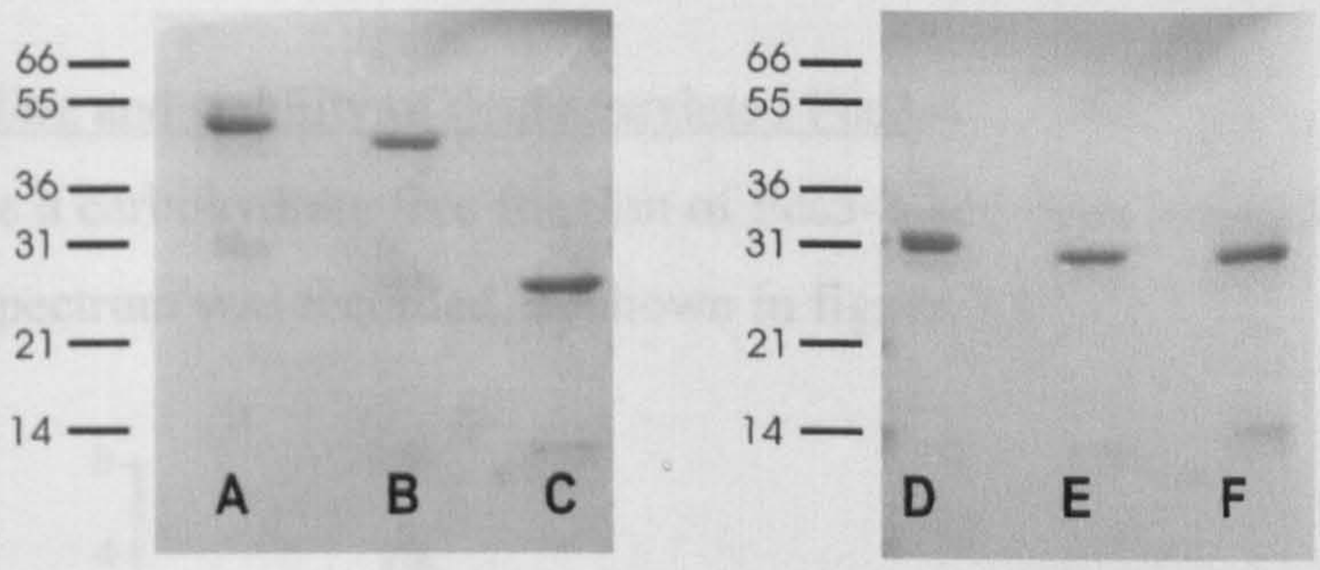

Figure 7.5: Non-reducing (left panel) and reducing (right panel) 15% SDS-PAGE of Fcε3-4 fragments. Left = mammalian Fcε3-4, middle = deglycosylated mammalian Fcε3-4, right = Fcε3-4ΔC (E. coli).

In addition to SDS-PAGE, the fragments collected for analysis were compared by gel filtration using an S200 column, as shown in figure 7.6. It is apparent from these profiles that the difference in elution time between the *E. coli* Fcε3-4ΔC and mammalian Fcε3-4 highlighted in Chapter 6 is not the result of deglycosylation. Furthermore, the analytical profile confirmed that once separation had taken place, the deglycosylated material remained free from aggregation and contamination with PNGase F. In fact, once isolated, the Fcε3-4 deglycosylated mammalian material remained as stable in solution as the

glycosylated material, an observation seemingly at odds with the precipitation problem experienced at early stages of the deglycosylation process.

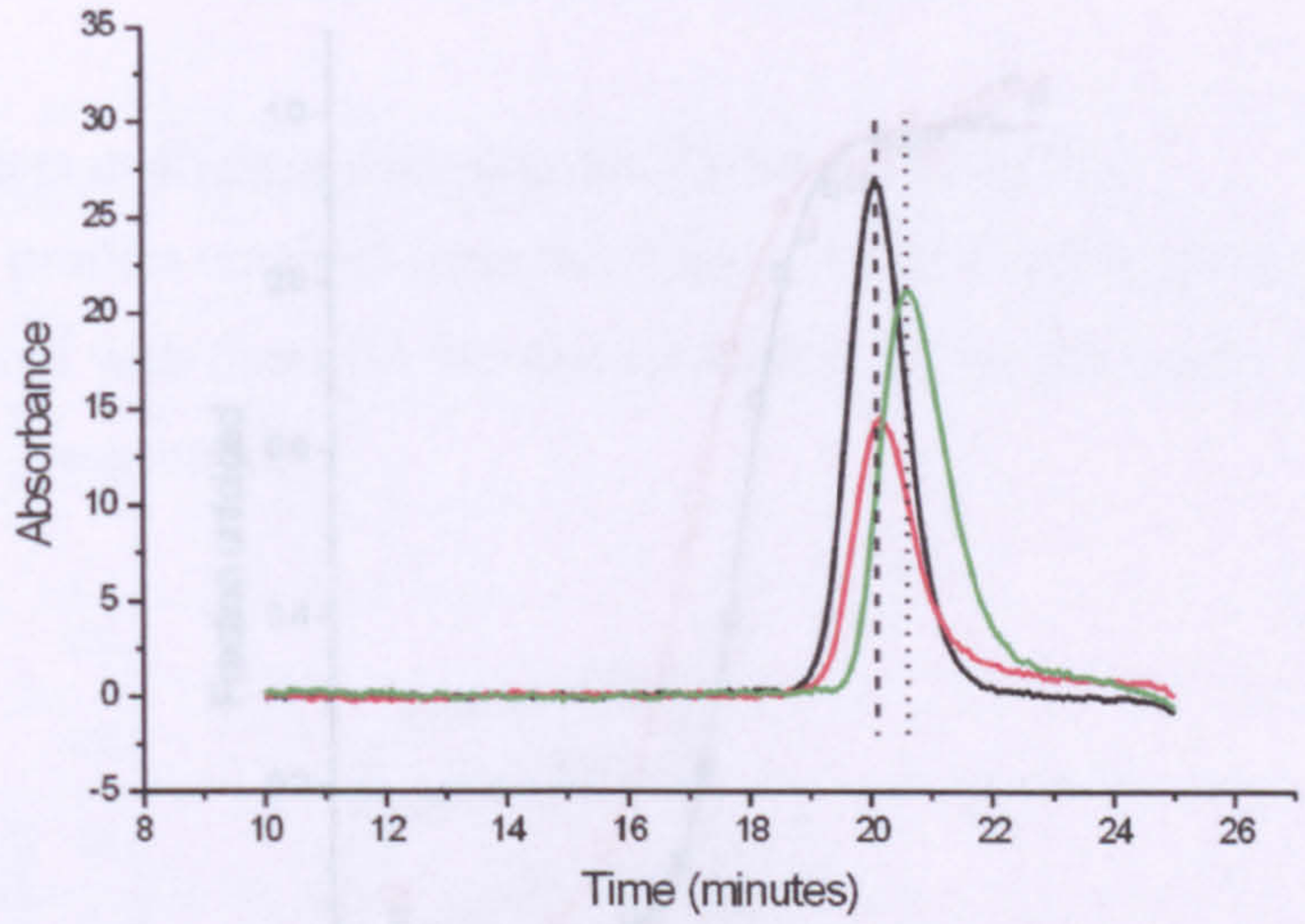

Figure 7.6: Gel filtration elution profiles of Fcε3-4 fragments (Superdex S200 HR column, run at 0.75 ml/min in gel filtration buffer – see section 2.1). Black = mammalian Fcε3-4, red = deglycosylated Fcε3-4, green = E. coli *Fcε3-4ΔC.*

7.3 Folding and stability of deglycosylated Fcε3-4

Once a carbohydrate free fraction of Fcε3-4 had been isolated, its circular dichroism spectrum was recorded, as shown in figure 7.7:

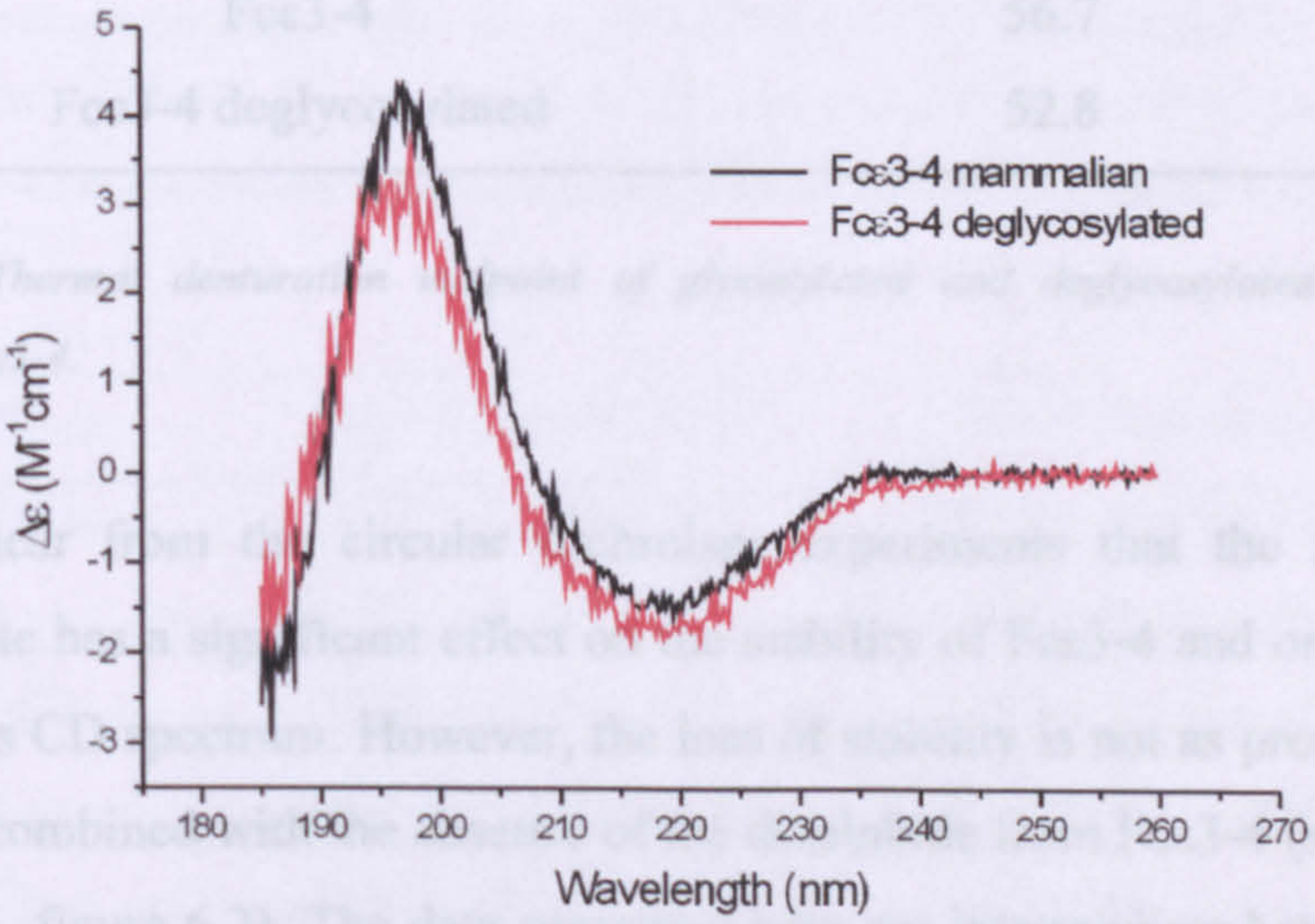

Figure 7.7: Circular dichroism spectra of deglycosylated and glycosylated mammalian expressed Fcε3-4. Data were acquired as outlined in section 2.4.1.

In addition, a thermal denaturation profile was recorded and the mid-point determined to yield a T_m value– see figure 7.8 and table 7.1:

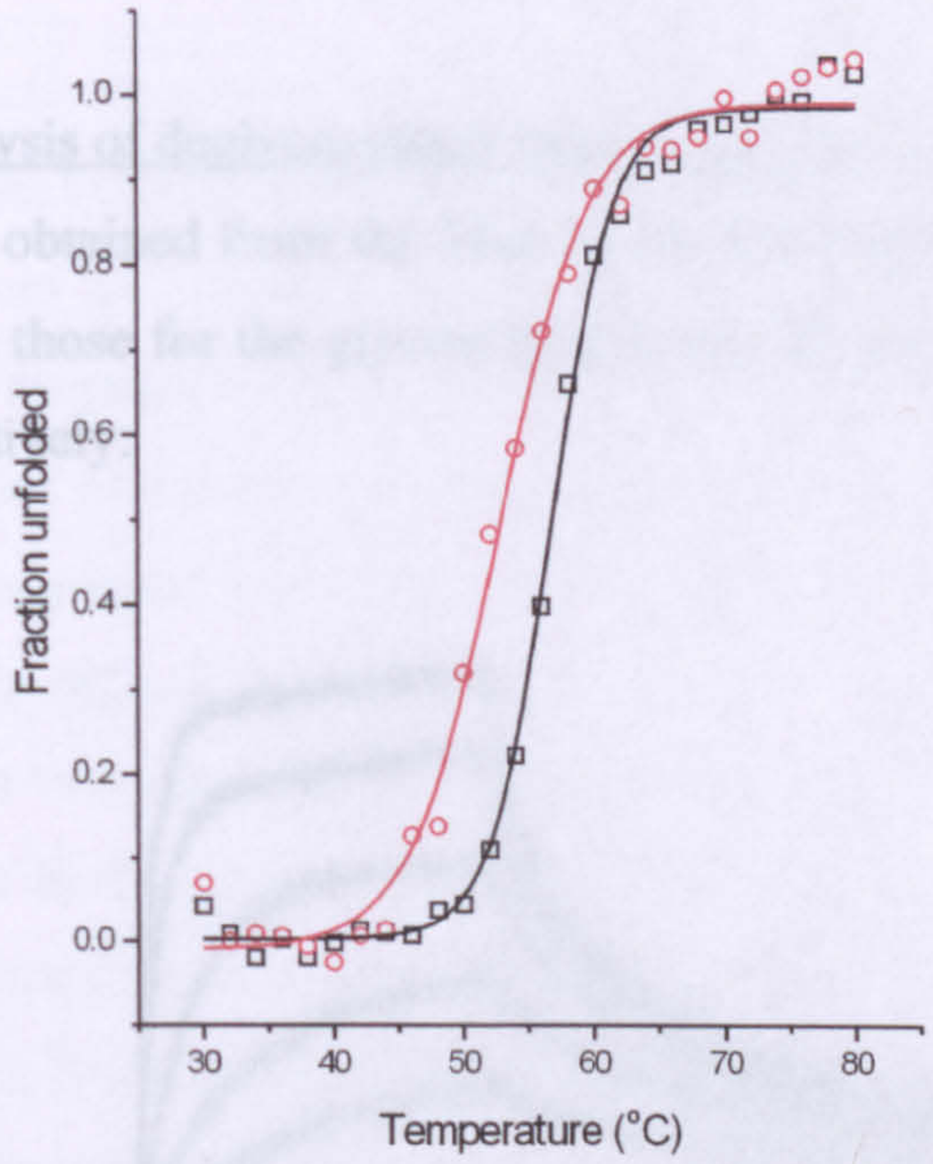

Figure 7.8: Thermal denaturation profile of mammalian Fcε3-4 glycosylated (black) and deglycosylated (red). Sigmoidal fits are shown from which temperature of melting mid-points were derived. Data was acquired as outlined in section 2.4.1.

Fragment	T_m (°C)
Fcε3-4	56.7
Fcε3-4 deglycosylated	52.8

Table 7.1: Thermal denturation midpoint of glycosylated and deglycosylated mammalian expressed Fcε3-4.

It is clear from the circular dichroism experiments that the absence of carbohydrate has a significant effect on the stability of Fcε3-4 and only a minor effect on its CD spectrum. However, the loss of stability is not as pronounced as that when combined with the absence of the disulphide from Fcε3-4 (see Chapter 6, table 6.1, figure 6.2). The data presented here are intermediate between those for *E. coli* Fcε3-4ΔC and glycosylated mammalian Fcε3-4 (see Chapter 6, figure 6.4, table 6.1).

7.5 Effect of glyscosylation on the interaction with FcεRI

The binding capabilities of deglycosylated Fcε3-4 were measured using the Biacore and AUC assays as before (see Chapter 6).

7.5.1 Biacore analysis of deglycosylated mammalian Fcε3-4

The profiles obtained from the Biacore for this fragment, and the kinetic data compared with those for the glycosylated material, are shown in figure 7.9 and table 7.2 respectively:

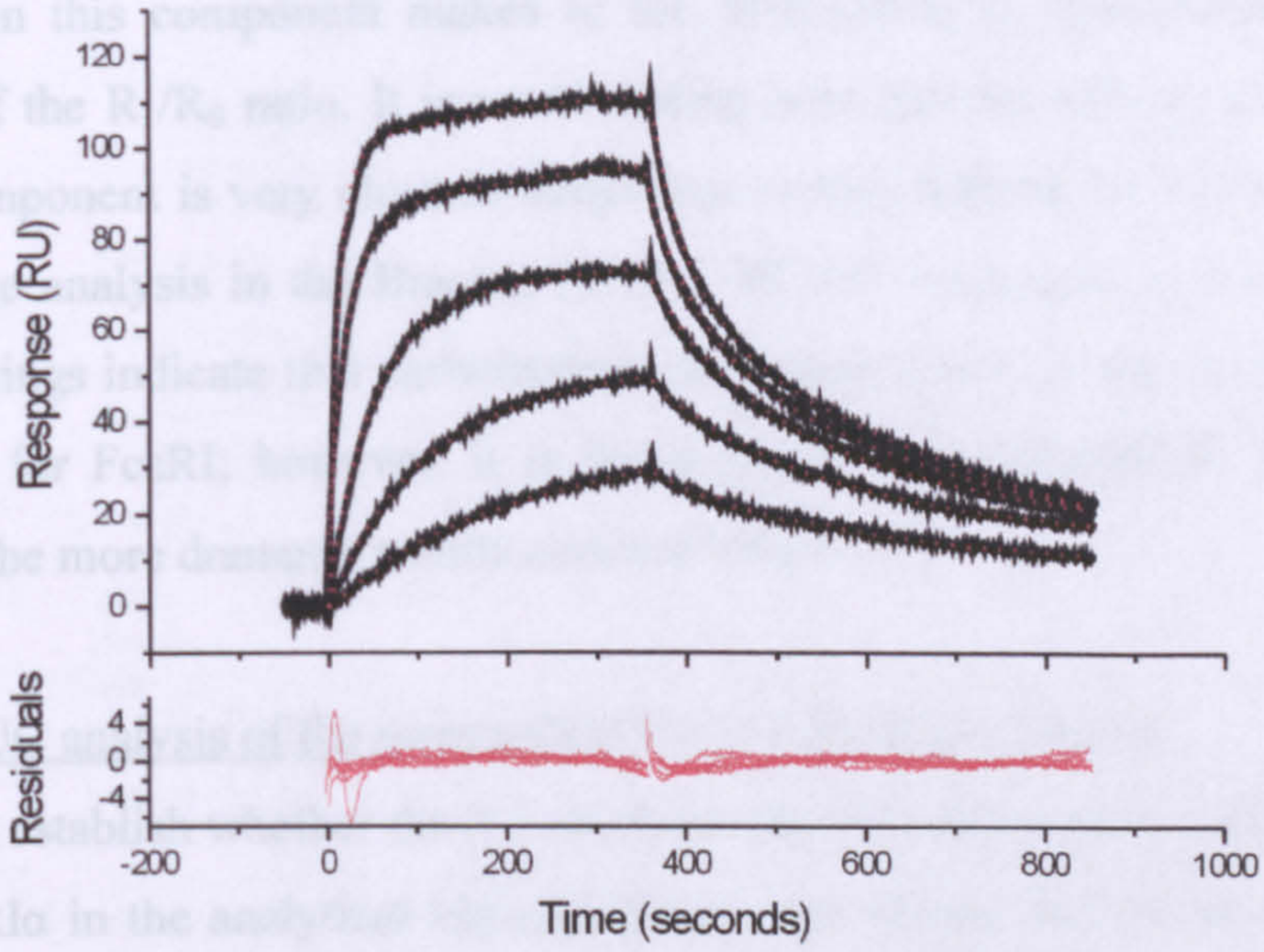

Figure 7.9: Biacore binding profiles for a concentration series of deglycosylated mammalian Fcε3-4 (100nM - 6.25nM). Fits based on a 1:1 biphasic competition model are shown as a red dotted line for each concentration and residuals for the fits are shown in the bottom panel.

Constant	Fcε3-4 glycosylated	Fcε3-4 deglycosylated
k_{a1} ($M^{-1}s^{-1}$)	$(4.77 \pm 1.88) \times 10^{5}$	$(4.88 \pm 1.97) \times 10^{5}$
k_{d1} (s^{-1})	$(1.21 \pm 0.19) \times 10^{-2}$	$(1.50 \pm 0.29) \times 10^{-2}$
k_{a2} ($M^{-1}s^{-1}$)	$(3.08 \pm 0.65) \times 10^{5}$	$(1.97 \pm 0.15) \times 10^{5}$
k_{d2} (s^{-1})	$(6.26 \pm 1.29) \times 10^{-4}$	$(1.73 \pm 0.23) \times 10^{-3}$
K_{a1} (M^{-1})	3.94×10^{7}	3.25×10^{7}
K_{a2} (M^{-1})	4.92×10^{8}	1.14×10^{8}
R_1/R_0	0.15 ± 0.03	0.38 ± 0.03
Overall K_A (M^{-1})	4.2×10^{8}	8.1×10^{7}

Previous page.

Table 7.2: Kinetic parameters derived from SPR analysis of deglycosylated mammalian Fcε3-4 compared with those of its glycosylated counterpart.

From the kinetic analysis it is clear that the behaviour of deglycosylated Fcε3-4 is similar to that of glycosylated material. The fit is biphasic, and most of the kinetic parameters are identical. However, there are differences, and the overall affinity has dropped by a factor of five. This is due principally to an increase in the off rate of the second component (k_{d2}) and a shift in the relative contribution this component makes to the interaction, as demonstrated in the increase of the R_1/R_0 ratio. It is worth noting here that the affinity constant for the k_{a2} component is very close in magnitude to that derived for Fcε3-4ΔC by a steady state analysis in the Biacore (3.25×10^7 M^{-1} compared to 3×10^7 M^{-1}). These findings indicate that carbohydrate does have a role to play in the affinity of Fcε3-4 for FcεRI; however, it is the removal of the disulphide bridge that results in the more dramatic results outlined Chapter 6.

7.5.3 AUC analysis of the mammalian Fcε3-4:sFcεRIα complex

To establish whether the 2:1 stochiometry seen between *E. coli* Fcε3-4ΔC and sFcεRIα in the analytical ultracentrifuge was wholly due to the removal of the disulphide, or whether it was a result of a combination with the effect of deglycosylation, fragments lacking just one of these two components thought to be critical (carbohydrate or disulphide linkage at Cys 328) were analysed with respect to their binding to sFcεRIα.

Deglycosylated mammalian Fcε3-4 binding to sFcεRIα was found to fit best to a model that describes a single ideal species. This is because above affinity constants of ~$10^8 M^{-1}$ the majority of the complexes formed prior to analysis do not dissociate. In the case of this single ideal species, the molecular weight corresponded to that of a single sFcεRIα bound to a single Fcε3-4, i.e. a 1:1 stoichiometry (see left hand panel of figure 7.10). This result confirmed that the absence of carbohydrate is not responsible for the 2:1 stoichiometry seen between *E. coli* Fcε3-4ΔC and sFcεRIα.

The disulphide linked, deglycosylated fragment was then compared to a mildly reduced, i.e. non-disulphide linked, but glycosylated Fcε3-4 under

identical conditions. The disulphide linkage at Cys 328 was disrupted with DTT. The minimal concentration of DTT required to achieve reduction of this single disulphide was determined by titrating Fcε3-4 (at the concentration used in AUC experiments) with DTT and running it out on SDS-PAGE (see figure 7.11). The minimum concentration of DTT for reduction of the inter-chain disulphide was 0.4 mM. According to previous disulphide mapping studies, this concentration is insufficient to reduce the internal disulphides (Takatsu *et al*, 1975). After reduction, samples were placed in a nitrogen-purged AUC cell to stop oxidation. The results obtained are compared with those for deglycosylated Fcε3-4 in figure 7.10.

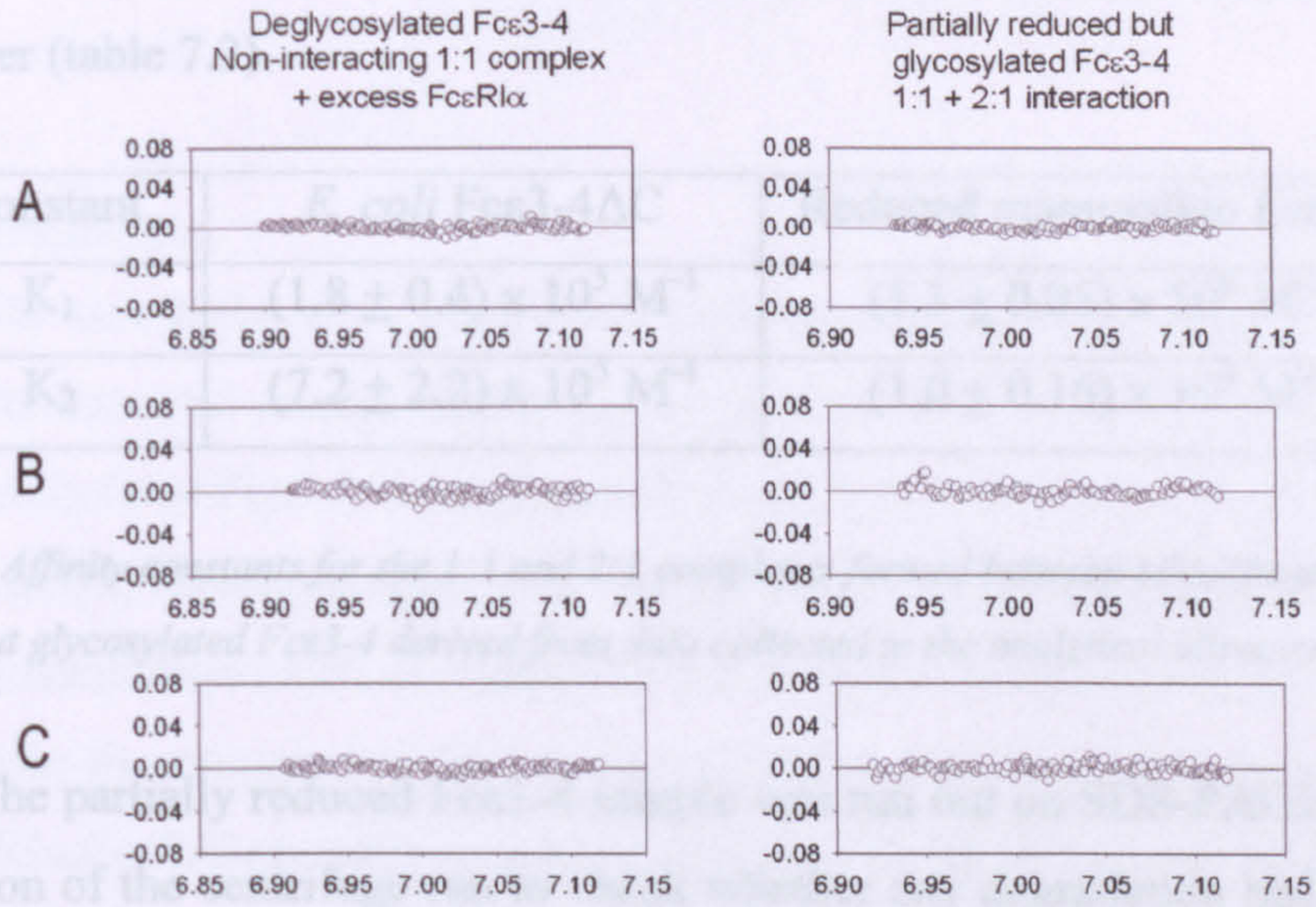

Figure 7.10: Sedimentation equilibrium analytical ultracentrifugation datasets. Residuals from fits based on a interaction stoichiometry of either 1:1 or 2:1 + 1:1 mix for three differing ratios of Fcε3-4 (deglycosylated or partially reduced) to sFcεRIα (1:1 - A, 2:1 - B, 1:2 - C).

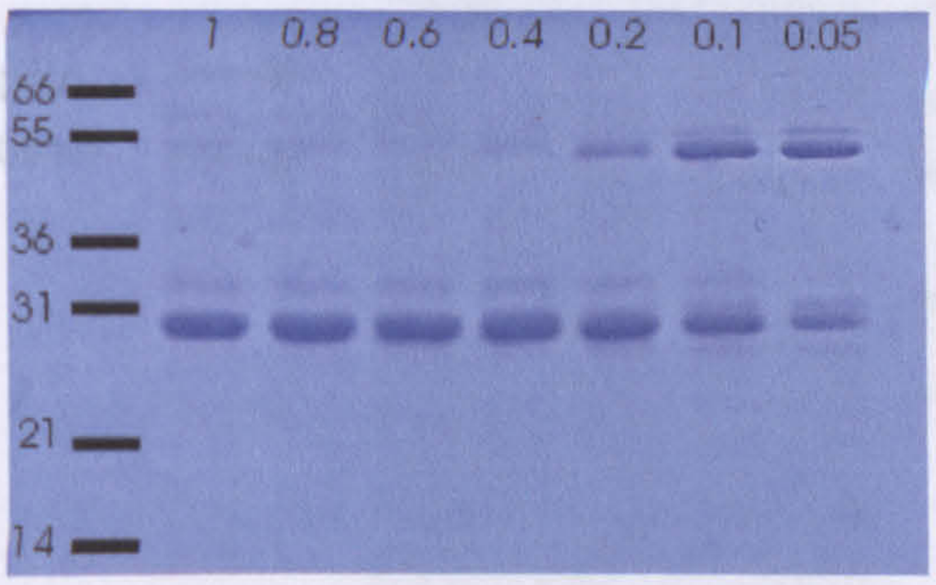

Figure 7.11: 15% SDS-PAGE of Fcε3-4 treated with various concentrations of DTT (mM) to determine the transition point from covalent dimer to monomer due to the reduction of the Cys 328 inter-chain disulphide bridge.

From the fitting procedure for the AUC data it was clear that the reduced sample adhered to the 1:1 + 2:1 interaction model. The scheme describing the interaction is shown in figure 7.12.

$$A + 2B \underset{K_1}{\longleftrightarrow} AB + B \underset{K_2}{\longleftrightarrow} AB_2$$

Figure 7.12: Scheme for the formation of a 2:1 complex between Fcε3-4 and sFcεRIα showing interactions that correspond to the affinity constants K_1 and K_2.

The K_1 value for the reduced but glycosylated Fcε3-4 fragment was higher than that derived for *E. coli* Fcε3-4ΔC, with K_2 value also altered, but this time lower (table 7.3).

Constant	*E. coli* Fcε3-4ΔC	Reduced mammalian Fcε3-4
K_1	$(1.8 \pm 0.4) \times 10^5\ M^{-1}$	$(1.3 \pm 0.05) \times 10^6\ M^{-1}$
K_2	$(7.2 \pm 2.2) \times 10^5\ M^{-1}$	$(1.0 \pm 0.16) \times 10^4\ M^{-1}$

Table 7.3: Affinity constants for the 1:1 and 2:1 complexes formed between sFcεRIα and partially reduced but glycosylated Fcε3-4 derived from data collected in the analytical ultracentrifuge.

The partially reduced Fcε3-4 sample was run out on SDS-PAGE after the completion of the centrifuge run to check whether any degradation had occurred and whether the Fcε3-4 had remained monomeric, as shown in figure 7.13.

Figure 7.13: 15% non-reducing SDS-PAGE of Fcε3-4:sFcεRIα mixes from ultracentrifuge cells after 100 hour sedimentation equilibrium experiments under reducing conditions. The three lanes correspond to the three different protein loading ratios used in the experiment.

From the gel it is clear that the majority of the Fcε3-4 inter-chain disulphides remained reduced. There is a very small amount of higher molecular weight material that corresponds to covalent dimer, visible as a faint band above the smeared sFcεRIα band. It is unlikely that this small amount of material would have interfered with the fitting procedure. It must be noted that there are differences between the figures obtained for *E. coli* Fcε3-4ΔC and the reduced mammalian Fcε3-4. However, such a pronounced effect may well be the result of the engagement of the second site being severely hampered by the presence of a first sFcεRIα, and it is this that leads to a reduction in its affinity constant. This will be discussed further in section 7.6.

7.6 Discussion

The aim of the work described in this chapter was to distinguish the role of carbohydrate and disulphide linkage in the interaction of Fcε3-4 with FcεRI. Kinetic analysis of Fcε3-4 lacking carbohydrate, but with the disulphide bridge at Cys 328 intact, showed a shift in the magnitude (a four fold reduction) and the relative contribution (38% compared to 15%) of the second component, K_{a2}, to the biphasic fit compared to the wild type Fcε3-4 (see table 7.2). According to the sFcεRIα:Fcε3-4 complex crystal structure only 100Å^2 of the total 1850Å^2 interaction surface is accounted for by contact with the first N-acetylglucosamine residue attached at Asn394, no other carbohydrate contacts are made. The effect removal of carbohydrate has on binding contrasts with the minimal contact observed in the crystal complex, thus suggesting glycosylation must exert its effect by other means also, possibly by altering the topology of the molecule so that when removed full engagement, and therefore full affinity, cannot be attained. According to Wurzburg *et al* (2000) the Fcε3-4 fragment needs to go through a large conformational change involving the Fcε3 domains to enable full engagement of FcεRI. This would contribute to a slower phase of association; the K_{a2} of the biphasic fit represents such a phase. It is precisely in this second phase of the interaction that the decrease in affinity after deglycosylation is observed.

Within the large contact area between Fcε3-4 and sFcεRIα there are a number of specific interactions that could be affected by the absence of carbohydrate. At the "top" of each Fcε3 domain (figure 7.14) sit three loops

containing important contact residues, including proline 426 that forms a "sandwich" with trytophan 89 and 113 of FcεRI, and a set of loops, structurally similar to CDRs, that make contact with another key residue of FcεRI, tyrosine 131 (Garman *et al*, 2000).

Figure 7.14: The crystal structure of the Fcε3-4:sFcεRIα complex (Garman et al, 2000). Soluble FcεRI alpha chain is shown in green (ribbon format). Fcε3-4 is shown in yellow and red (coloured by chain, ribbon format). Carbohydrate at Asn 394 is also coloured yellow. Proline 426 and interacting FcεRI residues, and tyrosine 131 of FcεRI and interacting residues, are shown space filled on the left and right hand side of the binding site respectively.

It is possible that only a minor shift in the way these clusters of residues were presented may significantly alter the overall nature of the complex by preventing the full engagement of one or more units that stabilises the interaction. Studies on truncated IgG Fc glycoforms, which have significantly altered receptor binding capabilities, have shown small shifts in the positions of the homologous loops at the "top" of the Fcγ2 domain depending on the level of glycosylation (Krapp *et al*, 2003). Glycosylation also determines the separation between opposing Fcγ2 domains, with sequential removal of carbohydrate residues causing a gradual closing (Mimura *et al*, 2001; Krapp *et al*, 2003). However, Fcε3-4 is already very closed in comparison (Wurzburg *et al*, 2000),

and perhaps this is why deglycosylation has a relatively minor effect in the IgE-Fc compared with IgG. Certainly, on complete deglycosylation a large shift in the size of Fcε3-4 is not seen in gel filtration analysis, although a large change is seen for IgG (Radaev and Sun, 2001). This does not however discount the subtle changes noted by Krapp *et al* (2003) when sugars are only partially removed from IgG. In earlier deglycosylation studies of the full IgE-Fc subtle changes in the binding of a panel of mAbs to Fcε3 were observed, suggesting that small structural rearrangements may take place when sugars are removed (Bjorklund *et al*, 2000).

The region of Fcε3 in which carbohydrate is most likely to have an effect is in the BC and DE loops. These form part of binding site 1 (including the region that binds Tyr 131, right hand side in figure 7.14). A highly structured region like this might be more susceptible to minor structural changes than others. This region has been suggested to establish specificity across the Ig receptor family (Wurzburg and Jardetzky, 2002). The overall contribution of these residues to the interaction is not large, and therefore loss of some, or all, of the contacts in this region may not lead to an enormous drop in affinity. Thus we have found that even though the kinetic differences are significant, the impact is only an ~ 3 fold increase in off rate when the relative contributions from the biphasic fit are taken into account (see table 7.2 for individual values; the overall k_d for each fragment can be calculated using a weighted average based on the relative contribution of each component according to the R_1/R_0 ratio, when this is done Fcε3-4 wild type has an off-rate of ~6 x 10^{-3} s^{-1} and deglycosylated Fcε3-4 has an off rate of ~2 x10^{-3} s^{-1}).

When observed in the analytical ultracentrifuge, the complex between purified deglycosylated Fcε3-4 and FcεRI still appears to be a single species. It must therefore still be considered "high-affinity", especially in comparison to the receptor complexes of IgG and the effects seen when IgG-Fc is deglycosylated, which experiences a total loss in binding capability. This explains why in assays which cannot assess binding in real time, effects of the removal of carbohydrate may have been difficult to detect (Basu *et al*, 1993; Henry, PhD thesis, 1997; discussed in Chapter 6, see table 6.6). Interestingly, studies in mice using an enzyme from humans that is known to deglycosylate IgE have shown that removal of carbohydrate disrupts effector function, but not antigen recognition

(Masuda *et al*, 2001). It may be that the body has already discovered an anti-allergic mechanism that involves deglycosylation, as by affecting the glycosylation status of the IgE-Fc it may be possible to dampen the hypersensitivity response that is dependent on the priming of FcεRI on the surface of mast cells and basophils with antigen-specific IgE. However, the mode of action is still to be determined, for although reduced persistence of receptor binding due to an increase in the off-rate is one possibility, another may simply be that removal of carbohydrate leads to aggregation and more rapid clearance of IgE.

The removal of carbohydrate was also confirmed to have an effect on the stability of the Fcε3-4 fragment. In comparison to the findings in Chapter 6, an intermediate result in terms of thermal denaturation mid-point (T_m) and CD spectrum was observed. This suggests that both disulphide linkage and carbohydrate contribute to maintaining the structure and stability of the Fcε3-4 fragment. In the previous chapter it was noted that this trend was also seen in differential scanning microcalorimetry studies carried out on IgG-Fc (Mimura *et al*, 2000l; Mimura *et al*, 2001), suggesting a common pattern for immunoglobulin Fc fragments. The further result, reported in this chapter, with disulphide linked but deglycosylated Fcε3-4 fits well with this pattern, as shown in table 7.4.

Species	Melting temperature T_m (°C)
IgG-Fc (native)	71 (Cγ2 value)*
IgG-Fc (deglycosylated)	65.7 (Cγ2 value)*
IgG-Fc (deglycosylated, reduced and alkylated)	63.5 (Cγ2 value)*
Fcε3-4 (mammalian)	56
Fcε3-4 (mammalian deglycosylated)	53
Fcε3-4ΔC (*E. coli*)	48

Table 7.4: DSC (IgG-Fc) and CD (Fcε3-4) thermal denaturation values. DSC can provide individual T_m values for each domain, and therefore the lower value for Fcγ2 is given (Data from Mimura et al,2000; Mimura et al, 2001).

The results obtained in the centrifuge for the glycosylated, but non-disulphide linked fragment, demonstrated that the 2:1 stochiometry, as observed for the Fcε3-4ΔC, is entirely due to the removal of any tethering at the N-terminus. Interestingly, there was a difference in the affinity constants obtained for the first component of the fit (K_1 = 1.3 x 10^6 M^{-1} for deglycosylated Fcε3-4; K_1 1.8 x 10^5 M^{-1} for Fcε3-4ΔC). This could be the result of the carbohydrate enhancing the affinity of a single Fcε3 domain by increasing the ordering of the N-terminal loops used for receptor engagement (as was found for IgG-Fc by Krapp *et al* 2003 – as discussed earlier).

The K_2 affinity constant for each fit was also different (1.0 x 10^4 M^{-1} for reduced mammalian Fcε3-4 compared to 7.2 x 10^5 M^{-1} for *E. coli* Fcε3-4ΔC). This may reflect the fact that engagement of the second Fcε3 domain by a second sFcεRIα fragment is more difficult for the glycosylated but reduced mammalian Fcε3-4. It is possible this is the result of the glycosylation introducing more rigidity into the Fcε3 domains and therefore reducing the conformational freedom that allowed the Fcε3-4ΔC fragment bind two sFcεRIα domains. In the model proposed in Chapter 6 (see figure 6.11), where the Fcε3 domains "roll" past one another to present the Fcε3 domains in such a way that it is possible to bind two sFcεRIα fragments, this process may be enhanced for the *E. coli* Fcε3-4ΔC fragment as a result of the need to find a way of shielding hydrophobic residues normally covered by the carbohydrate attached at Asn 394. The result of this requirement may be a greater than normal adjustment in the positioning of the flexible Fcε3 domains relative to one another. The need to cover hydrophobic residues in the cavity between opposing domains in the Fc effecting a conformational change has already been proposed as a mechanism for the compacting of the IgG-Fc (Radaev and Sun, 2001). The 2:1 stoichiometry is still seen for the glycosylated Fcε3-4 fragment because when the constraining disulphide is removed the Fcε3 domains are still enabled with a greater degree of conformational freedom (as a result of their inherent instability / flexibility), but because the carbohydrate is present the effect is not as dramatic as that seen for the *E. coli* Fcε3-4ΔC. Certainly, what could be interpreted as a strong requirement to shield the hydrophobic patch between the Fcε3 domains is apparent during the deglycosylation process, as much of the mammalian Fcε3-4 came out of solution during the PNGase F treatment process, all of this

precipitated material corresponded to the band observed for deglycosylated Fcε3-4 in SDS-PAGE (see figure 7.1).

The results reported in this chapter have allowed the contributions of carbohydrate and disulphide linkage to be distinguished. If the disulphide bridge is lost, so too is the high affinity interaction, and thus the disulphide linkage at the N-terminus has a critical role in enabling full engagement of FcεRIα and a 1:1 stoichiometry. The carbohydrate appears to have a subtler, but still significant part to play in establishing a high affinity interaction. The experiments described here, combined with those in the preceding chapter, show that independent of glycosylation state, N-terminal disulphide linkage is a key determinant in the affinity and mode of interaction of Fcε3-4 with FcεRI.

Discussion

Chapter 8: Discussion

In the introduction to this thesis two questions were highlighted. The first was: **What determines the correct folding of the Fcε3 domain in the IgE molecule?**

In the course of investigation it was discovered that to fold Fcε3, Fcε4 needs to be structured, and this can only be achieved when it is part of a homodimer. This was determined using a site-directed mutation that prevented dimerisation of the Fcε4 domain. Neither a monomeric Fcε4 domain, nor a monomeric Fcε3-4 was able to fold. In contrast, dimeric Fcε4 and Fcε3-4 did fold. Furthermore, a heterodimer of Fcε3-4 and Fcε4 appeared not to fold completely, but was stabilised to a greater degree than the Fcε3-4 monomer. This led to the conclusion that, in addition to Fcε4, some form of lateral contact is required for Fcε3 to fold fully, either from an adjacent Fcε3 domain, or glycosylation. It was clear however that Fcε4 was the major contributing factor to the stability of Fcε3. The minimal fragment within which Fcε3 can fold fully is therefore a dimer of Fcε3-4, either with or without carbohydrate, or possibly a Fcε3-4:Fcε4 heterodimer which is glycosylated. The pursuit of a folded heterodimer was not maintained, as the main aim of folding an individual Fcε3 domain was to determine the affinity of a single folded Fcε3 for FcεRI, and this was addressed by the study of the Fcε3-4ΔC fragment.

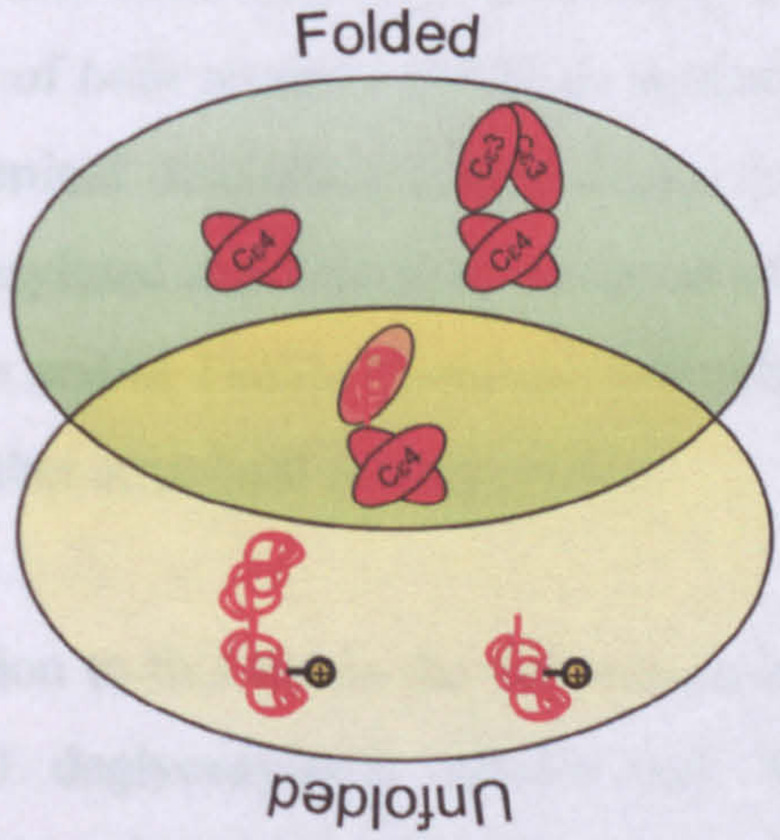

Figure 8.1: Overview of the fragments expressed in Chapters 3-5. The two lower fragments represent Fcε3-4ΔC F506R and Fcε4 F506R (monomeric fragments), the middle fragment is Fcε3-4(4) (the heterodimer) and the top two fragments are the Fcε4 and Fcε3-4ΔC homodimers.

The second question to be addressed was: **What are the minimal structural requirements for a fully active Fcε3 domain?**

To obtain an IgE fragment that retains native affinity it is necessary to glycosylate and disulphide link the receptor binding Fcε3 domains. If the Fcε3 domains are not disulphide linked they are able to function independently of one another, leading to a 2:1 stoichiometry between the receptor and the Fcε3-4 homodimer. The observation of a single Fcε3 domain engaging FcεRI has enabled the affinity of a single folded Fcε3 domain to be determined (~ $10^7 M^{-1}$ by Biacore, 10^6 M^{-1} by AUC), and this contrasts with an affinity of between 10^8 -10^9 M^{-1} for a disulphide linked Fcε3-4 (depending on glycosylation state). The value for a single Fcε3 domain binding was close to that measured for an unfolded Fcε3 domain (5 x 10^6 M^{-1} by Biacore – Henry *et al*, 2000). Therefore, to achieve native affinity for FcεRI, it is necessary for two domains to be present, but the affinity of these domains is not as greatly enhanced by their folding status as perhaps would be expected. In addition to a difference in the affinity between glycosylated and deglycosylated disulphide linked Fcε3-4 fragments, the affinity of the non-disulphide linked Fcε3-4 also depended on glycosylation state (~ 10^6 M^{-1} glycosylated, 10^5 M^{-1} unglycosylated, for a single Fcε3 domain binding FcεRI in the AUC). This result suggests that glycosylation has a direct role to play in presenting receptor-binding regions, and is not simply important for the correct juxtaposition of the Fcε3 domain pair. If the structural requirements were ranked in relation to their contribution to generating full binding affinity for FcεRI, the engagement of both receptor sub-sites is most important, which only occurs fully in a N-terminal disulphide linked dimer. It is less crucial that the Fcε3 domains are glycosylated and folded by virtue of interdomain contacts with Fcε4 (and carbohydrate and/or Fcε3). However, full native affinity can only be achieved with these further structural enhancements.

In the introduction to this thesis the differences in the behaviour of non-disulphide linked and deglycosylated IgE-Fc and IgG-Fc fragments was highlighted. It is now clear that disulphide linkage and glycosylation do have a role to play in affinity, but that Fcε3 has qualities that the receptor-binding region (Fcγ2) of IgG-Fc does not. A clue to how IgE manages the removal of these

structural features better than IgG may lie in data collected for the thermal stability of the IgE-Fc fragments.

The thermal stability of the IgE-Fc fragments, when compared to data collected for the IgG-Fc fragments (Mimura *et al*, 2000; Mimura *et al*, 2001), was found to be greatly reduced. The pattern observed for fragments that lacked certain structural features (glycosylation / disulphide linkage) within either IgE-Fc or IgG-Fc was however maintained. It is may be that this relative instability of IgE-Fc is a product of the necessity for greater flexibility required for full engagement of FcεRI with both Fcε3 domains. The crystal structures have already illustrated an array of conformations for the Fcε3 domain pair. The results described in this thesis show this flexibility at work (i.e. the potential for 2:1 stoichiometry). Perhaps the higher affinity shown by Fcε3-4 for FcεRI, compared to IgG-Fc for Fcγ receptors, is enabled by this flexibility. When the structures of the IgE and IgG crystal complexes are compared there is ~ 360 $Å^2$ more buried surface area attributable to the domain interface for IgE than for IgG. Having more "fluid" domains may be the only way that the greater variety of contacts shown by the Fcε3 domains can be accommodated. This is in contrast to the IgG-Fc, which has a greater degree of contact in the linker region and a reduced *domain* interface area. The linker regions are flexible because they are not constrained by a domain structure, although they cannot provide as broad an interface as the domains can, which display contact residues on several loops rather than a single continuous surface.

Given the observation of 2:1 stoichiometry between non-disulphide linked Fcε3-4, it is perhaps not surprising that IgG has evolved a reduced intra-domain flexibility. In the full IgE-Fc it appears that the presence of the Fcε2 domains would be sufficient to prevent engagement of a second receptor, and thus cross-linking and signalling in the absence of antigen, if the inter-chain disulphides were not formed. In IgG, the insurance against this happening may be reduced intra-domain flexibility, at the expense of a reduction in the potential affinity that IgG-Fc can show for its receptor; the more rigid domains of IgG may be unable to make the same contacts as the more flexible Fcε3 domains of IgE. This relative rigidity may also mean the IgG-Fc is less able to cope with modifications (such as deglycosylation) that alter the way in which the receptor binding site is presented.

How do these observations for the Fcε3-4 fragment sit within the broader context of the binding of the whole IgE-Fc (Fcε2-4) to FcεRI? For example, what is the relevance of the disulphide bridge? As alluded to in the previous paragraph, it may be that in the truncated fragment (Fcε3-4), the parallel disulphide (Cys 328–Cys 328) is playing part of the role that Fcε2 carries out. In the structure of the full Fc, one Fcε2 domain is folded back onto the Fcε3 of the opposite chain of the homodimer. To engage both sites it necessary to displace the Fcε3-bound Fcε2 domain. Therefore the Fcε2 domain only allows a single site to be seen by FcεRI, and then on receptor binding, it reveals the second site. In Fcε3-4 the parallel Cys 328-Cys 328 disulphide bridge tethers the sites together, with the result that once one sub-site is engaged, the second can only be bound by the opposite Fcε3 of the homodimer. In essence they both act to channel the Fc dimer towards the high-affinity complex. For IgE, the "cost" of retaining an extra domain within the Fc is justified, as Fcε2 has another role to play and makes contact with FcεRI after initial engagement via Fcε3 (McDonnell *et al*, 2001).

The presence of covalent linkage of opposing chains in the N-terminal region of the truncated Fcε3-4 fragment appears to allow enough freedom for the full engagement of both Fcε3 domains with FcεRI (Garman et al, 2000). However, given the fact that the disulphide arrangement in such fragments is incorrect (Cys 328-Cys 328, rather than Cys 328-Cys 241), and that evidence is presented in this thesis that demonstrates that the presence of the disulphide is critical for the correct engagement of sFcεRIα. It may well be that the inclusion of a parallel disulphide bridge in previous Fcε3-4 fragments used in biophysical studies of the FcεRI:IgE complex represents a fortunate addition. The inclusion of the Cys 328-Cys 328 disulphide has revealed what is almost certainly the correct mode of engagement of the Fcε3 domains of IgE-Fc with FcεRIα (Garman *et al*, 2000). However, it is now clear that the formation of the IgE:FcεRI complex actually comes about via a much more complicated process also involving Fcε2 (Wan *et al*, 2002). Therefore, it is clear that the true nature of the interaction between IgE and its high-affinity receptor will only be resolved by crystal structures of a complex composed of the whole Fc (Fcε2-4) fragment and sFcεRIα. Such a structure, in addition to resolving fully the role of Fcε2, may

also shed further light on the reasons for maintaining such a complex arrangement with respect to the inter chain disulphides.

Since the structure of the Fcε2-4 fragment reveals that the presence of Fcε2 would prevent the binding of a second receptor subunit, this suggests that the disulphide is less important in the full Fc. To some degree this statement is supported by a set of ΔC mutants made by Helm *et al* (Helm *et al*, 1991). Here the full Fc was made with and without the inter-domain disulphide bridges. In this study it was found that the complete ΔC mutant (i.e. a Fcε2-4 construct with the interchain 241 and 328 disulphides removed) displayed 20-fold lower affinity for FcεRI. The less drastic difference in affinity observed in these experiments, compared with those obtained for Fcε3-4, may be the result of a secondary role that the disulphide plays in local structuring of the linker in Fcε2-4, as opposed to pinning the Fcε3 domains together, as in the Fcε3-4 fragment.

The study of IgE-Fc fragments with differing post-translation features and domain structures has demonstrated a complex web of inter-domain contacts, covalent and non-covalent, that are organised to bring about the uniquely high affinity of IgE for FcεRI. Further work is now required to take the results from these experiments, and those carried out in the past, to focus on specific regions of IgE related to its binding to FcεRI, with the overall aim of inhibiting the interaction. Given these observations how can they be used to target the interaction?

Glycosylation would not appear to off much potential regarding inhibition of the formation of the IgE:FcεRI complex. A fragment that is deglycosylated is still seen as high affinity in the analytical centrifuge, for example. However, it should be noted that a deglycosylating enzyme has been identified in the urine of allergics (Masuda *et al*, 2001). This enzyme renders IgE non-functional with respect to receptor binding, although the mechanism by which this occurs is unclear. One aspect of the result obtained with deglycosylated Fcε3-4 that is particularly interesting is the fact that the carbohydrate may act in a similar fashion to the disulphide bridge. From the Biacore data it is clear that there are two components to the interaction, one lower in affinity than the other. This is consistent with the crystal structure of the FcεRI:Fcε3-4 complex that revealed binding across two sub sites in the Fcε3-4 dimer. The differences between the two components occur mainly in the off-

rates. When carbohydrate is removed it appears that fewer molecules are channelled to the higher affinity state, as is clear from the shift in the R_1/R_0 ratio (see table 7.2). The reasons for this may be two-fold. Firstly, the carbohydrate may aid in the contact of FcεRIα with the second sub site by virtue of orientating the Fcε3 domains with respect to one another. Secondly, as suggested by the affinities obtained from the AUC data, individual domains may also vary in affinity depending on their glycosylation state (the interaction of a single Fcε3 domain in Fcε3-4 with a single sFcεRIα is described by the K_1 affinity constant, this value rises from 1.8×10^5 M^{-1} to 1.3×10^6 M^{-1} when the fragment is glycosylated). This may reflect ordering of contact residues in loops due the presence of carbohydrate. This region is thought to distinguish affinities between antibody isotypes (Wurzburg et al, 2002), and is more extensive in the IgE:FcεRI complex compared to IgG:FcγRIII. Therefore, this region may represent an IgE specific target.

The necessity for IgE specific targets is particularly important if the similarities in binding modes, and therefore potential overlap in residues used by the different antibody isotypes is taken into account. Many peptides have been described in the past that inhibit IgE binding to FcεRI (for example Hamburger, 1975, Stanworth *et al*, 1990, McDonnell *et al*, 1997; reviewed in Beavil *et al*, 1993 and Helm *et al*, 1997). The most recent of these are a set of "zeta" peptides that present a small constrained peptide unit whose function is dependent on the presence of a proline residue at their centre (Nakamura *et al*, 2001; Nakamura *et al*, 2002). These peptides, despite their high affinity (30 nM), have not been advanced as a therapeutic option. This may be because they target the proline sandwich, which is a common motif for IgG as well as IgE. Certainly non-specificity has been seen previously with peptides, notably with linker peptides targeted to the IgG Fcγ interaction (Radaev and Sun, 2001). In these experiments it was found that an IgE linker peptide that has little sequence homology to the IgG peptide also inhibited IgG binding its receptor. This issue may be related to the folding of the domains. Minimally structured regions potentially yield a large amount of binding energy, as supported by the results obtained with the unstructured Fcε3 domain. However with this may come a degree of non-specificity. These initial interactions may represent only the first step, to be followed by more structure specific events lead to a channelling of the interaction

towards a high affinity state, for example those co-ordinated by carbohydrate or adjustment of the Fcε3 domain pair. Therefore, targeting the events subsequent to the initial interaction may be the key to inhibiting IgE binding to FcεRI without disrupting other isotypes binding to their respective receptors.

One such approach may be the pursuit of novel inhibitors of conformational change. This had previously been suggested by Wurzburg *et al* (Wurzburg et al, 2000) with respect to the flexing of the Fcε3 domains, and is equally relevant with respect to Fcε2. The work outlined in this thesis presents very striking evidence for an inherent flexibility of the Fcε3 domain pair, and it also shows that if a single binding site could be inhibited there is a potential for a 1000-fold reduction in affinity. If this observation is allied to those made with respect to the orientation of the Fcε2 domains in the full Fc, where it appears that only a single Fcε3 domain is open to binding, and that a conformational change is required to access the second site, there is an indication that it is not only direct inhibitors of binding that could work, but also inhibitors that act to prevent the accessibility of binding sites due to conformational change. For example, if the Fc could be locked into the conformation in which only one site is open for binding, the potential for disruption of receptor engagement is very apparent. Figure 8.2 illustrates the three different positions seen for opposing Fcε3 domains from the three known crystal structures of the IgE-Fc (Garman *et al*, 2000; Wurzburg *et al*, 2000; Wan *et al*, 2002).

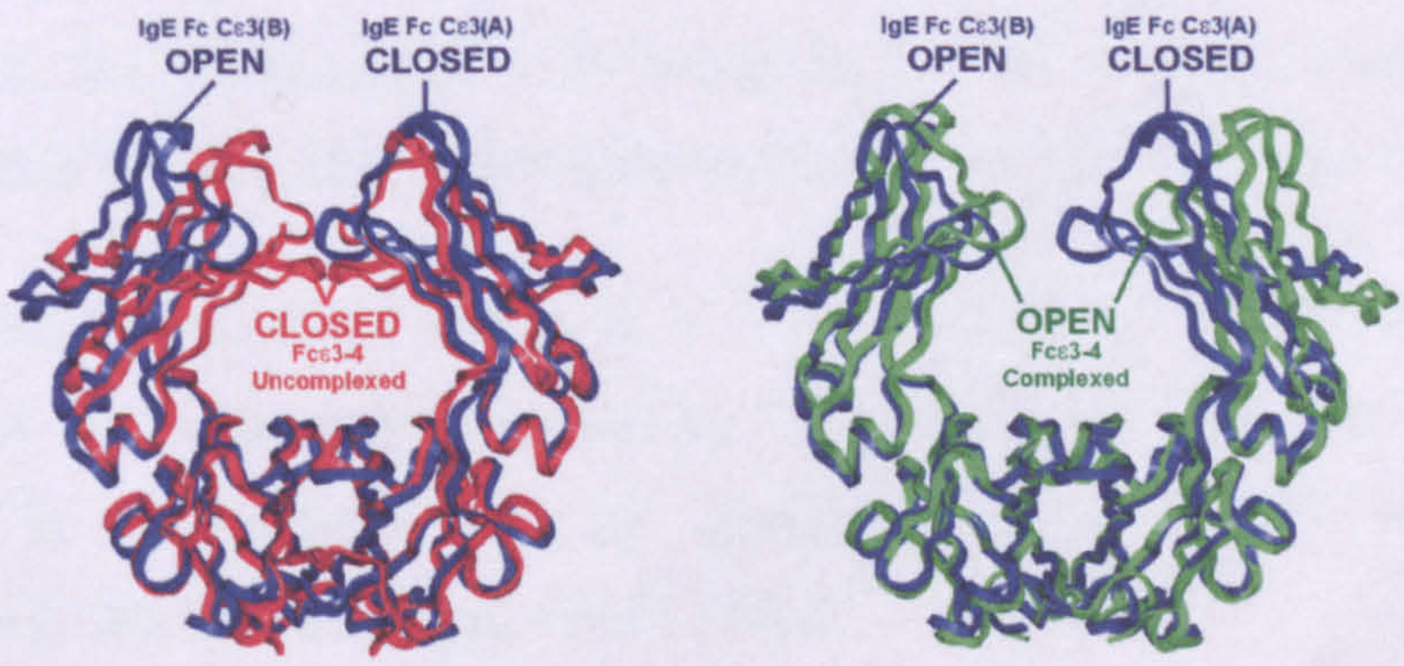

Figure 8.2: C-α backbones of Fcε3-4 complexed (red) and uncomplexed (green) superimposed on the Fcε3-4 of the full Fc (blue). This diagram shows that in the unbound full Fc one Fcε3 domain is open, and able to bind FcεRI, whereas the other is closed and cannot (based on Wan et al, 2002).

There is at present no direct evidence for the proposed conformational change, although the results reported in this thesis do reinforce the observations made with respect to the different crystal forms, i.e. that the Fc has an inherent flexibility. Therefore, one key focus for future work must be a method for testing the conformational change hypothesis. Such experiments could also form the foundation for assessing the potential of inhibitors of these conformational changes. The potential for stopping these events occurring is clear, as it is now possible to attach some quantitative figures to the likely effects of such inhibition As a the result of observing the interaction of a single Fcε3 domain with FcεRI in the experiments described in this thesis, it is clear that restricting receptor engagement to only one sub-site in IgE-Fc could lead to at least a 1000-fold reduction in binding affinity.

References

Aalberse, R., C. & Schuurman, J. 2002, "IgG4 breaking the rules", *Immunology*, vol. 105, pp 9-19.

Asai, K., Kitaura, J., Kawakami, Y., Yamagata, N., Tsai, M., Carbone, D. P., Liu, F. T., Galli, S. J., & Kawakami, T. 2001, "Regulation of mast cell survival by IgE", *Immunity.*, vol. 14, no. 6, pp. 791-800.

Baird, B. & Holowka, D. 1985, "Structural mapping of Fc receptor bound immunoglobulin E: proximity to the membrane surface of the antibody combining site and another site in the Fab segments", *Biochemistry*, vol. 24, no. 22, pp. 6252-6259.

Basu, M., Hakimi, J., Dharm, E., Kondas, J. A., Tsien, W. H., Pilson, R. S., Lin, P., Gilfillan, A., Haring, P., Braswell, E. H., & . 1993, "Purification and characterization of human recombinant IgE-Fc fragments that bind to the human high affinity IgE receptor", *J.Biol.Chem.*, vol. 268, no. 18, pp. 13118-13127.

Beavil, A. J., Edmeades, R. L., Gould, H. J., & Sutton, B. J. 1992, "Alpha-helical coiled-coil stalks in the low-affinity receptor for IgE (Fc epsilon RII/CD23) and related C-type lectins", *Proc.Natl.Acad.Sci.U.S.A*, vol. 89, no. 2, pp. 753-757.

Beavil, A. J., Beavil, R. L., Chan, C. M., Cook, J. P., Gould, H. J., Henry, A. J., Owens, R. J., Shi, J., Sutton, B. J., & Young, R. J. 1993, "Structural basis of the IgE-Fc epsilon RI interaction", *Biochem.Soc.Trans.*, vol. 21, no. 4, pp. 968-972.

Beavil, A. J., Young, R. J., Sutton, B. J., & Perkins, S. J. 1995, "Bent domain structure of recombinant human IgE-Fc in solution by X-ray and neutron scattering in conjunction with an automated curve fitting procedure", *Biochemistry*, vol. 34, no. 44, pp. 14449-14461.

Bebbington, C. R., Renner, G., Thomson, S., King, D., Abrams, D., & Yarranton, G. T. 1992, "High-level expression of a recombinant antibody from myeloma cells using a glutamine synthetase gene as an amplifiable selectable marker", *Biotechnology (N.Y.)*, vol. 10, no. 2, pp. 169-175.

Bjorklund, J. E., Karlsson, T., & Magnusson, C. G. 1999, "N-glycosylation influences epitope expression and receptor binding structures in human IgE", *Mol.Immunol.*, vol. 36, no. 3, pp. 213-221.

Bohmann, D. & Tjian, R. 1989, "Biochemical analysis of transcriptional activation by Jun: differential activity of c- and v-Jun", *Cell*, vol. 59, no. 4, pp. 709-717.

Borkowski, T. A., Jouvin, M. H., Lin, S. Y., & Kinet, J. P. 2001, "Minimal requirements for IgE-mediated regulation of surface Fc epsilon RI", *J.Immunol.*, vol. 167, no. 3, pp. 1290-1296.

Carter, P. 2001, "Bispecific human IgG by design", *J.Immunol.Methods*, vol. 248, no. 1-2, pp. 7-15.

Cathou, R.E. 1978. *Contemp. Immunol.*, vol 5, pp. 37-83.

Cook, J. P., Henry, A. J., McDonnell, J. M., Owens, R. J., Sutton, B. J., & Gould, H. J. 1997, "Identification of contact residues in the IgE binding site of human FcεRIα", *Biochemistry*, vol. 36, no. 50, pp. 15579-15588.

Dall'Acqua, W., Simon, A. L., Mulkerrin, M. G., & Carter, P. 1998, "Contribution of domain interface residues to the stability of antibody CH3 domain homodimers", *Biochemistry*, vol. 37, no. 26, pp. 9266-9273.

Deisenhofer, J. 1981, "Crystallographic refinement and atomic models of a human Fc fragment and its complex with fragment B of protein A from Staphylococcus aureus at 2.9- and 2.8-A resolution", *Biochemistry*, vol. 20, no. 9, pp. 2361-2370.

Dombrowicz, D. & Capron, M. 2001, "Eosinophils, allergy and parasites", *Curr.Opin.Immunol.*, vol. 13, no. 6, pp. 716-720.

Dorai, H., Wesolowski, J., S. & Gillies, S. D. 1992. "Role of inter-heavy and light chain disulphide bonds in the effector functions of human immunoglobulin IgG1", *Mol. Immunol.*, vol 29, no. 12, pp 1487 – 1491.

Dorrington, K. J. & Bennich, H. H. 1978, "Structure-function relationships in human immunoglobulin E", *Immunol.Rev.*, vol. 41, pp. 3-25.

Garman, S. C., Kinet, J. P., & Jardetzky, T. S. 1998, "Crystal structure of the human high-affinity IgE receptor", *Cell*, vol. 95, no. 7, pp. 951-961.

Garman, S. C., Wurzburg, B. A., Tarchevskaya, S. S., Kinet, J. P., & Jardetzky, T. S. 2000, "Structure of the Fc fragment of human IgE bound to its high-affinity receptor Fc epsilonRI alpha", *Nature*, vol. 406, no. 6793, pp. 259-266.

Garman S. C., Sechi S., Kinet J. P., Jardetzky T. S. 2001, "The analysis of the human high affinity IgE receptor FcεRIα from multiple crystal forms", *J Mol Biol.*, vol. 31;no. 311, part (5), pp. 1049-62.

Geha, R. S., Helm, B., & Gould, H. 1985, "Inhibition of the Prausnitz-Kustner reaction by an immunoglobulin epsilon-chain fragment synthesized in E. coli", *Nature*, vol. 315, no. 6020, pp. 577-578.

Gould, H. J., Sutton, B. J., Beavil, A. J., Beavil, R. L., McCloskey, N., Coker, H. A., Fear, D., & Smurthwaite, L. 2003, "The Biology of IgE and the Basis of Allergic Disease", *Annu.Rev.Immunol.* vol. 21, pp. 579-628.

Gould, H. J., Beavil, R. L., Reljic, R., Shi, J., Ma, C.W., Sutton, B. J., Gjirlando, R. 1997, "IgE homeostasis: is CD23 the safety switch?", *IgE regulation: Molecular mechanisms. Ed. Vercelli, D. John Wiley and Sons.*

Greenfield, N. & Fasman, G. D. 1969, "Computed circular dichroism spectra for the evaluation of protein conformation", *Biochemistry*, vol. 8, no. 10, pp. 4108-4116.

Hamburger, R. N. 1975, "Peptide inhibition of the Prausnitz-Kustner reaction", *Science*, vol. 189, no. 4200, pp. 389-390.

Hamelmann, E., Rolinck-Werninghaus, C., & Wahn, U. 2002, "From IgE to anti-IgE: where do we stand?", *Allergy*, vol. 57, no. 11, pp. 983-994.

Helm, B., Marsh, P., Vercelli, D., Padlan, E., Gould, H., & Geha, R. 1988, "The mast cell binding site on human immunoglobulin E", *Nature*, vol. 331, no. 6152, pp. 180-183.

Helm, B. A., Ling, Y., Teale, C., Padlan, E. A., & Bruggemann, M. 1991, "The nature and importance of the inter-epsilon chain disulfide bonds in human IgE", *Eur.J.Immunol.*, vol. 21, no. 6, pp. 1543-1548.

Helm, B. A., Spivey, A. C., & Padlan, E. A. 1997, "Peptide blocking of IgE/receptor interaction: possibilities and pitfalls", *Allergy*, vol. 52, no. 12, pp. 1155-1169.

Henry, A. J., Cook, J. P., McDonnell, J. M., Mackay, G. A., Shi, J., Sutton, B. J., & Gould, H. J. 1997, "Participation of the N-terminal region of Cε3 in the binding of human IgE to its high-affinity receptor FcεRI", *Biochemistry*, vol. 36, no. 50, pp. 15568-15578.

Henry, A. J., McDonnell, J. M., Ghirlando, R., Sutton, B. J., & Gould, H. J. 2000, "Conformation of the isolated Cε3 domain of IgE and its complex with the high-affinity receptor, FcεRI", *Biochemistry*, vol. 39, no. 25, pp. 7406-7413.

Henry, A. J., 1997, PhD thesis. University of London.

Holowka, D., Wensel, T., & Baird, B. 1990, "A nanosecond fluorescence depolarization study on the segmental flexibility of receptor-bound immunoglobulin E", *Biochemistry*, vol. 29, no. 19, pp. 4607-4612.

Hulett, M. D., McKenzie, I. F., & Hogarth, P. M. 1993, "Chimeric Fc receptors identify immunoglobulin-binding regions in human FcγRII and FcεRI", *Eur.J.Immunol.*, vol. 23, no. 3, pp. 640-645.

Ishizaka, K. & Ishizaka, T. 1967, "Identification of gamma-E-antibodies as a carrier of reaginic activity", *J.Immunol.*, vol. 99, no. 6, pp. 1187-1198.

Jefferis, R. & Lund, J. 2002, "Interaction sites on human IgG-Fc for FcγR: current models", *Immunol.Lett.*, vol. 82, no. 1-2, pp. 57-65.

Johansson, S. G. O., & Bennich, H. 1967, "Immunological studies of an atypical (myeloma) immunoglobulin", *Immunology*, vol. 13, no. 4, pp. 381-394.

Kalesnikoff J., Huber M., Lam V., Damen J. E., Zhang J., Siraganian R.P., and Krystal G. 2001, "Monomeric IgE stimulates signaling pathways in mast cells that lead to cytokine production and cell survival." *Immunity* vol 14, part (6), pp. 801-811.

Karagiannis, S. N., Warrack, J. K., Jennings, K. H., Murdock, P. R., Christie, G., Moulder, K., Sutton, B. J., & Gould, H. J. 2001, "Endocytosis and recycling of the complex between CD23 and HLA-DR in human B cells", *Immunology*, vol. 103, no. 3, pp. 319-331.

Karagiannis, S. N., Wang, Q., East, N., Burke, F., Riffard, S., Bracher, M. G., Thompson, R. G., Durham, S. R., Schwartz, L. B., Balkwill, F. R., & Gould, H. J. 2003, "Activity of human monocytes in IgE antibody-dependent surveillance and killing of ovarian tumor cells", *Eur.J.Immunol.*, vol. 33, no. 4, pp. 1030-1040.

Kenten, J. H., Molgaard, H. V., Houghton, M., Derbyshire, R. B., Viney, J., Bell, L. O., & Gould, H. J. 1982, "Cloning and sequence determination of the gene for the human immunoglobulin epsilon chain expressed in a myeloma cell line", *Proc.Natl.Acad.Sci.U.S.A*, vol. 79, no. 21, pp. 6661-6665.

Keown, M. B., Ghirlando, R., Young, R. J., Beavil, A. J., Owens, R. J., Perkins, S. J., Sutton, B. J., & Gould, H. J. 1995, "Hydrodynamic studies of a complex between the Fc fragment of human IgE and a soluble fragment of the FcεRI α-chain", *Proc.Natl.Acad.Sci.U.S.A*, vol. 92, no. 6, pp. 1841-1845.

Keown, M. B., Ghirlando, R., Mackay, G. A., Sutton, B. J., & Gould, H. J. 1997, "Basis of the 1:1 stoichiometry of the high affinity receptor FcεRI-IgE complex", *Eur.Biophys.J.*, vol. 25, no. 5-6, pp. 471-476.

Keown, M.B., 1997. PhD thesis, University of London.

Kessler, H., Mronga, S., Muller, G., Moroder, L. & Huber, R. 1991, "Conformational dynamics of a IgG1 hinge peptide derivative in solution

determined by NMR spectroscopy and refined by restrained molecular dynamics simulations", *Biopolymers*, vol 31, no. 10, pp 1189-1204.

Kinet, J. P. 1999, "The high-affinity IgE receptor (FcεRI): from physiology to pathology", *Annu.Rev.Immunol.*, vol. 17, pp. 931-972.

Kitaura, J., Song, J., Tsai, M., Asai, K., Maeda-Yamamoto, M., Mocsai, A., Kawakami, Y., Liu, F. T., Lowell, C. A., Barisas, B. G., Galli, S. J., & Kawakami, T. 2003, "Evidence that IgE molecules mediate a spectrum of effects on mast cell survival and activation via aggregation of the FcεRI", *Proc.Natl.Acad.Sci.U.S.A*, vol. 100, no. 22, pp. 12911-12916.

Kochan, J. P., Mallamaci, M., Gilfillan, A., Madison, V., & Basu, M. 1994, "Characterization of the human IgE Fc-FcεRIα interaction", *Adv.Exp.Med.Biol.*, vol. 347, pp. 31-38.

Krapp, S., Mimura, Y., Jefferis, R., Huber, R., & Sondermann, P. 2003, "Structural Analysis of Human IgG-Fc Glycoforms Reveals a Correlation Between Glycosylation and Structural Integrity", *J.Mol.Biol.*, vol. 325, no. 5, pp. 979-989.

Laemmli, U. K. 1970, "Cleavage of structural proteins during the assembly of the head of bacteriophage T4". *Nature,* vol. 227, pp. 680-685.

Lamers, M. C. & Yu, P. 1995, "Regulation of IgE synthesis. Lessons from the study of IgE transgenic and CD23-deficient mice", *Immunol.Rev.*, vol. 148, pp. 71-95.

Lund, J., Takahashi, N., Popplewell, A., Goodall, M., Pound, J. D., Tyler, R., King, D. J., & Jefferis, R. 2000, "Expression and characterization of truncated forms of humanized L243 IgG1. Architectural features can influence synthesis of its oligosaccharide chains and affect superoxide production triggered through human Fcγ receptor I", *Eur.J.Biochem.*, vol. 267, no. 24, pp. 7246-7257.

Maenaka, K., van der Merwe, P. A., Stuart, D. I., Jones, E. Y., & Sondermann, P. 2001, "The human low affinity Fcgamma receptors IIa, IIb, and III bind IgG with

fast kinetics and distinct thermodynamic properties", *J.Biol.Chem.*, vol. 276, no. 48, pp. 44898-44904.

Masuda, Y., Akagawa, Y., & Hishikawa, Y. 2001, "Another anti-allergic mechanism: antibody IgE deglycosylation induced by a substance extracted from human urine", *Yale J.Biol.Med.*, vol. 74, no. 3, pp. 145-149.

McDonnell, J. M., Beavil, A. J., Mackay, G. A., Henry, A. J., Cook, J. P., Gould, H. J., & Sutton, B. J. 1997, "Structure-based design of peptides that inhibit IgE binding to its high-affinity receptor FcεRI", *Biochem.Soc.Trans.*, vol. 25, no. 2, pp. 387-392.

McDonnell, J. M., Calvert, R., Beavil, R. L., Beavil, A. J., Henry, A. J., Sutton, B. J., Gould, H. J., & Cowburn, D. 2001, "The structure of the IgE Cε2 domain and its role in stabilizing the complex with its high-affinity receptor FcεRIα", *Nat.Struct.Biol.*, vol. 8, no. 5, pp. 437-441.

Mimura, Y., Church, S., Ghirlando, R., Ashton, P. R., Dong, S., Goodall, M., Lund, J., & Jefferis, R. 2000, "The influence of glycosylation on the thermal stability and effector function expression of human IgG1-Fc: properties of a series of truncated glycoforms", *Mol.Immunol.*, vol. 37, no. 12-13, pp. 697-706.

Mimura, Y., Sondermann, P., Ghirlando, R., Lund, J., Young, S. P., Goodall, M., & Jefferis, R. 2001, "Role of oligosaccharide residues of IgG1-Fc in FcγRIIb binding", *J.Biol.Chem.*, vol. 276, no. 49, pp. 45539-45547.

Nakamura, G. R., Starovasnik, M. A., Reynolds, M. E., & Lowman, H. B. 2001, "A novel family of hairpin peptides that inhibit IgE activity by binding to the high-affinity IgE receptor", *Biochemistry*, vol. 40, no. 33, pp. 9828-9835.

Nakamura, G. R., Reynolds, M. E., Chen, Y. M., Starovasnik, M. A., & Lowman, H. B. 2002, "Stable "zeta" peptides that act as potent antagonists of the high-affinity IgE receptor", *Proc.Natl.Acad.Sci.U.S.A* , vol. 99, no. 3, pp. 1303-1308.

Nettleton, M. Y. & Kochan, J. P. 1995, "Role of glycosylation sites in the IgE Fc molecule", *Int.Arch.Allergy Immunol.*, vol. 107, no. 1-3, pp. 328-329.

Nezlin, R.S., Zagyansky, Y.A., Kaivarainen, A.I., & Stefani, D.V. 1973, "Properties of myeloma immunoglobulin E(Yu). Chemical, fluorescence polarisationand spin-labeled studies", *Immunochemistry*, vol. 10, no.10, pp. 681-688.

Nissim, A., Jouvin, M.-H., & Eshhar, Z. 1991. "Mapping of the high affinity Fcε receptor binding site to the third constant region domain of IgE", *EMBO*, vol. 10, no. 1, pp. 101-107.

Novak, N., Kraft, S., & Bieber, T. 2001, "IgE receptors", *Curr.Opin.Immunol.*, vol. 13, no. 6, pp. 721-726.

Oi, V. T., Vuong, T. M., Hardy, R., Reidler, J., Dangle, J., Herzenberg, L. A., & Stryer, L. 1984, "Correlation between segmental flexibility and effector function of antibodies", *Nature*, vol. 307, no. 5947, pp. 136-140.

Padlan EA, Davies DR. 1986, "A model of the Fc of immunoglobulin E." *Mol. Immunol.*, vol. 23, part (10), pp. 1063-1075.

Payet, M. & Conrad, D. H. 1999, "IgE regulation in CD23 knockout and transgenic mice", *Allergy*, vol. 54, no. 11, pp. 1125-1129.

Prausnitz, C. & Kustner, H. 1921. *Zentralbat fur Bacteriologie, Infectionskrankheiten und Hygeine.* Abt., vol 1 no. 86, pp160-169.

Presta, L., Shields, R., O'Connell, L., Lahr, S., Porter, J., Gorman, C., & Jardieu, P. 1994, "The binding site on human immunoglobulin E for its high affinity receptor", *J.Biol.Chem.*, vol. 269, no. 42, pp. 26368-26373.

Radaev, S. & Sun, P. D. 2001, "Recognition of IgG by Fcgamma receptor. The role of Fc glycosylation and the binding of peptide inhibitors", *J.Biol.Chem.*, vol. 276, no. 19, pp. 16478-16483.

Radaev, S., Motyka, S., Fridman, W. H., Sautes-Fridman, C., & Sun, P. D. 2001, "The structure of a human type III Fcγ receptor in complex with Fc", *J.Biol.Chem.*, vol. 276, no. 19, pp. 16469-16477.

Radaev, S. & Sun, P. 2002, "Recognition of immunoglobulins by Fcγ receptors", *Mol.Immunol.*, vol. 38, no. 14, pp. 1073-1083.

Ravetch, J. V. & Kinet, J. P. 1991, "Fc receptors", *Annu.Rev.Immunol.*, vol. 9, pp. 457-492.

Riske, F., Hakimi, J., Mallamaci, M., Griffin, M., Pilson, B., Tobkes, N., Lin, P., Danho, W., Kochan, J., & Chizzonite, R. 1991, "High affinity human IgE receptor (FcεRI). Analysis of functional domains of the alpha-subunit with monoclonal antibodies", *J.Biol.Chem.*, vol. 266, no. 17, pp. 11245-11251.

Sayers I., Cain S. A., Swan J. R., Pickett M. A., Watt P. J., Holgate S. T., Padlan E. A., Schuck P., Helm B. A. 1998, "Amino acid residues that influence Fc epsilon RI-mediated effector functions of human immunoglobulin E." *Biochemistry*, vol 17 no. 37, part (46), pp. 16152-16164.

Shi, J., Ghirlando, R., Beavil, R. L., Beavil, A. J., Keown, M. B., Young, R. J., Owens, R. J., Sutton, B. J., & Gould, H. J. 1997, "Interaction of the low-affinity receptor CD23/FcεRII lectin domain with the Fcε3-4 fragment of human immunoglobulin E", *Biochemistry*, vol. 36, no. 8, pp. 2112-2122.

Siraganian, R. P. 2003, "Mast cell signal transduction from the high-affinity IgE receptor", *Curr.Opin.Immunol.*, vol. 15, no. 6, pp. 639-646.

Slattery, J., Holowka, D., & Baird, B. 1985, "Segmental flexibility of receptor-bound immunoglobulin E", *Biochemistry*, vol. 24, no. 26, pp. 7810-7820.

Smurthwaite, L., Walker, S. N., Wilson, D. R., Birch, D. S., Merrett, T. G., Durham, S. R., & Gould, H. J. 2001, "Persistent IgE synthesis in the nasal mucosa of hay fever patients", *Eur.J.Immunol.*, vol. 31, no. 12, pp. 3422-3431.

Sondermann, P., Huber, R., Oosthuizen, V., & Jacob, U. 2000, "The 3.2-A crystal structure of the human IgG1 Fc fragment-FcγRIII complex", *Nature*, vol. 406, no. 6793, pp. 267-273.

Stanworth, D. R., Jones, V. M., Lewin, I. V., & Nayyar, S. 1990, "Allergy treatment with a peptide vaccine", *Lancet*, vol. 336, no. 8726, pp. 1279-1281.

Sutton, B. J. & Gould, H. J. 1993, "The human IgE network", *Nature*, vol. 366, no. 6454, pp. 421-428.

Sutton, B. J., Beavil, R. L., & Beavil, A. J. 2000, "Inhibition of IgE-receptor interactions", *Br.Med.Bull.*, vol. 56, no. 4, pp. 1004-1018.

Takatsu, K., Ishizaka, T., & Ishizaka, K. 1975, "Biologic significance of disulfide bonds in human IgE molecules", *J.Immunol.*, vol. 114, no. 6, pp. 1838-1845.

Tao, M. H. & Morrison, S. L. 1989, "Studies of aglycosylated chimeric mouse-human IgG. Role of carbohydrate in the structure and effector functions mediated by the human IgG constant region", *J.Immunol.*, vol. 143, no. 8, pp. 2595-2601.

Taylor, A.J., Prat, K. A., Revell, D. F., Baker, K. C., Sumner, I. G., & Goodenough, P. W. 1992. "Active papain renatured and processed from insoluble recombinant propapain expressed in Escherichia coli", *Protein Eng.*, vol. 5, no. 5, pp. 455-9.

van der Heijden, F. L., Joost van Neerven, R. J., van Katwijk, M., Bos, J. D., & Kapsenberg, M. L. 1993, "Serum-IgE-facilitated allergen presentation in atopic disease", *J.Immunol.*, vol. 150, no. 8 Pt 1, pp. 3643-3650.

van der Merwe. 2000. "Surface plasmon resonance", *Protein-ligand interactions: A practical approach. Ed. Harding, S. and Chowdhry, P. Z. Oxford University Press.*

Vangelista, L. 2003, "Current progress in the understanding of IgE-FcepsilonRI interaction", *Int.Arch.Allergy Immunol.*, vol. 131, no. 4, pp. 222-233.

Vercelli, D., Helm, B., Marsh, P., Padlan, E., Geha, R. S., & Gould, H. 1989, "The B-cell binding site on human immunoglobulin E", *Nature*, vol. 338, no. 6217, pp. 649-651.

Wan, T., Beavil, R. L., Fabiane, S. M., Beavil, A. J., Sohi, M. K., Keown, M., Young, R. J., Henry, A. J., Owens, R. J., Gould, H. J., & Sutton, B. J. 2002, "The crystal structure of IgE Fc reveals an asymmetrically bent conformation", *Nat.Immunol.*, vol. 3, no. 7, pp. 681-686.

Weetal, M., Shopes, B., Holowka, D., & Baird, B. 1990, "Mapping the site of interation between murine IgE and its high affinity receptor with chimeric Ig^{1}", *J. Immunol.*, vol. 145, no. 11, pp. 3849-3854.

Wurzburg, B. A., Garman, S. C., & Jardetzky, T. S. 2000, "Structure of the human IgE-Fc Cε3-Cε4 reveals conformational flexibility in the antibody effector domains", *Immunity.*, vol. 13, no. 3, pp. 375-385.

Wurzburg, B. A. & Jardetzky, T. S. 2002, "Structural insights into the interactions between human IgE and its high affinity receptor FcεRI", *Mol.Immunol.*, vol. 38, no. 14, pp. 1063-1072.

Zheng, Y., Shopes, B., Holowka, D., & Baird, B. 1991, "Conformations of IgE bound to its receptor FcεRI and in solution", *Biochemistry*, vol. 30, no. 38, pp. 9125-9132.

Zheng, Y., Shopes, B., Holowka, D., & Baird, B. 1992, "Dynamic conformations compared for IgE and IgG1 in solution and bound to receptors", *Biochemistry*, vol. 31, no. 33, pp. 7446-7456.